

An investigation of the pyrolysis
of binary mixtures of wool with
other textile polymers and the
surface properties of the carbons produced

Neville Frank Ordoyno BSc CChem MRIC PGCEd

Awarded London University March 31st 1976

Department of Physical Sciences
Trent Polytechnic
Nottingham

1976

ProQuest Number: 10290239

All rights reserved

INFORMATION TO ALL USERS

The quality of this reproduction is dependent upon the quality of the copy submitted.

In the unlikely event that the author did not send a complete manuscript and there are missing pages, these will be noted. Also, if material had to be removed, a note will indicate the deletion.



ProQuest 10290239

Published by ProQuest LLC (2017). Copyright of the Dissertation is held by the Author.

All rights reserved.

This work is protected against unauthorized copying under Title 17, United States Code
Microform Edition © ProQuest LLC.

ProQuest LLC.
789 East Eisenhower Parkway
P.O. Box 1346
Ann Arbor, MI 48106 – 1346

TRENT POLYTECHNIC LIBRARY	
	PS. PHD 4

ABSTRACT

In this research project the pyrolysis behaviour of three series of binary polymer mixtures (wool/Terylene, wool/Courtelle, Terylene/Courtelle) was examined using the techniques of Differential Thermal Analysis, Thermogravimetry and Hot-Stage Microscopy.

Evidence from Differential Thermal Analysis and Thermogravimetry indicated that the thermal stability of Terylene is reduced when pyrolysed in binary mixtures with wool or Courtelle. It is suggested that this decrease in thermal stability may be attributed to chemical interaction between the Terylene and degradation products arising from the second polymer of the binary mixture.

The residual yields from large scale pyrolysis of the polymer mixtures wool/Courtelle and Terylene/Courtelle were observed to be excessively high.

Hot-Stage Microscope observations of these two binary mixtures during pyrolysis indicated that coating of the non-fusing polymer by the fusing polymer took place. It was considered that this coating trapped degradation products from the non-fusing polymer (Courtelle) and thus gave rise to the excessively high residual yields observed.

The various carbons prepared from the three series of binary polymer mixtures were activated by reaction with carbon dioxide. The adsorption of carbon dioxide by each carbon sample was measured at 195K.

Dubinín-Radushkevich type I plots were constructed from this adsorption data. Mercury density measurements were made on selected activated carbons.

Various types of deviations from linearity were observed in the Dubinín-Radushkevich type I plots. Further some of the highly activated carbons prepared from wool/Courtelle and Terylene/Courtelle polymer mixtures were found to adsorb negligible amounts of gas and had relatively high mercury densities.

The adsorption and mercury density data for carbons prepared from polymer mixtures wool/Courtelle and Terylene/Courtelle have been interpreted in terms of a model structure for these carbons based on the coating phenomena observed during pyrolysis by Hot-Stage Microscopy.

To my parents
and J.A.S.

ACKNOWLEDGEMENTS

I would like to thank Mr S M Rowan, my supervisor, for all the advice and encouragement given throughout this work.

Further I would like to thank all the people at Trent Polytechnic who have given help in this project including Dr D Harvey, Mrs S Roller, and the technical and academic staff of the departments of Physical Sciences and Textiles.

Finally I am indebted to the Wool Industries Research Association whose grant made this study possible and in particular the interest and help of Dr J C Fletcher.

INDEX

<u>Section number</u>	<u>Page</u>
Abstract	2
Acknowledgements	4
Index	5
 <u>Chapter 1</u>	
Introduction	7
1.1 The waste textile industry	7
1.2 Aims of the present work	9
 <u>Chapter 2</u>	
The pyrolysis of polymers	10
2.1 Pyrolysis - a general view	10
2.2 Structural behaviour during pyrolysis	13
2.3 Pore formation and its relation to structural changes during pyrolysis	17
 <u>Chapter 3</u>	
Review of physical and chemical changes taking place during the pyrolysis of wool and polyethylene terephthalate	20
3.1 Introduction	20
3.2 Wool	23
3.3. Polyethylene terephthalate	34
 <u>Chapter 4</u>	
The physical and chemical changes taking place during the pyrolysis of polyacrylonitrile	40
4.1 Introduction	40
4.2 Developments in the theory of pyrolytic changes in polyacrylonitrile	42
4.3 The role of defect structures and comonomer present within polyacrylonitrile and the effect of additives on polyacrylonitrile pyrolysis behaviour	60
 <u>Chapter 5</u>	
Review of the physical and chemical changes taking place during the pyrolysis of binary polymer mixtures	65
5.1 General survey of the pyrolysis behaviour of binary polymer mixtures	65
5.2 Types of interaction occurring during the pyrolysis of binary polymer mixtures	71
 <u>Chapter 6</u>	
Review of the characterisation of carbon surfaces	78
6.1 Physical adsorption	78
6.2 The implications of the D-R type I equation as a distribution function	88
6.3 Thermodynamic limitations of the theory of volume filling of micropores	95
6.4 Deviations observed in D-R type I plots	100

	<u>Page</u>
<u>Chapter 7</u>	
Experimental methods	116
7.1 Introduction	116
7.2 Textile fibres and their preparation	118
7.3 Large scale pyrolysis	119
7.4 Thermogravimetric analysis and gasification	120
7.5 Gas adsorption	122
7.6 'Mercury density' determination	127
7.7 Differential thermal analysis	129
7.8 Hot-stage microscopy	133
<u>Chapter 8</u>	
Results and discussion of the pyrolysis studies on single polymers	135
8.1 Introduction	135
8.2 Merino Top 64 wool	136
8.3 Terylene	146
8.4 Courtelle	154
<u>Chapter 9</u>	
Results and preliminary discussion of the pyrolysis studies on binary polymer mixtures	161
9.1 Wool/Terylene	161
9.2 Wool/Courtelle	179
9.3 Terylene/Courtelle	193
<u>Chapter 10</u>	
Introduction to adsorption results and discussion	209
10.1 A criterion for comparison of adsorption results	209
10.2 Format and treatment of adsorption results	211
<u>Chapter 11</u>	
Results and preliminary discussion of the adsorption studies on polymer carbons	215
11.1 (a) Wool carbon	215
(b) Terylene carbon	219
(c) Courtelle carbon	223
11.2 Wool/Terylene carbon	227
11.3 Wool/Courtelle carbon	250
11.4 Terylene/Courtelle carbon	276
<u>Chapter 12</u>	
'Mercury density' determination	303
12.1 Results and preliminary discussion	303
<u>Chapter 13</u>	
Final discussion of results and conclusions	315
13.1 Pyrolysis study	315
13.2 Adsorption study	
(a) Single polymer carbons	325
(b) Carbons prepared from binary polymer mixtures	330
13.3 Final conclusions	339
References	341

Introduction

1.1 The Waste Textile Industry

In 1801 a textile machine was invented which in the words of its specification¹ was designed "to recover materials of manufacture from articles that have been made of flax, hemp, silk, wool, cotton and other materials of the like nature, or of mixtures thereof, by reducing or teasing down all the said articles of materials into states capable of being manufactured or otherwise made use of."

The invention of this machine proved the starting point of the shoddy and mungo manufacturing industry which was and is now based almost exclusively in the West Riding of Yorkshire especially in the towns of Dewsbury, Batley and Ossett.

More specifically shoddy consists of ground woollen rags and knitted goods which being comparatively loose in structure yield a long staple fibre. Mungo consists of generally shorter staple because it is obtained from ground worsted rags which are closely woven from smooth tightly spun yarns which require a greater force in grinding².

The production of mungo and shoddy is preceded by a process of separation. The waste rags must be sorted according to fibre type, colour and quality. Any cotton fibres present in the rags are destroyed by an acid carbonisation process.

From the outset mungo and shoddy have been used principally for blending with virgin wool to reduce the price of woollen cloth for the mass market.

Table 1.1(1)³ indicates the extent of mungo and shoddy production in relation to home production and imports of wool.

During mungo and shoddy processing, quantities of fibres known commercially as flock are produced which are too short to be re-spun and are used instead for bedding, upholstery, cushions and pillows.

Increasing production of synthetic fibres has affected the mungo and shoddy industry in two ways.

Synthetic fibres offer alternative properties which are attractive to the consumer. Secondly, increasing use of synthetic fibres in blends with wool has made the process of rag sorting more difficult and has reduced the amount of mungo and shoddy available for re-use in the wool textile industry.

Table 1.1(1)

Comparison of wool consumption in Great Britain (Home produced and Imported Wool) with mungo and shoddy production.

Year	Home Wool Production	Wool Imports	Mungo and shoddy production
1965	83 (million lbs)	382 (million lbs)	63.4 (million lbs)
1966	86	355	61.1
1967	85	356	54.3
1968	80	383	49.7
1969	69	362	46.8
1970	68	314	41.9
1971	68	251	37.2

The mungo and shoddy producers are therefore faced with a contracting market.

However a stable supply of rags still exists although the proportion of pure wool rags has decreased through increased use of synthetic fibre blends.

Mungo and shoddy manufacturers must therefore find an alternative commercial use for wool/synthetic fibre rag mixtures. It is considered that one possible solution is the conversion of these rags into the commercially useful material active carbon.

1.2 Aims of the present work

This project has been totally supported by a Wool Industries Research Association grant and was commenced in 1971.

The aim of the project was to investigate the conversion of binary mixtures of textile fibres, containing wool as one fibre into active carbons. The other fibres selected for the investigation were Terylene and Courtelle.

The production of active carbon from textile fibres takes place through a three stage process.

The first stage involved pelletising the textile fibres to compact them. These pellets are then pyrolysed in an electric furnace under a flowing nitrogen atmosphere. In the final stage the resultant carbonaceous material was activated in a thermobalance to a predetermined percentage mass loss based on the initial mass prior to activation. This percentage mass loss or burn-out characterises the degree of activation.

The isothermal adsorption of gas by the active carbons over a range of relative pressures using carbon dioxide as the adsorbate was selected as a measure of the adsorptive behaviour of the product. Such a measurement served to characterise the surface properties of the carbons.

For the purpose of comparing the surface properties of the individual active carbons, the gas uptake (expressed as milligrams adsorbed per gram of active carbon) at an arbitrarily established relative pressure was taken as representative of the particular carbon.

The initial structure of the textile polymer and its subsequent behaviour during the pyrolysis process, to a significant extent, determine the surface properties of the final carbon and also those of the activated carbon⁴.

Differential Thermal Analysis (D.T.A.) was used to study the behaviour of the textile fibres during pyrolysis. The results of the technique in the form of exothermic and endothermic peaks reflect the thermal changes and hence the physical and chemical changes taking place.

The results from D.T.A. are somewhat ambiguous unless substantiated by complementary techniques.

Thus Thermogravimetric Analysis (T.G.) correlating mass changes with temperature and Hot Stage microscopy to follow visual changes were employed in parallel with D.T.A.

CHAPTER 2

The Pyrolysis of Polymers

2.1 Pyrolysis - a general view

The process of carbonisation has been defined as the gradual progress of a carbon compound towards carbon under the influence of increasing temperature⁵.

In the textile field the term carbonisation has a different meaning. In this context carbonisation describes the removal of organic impurities from natural fibres⁶.

It has therefore been decided that in this study the gradual progress of a carbon compound towards carbon under the influence of increasing temperature will be termed pyrolysis.

Several important industrial products are produced by the pyrolysis of organic raw materials, e.g. active carbons. Possible raw materials range in complexity from the simple linear polymer polyacrylonitrile to highly complex materials such as coal and crude petroleum residues.

The mechanism of the pyrolysis process is in the case of heterogeneous materials extremely complex and consequently not fully understood.

Even in the case of simple linear polymers the relative importance of the chemical and physical processes involved is not yet fully understood.

It is generally agreed^{4,7} that the residual yield and properties of the solid product from pyrolysis are determined by a number of factors including the chemical structure and physical form of the starting material, the heating rate, the final heat treatment temperature, and the pressure and type of gas atmosphere adopted for the pyrolysis process.

For brevity the term carbon will be used in this study to describe the solid product of pyrolysis. However at the final heat treatment temperature adopted in this study (1213K) it is more accurate to describe the solid residue as carbonaceous material.

Chemical analysis of the pyrolysis residues formed at these temperatures indicate that there may still be a significant proportion of elements other than carbon present. Thus the residue formed at 1273K from the pyrolysis of the polyacrylonitrile based

commercial fibre Courtelle was found to have a nitrogen content of 8.2% by mass⁸.

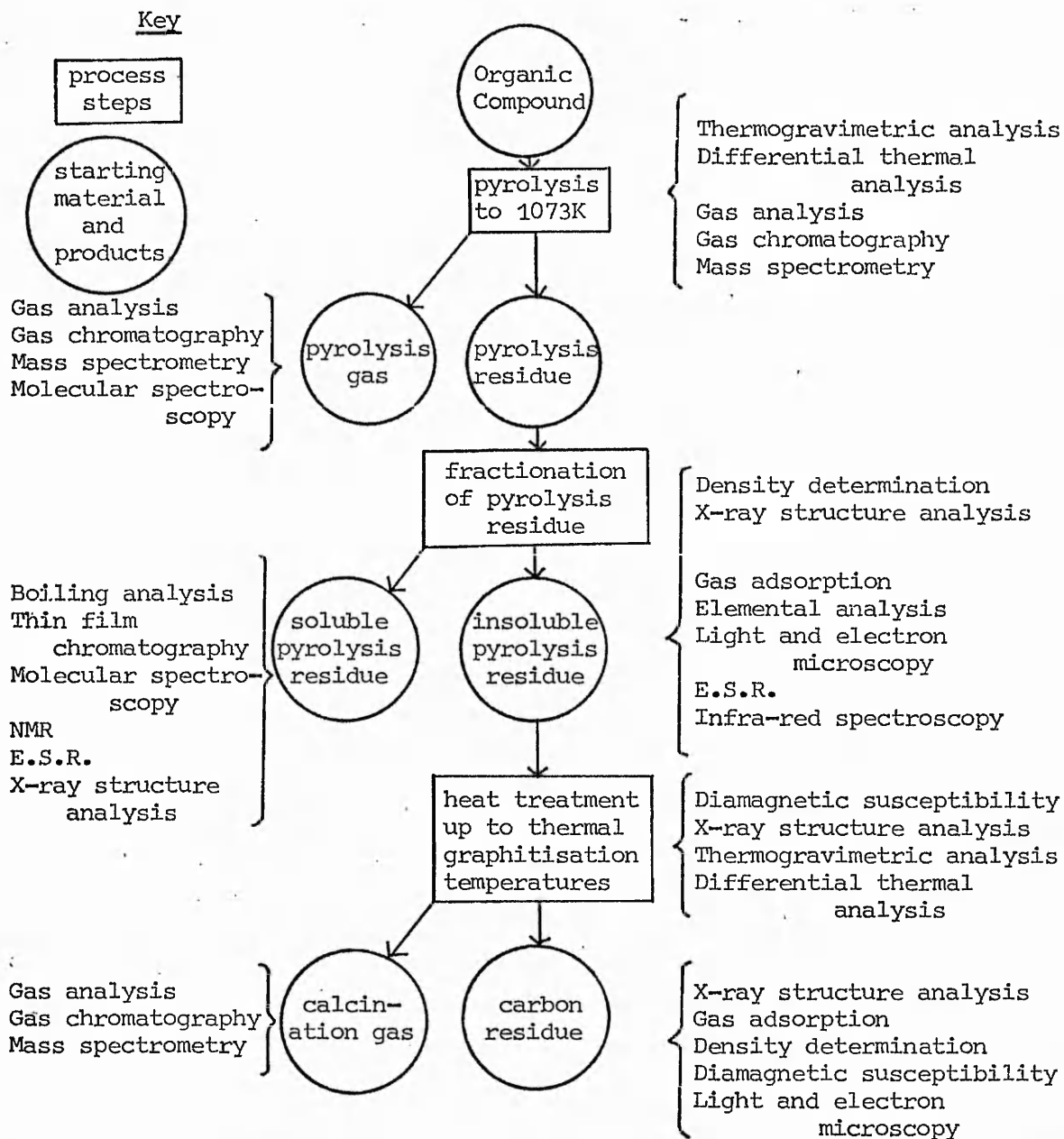
The proportion of non-carbon elements present in pyrolysis residues may generally be reduced by increasing the final heat treatment temperature.

A number of analytical techniques have been employed by previous workers to study the process of pyrolysis. These methods are illustrated schematically in figure 2.1(1)⁷.

Pyrolysis of organic materials generally produces gases, tars and a solid residue. Further heat treatment of the residue may produce gas evolution and concurrent structural changes.

Figure 2.1(1)

Schematic representation the analytical techniques available for the investigation of pyrolysis behaviour.



2.2 Structural behaviour during pyrolysis

The X-ray work of Franklin⁴ on crystallite growth in graphitising and non-graphitising carbons prepared from the pyrolysis of various materials in an inert atmosphere provides considerable information on the structural changes taking place during pyrolysis.

Franklin⁴ used the term crystallite to describe parallel layer groups where no true crystalline structure exists as well as those in which the three dimensional graphitic structure is either partially or wholly developed.

Graphite is an allotrope of carbon which occurs naturally and also may be synthesised. Its structure is well known⁹.

Carbons prepared by pyrolysis of organic materials to final heat treatment temperatures of about 1273K are described by Franklin⁴ as non-graphitic. Further heat treatment of certain of these non-graphitic carbons to temperatures in the range 1973-3273K may lead to the mutual orientation of the layer groups present in non-graphitic carbons resulting in the formation of a graphitic carbon⁴.

It must be stressed that these graphitic carbons only contain a partially developed three dimensional graphite structure.

The carbons which develop a graphitic structure on heating, Franklin⁴ referred to as graphitising carbons.

Franklin⁴ considers that the non-graphitising carbons arise through the formation of a strong system of cross-linking uniting the areas where crystallites exist. This cross-linking is postulated to form during the earliest stages of pyrolysis and leads to a random orientation of the crystallites in a rigid mass.

However in graphitising carbons the cross-linking is postulated⁴ to be less wide spread and weaker allowing growth and orientation of crystallites and the development of a compact and ordered graphitic structure on further heat treatment.

Franklin⁴ also observed that apart from the two main groups of carbons exhibiting graphitising and non-graphitising behaviour there are some carbons which exhibit an intermediate type of character.

Kipling et al^{10,11,12} have investigated the factors influencing graphitisation in a number of polymer carbons (i.e. carbons produced by the pyrolysis of polymeric materials).

It was observed¹⁰ that all the polymers producing graphitizing carbons underwent fusion at some stage during pyrolysis. However fusion was also observed during the pyrolysis of some polymers which give rise to non-graphitising carbons.

A Geisler plastometer was employed to examine the polymers during pyrolysis¹⁰. It was found that polymers giving rise to non-graphitising carbons either did not fuse or existed in the fused state at a single temperature. The existence of a fused state over a range of temperature characterised the behaviour of polymers giving rise to graphitising carbons.

In a later paper Kipling and Shooter¹¹ stated that for the pyrolysis of a polymer to produce a graphitising carbon, fusion must usually take place between 673K and 823K and accompany one of the stages of chemical decomposition of the polymer. In the case of purely aliphatic polymers, infra-red spectroscopy indicated that fusion should occur simultaneously with or follow aromatisation of the solid polymer residues¹¹. Even in the case of partially aromatic and polycyclic polymers the existence of a fused state over a range of temperature appears to be a necessary prerequisite for graphitising behaviour¹¹.

Kipling¹¹ has suggested that the maintenance of a fused state at this stage of decomposition allows sufficient mobility for the polycyclic layer structures to undergo a preliminary orientation.

It would appear that these polycyclic layer structures correspond to the layers constituting crystallites whose growth was described by Franklin⁴. In fact Franklin⁴ found that in carbons prepared at 1273K there exists disordered carbon together with many small crystallites. The relative proportions of disordered carbon to crystallites and the dimensions of the crystallites was found to vary from carbon to carbon.

It was found⁴ that on further heat treatment the crystallites grow laterally until most of the disordered carbon has been consumed. At this point distinct differences in the behaviour shown by graphitising and non-graphitising carbons begin to emerge.

Once the disordered carbon has been consumed the number of layers in the crystallites increases with increasing temperature. In non-graphitising carbons the layer diameter and number of layers per crystallite reach a finite limiting value. However in graphitising carbons the layer diameter and the number of layers per crystallite both increase rapidly with increasing temperature as graphitisation

sets in.

For extensive crystallite growth and hence graphitisation to be possible Franklin⁴ considers that a considerable degree of preliminary orientation is necessary. It is presumably the occurrence of fusion during pyrolysis, suggested by Kipling¹¹ as a necessary but not sufficient prerequisite for graphitisation, which allows this preliminary orientation to take place.

Ramdohr¹³ using polarised light microscopy observed that coke carbons exhibit optical anisotropy.

Kipling et al¹⁰ using the results obtained by Blayden¹⁴ observed that non-graphitising carbons were optically isotropic at all stages of development whereas graphitising carbons showed distinct optical anisotropy. This anisotropy they¹⁰ ascribed to the flow of decomposing material during pyrolysis resulting in a degree of long range order.

The fact that graphitising carbons exist in a fused state at some stage during decomposition facilitates this explanation.

Brooks and Taylor¹⁵ using polarised light microscopy observed the pyrolysis behaviour of organic materials which form a fluid or plastic state. They¹⁵ observed that from the optically isotropic melt an optically anisotropic mesophase formed, initially as very small spheres. These spheres were initially observed at about 673K. The spheres were observed to grow and coalesce until the optically isotropic material had been totally transformed to mesophase.

During this process the viscosity increased and the carbon finally hardened.

In a coke pitch examined by Brooks and Taylor¹⁵ the average relative molar mass was of the order 400-700. The initially formed mesophase had a relative molar mass of the order of 1700.

According to Brooks¹⁵ the mesophase formation and subsequent solidification may take a few degrees or extend over tens of degrees. It is however generally complete by 823K¹⁶.

It was found¹⁵ that using selected area electron diffraction that the mesophase spheres consist of planar molecules in approximately common alignment and parallel orientation but in no general three dimensional order.

This orientation is parallel with a sphere diameter. However since the planar molecules meet the surface normally some bending of the layers must therefore take place.

The growth of these spheres leads to the formation of large regions of extended order and their coalescence to regions where layers are somewhat curved¹⁵.

The fact that these processes occur in the temperature range 673-823K and involve the formation of a fused state and its maintenance over a range of temperature lends further support to the postulate that a zone of fusion is necessary to allow orientation before graphitising behaviour may be observed for a particular carbon¹¹.

2.3 Pore Formation and its relation to structural changes during pyrolysis

Franklin⁴ observed the presence of considerable fine structure porosity in some carbons from low angle X-ray scattering measurements.

The results⁴ from a range of carbons indicated that generally non-graphitising carbons exhibit considerable fine structure porosity. Little fine structure porosity was observed in graphitising carbons.

Franklin⁴ rationalised the occurrence of this fine structure porosity in terms of the differences in pyrolysis behaviour of materials which separately give rise to graphitising and non-graphitising carbons.

In materials producing non-graphitising carbon the initial presence of a strong three dimensional cross-linked framework or its formation in the low temperature stage of pyrolysis prevents fusion from taking place. The rigidity of this structure prevents orientation and therefore limits the growth of crystallites and the formation of a compact structure.

Fine structure porosity presumably develops therefore through the combined effects of material loss due to decomposition and limited crystallite growth within a rigid structural framework.

In contrast the fusion apparently necessary for the formation of a graphitising carbon allows considerable movement of material and therefore orientation to take place thus precluding the permanent establishment of extensive fine structure porosity. Some small pores may be present between crystallites in graphitising carbons, however in view of the orientation already present and the observed crystallite growth in graphitising carbons these ^{small pores} are progressively eliminated by further heat treatment.

Some gross defects are however observed in graphitising carbons as a result of bubble formation in the liquid mass during decomposition.

Loch and Austin¹⁷ using X-ray diffraction and sink-float density measurements found that the fine structure porosity increased with decreasing crystallite size in a range of carbons heat treated to 2843K. They¹⁷ suggested that these fine pores existed as small spaces between crystallites.

From X-ray data and sink-float density determinations Franklin⁴ found that in the carbons examined the fine structure porosity of the

non-graphitising carbons varied between 20% and 50% of the bulk volume of the carbon. It was further concluded from X-ray measurements that the diameter of the fine pores was not more than a few tens of angstroms. Loch and Austin¹⁷ determined a fine structure porosity of 4% of the bulk volume of the carbon in a commercial graphite using similar methods.

Franklin⁴ also noted that generally where fine structure porosity is developed at low temperatures it is substantially preserved after heat treatment to higher temperatures.

Kipling et al¹⁸ have investigated changes in pore structure in a set of graphitising and non-graphitising carbons over the temperature range 973-3273K. Some important conclusions may be drawn from the mercury density and helium density results, however the accuracy of some of the helium density results is open to doubt.

Mercury at atmospheric pressure will not penetrate pores less than about 10^{-5} m (100,000A) in diameter¹⁰ and thus densities measured by mercury displacement represent the density of the carbon and those large pores not penetrated by mercury.

Helium however is considered to penetrate the vast majority of small pores and thus densities measured by helium displacement represent the density of the carbon and those closed pores not accessible to helium.

Rossman and Smith¹⁹ have observed a drift in the observed value of the helium density with time, possibly indicating restricted penetration of helium into the very small pores.

A major assumption²⁰ in the use of helium for density determination is that negligible physical adsorption of helium occurs at the temperature of the density determination. Maggs²¹ has however observed physical adsorption of helium at room temperature in carbons with considerable fine structure porosity resulting in anomalously high density values.

In an attempt to obviate this problem Kipling et al²⁰ repeated some of their helium density determinations at 573K. At this temperature Kipling²⁰ considered that there was very little physical adsorption of the helium gas. However further anomalous results were obtained, possibly reflecting activated diffusion effects or pore opening effects at the higher temperatures.

Kipling¹⁸ found that both the helium and 'mercury densities' rise with increasing heat treatment temperature for graphitising carbons.

Adopting 2.26 g cm^{-3} and 2.10 g cm^{-3} as the 'true' densities of graphitic and non-graphitic carbons respectively, Kipling¹⁸ observed the general result that graphitising carbons contain no appreciable closed pore volume and only a small degree of open pore volume. This open pore volume is little affected by increasing heat treatment temperature and may be related to gross defects formed by gas evolution from the liquid state during pyrolysis.

The general increase in densities observed for graphitising carbons¹⁸ indicates an overall contraction of the mass of carbon as the result of continued growth of crystallites and elimination of defects.

The 'mercury densities' of non-graphitising carbons¹⁸ were observed to remain approximately constant with increasing heat treatment temperature indicating that the total pore volume was unchanged.

In view of the anomalous behaviour observed and discussed previously, the interpretation of the helium density data for non-graphitising carbons is somewhat restricted although there are indications that with increasing heat treatment temperature the open pore volume is reduced, probably with some conversion to closed pores. Kipling¹⁸ thus observed a fairly clear difference in the properties of graphitising and non-graphitising carbons on further heat treatment, in substantial agreement with the results of Franklin⁴.

CHAPTER 3

Review of Physical and Chemical Changes Taking Place during the Pyrolysis of Wool and Polyethylene Terephthalate

3.1 Introduction

The physical and chemical changes which take place during the pyrolysis of textile polymers have been examined by a variety of analytical techniques⁷. Generally the main chemical changes significant in the formation of carbon are complete by 773-873K.

From an examination of the results obtained using Differential Thermal Analysis (D.T.A.) and Thermogravimetry (T.G.) it is usually possible to distinguish between chemical and physical changes.

Mackenzie²² has published a comprehensive review of all aspects of D.T.A.

The technique of D.T.A. is based on the principle that chemical or physical changes taking place in a material as a result of increase in temperature are accompanied by the absorption of heat from or the evolution of heat to the surroundings.

The material under test and a thermally inert reference material with similar thermal characteristics are subjected to identical thermal environments. At temperatures at which a chemical or physical change takes place in the sample material there will be a detectable difference in temperature between the sample material and the thermally inert reference.

If the sample and reference materials have similar thermal characteristics and no chemical or physical changes take place in the sample then no temperature difference can be detected and the D.T.A. curve should take the form of a horizontal line.

In practice the thermal characteristics of sample and reference materials are not exactly matched and at low temperatures an initial displacement is observed. Prior to this initial displacement the position of the differential temperature pen defines what is termed the zero differential.

The linear portion of the curve (AB Figure 3.1(1)) following the initial displacement establishes what is termed the base-line.

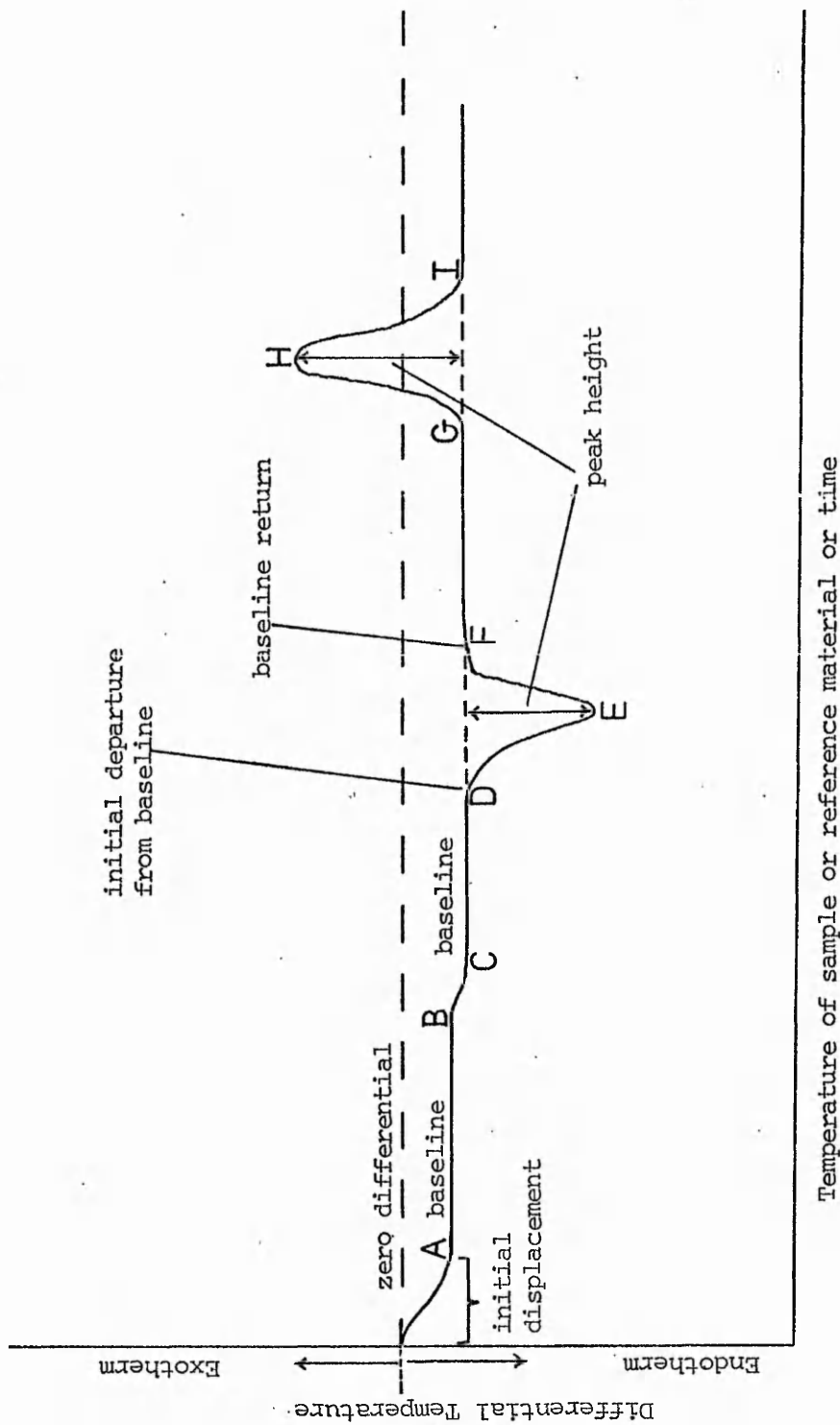


Figure 3.1(1)
Schematic representation of a D.T.A. curve illustrating some of the terminology employed.

The occurrence of a second order transition within the sample material (e.g. a glass transition) may result in a displacement of the base-line as indicated by BC in figure 3.1(1). Following this second order transition a base-line is established as the portion of the curve CD (figure 3.1(1)) parallel with initial section of base-line AB.

If an endothermic change (e.g. fusion) takes place in the sample then a peak is observed below the new base-line in the endothermic direction (e.g. peak DEF figure 3.1(1)). Alternatively if an exothermic change occurs within the sample (e.g. a degradation reaction) a peak is observed above the base-line in the exothermic direction (peak GHI figure 3.1(1)).

As indicated in figure 3.1(1) each peak observed has its own peak height relative to the base-line.

In practice the sample and reference materials are sited symmetrically within a furnace and are subjected to a constant rate of temperature increase.

With most commercial apparatus both vacuum and controlled gas atmospheres are available.²²

The results from D.T.A. are dependent upon both the specific design of the particular apparatus employed and the particular experimental techniques employed.²² It is usual where first order transitions are involved to quote D.T.A. results in terms of peak temperatures. The significance of the peak temperature depends not only upon the instrument design but also upon the actual type of change involved (e.g. fusion, decomposition).

As indicated in figure 3.1(1) the difference in temperature between the sample and reference material (ΔT) is plotted against either the sample temperature or the reference material temperature.

Thermogravimetry is often used as a complementary technique to D.T.A. The sample under test is again heated at a constant rate of temperature rise and any resulting changes in mass are plotted against either sample or furnace temperature.

A comparison of the results from D.T.A. and T.G. usually facilitates the identification of physical and chemical changes if it is assumed that identical samples have been subjected to similar thermal treatments in the two respective techniques.

D.T.A. has been employed to study the effects of chemical modification of some textile fibres including wool.

In attempts to relate D.T.A. peaks with particular chemical changes several workers have used treatments designed to modify specific chemical features of the wool structure. Some of these chemical treatments will be discussed in the following sections.

However the specificity of some of these treatments must be in doubt and hence in some cases any inferences drawn from such experiments must be viewed with caution. In addition D.T.A. results, even when combined with those from T.G. are not completely unambiguous. Hence visual observation of sample behaviour using Hot-Stage Microscopy (H.S.M.) and changes in measured mechanical properties of fibres are often sought in addition to data obtained from D.T.A. and T.G.

Thermoanalytical techniques and in particular D.T.A. have been widely adopted to facilitate the problem of textile fibre identification.^{23,24}

More detailed information concerning the chemical changes taking place during pyrolysis may be derived from the detection and analysis of evolved gases and volatiles. Limited information is also available from chemical analyses of the solid residues formed at various stages during pyrolysis.

However Franklin⁴ found that a quantitative X-ray analysis of carbonaceous residues formed below 1273K was not generally possible in view of the presence of oxygen or other impurity.

The chemical and physical changes taking place during the pyrolysis of textile fibres will be reviewed in the four following sections in the light of current experimental techniques employed and with particular reference to the fibres utilised in this project.

3.2 Wool

Before reviewing the chemical and physical changes occurring during the pyrolysis of wool it is necessary to consider the chemical and physical structures of wool.

Wool is a protein and as such consists of long chains of amino acids joined together through amide links.

Approximately nineteen amino acids have been isolated from wool in various sequences along the protein chains. The amino acid composition has been found to vary with both wool type and quality. It is believed that the amino acid composition may vary along the length of individual wool fibres.²⁵

A further complication with a natural fibre such as wool is that its morphology is complex compared with that of a synthetic fibre (see figure 3.2(1)).

Essentially wool consists of an outer skin or cuticle and an inner cortex. The cortex is responsible for the principal physical properties of wool. Woods²⁶ has shown that the cortical cell is the elastic unit of the fibre.

The cortex also constitutes the major part of the fibre mass²⁷ (86.5% of mass in fine wools).

Two types of cortical cell have been observed through their differing accessibility to dyes.²⁸ The two cell types occur in different regions of the cortex, the orthocortex and paracortex (see figure 3.2(1)).

Observations made using light microscopy indicate that both types of cortical cells contain bundles of what are termed macrofibrils (see figure 3.2(1)).

There are two major differences between the orthocortex and paracortex. First the individual macrofibrils within the orthocortex are surrounded by non-keratinous material of low cystine content.²⁹ Non-keratinous material in the paracortex is mainly located in a few large areas however.

As illustrated in figure 3.2(1) each macrofibril is made up of bundles of microfibrils and it is at this level that the second major difference exists. The microfibrils in each macrofibril are embedded in an amorphous matrix material which is believed to be heavily cross-linked with disulphide bonds.³⁰

Leach³¹ estimates that the volumes occupied by the microfibrils in each macrofibril in the paracortex and orthocortex are ~50% and ~80% respectively. Hence there is a high proportion (in terms of volume occupied) of matrix material relative to microfibrils in the paracortex.

The substructure of the individual microfibrils is open to discussion. Some form of structural order is believed to exist

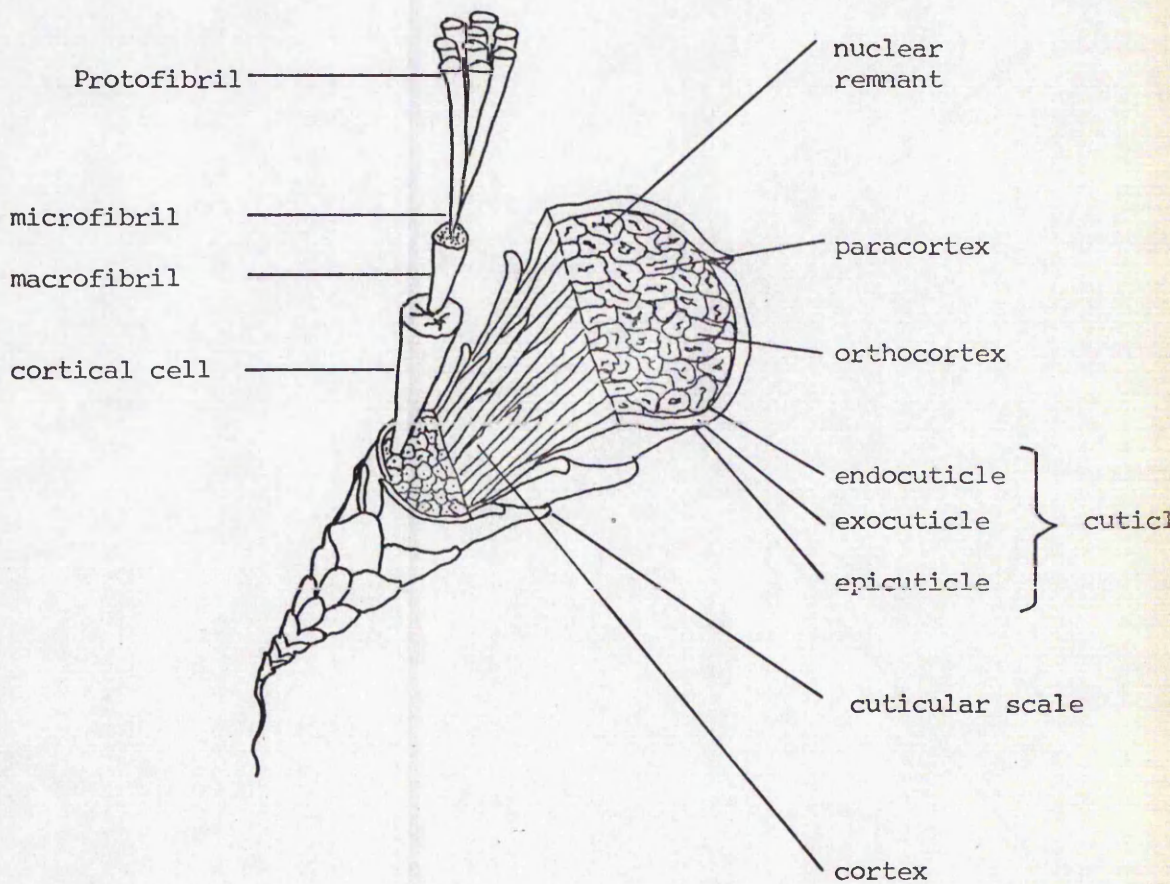


Figure 3.2(1)
Morphology of the wool fibre

within the microfibrils, the sub-units being termed protofibrils.

An α -helical configuration for the individual protein chains has been suggested³², although how this configuration is arranged within the individual protofibrils is again open to further discussion.

Separation of these morphological components without modification appears difficult but variations in chemical behaviour of these structural components may be indicative of variations in amino acid composition.

Approximately 50% of the weight of wool is accounted for by side-chain structures.³³

As previously discussed it is believed that in the protofibrils the protein chains exist in a helical configuration known as α -keratin, as postulated by Pauling et al.³²

In this configuration an optimum number of intra-chain hydrogen bonds is achieved between amide links.

When a tensile stress is applied to wool fibre the helical coils unwind and intra-chain hydrogen bonds are replaced by interchain hydrogen bonds between parallel protein chains to give the β -keratin structure.³⁴

In the helical α -keratin structure the hydrogen bonds are parallel to the fibre axis. In β -keratin the hydrogen bonding is perpendicular to the fibre axis.

Estimates of the extent of highly ordered regions corresponding to α -keratin vary between 10% and 50% of the fibre mass.²⁵ The major proportion of this ordered material is contained within the microfibrils. A considerable proportion of the remaining amorphous material is presumably matrix material.

Chemical and mechanical studies have shown that another important factor in determining fibre properties are the attractive interactions of side chains which are found mainly in the amorphous regions of the fibre.

These attractions are considered to arise from salt links formed from amino groups and carboxylic acid groups on adjacent chains and hydrogen bonds between oppositely charged or polarisable groups in adjacent chains.

Amino groups and carboxylic acid groups present in side chains may arise through the incorporation in the polymer chain of amino

acids containing three functional groups (e.g. diamino carboxylic acids and amino dicarboxylic acids).

The amino acid cystine may be incorporated into a single protein chain or two adjacent chains. The result of the incorporation of cystine into two adjacent chains is known as a disulphide link. This disulphide linkage is also generally observed in the amorphous regions of the fibre.

Before discussing the various experimental results concerning the pyrolysis of wool fibres it is important to consider that these results are derived from a variety of keratin fibre types and under a variety of experimental conditions. Caution must therefore be exercised when comparing the results from different workers.

Crighton and Happey³⁵ attempted to relate structural features to thermal changes, characterised by D.T.A. occurring in a range of wool and related protein fibres. The D.T.A. curves for various types of wool fibre were found to be essentially similar.

In all thermoanalytical work the temperatures quoted by Crighton and Happey³⁵ refer to the temperature of the sample material. They³⁵ adopted a heating rate of 20 degrees min⁻¹ for D.T.A. work and used separately, flowing nitrogen and air atmospheres to isolate oxidative reactions. D.T.A. results utilising continuous evacuation were also reported.

In both nitrogen and air atmospheres they³⁵ observed a broad endotherm in the temperature range 363-473K. Felix et al³⁶ have associated this peak with bound water. Under continuous evacuation two endothermic peaks were resolved in this temperature range. One large peak occurring in the temperature range 313-393K and a much smaller peak at 413-428K.

Crighton and Happey³⁵ suggest that the major peak represents the loss of loosely bound water and the smaller peak the loss of water more strongly bound at hydrophilic sites. The existence of this strongly bound water was first suggested by Watt.³⁷

Horio et al³⁸ have observed that the thermal behaviour of wool is sensitive to the presence of moisture. Thus air dried wool heated in a sealed tube was observed to melt at 473K. This compares with the melting point of 523-533K observed for wool heated in a flowing nitrogen atmosphere by Felix et al³⁶. Horio et al³⁸ believe that the residual moisture content of the air dried wool in the sealed tube is

responsible for the decreased thermal stability.

Crighton and Happey³⁵ therefore isothermed wool samples at 421K for 3 hours to remove all traces of water. On cooling to room temperature and reheating they detected a movement in the D.T.A. curve base-line at 438K of the type illustrated in figure 3.1(1) by the portion BC. On further heating to 523K followed by unprogrammed cooling a more clearly defined base-line deflection was observed at 433K. This behaviour Crighton and Happey³⁵ associated with a glass transition in the amorphous regions of the fibre.

Crighton³⁵ using Merino 70 wool samples heated under continuous evacuation after a 3 hour isotherm period at 421K observed further endotherms occurring in the temperature ranges 493-503K and 503-523K although the relative sizes and exact positions of these peaks were found to vary with wool type. (The endotherm at 493-503K being a shoulder to the endotherm at 503-523K for Merino 70 wool).

The occurrence of this pair of endotherms in the approximate temperature range 473-523K is well established.^{36,39,40}

The D.T.A. curve of silk run in a nitrogen atmosphere exhibits no major endotherms in the temperature range 473-523K.³⁹ However a large endotherm in the D.T.A. curve of silk has been observed by Schwenker and Dusenbury³⁹, with a peak temperature of 599K.

It has been postulated³⁹ that this difference in thermal behaviour between silk and wool is related to differences in structure at the molecular level. Silk is generally considered to consist of protein chains in essentially a β -keratin configuration. Wool fibres however are believed to consist mainly of α -keratin although small amounts of β -keratin may be present.

Thus the endotherms occurring in the temperature range 473-523K in the D.T.A. curve of wool are considered to be associated with disordering or melting of α -keratin. The endotherm in the D.T.A. curve of silk at 599K is thought to represent the disordering or melting of β -keratin.³⁹

The occurrence of small endotherms in the temperature range 589-597K in the D.T.A. curves of wool fibres run in nitrogen may, it is considered, indicate disordering within the small β -keratin component.³⁹

T.G. data indicates that in the temperature range 473-523K, a mass loss of 10% is recorded for the keratin fibre vicuna.³⁹ Mass losses of this order indicate that endotherms observed in this temperature range for keratin fibres do not reflect extensive structural degradation.

An alternative explanation put forward initially by Schwenker and Dusenbury³⁹ for the two endotherms observed in the D.T.A. curve of wool in the temperature range 473-523K, is related to the relative orthocortex and paracortex content of the fibre. Correlations exist between the relative orthocortex and paracortex content of human hair, wool, and mohair and the relative sizes of the two endotherms in this temperature range.

Moreover Horio et al³⁸ later published birefringence data suggesting that the paracortex exhibits a lower thermal stability than the orthocortex.

It is possible, if this latter suggestion is correct that this difference in thermal stability may be related to the relatively higher proportion of matrix material in the paracortex.

Felix et al³⁶ applied various chemical treatments to wool fibres. These treatments are believed to break disulphide cross-links. They³⁶ observed that the endotherms originally in the temperature range 473-523K occurred at lower peak temperatures after the chemical treatment.

Similar behaviour after the chemical pre-treatment of wool has been observed by Haly and Snaith⁴¹ and Crighton and Findon.⁴⁰ Chemical reconstruction of the cross-links was found to restore the thermal stability.

C.Z. Carroll-Porczynski⁴² using a step-wise temperature programme investigated the thermal behaviour of wool in a helium atmosphere.

The results from simultaneous D.T.A./Mass Spectrometry indicate⁴² the release of sulphur compounds including carbon disulphide, carbon oxysulphide and sulphur dioxide in the temperature range 501-550K. Measured temperatures refer to the D.T.A. sample temperature.

These sulphur containing compounds are thus released in the temperature range of the two endotherms previously discussed as occurring at 473-523K in the D.T.A. curve. The nature of these products points to their formation through cleavage of disulphide links. These data correlate with those derived from the application of chemical pre-treatments and point to the importance of disulphide links in

maintaining the thermal stability of wool.

Haly and Snaith⁴¹ using D.T.A. and X-ray diffraction examined the thermal behaviour of wool under continuous evacuation and also sealed with varying amounts of water. The D.T.A. temperatures quoted by Haly and Snaith⁴¹ refer to the temperature of the reference material.

They⁴¹ observed that the endothermic peaks detected in the temperature range 473-523K under continuous evacuation moved to lower temperatures when water was present. This observation correlated with the birefringence data of Horio et al.³⁸

Haly and Snaith⁴¹ also found that the actual temperature at which these endothermic peaks occurred depended upon fibre type, heating rate and level of disulphide bond reduction.

They⁴¹ found fairly clear evidence from X-ray diffraction results that the endotherms in the temperature range 473-523K are associated with phase transitions. Haly and Snaith⁴¹ suggest that this pair of endotherms may represent melting of α -keratin with some formation of β -keratin followed by melting of this β -keratin.

Bendit⁴³ has previously reported the melting of α -keratin in vacuo at 473-498K.

An alternative explanation offered by Haly and Snaith⁴¹ concerns the relative stabilities of the orthocortex and paracortex and resembles that previously suggested by Schwenker and Dusenbury.³⁹

Menefee and Yee⁴⁴ investigated the changes in mechanical properties of wool fibres heated under vacuum. Their results⁴⁴ indicated a possible glass transition at about 433K. These may be correlated with base-line displacement in the D.T.A. curve of wool detected by Crighton and Happey³⁵ at 433K during cooling.

A slow formation of amide cross-links at 433K was postulated by Menefee and Yee⁴⁴. At 488K melting of a small part of the ordered wool was detected with rapid amide cross-link formation in this newly formed amorphous material.

Dry wool heated to between 413K and 443K shows a decrease in both acid and base groups together with a decreased solubility in sodium bisulphite.⁴⁵ From this data Mecham⁴⁵ postulated the formation of amide cross-links in this temperature range.

Melting of the major part of the wool was detected at 508K by

Menefee and Yee⁴⁴ with disulphide bond cleavage occurring in the temperature range 503-523K.

Menefee and Yee⁴⁴ suggested that amide cross-link formation may stabilise the structure to about 523K, above this temperature large scale degradation takes place.

C.Z. Carroll-Porczynski⁴² detected products indicative of general degradation above 550K from a wool sample heated in a helium atmosphere.

Felix et al³⁶ using wool heated in a nitrogen atmosphere observed fusion at 523-533K. Haly and Snaith⁴¹ using wool samples heated under continuous evacuation observed gradual discolouration and at 533K the formation of a fused black mass.

Crighton and Happey³⁵ observed two further endothermic peaks occurring in the D.T.A. curve of Merino 70 wool heated under continuous evacuation, in the temperature ranges 533-543K and 553-563K. These peaks they associated with thermal degradation.

In another D.T.A. curve of Merino 70 wool heated under continuous evacuation Crighton and Happey³⁵ illustrated a further endothermic peak at 598K. They added however that this peak was variable in height. As it occurred in the temperature region of thermal degradative reactions, height variations may be attributed to a lack of base-line stability.

Crighton and Findon⁴⁰ using Merino Top 64 wool samples run under continuous evacuation observed endothermic peaks at 507K (shoulder), 516K, 566K and 599K in the D.T.A. curve. All quoted temperatures for both D.T.A. and T.G. refer to the temperature of the sample. Their T.G. data⁴⁰ for a Merino Top 64 wool sample run under similar conditions indicated that mass loss commenced above 484K. An approximate 10% mass loss was recorded between 484K and 543K. The most significant mass losses (30%) were observed in the temperature range 543-603K.

Tarim and Cates⁴⁶ reported D.T.A. and T.G. data for wool heated in a static air atmosphere at $10^{\circ} \text{ min}^{-1}$ and $5^{\circ} \text{ min}^{-1}$. Quoted peak temperatures refer to the temperature of the reference material. Tarim and Cates' results⁴⁶ are somewhat difficult to interpret because of extensive base-line drift.

Crighton and Happey³⁵ reported D.T.A. curves for wool samples run in air and these exhibited a fairly stable base-line. Moreover

only endothermic peaks were recorded up to approximately 573K, above this temperature the curve falls away in the exothermic direction and becomes somewhat unstable.

Tarim and Cates⁴⁶ reported D.T.A. curves for wool which although exhibiting similar peak temperatures to those reported by Crighton and Happey³⁵, were attributed⁴⁶ to exothermic transitions. This assignment may be unsound in view of the extensive base-line drift.

The T.G. data of Tarim and Cates⁴⁶ indicated that after initial loss of water (12%) the wool began to degrade at 513K at a rate which slowed in the region of 613K. At 773K a mass loss of 63% was reported.

More complete T.G. data for wool heated in a nitrogen atmosphere have been published by Schwenker et al.⁴⁷

Initial water loss (9%) was complete at 433-443K. An initial decomposition process was observed in the temperature range 493-578K accompanied by a further mass loss of 19%. A second decomposition stage was observed from 578K to 673K (30% mass loss) followed by more gradual mass loss as the temperature was further increased.⁴⁷

Above about 603K little D.T.A. data have been reported for wool. The large changes in sample mass, thermal conductivity and thermal contact between sample and thermocouple in most types of D.T.A. apparatus render unreliable the curve obtained. However it may be observed that the D.T.A. curve for wool samples heated under nitrogen atmospheres break away in the exothermic direction.

In a very recent study¹³¹ the pyrolysis of wool in a nitrogen atmosphere has been investigated at temperatures in the range 373-1273K.

The actual pyrolysis temperatures employed ranged from 373K to 1273K in increments of 100 degrees. In this investigation of the pyrolysis behaviour of wool at a particular temperature, the wool sample was introduced into the furnace which was held at that temperature i.e. no programmed heating cycle was employed.

A qualitative determination of the majority of degradation products was achieved through the use of a gas chromatograph coupled to a mass spectrometer.

The degradation products below 673K were found to include carbon dioxide, hydrogen cyanide, ammonia, organic nitriles, saturated and unsaturated hydrocarbons, hydrogen sulphide and phenols. However no amines, amides or carboxylic acids were detected.

Between 673K and 973K the products detected included carbon dioxide, carbon monoxide, hydrogen cyanide, ammonia, saturated and unsaturated hydrocarbons, organic nitriles and hydrogen sulphide.

The hydrocarbons, organic nitriles and particularly hydrogen sulphide were formed in substantially smaller amounts than those detected below 673K. Further no amines, amides or carboxylic acids were detected.

In the temperature range 973-1273K the following products were detected, carbon dioxide, carbon monoxide, hydrogen cyanide, ammonia, benzonitrile, unsaturated hydrocarbons and organic sulphur compounds. Again no amines, amides or carboxylic acids were detected.

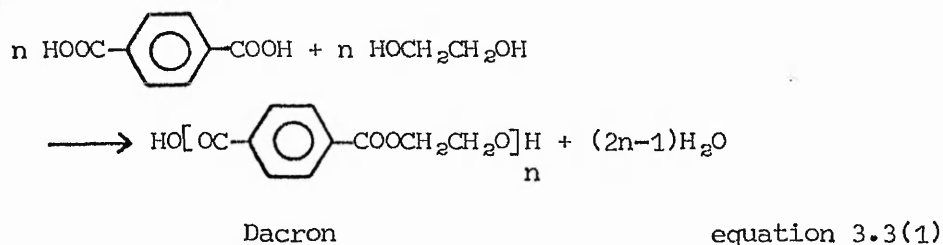
This product analysis was achieved by trapping the pyrolysis products at 77K and then flash vapourising them into the gas chromatograph. In such an analysis system it is possible that pyrolysis products formed initially as primary products may further react whilst in the pyrolysis tube. Thus the final product analysis may not necessarily reflect the whole range of primary pyrolysis products.

Indeed it was postulated¹³¹ that the formation of unsaturated conjugated hydrocarbon products may be the result of the combination of hydrocarbon fragments to form more stable compounds.

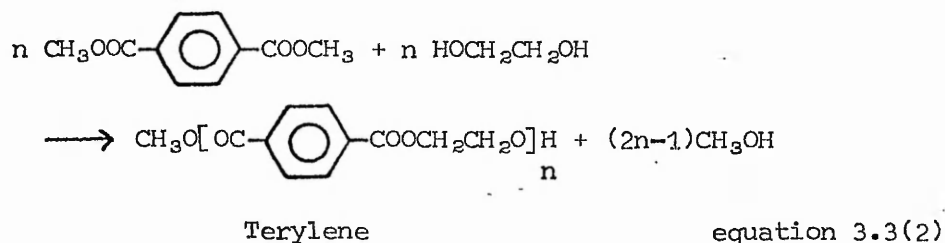
3.3 Polyethylene terephthalate

A number of polyester fibres are manufactured commercially under various trade names.

Polyester fibre is formed by reacting a bifunctional carboxylic acid (terephthalic acid) with a bifunctional alcohol (ethylene glycol). Dacron (Du Pont de Nemours and Co. USA) is manufactured in this way⁴⁸ and the essential reaction may be represented by equation 3.3(1).



Terylene is the commercial polyester fibre manufactured by (ICI Fibres Ltd), and is prepared by polymerising the dimethyl ester of terephthalic acid with ethylene glycol.⁴⁸ The reaction may be represented by equation 3.3(2).



Thus Terylene and Dacron are essentially similar in structure except that one end group may be an ester group in Terylene or a carboxyl group in Dacron⁴⁸.

Polyester produced by the polymerisation of an equimolar mixture of terephthalic acid (or an ester of terephthalic acid) and ethylene glycol may be termed polyethylene terephthalate (PET).

Gillham and Schwenker⁴⁹ using Torsional Braid Analysis (TBA), D.T.A. and T.G. techniques have examined the changes taking place in PET heated at a constant rate of increase of temperature, run in a nitrogen atmosphere, in the temperature range ambient - 773K. Peak temperatures quoted for D.T.A. data refer to the temperature of the reference material.

The PET examined⁴⁹ was in the form of a film obtained from

solution of Dacron fibre in hexafluoroacetone ^Sequihydrate. An initial heat treatment to 423K was employed to effect solvent volatilisation.

The D.T.A. curve reported by Gillham and Schwenker⁴⁹ for PET indicated an endothermic base-line displacement in the temperature range 338-361K corresponding to the occurrence of a previously reported glass transition.⁵⁰

Gillham and Schwenker⁴⁹ postulated that an exothermic change beginning at approximately 443K represented a secondary crystallisation process.

Fusion of the Dacron was detected as a sharp endotherm in the D.T.A. curve beginning at 501K with a peak temperature of 522K.

The T.G. data⁴⁹ indicated no significant mass losses in this temperature range. Following the fusion endotherm Gillham and Schwenker⁴⁹ reported the occurrence of an exotherm (peak temperature 653K) and an endotherm (peak temperature 701K) in the D.T.A. curve of Dacron.

Following the endotherm (peak temperature 701K) the D.T.A. curve moved in the exothermic direction and an exothermic peak was recorded at 748K.

Schwenker and Beck⁵¹ have published a D.T.A. curve for drawn Dacron fibre run in a nitrogen atmosphere. Following the initial fusion endotherm (peak temperature 534K) an exotherm (peak temperature 662K) and then an endotherm (peak temperature 720K) were recorded. These peaks correspond to those observed by Gillham and Schwenker⁴⁹ in this temperature range.

Both Schwenker⁵¹ and Pande⁵² considered the endothermic peak recorded by Schwenker⁵¹ at 720K (Gillham and Schwenker⁴⁹ 701K) to represent depolymerisation of PET.

The T.G. data of Gillham and Schwenker⁴⁹ support this conclusion for a considerable mass loss was recorded in the temperature range 663-773K (80% mass loss). The major proportion of this mass loss occurring in the region of the endothermic peak at 701K.

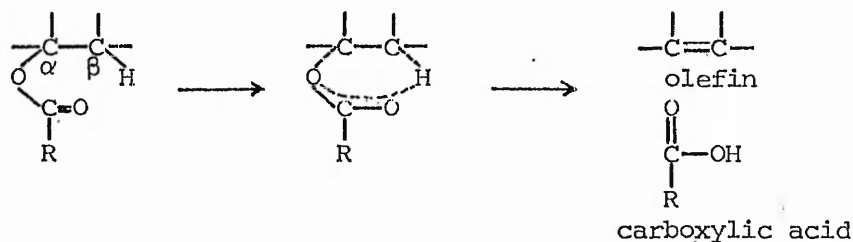
Mechanical measurements by Gillham and Schwenker⁴⁹ are consistent with the formation of a strongly cross-linked network in the residue formed at 773K.

Studies of the mechanism of thermal degradation of PET have been reviewed by Buxbaum⁵³. These studies rely to some extent on the

results from model compounds and Buxbaum⁵³ points out that caution is necessary in correlating the results from model compounds with the reactions of PET itself.

It seems however that in the case of PET the pyrolysis behaviour of model compounds does not differ to any great extent from those occurring in the polymer itself especially in the temperature range 473-573K.

Generally, carboxylic esters containing at least one β -hydrogen are believed⁵⁴ to decompose pyrolytically to give olefins and carboxylic acids through a cyclic transition state (see equation 3.3(3)).



equation 3.3(3)

In view of the similarity of products obtained from the pyrolysis of PET and model compounds Buxbaum⁵³ considered that the mechanism for PET degradation during pyrolysis is probably similar to that for simple ester pyrolysis.

In fact Pohl⁵⁵ has proposed that the principal point of weakness in the PET chain is the β -methylene group. Buxbaum⁵³ has summarised the main reactions involved in the pyrolytic degradation of PET (see figure 3.3(1))

As is illustrated in figure 3.3(1) the initial degradation products consist of olefins and carboxylic acids. An equilibrium between these products once formed and an anhydride and acetaldehyde illustrates a possible reaction of the immediate products of PET pyrolysis.

Additional degradation reactions are postulated to occur during pyrolysis if 2-hydroxyethyl end groups are present in the PET chain (see figures 3.3(2) and 3.3(3)). Thus the 2-hydroxyethyl end group may itself break down to give a carboxylic acid and an active species. This active species may give rise to acetaldehyde or react with a 2-hydroxyethyl end group if available (see figure 3.3(2)).

Illustrated in figure 3.3(3) are possible reactions between 2-hydroxyethyl end groups and products of PET pyrolysis.

Figure 3.3(1)

Main reactions in the pyrolytic degradation of PET

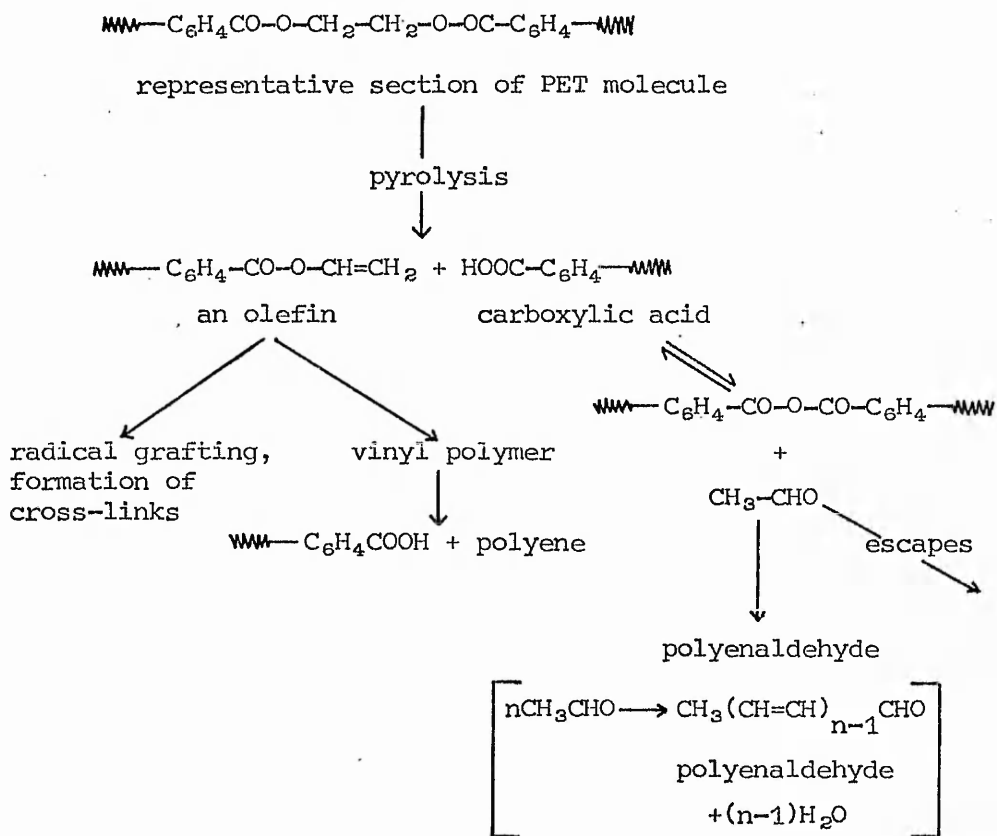
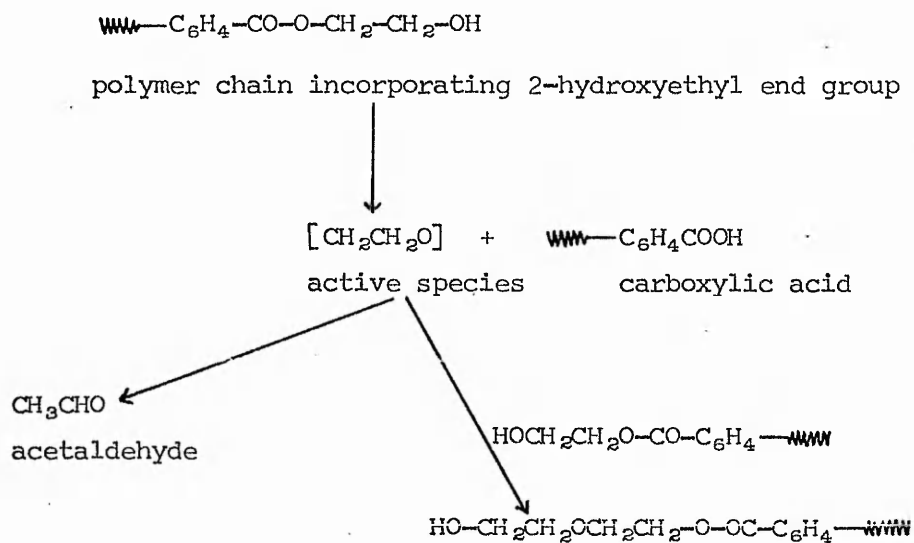


Figure 3.3(2)

Pyrolytic breakdown of the 2-hydroxyethyl end group.



CHAPTER 4

The physical and chemical changes taking place during the pyrolysis of polyacrylonitrile

4.1 Introduction

Considerable interest exists in the physical and chemical changes taking place in polyacrylonitrile (PAN) fibres during pyrolysis. Under certain pyrolysis conditions⁵⁶ PAN fibre yields a carbon fibre of considerable tensile strength and elastic modulus. Commercial and technical applications are believed possible for composite materials containing carbon fibres in view of their apparent high strength and low mass properties.

The main aim of previous workers in the carbon fibre field has been to relate the structure and hence properties of the final carbon fibre product to the structure of the precursor textile fibre through an understanding of the chemical changes taking place during pyrolysis. A large volume of information has therefore already been reported in this field.

In so far as the work reported in this thesis is related to carbon fibre research several important points must be made. The PAN fibre utilised in this research (Courtelle, Courtaulds Ltd) was in the form of cut fibres 5×10^{-4} m in length. The fibre was pyrolysed by heating from ambient to 1213K at a constant rate of temperature increase in a flowing nitrogen atmosphere. Carbon fibre research however has tended to concentrate on the pyrolysis of pre-oxidised, tensioned fibres in an inert atmosphere.

Analytical studies of gaseous and volatile products and solid residues have been utilised by various workers in attempts to determine the mechanism of pyrolysis reactions. These analyses are generally made at a series of temperatures rather than a continuous analysis from pyrolysis at a constant rate of temperature increase.

As the mode of temperature increase during pyrolysis may affect the pyrolytic reactions taking place some limitation therefore exists in the direct use of such analytical data.

It is also relevant to consider the variety of materials employed in carbon fibre studies. Whilst most are PAN based materials, usually taking the form of commercial fibres, laboratory produced PAN has also been employed.

The commercial PAN fibres differ not only in the number and type of comonomers present but also in the commercial finishes applied to the fibre.

PAN produced in the laboratory may be in powder, film or fibre form. As with commercial PAN fibres the laboratory produced PAN may be made by one of several types of polymerisation process. The PAN may be polymerised in a range of molecular weights, using different initiators and containing different comonomers.

The pyrolytic conditions employed in carbon fibre research also vary from flowing inert gas atmospheres to in some cases conditions of continuous evacuation. Of all the carbon fibre research data presently available, the research programme sponsored by Rolls Royce Ltd (Derby) is considered particularly relevant to the work contained in this thesis.

In the first part of their programme Turner and Johnson^{8,57} utilised Courttelle pyrolysed under an inert atmosphere at a constant rate of temperature increase. Thus both the type of fibre adopted and the particular pyrolytic conditions are directly comparable with those employed in this study. Their aim was to examine the nature and sequence of the chemical and physical changes taking place in Courttelle during pyrolysis.

In the second part of the Rolls Royce research programme Grassie and McGuchan⁵⁸⁻⁶⁶ examined the broader aspects of PAN pyrolysis behaviour through a systematic variation of both pyrolysis parameters and type of PAN based material.

4.2 Developments in the Theory of Pyrolytic Changes in Polyacrylonitrile

Houtz⁶⁷ first observed the progressive darkening of the commercial PAN fibre Orlon (Du Pont de Nemours and Co. USA) on heating in air.

Houtz⁶⁷ heated fibres for 60 hours at 473K and produced a black yarn which appeared stable to further heating in a bunsen flame. The black yarn still had considerable strength and flexibility although it was somewhat brittle.

In order to explain the darkening of the fibres and the maintenance of fibre properties by the black yarn, Houtz⁶⁷ postulated that the product must be still essentially linear polymer in form. He⁶⁷ proposed the formation of condensed aromatic ring systems along the original polymer chains [see figure 4.2(1)].

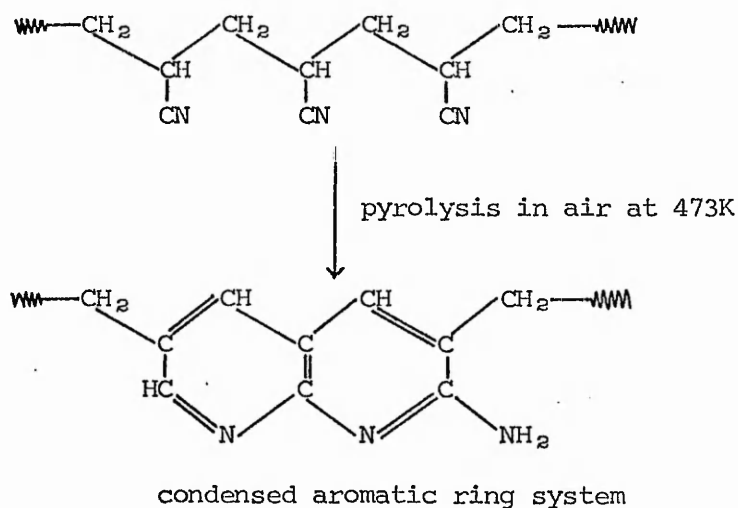


Figure 4.2(1)

Condensed aromatic ring system formed by pyrolysis of Orlon in air at 473K as proposed by Houtz.⁶⁷

Further work to determine the nature of the darkening observed in PAN fibres after pyrolysis was carried out by Grassie and Hay⁶⁸.

Samples of finely divided PAN and various copolymers of PAN (B.S.S. 120 mesh) were heated in a vacuum at 473K. The residue was examined using infra-red spectroscopy after various periods of time at 473K. A reduction in peaks associated with absorption by nitrile groups was observed together with an increase in absorption of peaks

attributed to conjugated nitrile groups.⁶⁸

From these results Grassie and Hay⁶⁸ postulated the formation of a ladder polymer structure (see figure 4.2(2)).

This structure differs from that originally proposed by Houtz⁶⁷ (figure 4.2(1)) which is partially dehydrogenated.

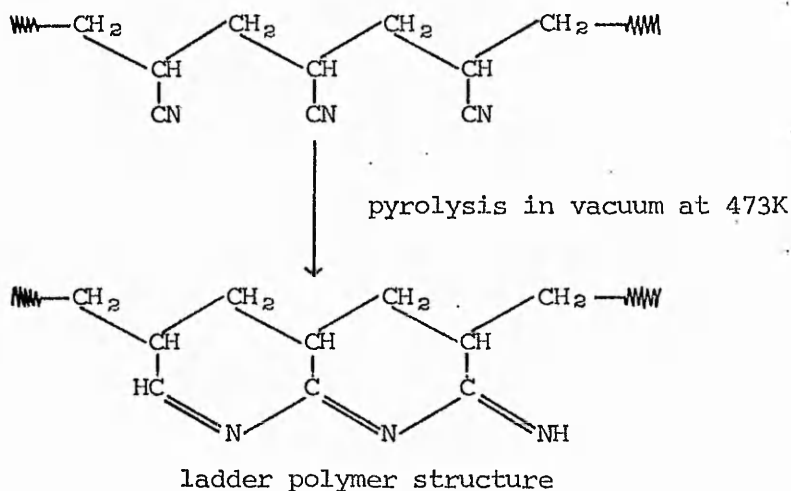


Figure 4.2(2)

Ladder polymer structure formed during PAN pyrolysis at 473K in vacuum as proposed by Grassie and Hay⁶⁸.

Grassie and Hay⁶⁸ concluded that this ladder polymer structure was responsible for the darkening of the PAN during pyrolysis.

Takarta and Hiroi⁶⁹ have examined the pyrolytic behaviour of model compounds using infra-red and ultra-violet absorption spectroscopy. The data obtained from this study supports the postulate of Grassie and Hay⁶⁸ that darkening of PAN during pyrolysis results from the formation of a ladder polymer structure (figure 4.2(2)).

Thompson⁷⁰ was one of the first workers to report DTA curves for PAN. He observed a large exotherm with a peak temperature in the range 506-546K. Thompson⁷⁰ noted that the peak temperature of the exotherm decreased with decrease in the molecular weight of the PAN sample examined. No firm conclusions were however advanced concerning the nature of the PAN pyrolysis reactions.

Hay⁷¹ has attempted to clarify the situation concerning the pyrolysis reactions of PAN by reviewing the experimental results obtained by himself and other workers.

Hay⁷¹ considered that the chemical reactions occurring during the pyrolysis of PAN could be divided into a low temperature reaction (373-473K) and a high temperature reaction occurring above 513K.

Hay⁷¹ postulated that the low temperature reaction resulted in the formation of a ladder polymer structure similar to that proposed by Grassie and Hay⁶⁸ (figure 4.2(2)). This ladder polymer structure was also believed to give rise to the darkening of the PAN during pyrolysis. Hay⁷¹ further pointed out that little evolution of volatiles was observed in this temperature range.

At temperatures above 513K Hay⁷¹ considered that the ladder polymer structure was stabilised through the process of aromatisation. The observed evolution of volatile materials he correlated with the occurrence of chain scission reactions.

The large exotherm observed by Thompson⁷⁰ in the D.T.A. curve of PAN (peak temperature in the range 506-546K), Hay⁷¹ considered was associated with the evolution of ammonia from the occurrence of two types of reaction (figures 4.2(3) and 4.2(4)) involving portions of the ladder polymer structure formed as previously discussed in the low temperature reaction.

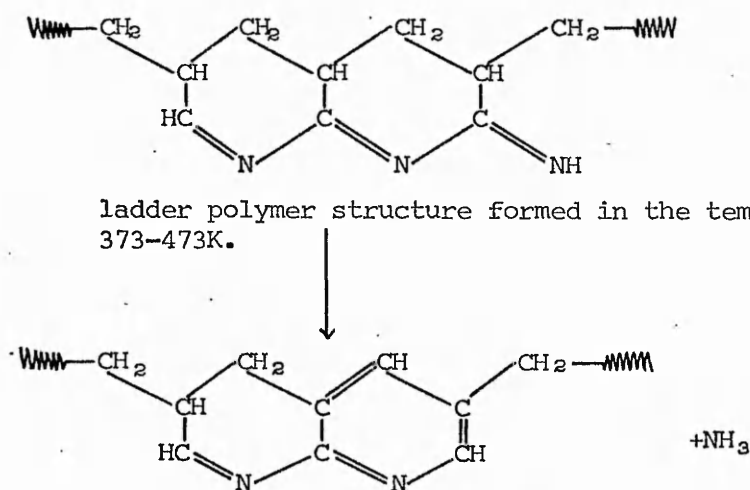


Figure 4.2(3)

First mechanism for ammonia evolution from terminal ring in a ladder polymer structure as proposed by Hay.⁷¹

In the first type of reaction (figure 4.2(3)) Hay⁷¹ postulated that aromatisation of the terminal ring of a ladder polymer structure occurred with the consequent evolution of ammonia.

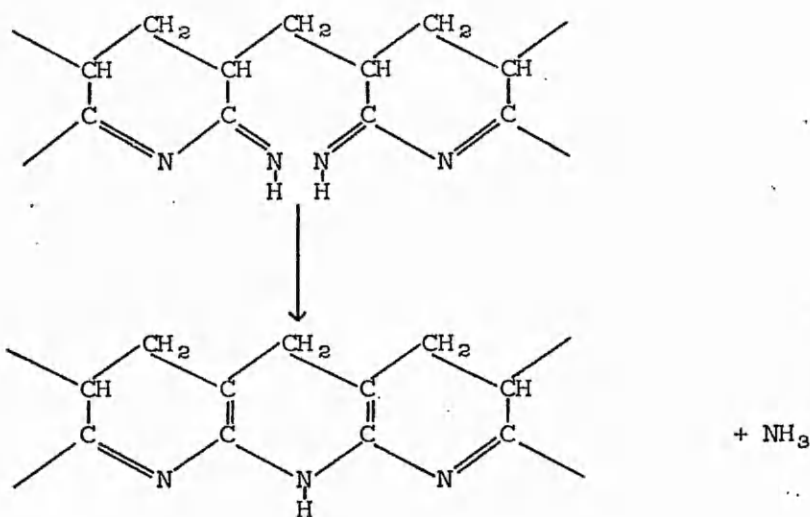


Figure 4.2(4)

Second mechanism for ammonia evolution from interaction of terminal rings in adjacent ladder polymer structures as proposed by Hay.⁷¹

In the second type of reaction (Figure 4.2(4)) ammonia was considered to result from the interaction of adjacent terminal rings in two ladder polymer structures formed through propagation of the ladder structure in opposite directions along the polymer chain.⁷¹ The evolution of ammonia during the pyrolysis of PAN has in fact been detected by several workers as will be discussed later in this section.

Hay⁷¹ did in fact consider the possibility that the large exothermic peak observed by Thompson⁷⁰ in the D.T.A. curve arose as a result of the reaction involving formation of the polymer ladder structure. However in view of the observed thermal behaviour of polymethacrylonitrile (PMAN)⁷² he considered that this was unlikely.

Polymethacrylonitrile is believed to colour during pyrolysis by a mechanism similar to that for PAN (i.e. formation of a ladder polymer type structure) but, however, does not produce ammonia or exhibit an exotherm in the D.T.A. curve⁷² (c.f. PAN).

This argument would now seem unsound for as Grassie⁵⁸ points out, PMAN unlike PAN, fuses and undergoes extensive depolymerisation during pyrolysis. Both fusion and depolymerisation would be expected to be endothermic processes and may thus mask the occurrence of any exotherm related to formation of a polymer ladder structure in PMAN. Further the bulky methyl groups in PMAN make the formation of a ladder polymer structure less favourable sterically and hence less exothermic.

It would seem relevant to observe at this point that large exothermic peaks are a general feature of the D.T.A. curves of most polymers of high acrylonitrile content.

In more recent work Turner and Johnson⁵⁷ concluded that the large exotherm observed in the D.T.A. curve of Courttelle fibre (peak temperature 535K, rate of temperature increase 1 degree min⁻¹) correlated with the extent of ladder polymer formation as determined by infra-red spectroscopy, and was not in fact related to reactions involving ammonia evolution as postulated previously by Hay.⁷¹

In support of this theory Turner and Johnson⁵⁷ calculated that the quantity of ammonia produced was insufficient to account for an exotherm measured as 33.5 - 46.5 kJ mole⁻¹. However the reaction to form the ladder polymer structure (Figure 4.2(2)) was calculated as exothermic to the extent of 21.0 - 42.0 kJ mole⁻¹.

Grassie and McGuchan⁵⁸ have reached similar conclusions concerning the origin of the large exotherm observed in the D.T.A. curve of PAN.

Further they⁵⁸ consider that the formation of polymer ladder structure during pyrolysis, in free radical polymerised PAN, proceeds by a free radical mechanism. The general structure of the product, reported by Grassie and McGuchan⁵⁹ is as illustrated in Figure 4.2(5) and is similar in general features to that proposed by Grassie⁶⁸ (Figure 4.2(2)).

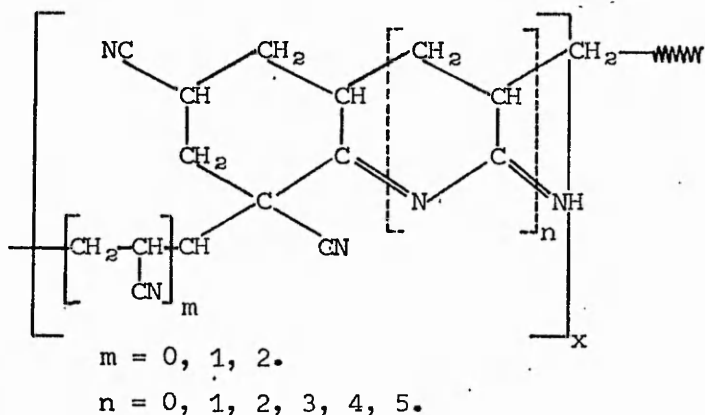


Figure 4.2(5)

The general structure of pyrolysed PAN after the formation of the ladder polymer structure, as proposed by Grassie and McGuchan.⁵⁹

Turner and Johnson⁵⁷ found that the infra-red data from pyrolysed Courttelle was consistent with the formation of a ladder polymer structure similar to that proposed by Grassie⁶⁸ (Figure 4.2(2)).

Utilising the technique of mass-spectrometry Turner and Johnson⁵⁷ detected ammonia evolution initially at 498K with a maximum in the rate of evolution at 553K.

Several other workers pyrolysing PAN in an inert atmosphere have detected ammonia in the gaseous products.⁷³⁻⁷⁵ However both Strauss⁷⁶ and Monahan⁷⁷ studied the pyrolysis of PAN in vacuo and were unable to detect ammonia. Monahan⁷⁷ thus suggested that any ammonia detected during pyrolysis was the result of a secondary reaction involving water within the fibre (See equation 4.2(1)).



Turner and Johnson⁵⁷ have postulated that one reaction giving rise to evolution of ammonia is that between imide and amide groups (see Figure 4.2(6)).

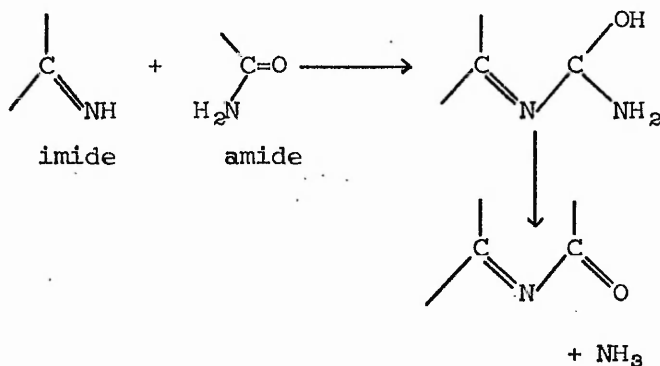


Figure 4.2(6)

Ammonia evolution from the reaction between amide and imide groups as postulated by Turner and Johnson.⁵⁷

The amide groups are postulated either to exist in the precursor polymer or form during the early stages of pyrolysis by reaction of the polymer with water vapour.⁵⁷

Both Turner⁵⁷ and Watt⁷⁸ consider that the mechanism postulated by Hay (see Figure 4.2(4)) is also a likely route to ammonia formation.

It would seem however that in the absence of water and amide groups in the precursor polymer both the mechanisms postulated by Hay (Figures 4.2(3) and 4.2(4)) remain as possible explanations of the observed ammonia evolution. However it is possible that ammonia is produced by several mechanisms, one or more of which involve the

participation of water.

Turner and Johnson⁵⁷ concluded from tensile strength measurements that in Courtelle heated at a constant rate of temperature increase, chain scission reactions occurred above 473K. Cross-linking reactions were not detected below 573K, the upper temperature limit of the mechanical measurement.

A pale yellow liquid was observed to condense in the liquid nitrogen cold trap in the temperature range of the large exotherm observed in the D.T.A. curve for Courtelle.⁵⁷ This liquid accounted for 7% of the mass loss up to 573K. On standing it was observed that the liquid polymerised slowly and gave an elemental analysis similar to that of the precursor polymer. Turner and Johnson⁵⁷ have postulated that this liquid product consists of chain fragments formed as a result of chain scission reactions.

From T.G. data for the pyrolysis of Courtelle in an argon atmosphere. Turner and Johnson⁸ postulate that chain scission reactions account for a major proportion of the mass loss observed in the temperature range 523-723K.

As will be discussed in the following section Grassie and McGuchan⁶¹ found that certain additives were efficient in initiating the reaction involving the formation of the ladder polymer structure.

In the presence of such additives Grassie and McGuchan⁶¹ observed two effects. First the residual yields at both 773K and 1273K were increased and second the peak height (ΔT) of the large exotherm in the D.T.A. curve was reduced.

They⁶¹ concluded that the result of a less intense exotherm was a decrease in the extent of chain scission reactions occurring during the exotherm and hence an increase in the residual yield.

It is believed⁷⁸ that chain scission reactions occur in portions of the polymer chain where the ladder polymer structure is absent.

Watt and Green⁷⁸ and to a more limited extent Turner and Johnson^{8,57} determined the various volatile and gaseous products evolved during the pyrolysis of PAN. Watt and Green⁷⁸ in fact examined the pyrolysis behaviour of homopolymer PAN fibre utilising a step-wise temperature programme with 100 degree temperature increments. The pyrolysis chamber was continuously evacuated and the products collected in cold traps at different temperatures. The qualitative and quantitative analysis of these products was achieved by mass spectrometry. Some of the major products detected, together with a measure of their relative abundance

are listed in table 4.2(1). In addition to the products listed in table 4.2(1) hydrogen cyanide, ammonia, nitrogen, hydrogen and methane were also detected all in fairly significant quantities. References will be made to the temperatures at which some of the latter degradation products are observed later in this section.

From 573K to 673K hydrogen cyanide was found as a major product from the pyrolysis of Courtelle.⁵⁷ Watt and Green⁷⁸ detected hydrogen cyanide evolution in the temperature range 573K to 1173K, the greatest amounts being detected between 973K and 1073K.

Both Watt⁷⁸ and Turner⁸ have suggested that the hydrogen cyanide arises by a reaction illustrated in figure 4.2(7), taking place in portions of the polymer chain where the ladder polymer structure is absent.

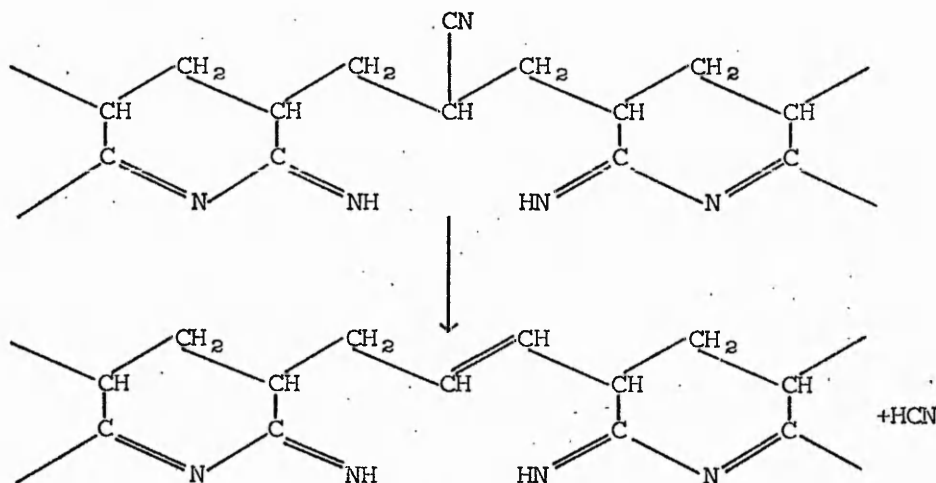


Figure 4.2(7)

Reaction resulting in the formation of hydrogen cyanide from a portion of the polymer chain where the ladder polymer structure is absent. As suggested by Watt⁷⁸ and Turner.⁸

Further Watt and Green⁷⁸ suggest that the preponderance of C₃ hydrocarbons detected in the pyrolysis products [table 4.2(1)] may arise from C₃ links occurring in the polymer chain between sections of the ladder polymer structure. [see figure 4.2(8)].

Table 4.2(1)

Major products of PAN pyrolysis under reduced pressure, together with a measure of their relative abundance. Experimental conditions - low pressure pyrolysis system (initial pressure 4×10^{-6} torr), PAN fibre heated at 2.6 degrees min^{-1} to 573K. Analysis of volatile products over 2 hour period at 573K by mass spectrometry. Then sample heated to 673K and procedure repeated (Watt and Green⁷⁸).

Temperature	Products	Relative quantities in Mass spectrometer units	Temperature	Products	Relative quantities in Mass spectrometer units
584K	propylene	4,000	979K	trace of hydrocarbons	
	acetonitrile	1,500			
	acrylonitrile	1,000			
682K	ethane	7,000	1079K	propylene	2,400
	propane	16,000		propadiene	750
	propylene	9,000		acetylene	500
	propadiene	600	1183K	propylene	1,000
	acetonitrile	2,200		acetylene	450
	acrylonitrile	300		propadiene	400
780K	vinyl-acrylonitrile	3,000		trace of C_4 hydrocarbons probably butadienes	
	propane	4,000	1233K		
	propylene	2,500		acetylene	860
	ethane	1,400		propylene	1,400
	acetonitrile	1,000		propadiene	750
881K	trace of hydrocarbons				

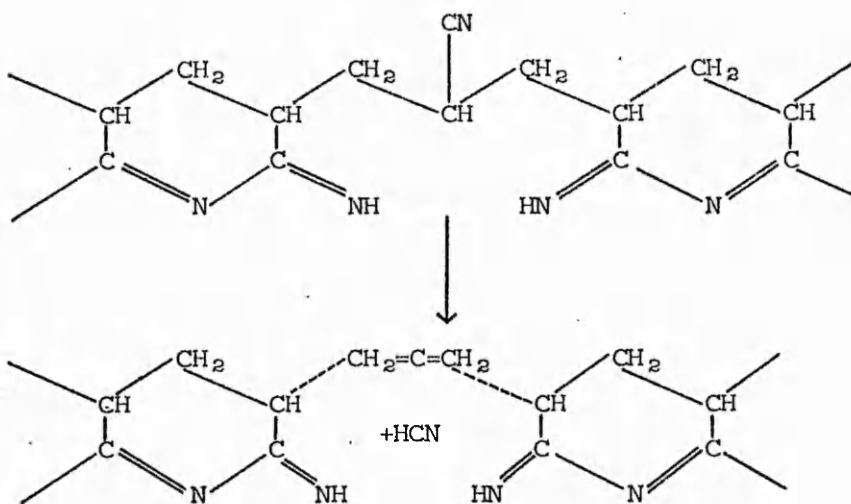


Figure 4.2(8)

Reaction resulting in the formation of C₃ hydrocarbons as proposed by Watt and Green.⁷⁸

They suggest⁷⁸ that the propadiene once formed may be hydrogenated to propylene and propane by hydrogen evolved through general dehydrogenation reactions.

As PAN is an atactic polymer, steric effects will limit the extent of ladder polymer formation. Further, De Winter⁷⁹ using statistical theory has predicted that in a reaction along an isotactic polymer chain, where reactive side groups are capable of ring closure with their neighbours on either side, 14% of these reactive side groups will remain unchanged. If PAN could be considered as an isotactic polymer, one in seven nitrile groups in PAN should be unable to participate in ladder polymer formation and the average ladder length after full reaction might be expected to be six rings.

PAN is in fact, however, an atactic polymer and therefore the average ladder length would be expected to be less than six rings. Turner and Johnson⁸ in a further study examined the hydrogen cyanide evolution from Courtelle pyrolysed in an inert atmosphere to 1273K. Hydrogen cyanide evolution was found to have subsided at 823K, only small amounts were detected above this temperature.

The total hydrogen cyanide evolution was found⁸ to represent 20% of the nitrile groups in the precursor polymer. This proportion may be compared with the 20% of unreacted nitrile groups found by Noh and Yu⁸⁰ in a PAN sample after a long heat treatment in vacuo at 493K.

This evidence would seem to support Watt's theory⁷⁸ that hydrogen cyanide is evolved from nitrile groups in portions of the polymer chain where the polymer ladder structure is incomplete.

Turner and Johnson⁸ observed from T.G. data (sample size 0.2 g, heating rate 1 degree min⁻¹, flowing argon atmosphere) that the Courtelle residue head stabilised by 773K, only a further 10% mass loss being recorded in temperature range 773-1273K.

Watt⁷⁸ used changes in the measured value of the Young's modulus of fibres as a measure of intermolecular cross-linking reactions. Using PAN fibres heated in vacuo he⁷⁸ found that intermolecular cross-linking reactions occurred between 673K and 773K.

In Courtelle fibres (sample size 0.3 g, heating rate 3 degrees min⁻¹, continuous evacuation) hydrogen evolution was initially detected at 673K.⁸ The rate of evolution of hydrogen was observed to reach two separate maxima at 823K and 953K, with continued and steadily decreasing evolution up to 1273K.⁸ Nitrogen evolution during Courtelle pyrolysis became significant above 1073K with a maximum rate at 1253K.⁸

Turner and Johnson⁸ have attempted to explain the mode of hydrogen and nitrogen evolution from Courtelle during pyrolysis in terms of structural changes which are presumably significant in improving the tensile properties of the fibre.

They⁸ have postulated that the first stage in hydrogen evolution (maximum rate at 823K) represents dehydrogenation of the ladder polymer structure to give an aromatic ladder polymer structure (see figure 4.2(9)).

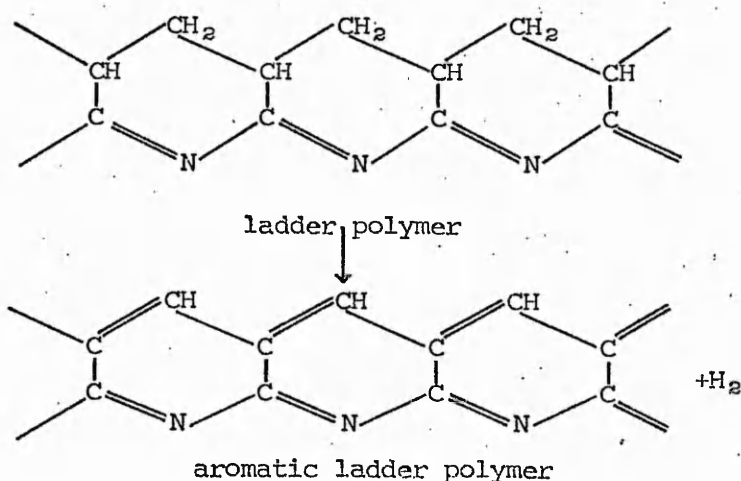


Figure 4.2(9)

Aromatisation of a portion of ladder polymer structure as proposed by Turner and Johnson.⁸

The higher temperature hydrogen evolution with a maximum observed rate at 953K has been postulated⁸ to reflect a back to back condensation reaction of aromatic fragments to give a multi-strand structure (see figure 4.2(10)).

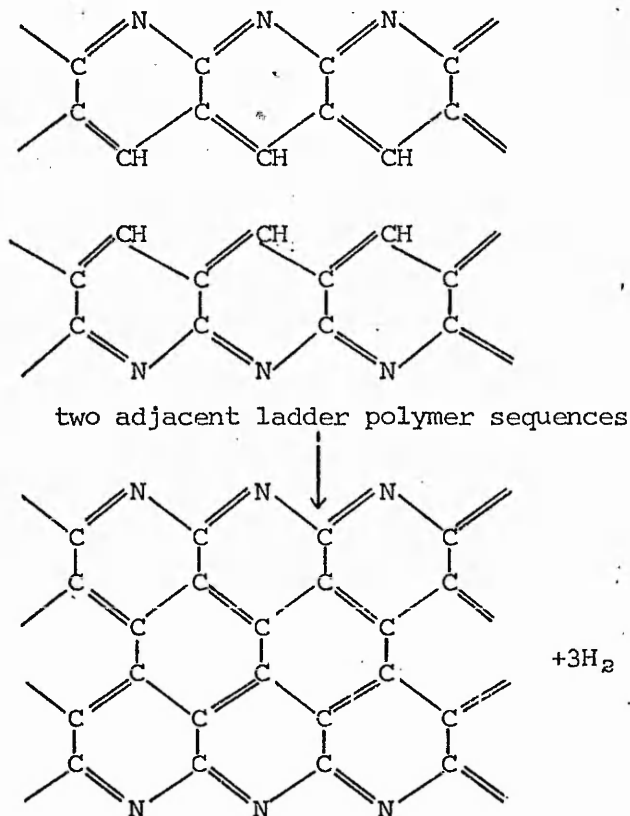


Figure 4.2(10)

Back to back condensation of aromatic ladder polymer sequences to form a multi-strand structure as proposed by Turner and Johnson.⁸

Turner and Johnson⁸ consider that the nitrogen evolution observed with a maximum at 1253K from Courtelle may be formed in a similar back to back condensation mechanism (see figure 4.2(11)).

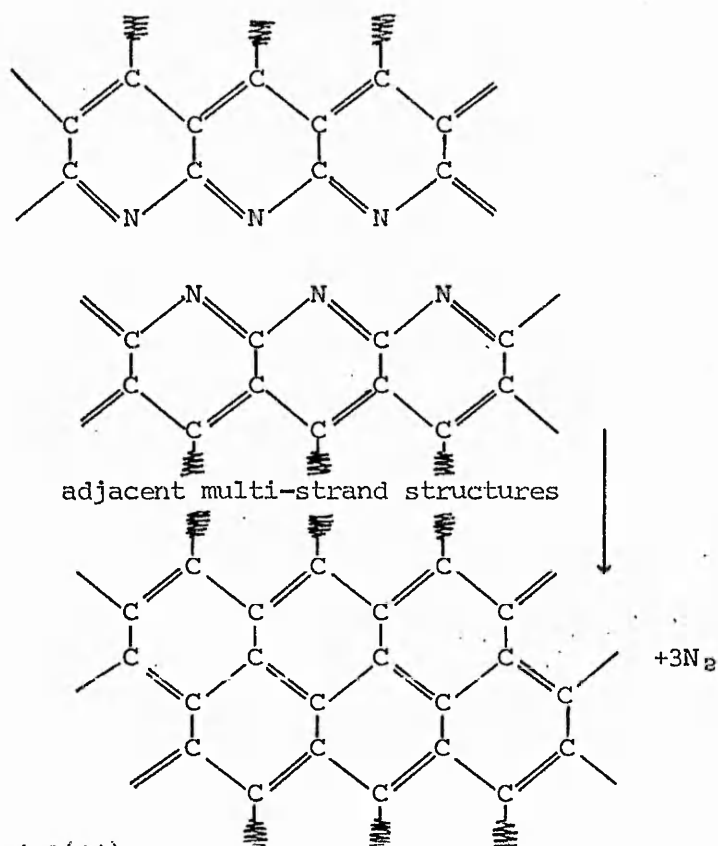


Figure 4.2(11)

Back to back condensation of aromatic multi-strand structures with resultant nitrogen evolution as proposed by Turner and Johnson.⁸

Turner and Johnson⁸ have attempted to assess the relative favourability of the reactions illustrated in figures 4.2(10) and 4.2(11).

They⁸ point out that these processes appear energetically unfavourable especially from a consideration of the degree of orientation required. Two factors they⁸ suggest are relevant in favouring these reactions. First the carbon-carbon back-bone of the ladder polymer structure and therefore the aromatised ladder polymer structure lies in the same direction as the polymer chains in the precursor fibre (i.e. along the fibre axis), thus reducing the steric requirements for lateral fusion of the chains.

Second, if as Watt⁷⁸ has suggested the lengths of ladder polymer structure and hence aromatised ladder polymer structure are relatively short, sufficient mobility may be present for final orientation prior to reaction.

Thus Turner and Johnson⁸ consider that through the reactions illustrated in figures 4.2(10) and 4.2(11) it is possible for a graphite like structure to be formed with the evolution of hydrogen and nitrogen.

Kasatochkin^{81,82} has investigated the chemical and physical changes taking place during the pyrolysis of PAN fibres in both air and inert gas atmospheres using X-ray analysis and infra-red spectroscopy.

Kasatochkin^{81,82} postulated that concurrent with the formation of ladder polymer structure, the formation of valence bonds cross-linking adjacent chains as suggested originally by Schurz⁸³ (see figure 4.2(12)) and partial dehydrogenation of the polymer chains (see figure. 4.2(13)) take place.

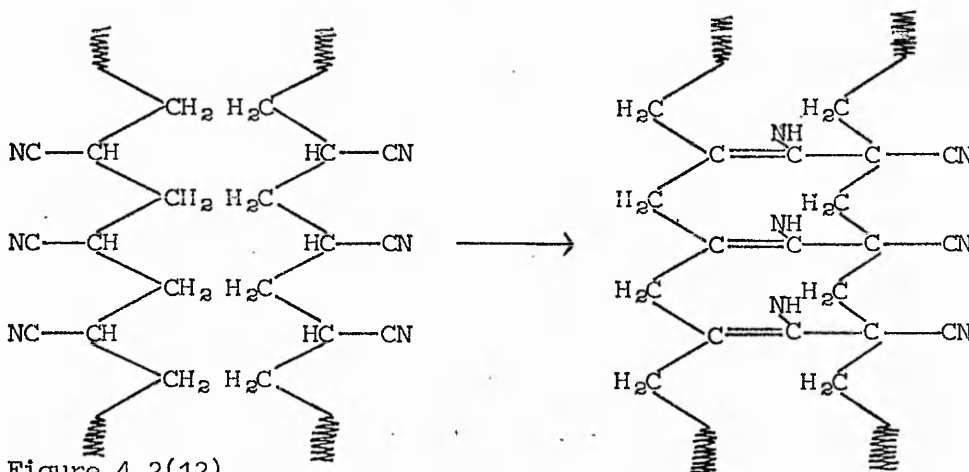


Figure 4.2(12)

Formation of valence bond cross-links between adjacent PAN chains during pyrolysis as postulated originally by Schurz.⁸³

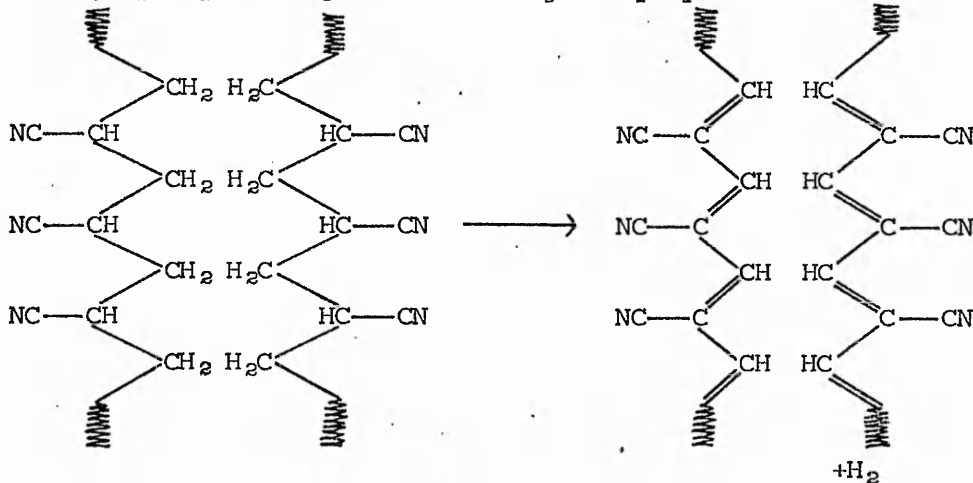


Figure 4.2(13)

Partial dehydrogenation of PAN chains during pyrolysis as postulated by Kasatochkin.⁸¹

Kasatochkin⁸¹ suggests that the relative rates of these three types of reaction depend upon both pyrolysis conditions and fibre structure. His⁸¹ results, however, would appear to indicate that the formation of ladder polymer structure is the most important reaction occurring during pyrolysis in an inert atmosphere.

Kasatochkin^{81,82} reports no D.T.A. data for his PAN samples. It would seem reasonable to assume that the large exotherm observed in the D.T.A. curve of PAN by other workers reflects ladder polymer formation, but in view of the lack of D.T.A. data it is impossible to estimate the temperature range in which the formation of ladder polymer structure occurs in Kasatochkin's^{81,82} experiments. He does however consider that all three types of reaction i.e. cross-linking, dehydrogenation and ladder polymer structure formation take place below 523K.⁸¹

No hydrogen evolution has been detected by Turner and Johnson⁸ below 673K from Courtelle nor by Grassie and McGuchan⁵⁸ below 623K from homopolymer PAN. These data would appear to conflict with the occurrence of partial dehydrogenation of the polymer chain as proposed by Kasatochkin.⁸¹ It is however possible that the hydrogen evolved may be immediately consumed in a secondary reaction.

A further comment may be made, concerning the evidence from infra-red spectroscopy Kasatochkin utilises⁸¹ in proposing the occurrence of the dehydrogenation reaction. Kasatochkin⁸¹ suggests that the infra-red absorption at 1600 cm^{-1} observed from PAN pyrolysis residues may be attributed to the presence of conjugated carbon-carbon double bonds. This same absorption has been observed by Turner and Johnson⁸ who have attributed it to the presence of a conjugated carbon-nitrogen double bond system.

The reaction scheme for the formation of graphite-like layers with consequent evolution of hydrogen and nitrogen proposed by Turner and Johnson⁸ is also postulated by Kasatochkin.⁸¹ Agreement also exists for the temperature ranges in which these reactions occur.

Whilst no direct evidence exists to confirm the postulate, Kasatochkin⁸¹ suggests that at high pyrolysis temperatures the valence bond cross-links are converted into shorter carbon chains, possibly of the cumulene type, covalently bonded to aromatic layers.

Kasatochkin⁸² confirmed by X-ray analysis that the orientation of the PAN polymer chains in the precursor fibre along the fibre axis is retained in the ladder polymer structure and hence in the high temperature carbon fibre product.

Kasatochkin⁸² considers that when the carbon layers are orientated preferentially along the fibre axis, cumulene type links between these layers may increase the overall strength of the fibre. In addition these links may prevent a final transformation to a true graphite structure at higher heat treatment temperatures.

In the light of Kipling's work¹⁰ on graphitising and non-graphitising behaviour it may be the formation of these same cross-links at low pyrolysis temperatures which prevents PAN fusion from taking place.

Dunn and Ennis⁸⁴ have reported the occurrence of an endothermic peak in the Differential Scanning Calorimetry (D.S.C.) curve of Courtelle at approximately 560K when the heating rate was in excess of 80 degrees min⁻¹. They⁸⁴ relate this endotherm to fusion of the Courtelle fibre.

It would seem that at such rapid heating rates, fusion may take place because cross-linking reactions are not sufficiently rapid. There are therefore insufficient cross-links available to stabilise the polymer structure as the temperature rapidly increases.

The formation of these cross-links below 523K as proposed by Kasatochkin⁸¹ would appear to conflict with Watt's findings⁷⁸ that cross-linking reactions are important in the temperature range 673K-773K. A partial explanation of this apparent contradiction may be that at temperatures below 673K the effects of cross-linking and chain scission reactions cancel. Therefore apparently only at temperatures above 673K are the effects of cross-linking reactions detected.

This is however only a partial explanation as Kasatochkin⁸¹ would appear to consider that cross-linking reactions are only significant below 523K.

Whilst the primary carbon in PAN pyrolysis residues is anisotropic Kasatochkin⁸² has observed that isotropic secondary carbon may be deposited on this anisotropic primary carbon as a result of the decomposition in situ of pyrolysis fragments formed during the low temperature chain scission reactions. Grassie and McGuchan⁵⁸ have

however postulated that under conditions of continuous evacuation most of the fragments are removed, resulting in a lower overall residual yield.

In view of the adoption of D.T.A. as a technique employed in this study it seems worthwhile to consider the shape of the D.T.A. curve following the large exotherm observed for polyacrylonitrile samples at c.a. 573K. Whilst the occurrence of chain scission reactions and the formation of the ladder polymer structure during polyacrylonitrile pyrolysis seem to be generally accepted, the nature of the higher temperature reactions would seem as yet not firmly established.

This uncertainty reflects itself in the lack of any real discussion of the shape of the D.T.A. curve following the large exotherm previously discussed.

A second exotherm has been observed (peak temperature unspecified) following the large exotherm in the D.T.A. curve of Orlon run in an air atmosphere by both Schwenker⁵¹ and Tarim.⁴⁶ Schwenker⁵¹ did not however observe this second exotherm when employing a nitrogen atmosphere.

Gillham and Schwenker⁴⁹ have also observed an exothermic peak (peak temperature 703K) following the large exotherm at 596K in the D.T.A. curve of a PAN film run in a nitrogen atmosphere.

It would seem therefore that the form of the D.T.A. curve following the well characterised exotherm reflecting formation of the polymer ladder structure, is not well established. This topic will be discussed later in relation to the results obtained in this study.

A final comment may be made concerning the products of pyrolysis of PAN based materials detected by Turner^{8,58} and Watt.⁷⁸

Except for methane evolution in the temperature range 573-878K, Turner and Johnson⁸ record no significant evolution of other hydrocarbons. This contrasts with the significant evolution of various hydrocarbons detected by Watt and listed in table 4.2(1).

This and any other differences in the evolution of degradation products detected by Turner^{8,58} and Watt⁷⁸ may be attributable to differences in pyrolysis procedure and also the different types of PAN polymer utilised.

Some of the effects of differences in the type of PAN polymer employed, upon pyrolysis observations will be discussed in the following section.

4.3 The role of defect structures and comonomer present within polyacrylonitrile and the effect of additives on polyacrylonitrile pyrolysis behaviour

As previously discussed the reaction involving the formation of ladder polymer structure is believed to be responsible for the large exothermic peak observed in the D.T.A. curve of PAN.

Grassie and McGuchan⁵⁹ have proposed that this process is free radical in nature and may be initiated by traces of polymerisation catalysts, polymerisation initiators, residual solvent and defect structures incorporation in the polymer structure.

The presence of the defect structures in PAN was first postulated by Peebles et al.⁸⁵ The defect structures were postulated to arise from side reactions during the free radical polymerisation of PAN (see figure 4.3(1)). Their decomposition during pyrolysis provides free radicals capable of initiating the formation of the ladder polymer structure.

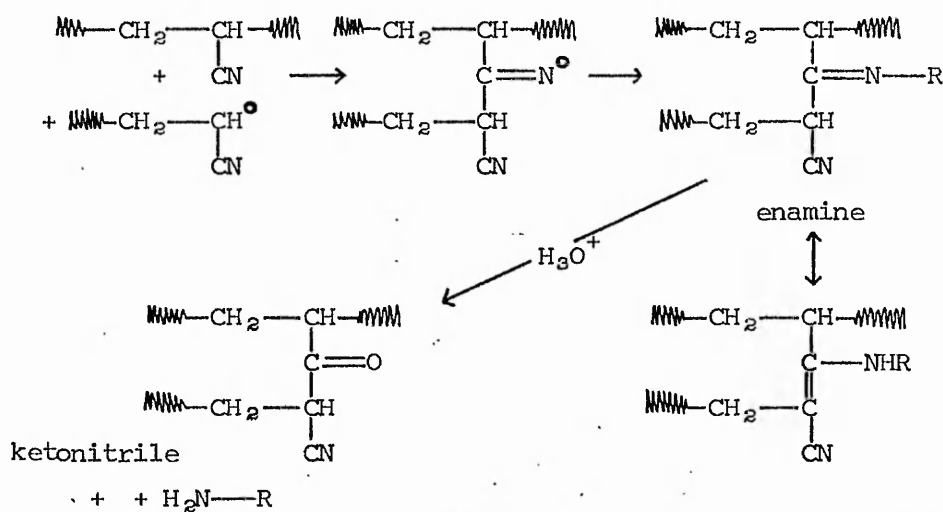


Figure 4.3(1)

Side reaction occurring during the free radical polymerisation of PAN resulting in the formation of an enamine or through hydrolysis a ketonitrile structure as proposed by Peebles.⁸⁵

Peebles et al.⁸⁵ believe that all free radically initiated PAN polymers incorporate either enamine structures, or if polymerisation conditions favour hydrolysis then ketonitrile structures.

Grassie and McGuchan⁶¹ were able to confirm the free radical nature of the reaction forming the ladder polymer structure by using a free radical inhibitor. They observed⁶¹ that the large exotherm in the PAN D.T.A. curve arising as a result of the reaction forming ladder polymer was markedly retarded in the presence of a free radical inhibitor.

They also observed however⁶¹ that a free radical inhibitor had no corresponding effect on the thermal behaviour of PAN produced by an anionic initiator mechanism.

In low molecular weight PAN polymer produced by free radical polymerisation Grassie and McGuchan⁵⁹ found that polymerisation catalysts, polymerisation initiators or solvent incorporated into the polymer structure at the chain ends were more effective in initiating the formation the ladder polymer structure than the defect structures whose existence was proposed by Peebles et al.⁸⁵ This conclusion was based on the D.T.A. curves obtained⁵⁹ when such chain end groups were present. Thus the large exotherm had a lower initiation temperature (T_I) than the exotherm observed for PAN where initiation of the reaction involving the formation of the ladder polymer structure was occurring at the defect structures previously discussed. A reduction in the height of this exotherm (ΔT) was also observed for initiation by end groups.⁵⁹

However it was observed⁵⁹ that the height of the exotherm (ΔT) was generally independent of polymer molecular weight and hence end group concentration above a viscosity of 0.5-1 dl g⁻¹. In polymers of higher molecular weight initiation through defect structures was postulated⁵⁹ as more important than initiation at chain ends.

Grassie and McGuchan⁶¹ have investigated the effects of various additives on the pyrolysis behaviour of PAN and in particular the changes observed in the D.T.A. curves when additives are present. They observed⁶¹ that some additives reduced both the initiation temperature (T_I) and the peak height (ΔT) of the large exotherm in the PAN D.T.A. curve. They considered⁶¹ that these particular additives were also effective in initiating the reaction leading to the formation of the polymer ladder structure.

Both acidic and basic organic compounds together with some inorganic salts were found to behave in this way.⁶¹

In the free radical initiation of the reaction leading to the formation of the ladder polymer structure Grassie and McGuchan⁶¹ believe initiation is the slow step and propagation the fast step. The related exotherm observed in the D.T.A. curve is thus sharp and intense. However in the presence of such additives they postulate⁶¹ an ionic initiation and propagation mechanism where propagation represents the slow step. Hence in this case the related exotherm appears much broader and less intense, i.e. low peak initiation temperature (T_I) and smaller peak height (ΔT).

D.S.C. results have indicated⁶¹ that in the presence of additives which are effective in initiating the reaction the total amount of heat liberated per mole of monomer during the formation of the ladder polymer structure is the same or somewhat higher than that observed in the absence of such additives.

Grassie and McGuchan⁶¹ have argued that the observed reduction in the peak height of the large exotherm in the PAN D.T.A. curve in the presence of these additives means a reduction in concurrent endothermic chain scission reactions and this therefore accounts for any observed increase in the heat of reaction per mole of monomer unit discussed in the previous paragraph.

In the final part of this section the role of comonomer in PAN will be discussed by comparing the thermal behaviour of homopolymer PAN and the commercial PAN fibre Courtelle (Courtaulds Ltd).

Grassie and McGuchan⁶⁴ have observed that the characteristics of the large exotherm reflecting formation of the ladder polymer structure are somewhat different in the D.T.A. curves of Courtelle and PAN homopolymer produced by free radical polymerisation.

For similar sample masses of PAN homopolymer and Courtelle, run under nitrogen atmospheres the peak temperatures (T_{ref}) observed for the large exotherm were approximately the same. However the initiation temperatures (T_I) and the peak heights (ΔT) of this exotherm were 548K and 44 degrees for PAN homopolymer and 483K and 7 degrees respectively for Courtelle.⁶⁴

Courtelle is in fact a copolymer⁸⁶ containing mainly acrylonitrile, some methyl acrylate (6% by mass) and small quantities of a third comonomer which is probably included to improve dyeing characteristics.

In an attempt to assess the role of comonomers in influencing thermal behaviour, Grassie and McGuchan⁶⁴ investigated the pyrolysis behaviour of a group of acrylonitrile/methyl acrylate copolymers of varying composition.

They concluded⁶⁴ that as the extent of the reaction involving the formation of the ladder polymer structure was not reduced in these samples the methyl acrylate although not taking part can be by-passed by the reaction. Thus although the extent of the reaction was not diminished, the presence of methyl acrylate comonomer resulted in a reduction in the rate of propagation of the reaction.

The changes observed in the D.T.A. curves were not perfectly regular through the range of copolymer compositions investigated.⁶⁴ However with increasing methyl acrylate content the large exotherm in the D.T.A. curve became broader and less intense. A progressive reduction in the peak height (ΔT) was thus observed.⁶⁴

The peak broadening was found to be due, not to a decrease in the initiation temperature (T_I), but rather to an increase in the peak temperature measured relative to the reference material (T_{ref}).⁶⁴ This observed increase in the peak temperature (T_{ref}) presumably resulted from the postulated decrease in the rate of propagation of the reaction leading to the formation of the ladder polymer structure in the presence of comonomer.

The large exotherm in the D.T.A. curve of Courtelle was observed to exhibit a lower peak initiation temperature (T_I) and a smaller peak height (ΔT) compared with the large exotherm observed for PAN homopolymer.⁶⁴ The peak temperature of the large exotherm (T_{ref}) for Courtelle was however slightly higher than that observed for PAN homopolymer.⁶⁴

Grassie and McGuchan⁶¹ postulated that the third comonomer present in Courtelle acts to initiate the reaction involving the formation of ladder polymer structure at lower temperatures than initiation through the decomposition of the previously discussed defect structures.

D.S.C. measurements indicated⁶⁴ that despite the change in shape of the large exotherm observed for both the acrylonitrile/methyl acrylate copolymers and Courtelle in comparison with that observed for

CHAPTER 5

Review of the physical and chemical changes taking place during the pyrolysis of binary polymer mixtures

5.1 General Survey of the pyrolysis behaviour of binary polymer mixtures

The pyrolysis behaviour of binary polymer mixtures has been examined by several workers. The actual systems examined vary in the types of the polymers present and the methods of mixing employed.

Tarim and Cates⁴⁶ used mixtures of chopped textile fibre and fabric. They studied the pyrolysis behaviour of these mixtures through application of D.T.A. and T.G. A static air atmosphere was adopted for both techniques and rates of temperature increase of 5 degrees min^{-1} and 10 degrees min^{-1} employed for T.G. and D.T.A. respectively.

The technique of sandwich packing using aluminium oxide as the inert support material was employed for the D.T.A. sample presentation.

Using principally wool (type not specified), Cotton, Dacron and Orlon they⁴⁶ reported that the results showed some variations from those expected on the basis of the behaviour of the single polymer fibres.

The T.G. and D.T.A. data obtained from their study for Dacron/wool, Orlon/wool and Dacron/Orlon⁴⁶ are included for comparison with the results from this study in the appropriate results section.

The T.G. data obtained for both Dacron/wool and Dacron/cotton mixtures indicated that the mass losses associated with Dacron degradation reactions were occurring at lower temperatures in these mixtures.⁴⁶ The observed decrease in the Dacron degradation temperatures being 50 degrees and 18 degrees for the Dacron/wool and Dacron/cotton mixtures respectively.

In addition higher residual yields than would be expected on the basis of the yield behaviour of the single polymer fibres were observed for these two systems at 753K.⁴⁶

Tarim and Cates⁴⁶ obtained D.T.A. curves for the different fibre mixtures. They also employed a cross-differential technique in their D.T.A. studies in order to obtain additional information about pyrolysis behaviour.

In this cross-differential technique the binary mixture (e.g. Dacron/wool) in the sample cell was run against a mixture of asbestos and one of the polymer fibres in the reference cell.

The quantity of polymer fibre (e.g. wool) in the reference cell was chosen to balance the thermal effects of the same fibre in the sample cell. The resulting D.T.A. curve thus reflected the thermal changes in the second fibre (e.g. Dacron in this example) in a Dacron/wool mixture as it was heated in the environment of the first fibre.

Using this technique for Dacron/wool and Dacron/Orlon mixtures they observed⁴⁶ the displacement of peaks associated with degradation reactions of pure Dacron to lower temperatures in the mixtures.

Some peak displacements were also observed in the D.T.A. curves of other simple fibre mixtures without applying the cross-differential technique. Thus the major Orlon exothermic peak (581K) was observed at 571K in a wool/Orlon mixture of unspecified composition⁴⁶ (see figure 5.1(1)).

In the Dacron 50/Cotton 50 (mass%) mixture, cotton peaks normally occurring in the D.T.A. curve at 601K (exotherm) and 638K (endotherm) were observed at 606K and 620K. Further the Dacron peaks at 695K (exotherm), 720K (endotherm) and 753K (exotherm) were observed at 661K, 707K and 743K respectively in the mixture⁴⁶ (see figure 5.1(2)).

Gokcen and Cates⁸⁷ employed pyrolysis gas chromatography to study the degradation products from mixtures of textile fibres ground separately in a mill.

Thermal degradation was achieved by both hot wire pyrolysis, reaching temperatures of 1373-1473K and hot chamber pyrolysis at 1023K. Some evidence for interaction (i.e. an unassigned peak from a Dacron/wool mixture) was obtained.⁸⁷

Tarim and Cates⁴⁶ claim to have observed an additional exothermic peak at 763K in the D.T.A. curve of a Dacron 75/Orlon 25 (mass %) mixture. This peak they⁴⁶ consider cannot be attributed to peaks arising from the thermal behaviour of the individual fibres present.

Crighton and Holmes⁸⁸ have employed D.T.A. in an attempt to characterise textile fibre mixtures.

Binary textile mixtures including either Nylon-6 or Nylon-66 together with Merino Top 64 wool, viscose rayon and cellulose triacetate were examined at a nominal rate of temperature increase of 20 degrees min⁻¹ in a static 'oxygen free' nitrogen atmosphere at 5.3×10^3 Nm⁻².

Some evidence of interaction was found in the Nylon-6/viscose rayon mixture.⁸⁸ The Nylon-6 degradation endotherm (733K) following

the Nylon-6 fusion endotherm (508K) and viscose rayon degradation endotherm (623K) was observed at a lower temperature (673K) in the mixture. No other such peak displacements were however reported for the other mixtures.⁸⁸

C.Z. Carroll-Porczynski⁴² examined the flammability behaviour of textile fibre mixtures using various techniques including simultaneous D.T.A./T.G. and also simultaneous D.T.A./Mass Spectrometry.

These experiments were conducted in a flowing air atmosphere at a rate of temperature increase of 10 degrees min^{-1} . Several mixtures were observed to give higher residual yields at 873-973K than would be expected on the basis of the yield behaviour of the single fibres.⁴²

In parallel flammability experiments a lower degree of flammability was observed with the fibre mixtures where higher than predicted residual yields were observed.⁴²

One of the mixtures exhibiting the type of behaviour outlined in the two preceding paragraphs was wool 50/Kynol 50 (mass%) (Kynol is a phenolic fibre).⁴²

Fusion of wool during pyrolysis is known to take place, however the D.T.A. curve of Kynol exhibits no endothermic peak corresponding to the occurrence of fusion. Further it was observed that in the presence of Kynol the thermal breakdown of wool was neither prevented nor was there any change in the temperature at which it took place.

However, evidence from mass spectrometry indicated a greater release of carbon dioxide from the mixture in comparison with the sum of the total released from the separate pyrolysis of the single fibres. Porczynski⁴² suggests that this additional carbon dioxide may arise from the Kynol. The pyrolysis behaviour of this mixture will be further discussed in the following section.

Perkins et al⁸⁹ have investigated the thermal behaviour separately in nitrogen and oxygen atmospheres of cotton chemically modified with resins designed to impart flame resistance. They employed⁸⁹ both D.T.A. and T.G. techniques adopting as standard a rate of temperature increase of 15 degrees min^{-1} .

The T.G. results obtained in both oxygen and nitrogen atmospheres indicated that the decomposition temperature of the cotton in the resin treated fabric was reduced relative to that observed for the untreated cotton fabric. An increase in the yield of carbonaceous residue was also observed compared with the yield behaviour of the

untreated cotton fabric.⁸⁹

Schwenker et al⁴⁷ have investigated the thermal behaviour of cotton fibre carrying a polyacrylonitrile graft. The grafted fibre was believed to be a copolymer of cellulose and polyacrylonitrile.

Schwenker⁴⁷ using D.T.A. observed that following the large PAN exotherm at 580K a further broad exotherm occurred with a peak temperature of 658K. In the temperature range of this second exotherm a mass loss of 35% was recorded.

The D.T.A. curve of cotton alone contains an endothermic peak reflecting thermal degradation reactions at 631K. This endotherm was found to be absent from the D.T.A. curve of the graft material.

The presence of the exothermic peak at 658K in the graft material Schwenker⁴⁷ attributed to possible interaction of PAN and cellulose degradation products. Schwenker⁴⁷ thus suggested that the material may be simply a cotton/PAN mixture rather than a copolymer.

Schwenker et al⁹⁰ employed separately both air and nitrogen atmospheres in a T.G. study of the thermal stability of cotton fabric and Nylon-66 fabric, each coated with neoprene-W.

In the cases of both the cotton fabric and the Nylon-66 fabric a decrease in thermal stability was observed for the coated relative to the uncoated fabric.⁹⁰ This decrease in thermal stability was observed in both nitrogen and air atmospheres.

Schwenker et al⁹⁰ postulated from the T.G. data that interaction between the neoprene-W coating and the base fabric was taking place. These observations will be further discussed in the following section.

Ubaidullaev et al⁹¹ investigated the thermal behaviour of various polymer mixtures containing PAN as one component by D.T.A. Mixtures of various compositions (mass %) of PAN and separately cellulose triacetate (CTA), polyvinyl alcohol (PVALc) and polyvinyl chloride (PVC) were prepared by solution and reprecipitation in fibre form from dimethyl sulphoxide.

Employing a rate of temperature increase of 2 degrees min⁻¹ and an unspecified gas atmosphere Ubaidullaev⁹¹ found that the initiation temperature (T_I) of the large exotherm (T_I 465-467K) observed in the D.T.A. curve of pure PAN was displaced to higher temperatures in the polymer mixtures.

This displacement of T_I was greatest in PAN/PVC mixtures, reaching a maximum value of approximately 60 degrees with a PVC content of 80% by mass. In PAN/PVALc mixtures of high PVALc content the maximum

observed displacement of T_I was approximately 40 degrees.⁹¹

In PAN/CTA mixtures however the displacement was observed to be an irregular function of composition varying between 0 and 40 degrees. It was concluded simply that the introduction of polymeric additives resulted in the inhibition of the reaction leading to the formation of the ladder polymer structure corresponding to the large exothermic peak in the PAN D.T.A. curve.⁹¹

It should be noted that in both the PVC and PVAlc D.T.A. curves endothermic peaks were observed at 525K and 493K respectively immediately preceding the large PAN exothermic peak observed at 528-533K.

It is therefore possible that the endothermic effects of these peaks masked the initiation of the reaction leading to the formation of the ladder polymer structure. Thus the inhibition observed by Ubaidullaev⁹¹ in PAN/PVC and PAN/PVAlc mixtures may only be apparent. A complementary technique, e.g. infra-red spectroscopy, would be required to estimate the true extent of the reaction leading to formation of the ladder polymer structure at a particular temperature.

In the case of the PAN/CTA mixture no endothermic peaks arising from CTA occur immediately preceding the large PAN exotherm (528-533K). Therefore the somewhat irregular variation of T_I with composition cannot be explained in analogous terms.

5.2 Types of Interaction occurring during the pyrolysis of binary polymer mixtures

It is clear from the review of the pyrolysis behaviour of binary polymer mixtures that in many cases interaction is taking place.

This interaction may be solely physical or solely chemical in nature. However it would seem that in some cases a combination of the two types may be operative.

In discussing the possible modes of interaction, physical interactions will be considered first.

Tarim and Cates⁴⁶ attempted to interpret the D.T.A. and T.G. data from binary polymer mixtures in terms of simple heat transfer effects. At the same time they⁴⁶ acknowledged that in some cases interactions other than those due to heat transfer effects were probably occurring.

Their⁴⁶ basic argument concerning heat transfer is relatively simple. Any exothermic process taking place in one polymer may raise the temperature of the sample as a whole sufficiently to cause reactions in the second polymer to take place. These reactions are considered to occur before the temperature of the heater block and hence the temperature sensing thermocouple in the reference cell register the normal temperature for the particular changes in the second polymer.

The peak in the D.T.A. curve for the particular thermal change is therefore observed at an apparently lower temperature in the polymer mixture.

Thus Tarim and Cates⁴⁶ observed peaks in pure Dacron at 695K (exotherm), 720K (endotherm) and 753K (exotherm). In a cross-differential experiment [i.e. Dacron 35/wool 65 (mass %) mixture in sample cell and asbestos 35/wool 65 (mass %) mixture in reference cell] these peaks were reported to occur at 623K, 673K and 743K respectively.⁴⁶

Tarim and Cates⁴⁶ postulated therefore that this decrease in the temperature of peaks associated with Dacron degradative reactions is the result of the exothermic behaviour of wool, reducing the temperature of the Dacron peaks through a heat transfer mechanism.

Similar behaviour has been observed for Dacron degradative peaks in cotton/Dacron mixtures⁴⁶ as previously discussed. Here again Tarim and Cates⁴⁶ considered that exothermic behaviour in the second component coupled with heat transfer is responsible for the observed peak displacement (see figure 5.1(2)).

The occurrence of major endothermic changes in one polymer might be expected to delay thermal changes in the second polymer thus increasing the temperatures of peaks related to the second fibre in the D.T.A. curve.

However Tarim and Cates⁴⁶ considered that unless the endotherm associated with one polymer is followed within a few degrees by a thermal change in the second polymer, the effects of the furnace acting as a major heat source nullifies this temperature pause in the sample.

Tarim and Cates⁴⁶ suggested that differences in the extent of observed peak displacement may be related to the formation of gaseous products. At higher temperatures the formation and removal of gaseous products occurs rapidly without adequate opportunity for heat transfer to take place. This postulate therefore explains the relatively greater peak displacement associated with the exotherm in Dacron at 695K compared with the exotherm at 753K.

In assessing the relative importance of heat transfer effects a knowledge of the value of the differential temperature (ΔT) associated with each particular peak in the D.T.A. curve is necessary.

Tarim and Cates⁴⁶ gave no indication of the magnitude of the differential temperature in their D.T.A. curves. However as an example a differential temperature of 72 degrees associated with a wool exothermic peak prior to the Dacron degradation peaks is required to account for the movement of the exotherm observed in pure Dacron at 695K to 623K in the cross differential experiment. The sample size in this experiment was 0.1 g comprising Dacron (0.035 g) and wool (0.065 g).

Large differential temperatures have been previously reported (e.g. $\Delta T = 48$ degrees for the large PAN exotherm,⁵⁹ sample size 0.01 g), however the differential temperatures observed in this current study utilising somewhat smaller samples never exceed 4 degrees.

At this point a qualification concerning the magnitude of observed differential temperatures is necessary.

The temperature recorded on the D.T.A. curve may be the temperature of the sample itself or the reference material. In the latter case, with a knowledge of the differential temperature and the temperature of the reference material at a particular peak in the D.T.A. curve, the sample temperature may be calculated by simple algebraic addition

i.e. $\Delta T + T_{\text{ref}} = T_{\text{sample}}$.

In the D.T.A. equipment employed in this study the junctions of the thermocouples associated with the sample and reference material are located beneath the sample and reference platforms. It is conceivable in this type of system that the total extent of localised heat evolution within the sample itself may not be detected by the sample thermocouple simply through limitations in the thermal conductivity properties of the sample.

Therefore the observed differential temperature may not reflect the true difference in temperature between the sample and reference material for a particular peak in the D.T.A. curve.

Whilst heat transfer effects may account for observed peak movement in the D.T.A. curves of some polymer mixtures, it seems doubtful that heat transfer effects are responsible for the Dacron peak movements observed by Tarim and Cates⁴⁶ in the mixture Dacron 35/wool 65 (mass %).

As previously discussed both in this study and elsewhere³⁵ wool degradative reactions are found to be endothermic up to a temperature of c.a. 673K contrary to Tarim and Cates⁴⁶ who consider such thermal activity to be exothermic. Results in this study indicate that exothermic behaviour in wool is only observed at temperatures greater than or equal to 673K.

As previously discussed Tarim and Cates⁴⁶ using T.G. observed that for both Dacron/wool and Dacron/cotton mixtures the mass losses associated with Dacron degradation occurred at apparently lower temperatures in the mixtures. This observation they⁴⁶ attributed to the effects of heat transfer. Thus exothermic behaviour in the second polymer raised the temperature of the sample. This localised rise in temperature was not detected by the temperature sensing thermocouple located beneath the sample container.

If in fact wool degradative behaviour was endothermic the decrease in the Dacron degradation temperature could not be explained in terms of the heat transfer effect.

Tarim and Cates⁴⁶ considered that the higher than predicted residual yields observed at 753K for Dacron/wool and Dacron/cotton mixtures arise from an interaction of a type other than heat transfer.

In an Orlon 50/polystyrene 50 (mass %) mixture it was observed⁴⁶

that at a temperature of 393K the polystyrene was liquid. Further at 513K the liquid polystyrene appeared to coat the surface of the Orlon fibres.

Tarim and Cates⁴⁶ considered that this coating was effective in reducing the mass loss in the mixture associated with Orlon, presumably by retention of Orlon degradative products within the polystyrene coating.

The coating process may therefore be effective in increasing the residual yields. However it would seem that the coating process must occur before degradation of the non-fusing fibre to be effective in trapping degradation products and increasing residual yields.

It is possible however that the fusing and therefore coating polymer may incur greater mass losses by spreading over the surface of the second fibre, for this may facilitate the loss of volatiles from the fused polymer. In this case the unchanged second polymer fibre merely acts as an inert support over which the fused polymer may spread.

Tarim and Cates⁴⁶ postulated that an endotherm observed in the D.T.A. curve of an Orlon 50/polystyrene 50 (mass%) mixture at 545K prior to the occurrence of the large Orlon exotherm and absent from the curves of the single components may represent the wetting or coating process previously described. They⁴⁶ consider that this endotherm at 545K occurs sufficiently close to the large Orlon exotherm (588K) to cause an increase in the peak temperature of 10 degrees to 598K by the mechanism of heat transfer.

It would however appear doubtful that the endotherm observed at 545K does in fact represent wetting as wetting processes are predominantly exothermic in nature. If this is the case then the source of this endotherm requires some other explanation.

As previously discussed the large exothermic reaction in PAN is effective in causing chain scission reactions and hence mass loss.⁶¹ The occurrence of the Orlon exotherm 10 degrees higher at 598K thus correlated with an increase of 7 degrees in the temperature at which significant Orlon mass loss was first detected.⁴⁶

The second type of interactions possible between polymers during pyrolysis are chemical interactions.

Direct chemical interaction between fibres may occur before either fibre starts to degrade. This type of direct reaction may be favoured by the intimate contact achieved through the fusion and coating process previously discussed.

Direct chemical interaction of polymer fibres with additives at elevated temperatures has been observed by both Grassie and McGuchan⁶¹ and Perkins et al.⁸⁹

In both these studies additives were observed to decrease the initial degradation temperature of the polymer and produce a higher residual yield.

It would seem that fibre degradation at lower temperatures results in either less extensive fragmentation or the formation of fragments too involatile to escape at the decreased degradation temperature.

Perkins et al.⁸⁹ quoted increased residual yields at 673K from resin treated cotton fibre compared with the yield from untreated cotton fibre. It is however possible that at higher temperatures greater mass losses may be observed for the resin treated relative to the untreated cotton fibres.

Thus the extent of the increase in residual yield over that expected may be a function of the temperature at which the yield is recorded.

Chemical interactions may also take place between degradation products themselves or between degradation products from one polymer and the unchanged second polymer.

Crighton and Holmes⁸⁸ obtained a D.T.A. curve (static nitrogen atmosphere) for a Nylon-6/viscose rayon mixture of unspecified composition. They⁸⁸ observed that the Nylon-6 degradation endotherm normally occurring at 733K appeared in the mixture at a lower temperature (673K). The peak movement observed was thus 60 degrees. This cannot be explained in terms of heat transfer for no exotherm of sufficient magnitude occurs prior to the Nylon-6 degradation endotherm in the D.T.A. curve of the mixture.

It may however be possible that products from the degradation of viscose rayon (T_I for the viscose rayon degradation reaction 573K) attack the fused Nylon-6 and bring about degradation at lower temperatures.

In the pyrolysis of Nylon-6 and cotton fibres coated with neoprene-W discussed previously, Schwenker⁹⁰ proposed that hydrogen chloride formed during the degradation of neoprene-W attacked the base fibre. Thus the mechanism of degradation of the base fibre (i.e. Nylon-6 or cotton) changed in the presence of the neoprene-W coating, the degradation reaction of the base fibre being observed at lower temperatures in the T.G. curve.

C.Z. Carroll-Porczyński⁴² has postulated that interaction occurring in a Kynol 50/wool 50 (mass %) mixture during pyrolysis in air leads to increased evolution of carbon dioxide from the Kynol fibre. Porczyński has further suggested⁴² that this increased evolution of carbon dioxide may lead to the formation of a carbon layer surrounding the fibres through the exclusion of air from the immediate vicinity of the degrading fibres.

He considered⁴² that this carbon layer acts as a protective skin capable of retaining degradation products and resulting in a decrease in the mass losses observed in later stages of pyrolysis.

If chemical interactions take place during the pyrolysis of polymer mixtures then some change in the type and relative quantities of the degradation products might be expected. In addition the thermal changes reflecting the occurrence of such chemical interactions should also be evident.

Various new peaks have indeed been observed in the D.T.A. curves of polymer mixtures, e.g. exothermic peak at 763K in the D.T.A. curve of a Dacron 75/Orlon 25 (mass %) mixture⁴⁶, exothermic peak at 658K in the D.T.A. curve of cotton fibre treated with PAN.⁴⁷

Tarim and Cates⁴⁶ considered that the additional exothermic peak observed in the D.T.A. curve of the Dacron/Orlon mixture represents the degradation of a new compound formed from reaction of the degradation products of the two polymers.

Schwenker⁴⁷ has suggested that the additional exothermic peak in the D.T.A. curve of cotton treated with PAN represents the interaction of PAN and cellulose degradation products.

Further Gokcen and Cates⁸⁷ using pyrolysis gas chromatography detected an additional product from the pyrolysis of a Dacron 50/wool 50 (mass %) mixture, not observed during the pyrolysis of either of the

single polymers. Gokcen and Cates⁸⁷ consider that the occurrence of this additional peak reflects some kind of chemical interaction taking place during pyrolysis of the polymer mixture.

In conclusion it is considered that increased or decreased residual yields and changes in T.G. and/or D.T.A. curves observed for polymer mixtures when compared with single polymer behaviour may indicate interaction during pyrolysis between the polymers.

It is however possible that more than one form of interaction may be present during the pyrolysis of a particular polymer mixture.

CHAPTER 6

Review of the characterisation of carbon surfaces

6.1 Physical Adsorption

The physical adsorption of gases (adsorbates) on solids (adsorbents) takes place by virtue of attractive forces between the adsorbate and the adsorbent.

If the adsorbate has no permanent multi-pole moment and the adsorbent itself has no external electric field then the attractive interaction is due solely to non-polar dispersion forces.

If however the adsorbent is an ionic compound then the electric field of the adsorbent will induce electric moments in the adsorbate. An attractive interaction will thus arise in addition to that due to dispersion forces.

The presence in the adsorbate atom or molecule of multipole moments will create additional interactions with the adsorbent. Thus the multi-pole of the adsorbate may interact with any permanent field of the solid or may simply induce a charge distribution in the adsorbent leading to attractive interaction.

Dispersion forces are always present in adsorbate-adsorbent systems and represent the attractive interactions of instantaneous multipoles occurring in the adsorbate and adsorbent.

Thus in the case of a non-polar adsorbate and adsorbent, dispersion forces constitute the only form of attractive interaction.

At the equilibrium position adopted by the adsorbate in any adsorbate-adsorbent system the attractive forces are balanced by short range repulsive forces.

Experimentally, measurements of the mass of material adsorbed (a) as a function of pressure (P) at constant temperature (T) may be plotted in the form of an adsorption isotherm (equation 6.1(1)).

$$a = f(P)_T \quad \text{Equation 6.1(1)}$$

Basic theoretical interpretations of physical adsorption have been formulated.^{92,93} These interpretations employ a particular simplified model for the adsorption process and incorporate certain basic assumptions.

The Potential theory as postulated by Polanyi^{94,95,96} is however based on thermodynamic considerations and does not offer a detailed mechanism for the adsorption process.

Polanyi considered that forces emanating from the surface of the adsorbent attract adsorbate atoms or molecules. These forces are the previously discussed dispersion forces and are considered to decay with distance from the surface. Polanyi considered that above the surface of the adsorbent there exists an adsorption space as illustrated in figure 6.1(1) which is gradually filled with adsorbate during the adsorption process.

The broken lines in figure 6.1(1) above the adsorbent surface represent planes connecting points of equal adsorption potential. The adsorption potential decays from its maximum value (ϵ_{\max}) at the adsorbent surface to zero (ϵ_{\min}) at some distance from the surface.

Volumes enclosed between each equipotential layer and the adsorbent surface are denoted by the various values of W between W_{\min} (=0) and W_{\max} . The adsorption process as represented by the Potential Theory may be described by equation 6.1(2).

$$\epsilon = f(W) \quad \text{Equation 6.1(2)}$$

Polanyi assumed that the adsorption potential at a point above the adsorbent surface was independent of temperature and therefore the curve $\epsilon = f(W)$ should be the same for a given gas or vapour on a given adsorbent at all temperatures. (Hence it is known as the Characteristic curve.)

The Potential Theory however does not give an explicit isotherm equation.

In order to calculate the Characteristic curve Polanyi⁹⁶ recognised three different cases which are described in table 6.1(1).

Table 6.1(1)

Case	Temperature	State of Adsorbate
I	$\ll T_c$	Liquid
II	Just below T_c	Liquid + compressed gas
III	$> T_c$	Compressed gas

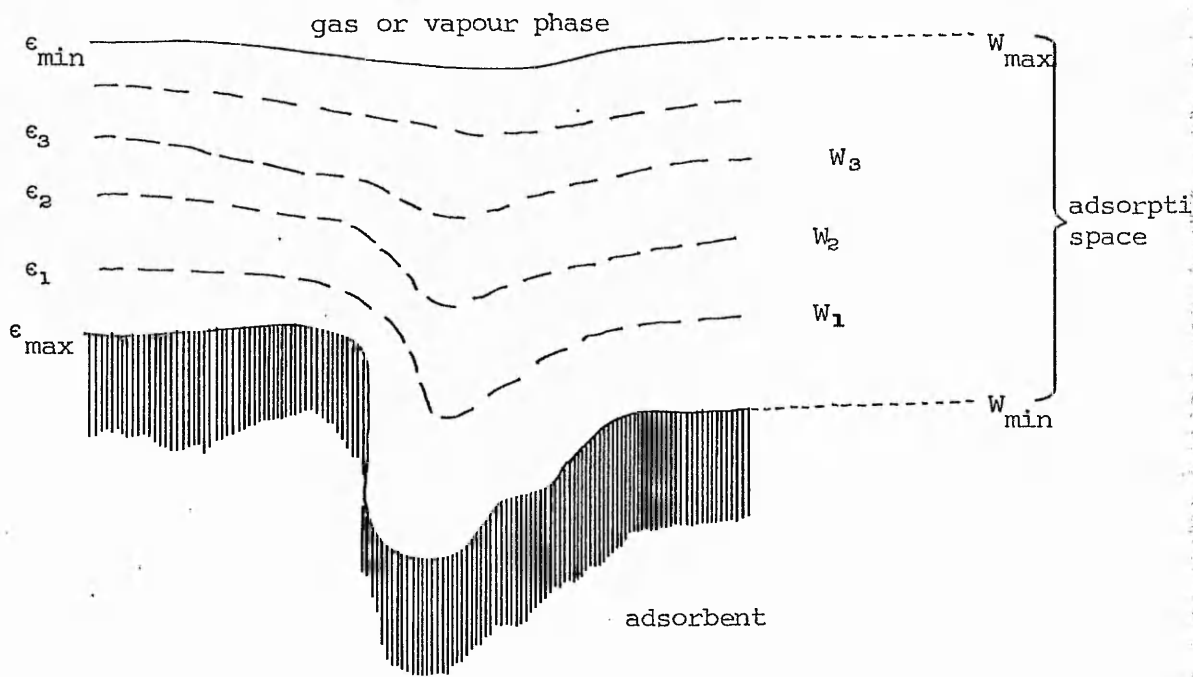


Figure 6.1(1)
 Schematic representation of adsorption space above the surface of an adsorbent.

For adsorption at temperatures below the critical temperature (T_c) of the adsorbate (i.e. Case I, table 6.1(1) Polanyi made three assumptions).

The vapour was assumed to behave as an ideal gas to a first approximation. Secondly the adsorbed vapour in the form of a liquid film on the adsorbent surface was considered incompressible.

Finally it was considered that negligible work was expended in forming the liquid surface.

The adsorption potential at a point in the adsorbed film is defined as the work done in bringing a molecule from the vapour phase to that point.

In the process of physical adsorption and in Case I the adsorption potential may be equated with the work done in compressing one mole of vapour from the equilibrium pressure P at temperature T to the saturated vapour pressure P_0 at temperature T . (equation 6.1(3)).

$$\begin{aligned} \epsilon &= RT \ln \frac{P_0}{P} && \text{Equation 6.1(3)} \\ \left[\text{c.f. } \epsilon &= RT \ln \frac{P_0}{P} \right] \end{aligned}$$

The corresponding value of the adsorption volume (W) is given by equation 6.1(4).

$$W = \frac{a}{\rho T} \quad \text{Equation 6.1(4)}$$

where a = mass of adsorbate adsorbed

ρ = liquid density of adsorbate at Temperature T .

Thus equations 6.1(3) and 6.1(4) allow the Characteristic curve to be constructed from the data of a single isotherm.

The Potential Theory is regarded as successful in that it correctly predicts the temperature dependence of physical adsorption for many systems. This may be illustrated by the following example. Titoff⁹⁷ determined the adsorption isotherms for carbon dioxide on charcoal over a wide temperature range including the critical temperature. Berenyi⁹⁸ utilising the isotherm determined at 273K by Titoff constructed a characteristic curve and from this calculated the isotherms obtained experimentally by Titoff⁹⁷ at the remaining

temperatures. Substantial agreement was found between the calculated and experimental isotherm data. In such a case therefore the characteristic curve successfully describes the process of adsorption and may be regarded as a distribution relating adsorption potential to filled adsorption volume.

Polanyi⁹⁵ derived theoretical expressions to describe the adsorption potential experienced by adsorbates on both a planar adsorbent and a porous adsorbent where the pores are of molecular dimensions. He considered that the close proximity of pore walls in the latter led to an overlap and hence reinforcement of adsorption potential.

This increase in adsorption potential at a given adsorption volume is illustrated clearly in figure 6.1(2).

The shape of characteristic curves calculated from experiment, when compared with those illustrated in figure 6.1(2) give a qualitative indication of the extent of porosity, if any, present in the adsorbent. Dubinin's Theory of Volume filling of micropores⁹⁹ represents a development of the Potential Theory.

Dubinin considered that for adsorbents with pores of molecular dimensions, layer by layer filling of the adsorption volume was unrealistic. Instead, in these small pores he adopted the concept of volume filling of the adsorption space.

Further he considered that the interpretation of \mathcal{E} as the adsorption potential was physically invalid¹⁰⁰ as it implied that in the adsorbent pores an equipotential surface exists on which the adsorbate pressure is equal to the saturated vapour pressure (p_0)

Dubinin¹⁰⁰ considered that the quantity \mathcal{E} should be interpreted as the change in partial molar free energy ($\Delta\bar{G}$) during the reversible isothermal transfer of a mole of adsorbate from a bulk liquid to an infinitely large amount of adsorbent. In more practical terms $\Delta\bar{G}$ therefore represents the difference in the chemical potentials of the adsorbate in the adsorbed state and the bulk liquid state at the same temperature (equation 6.1(5)). It may also be considered as the molar work of adsorption.¹⁰²

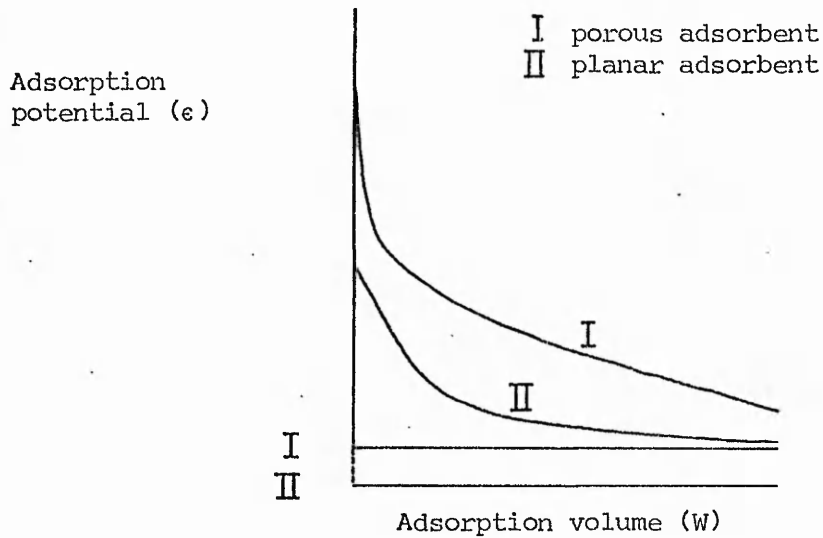


Figure 6.1(2)

Variation of adsorption potential (ϵ) with adsorption volume (W) for a porous adsorbent (I) and a planar adsorbent (II)

$$\begin{aligned}\Delta\bar{G} &= \bar{G}_{\text{adsorbed}} - \bar{G}_{\text{liquid}} \\ &= RT\ln P/P_0\end{aligned}\quad \text{Equation 6.1(5)}$$

$$\left[\begin{array}{l} \text{adopting the notation of Young and Crowell}^{101} \\ \Delta\bar{G} = RT\ln P/P_0 \quad \text{and} \quad \mathcal{E} = RT\ln P_0/P \\ \therefore \Delta\bar{G} = -\mathcal{E} \end{array} \right]$$

The second parameter of the Potential theory, the filled adsorption volume also appears in Dubinin's Theory (equation 6.1(6)).

$$W = aV^* \quad \text{Equation 6.1(6)}$$

where

a = number of moles of adsorbate adsorbed

V^* = molar volume of adsorbate in adsorbed phase.

The first proposition of Dubinin's theory concerns the temperature independence of the Characteristic curve (equation 6.1(7)) for a particular adsorbent-adsorbate system.

$$\left(\frac{\partial \Delta\bar{G}}{\partial T} \right)_{aV^*} = 0 \quad \text{Equation 6.1(7)}$$

A similar conclusion concerning the temperature independence of attractive dispersion forces emanating from a solid surface was reached by Polanyi⁹⁵ as previously discussed.

For the second proposition of his theory, Dubinin considered that at equal filled volumes of adsorption space (aV^*) the ratio of the partial molar free energy change on adsorption ($\Delta\bar{G}$) for a given vapour to the partial molar free energy change on adsorption ($\Delta\bar{G}_s$) for a vapour chosen as standard has a constant value (equation 6.1(8)).

$$\left(\frac{\Delta\bar{G}}{\Delta\bar{G}_s} \right)_{aV^*} = \beta \quad \text{Equation 6.1(8)}$$

The quantity β is often called the affinity coefficient of the characteristic curve. The use of the affinity coefficient allows characteristic curves of different adsorbates on the same adsorbent to coalesce.

It has been found that the ratio of molar volumes of the given adsorbate to the standard adsorbate in the liquid state approximate to observed β values (equation 6.1(9)).

$$\frac{V^*}{V_s} = \beta \quad \text{Equation 6.1(9)}$$

Thus it would appear that liquid state molar volumes can give a realistic measure of likely adsorptive behaviour. However Marsh and Rand¹⁰³ argue that when the adsorbates are polar both the temperature invariance of the characteristic curve and the use of β may be suspect.

Temperature dependence of characteristic curves have been observed by both Freeman et al¹⁰⁴ and Dubinin.¹⁰⁵ Both workers used polar adsorbates (e.g. ammonia and pyridine respectively) on activated carbon adsorbents.

It would seem therefore that only when adsorption takes place solely through the mechanism of dispersion forces can the basic temperature independence of the characteristic curve be maintained. It would appear that when this requirement is fulfilled then characteristic curves for different adsorbates can be made to coalesce. Marsh and Rand¹⁰² and Freeman et al¹⁰⁴ suggest that under these conditions the shape of a characteristic curve depends only upon the structure of the adsorbent.

After considerable experimental work Dubinin¹⁰⁶ defined the function relating the partial molar free energy change on adsorption to the adsorption volume (equation 6.1(10)) for carbons containing pores of molecular dimensions.

$$\Delta\bar{G} = \beta f(w) \quad \text{Equation 6.1(10)}$$

This function appears in equation 6.1(11). Radushkevich¹⁰⁷ has attempted to justify the form ^{of} the equation from a theoretical viewpoint.

$$W = W_0 \exp(-k\Delta\bar{G}^2/\beta^2) \quad \text{Equation 6.1(11)}$$

where W = volume of adsorption space filled at pressure P

W_0 = total volume of adsorption space available, defined for an adsorbent containing pores of molecular dimensions i.e. microporous adsorbent, as the micropore volume

β = affinity coefficient of adsorbate relative to an adsorbate chosen as standard

k = constant.

The Dubinin-Radushkevich or D-R Type I equation (equation 6.1(11)) may be written in a linear form (equation 6.1(12)) substituting for $\Delta\bar{G}$ from equation 6.1(5).

$$\log W = \log W_0 - D(\log P/P_0)^2 \quad \text{Equation 6.1(12)}$$

$$\text{where } D = 2.303 \frac{R^2 T^2 k}{\beta^2}$$

Thus the D-R Type I equation represents the equation of the characteristic curve for adsorption on a microporous adsorbent. Further it predicts a rectilinear plot of $\log W$ against $(\log P/P_0)^2$.

Dubinin¹⁰⁸ has suggested that the constant k and hence the gradient of this plot are a measure of the average pore size.

Dubinin¹⁰⁶ also considered adsorption by non-porous adsorbents, or adsorbents with large pores where no overlap of adsorption potential was possible.

For this second structural type he postulated an equation to describe the characteristic curve of the form of equation 6.1(13).

$$W = W'_0 \exp\left(-\frac{k'\Delta\bar{G}}{\beta}\right) \quad \text{Equation 6.1(13)}$$

where W = volume of adsorption space filled at pressure P .

W'_0 = total volume of available adsorption space

β = affinity coefficient

k' = constant.

substituting for $\Delta\bar{G}$ from equation 6.1(5) the linear form of equation 6.1(13) may be written as equation 6.1(14).

$$\log W = \log W'_0 - D' \log P/P_0 \quad \text{Equation 6.1(14)}$$

$$\text{where } D' = \frac{k'RT}{\beta}$$

Equation 6.1(13) is often described as the Dubinin-Radushkevich Type II equation.

The D-R Type I equation has been shown to represent adsorption data on microporous carbon adsorbents over a wide range of relative pressure.^{99,106}

The data for benzene adsorption at 293K on highly activated (>75% burn-out) charcoals has been found to be well represented by the D-R Type II equation.¹⁰⁶

It has been found however that in some adsorbate-microporous adsorbent systems considerable deviations from linearity are observed when the isotherm data is plotted in coordinates $\log W$ against $(\log \frac{P}{P_0})^2$. The possible reasons for these deviations will be discussed in the later section.

Freeman et al¹⁰⁴ have discussed the criticism of the Dubinin equations voiced by Sutherland.¹⁰⁹ This criticism attributes the general applicability of the Dubinin equations [D-R Type I and D-R Type II] to the ability of log-log plots to linearise curves.

Freeman et al¹⁰⁴ have pointed out that in the case of the D-R Type I equation the plot is of the log-log² type, the difference between this plot and a log-log plot being significant.

In addition Marsh and O'Hair¹¹⁰ found that neither curves, drawn at random to resemble isotherms, nor experimental isotherms on non-carbonaceous adsorbents could be linearised by a log-log² plot.

Finally isotherm data for adsorption on some carbonaceous adsorbents as published by Dubinin⁹⁹ cannot be linearised by a single log-log² plot.

6.2 The implications of the D-R Type I equation as a distribution function

The D-R Type I equation as previously discussed (equation 6.1(11)) was suggested by Dubinin¹⁰⁶ on the basis of an empirical approach.

The first derivative of this equation (i.e. adsorption volume (W) with respect to change in partial molar free energy on adsorption ($\Delta\bar{G}$)) provides the mathematical form of the distribution of partial molar free energy change with adsorption volume (equation 6.2(1)).

$$\frac{dW}{d(\Delta\bar{G})} = \frac{-2W_0 k \Delta\bar{G}}{\beta^2} \exp\left(\frac{-k(\Delta\bar{G})^2}{\beta^2}\right) \quad \text{Equation 6.2(1)}$$

Marsh and Rand¹⁰² have pointed out that this equation (equation 6.2(1)) has the form of a Rayleigh distribution.

Freeman et al¹⁰⁴ have argued that the microporosity present in cokes and carbons arises through the presence of extensive structural defects of varying types. They further argue that there will be a continuous distribution of shapes and dimensions within the microporosity arising through these defects.

The success of the D-R Type I equation in representing adsorption data in cokes and carbons they¹⁰⁴ attribute to the form of the equation. In other words the Rayleigh type of distribution of change in partial molar free energy change with adsorption volume required by the D-R Type I equation is in fact present in many carbonaceous adsorbents.

Further Brunauer¹¹¹ considers that the $\Delta\bar{G}$ value for adsorption as defined by Dubinin⁹⁹ is a measure of the adsorption potential in the micropore volumes. Flood¹¹² has argued that for some carbonaceous materials the adsorption potential is essentially a property of the diameter of micropores and is not significantly related to surface heterogeneity.

Utilising these assumptions of Brunauer¹¹¹ and Flood¹¹² leads to the conclusion that at least in some microporous adsorbents the distribution of change in partial molar free energy change on adsorption with adsorption volume is in fact related to the micropore size distribution.

The constant k of the D-R Type I equation controls both the mode and the spread of the distribution of change in partial molar free energy with adsorption volume (see later in section). Thus k has been considered by Dubinin to be a measure of average pore size when a linear D-R Type I plot is observed.

An alternative approach is to relate experimentally observed changes in the distribution function with expected structural changes if for example a gasification treatment is applied.

It has been observed in a series of progressively activated carbons that the mode of the distribution moves to lower values of $\Delta\bar{G}$ with increasing activation.¹¹³ Further, gasification of carbons has been postulated to lead to widening of micropores by erosion of the pore walls.^{114,115} Thus if the process of activation is postulated to lead to pore widening the lower $\Delta\bar{G}$ value might be expected.

It is clear from the opening paragraphs of this section that a linear D-R Type I plot is only obtained when a Rayleigh distribution of change in partial molar free energy adsorption volume exists in the adsorbent.

It is however clear that only if this observed Rayleigh distribution is governed primarily by the micropore size distribution can any relationship between the Rayleigh distribution parameters and micropore size parameters be assumed. Although Freeman et al¹⁰⁴ consider that correlations between values of k and pore size from adsorption data may be substantiated by measurements of low angle X-ray scattering, no evidence from this latter technique is offered by Freeman.¹⁰⁴

Thus until clear evidence is presented there appears to be no independent evidence to correlate the mode of an observed Rayleigh distribution with for example average pore size.

A further point must be considered for pores of the dimensions of adsorbate molecules. It may not in these cases be realistic to consider micropore diameters, as in these small pores surface heterogeneity may also be a factor in determining adsorbate penetration.

Marsh and Rand¹⁰³ have discussed the role of surface heterogeneity in micropores and its effect on the adsorption process. They consider that different adsorption interaction energies arise from edge and basal planes of graphitic structures, aliphatic linkages, surface oxide and other impurity atoms.

Radushkevich¹⁰⁷ considers that each micropore may be described by an average value of $-\Delta\bar{G}$. As Marsh and Rand¹⁰³ point out this assumes that enhancement of dispersion interaction by overlap from adjacent pore walls completely masks surface heterogeneity effects. However they¹⁰³ argue that in micropores where the adsorbate atom or

molecule does not experience this enhanced dispersion interaction surface heterogeneity is no longer masked.

They¹⁰³ thus consider that adsorption governed solely by dispersion interaction in the smaller micropores gives a distribution of change in partial molar free energy of adsorption against adsorption volume which may give a qualitative measure of micropore size distribution. However in the larger micropores where overlap of dispersion forces is absent no consistent argument exists relating the distribution of W with $\Delta\bar{G}$ to the micropore size distribution.

This would seem to imply that in the larger micropores the distribution of W with $\Delta\bar{G}$ may be related to some distribution function arising from surface heterogeneity.

The Rayleigh distribution is one of several functions which describe naturally occurring phenomena. This distribution is not symmetrical about the mode but is pulled out in the direction of high $\Delta\bar{G}$ values (figure 6.2(1)a).

The position of the mode can be obtained from the second derivative of equation 6.2(1) (i.e. equation 6.2(2)).

$$\frac{d^2(W)}{d(\Delta\bar{G})^2} = \frac{2W_0k}{\beta^2} e^{-\frac{k(\Delta\bar{G})^2}{\beta^2}} \left[\frac{2k(\Delta\bar{G})^2}{\beta^2} - 1 \right] \quad \text{Equation 6.2(2)}$$

$$\text{when } \frac{d^2(W)}{d(\Delta\bar{G})^2} = 0$$

$$2k \frac{\Delta\bar{G}^2}{\beta^2} = 1$$

$$\therefore \Delta\bar{G}_{\max} = \sqrt{\frac{\beta}{2k}}$$

$$\text{substituting } \beta = RT \frac{\sqrt{2.303k}}{D}$$

$$\Delta\bar{G}_{\max} = RT \frac{\sqrt{2.303}}{2D} \quad \text{Equation 6.2(3)}$$

$$\text{where } D = \frac{kR^2 T^2 (2.303)}{\beta^2}$$

Thus as the value of k and therefore D increases the mode as given by $\Delta\bar{G}_{\max}$ moves to smaller values of $\Delta\bar{G}$. The width of the distribution is also controlled by the k and therefore D value. (see figure 6.2(1)a).

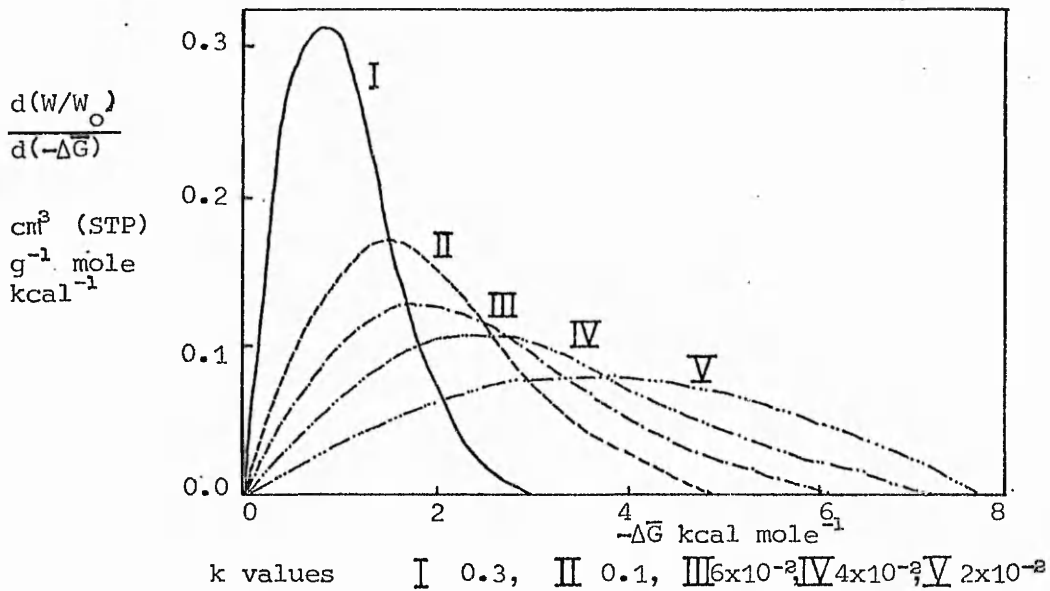


Figure 6.2(1) a
 Distributions of W with $\Delta\bar{G}$ from idealised D-R type I plots¹⁰³

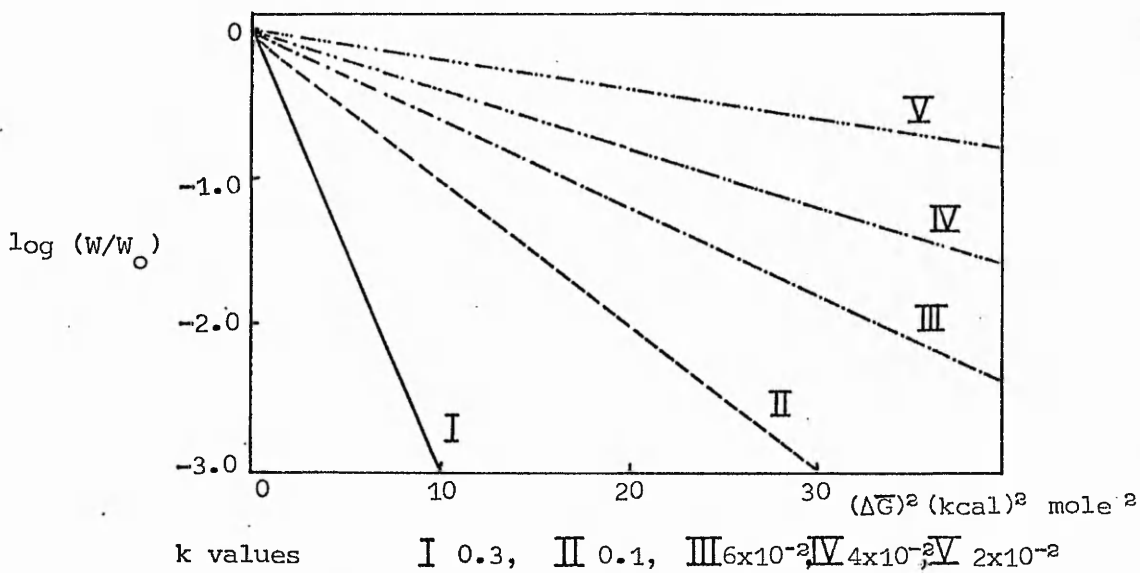


Figure 6.2(1) b
 Idealised D-R type I plots¹⁰³

The D-R Type I plot is only completely linear if a Rayleigh distribution of change in partial molar free energy exists over the entire adsorption volume.

Thus when other distribution functions describing naturally occurring phenomena are plotted in D-R Type I coordinates curved plots are generally obtained. This is illustrated¹⁰³ in figures 6.2(2), 6.2(3) and 6.2(4) for log-normal, Gaussian and Poisson distributions of change in partial molar free energy with adsorption volume.

It is however interesting that, as illustrated in figure 6.2(4)¹⁰³ at least portions of the Poisson type distribution are linear. Marsh and Rand¹⁰³ thus make the point that the whole range of the distribution relating the change in partial molar free energy with adsorption volume should be investigated before the existence of a Rayleigh distribution is claimed.

Whilst Marsh and Rand¹⁰³ consider that the adsorption data must be recorded over a wide range of partial pressures to include the whole of the distribution as discussed above, Dubinin⁹⁹ and later Dovaston¹¹⁶ have both recognised a thermodynamic limitation to the theory of volume filling of micropores. The details of this limitation will be discussed in the next section.

Here it is sufficient to state that at low relative pressures the condition of temperature invariance (equation 6.1(7))

$$\left(\frac{\partial \Delta \bar{G}}{\partial T} \right)_{aV^*} = 0 \quad \text{Equation 6.1(7)}$$

postulated by Dubinin⁹⁹ does not hold.

Thus since one of the basic conditions of Dubinin's Theory of Volume filling of micropores⁹⁹ is violated no significance can be placed on the D-R Type I plot at these low relative pressures even when linearity is observed.

In addition, in many D-R Type I plots deviations from linearity are observed at higher relative pressures¹⁰³, these too will be discussed in a later section. It is sufficient here to consider Dovaston's¹¹⁶ postulate that the upper pressure limit for the application of the D-R Type I equation is usually determined by the onset of capillary condensation in the larger pores, i.e. transitional and macropores at about $P/P_0 = 0.4$.

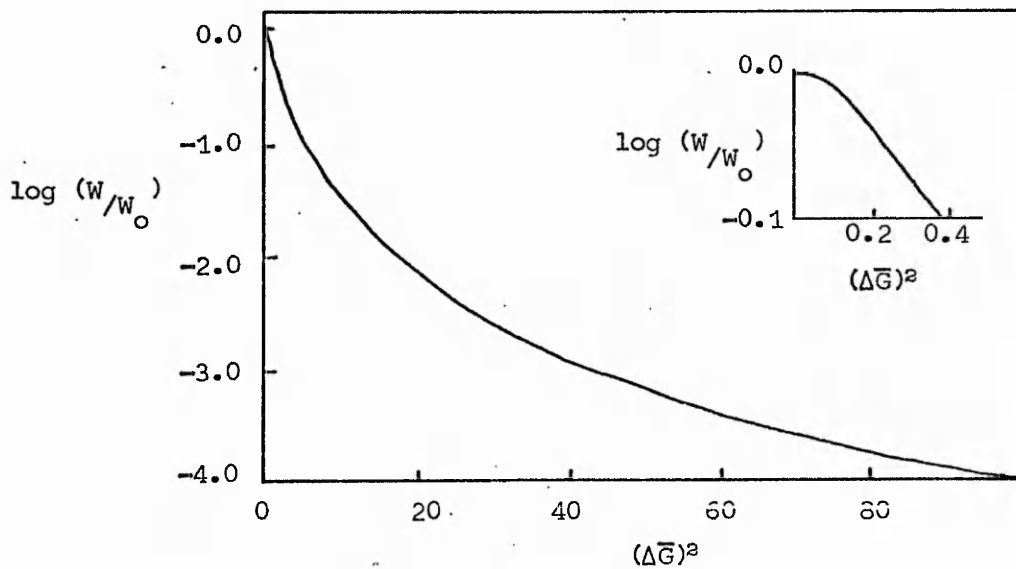


Figure 6.2(2)
D-R type I plot of log-normal distribution of W with $\Delta\bar{G}^{(103)}$

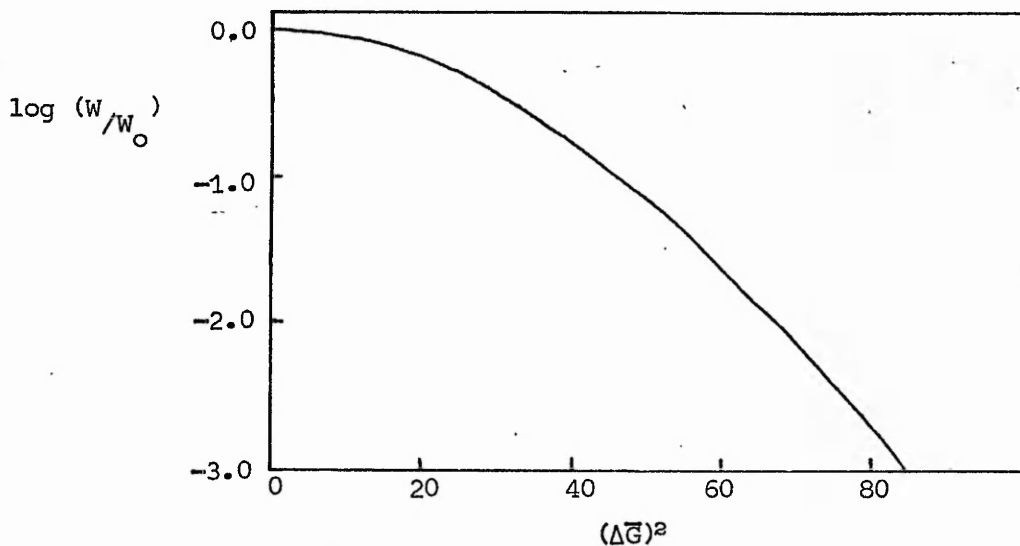


Figure 6.2(3)
D-R type I plot of Gaussian distribution of W with $\Delta\bar{G}^{(103)}$

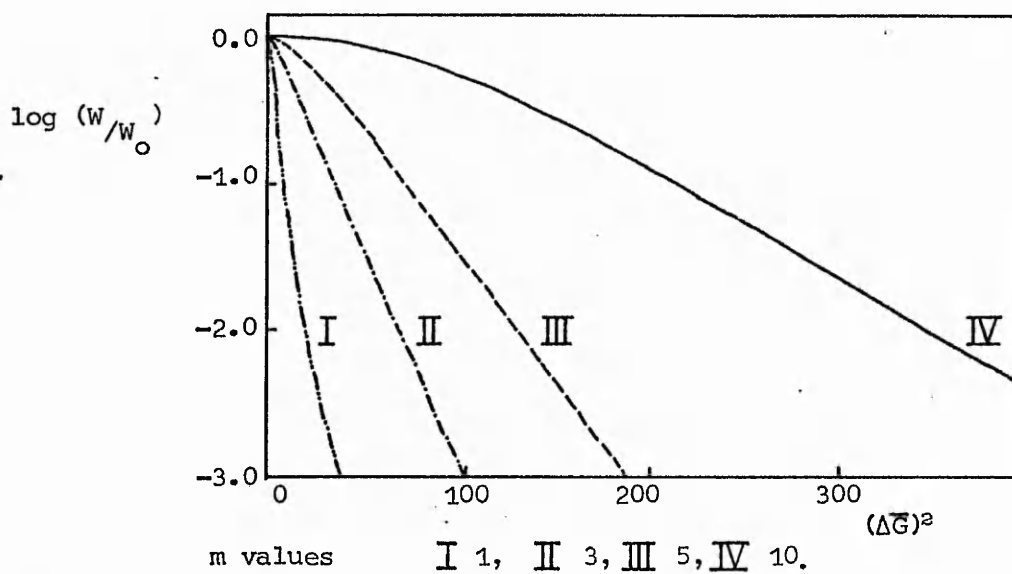


Figure 6.2(4)
 D-R type I plot of Poisson distributions of W with $\Delta \bar{G}^{(103)}$

6.3 Thermodynamic Limitations of the Theory of Volume Filling of Micropores

Dubinin⁹⁹ and later Dovaston et al¹¹⁶ have recognised that a thermodynamic limitation restricts the range of applicability of the theory of volume filling of micropores.

In the original Potential theory Polanyi⁹⁵ postulated that the adsorption potential (\mathcal{E}) at a particular point above the adsorbent surface is independent of temperature. This postulate may be represented by equation 6.3(1).

$$\left(\frac{\partial \mathcal{E}}{\partial T} \right)_W = 0 \quad \text{Equation 6.3(1)}$$

where W = volume of adsorption space.

The Polanyi⁹⁵ condition of temperature independence of the adsorption potential at a given adsorption volume was included in Dubinin's⁹⁹ theory as the temperature independence of the change in partial molar free energy at a given adsorption volume (equation 6.3(2)).

$$\left(\frac{\partial \Delta \bar{G}}{\partial T} \right)_W = 0 \quad \text{Equation 6.3(2)}$$

where W = volume of adsorption space.

Thus Dubinin⁹⁹ considers that only when the condition of equation 6.3(2) is fulfilled can the D-R Type I equation represent the characteristic curve for the adsorption in microporous adsorbents.

In discussing the thermodynamic limitations restricting the applicability of the theory of volume filling it is necessary to consider the partial molar entropy change on adsorption.

This entropy change is defined relative to the entropy of the adsorbate in the bulk liquid form (equation 6.3(3)).

$$\Delta \bar{S} = \bar{S}_{\text{adsorbed}} - \bar{S}_{\text{liquid}} = - \left(\frac{\partial \Delta \bar{G}}{\partial T} \right)_a \quad \text{Equation 6.3(3)}$$

where a = mass of adsorbate adsorbed.

Alternatively the partial molar entropy change on adsorption can be considered as the sum of the partial molar entropy changes in going from bulk liquid adsorbate at temperature T via vapour at T and pressure P_0 , vapour at T and P to adsorbed vapour (equation 6.3(4)).

$$\Delta \bar{S} = (\lambda_v - q_{st})/T + 2.303R \log P/P_0 \quad \text{Equation 6.3(4)}$$

where λ_v = latent heat of vapourisation of bulk liquid adsorbate
 q_{st} = isosteric heat of adsorption.

Dubin⁹⁹ has stated that $\left(\frac{\partial \Delta \bar{G}}{\partial T}\right)_W$ and $\left(\frac{\partial \Delta \bar{G}}{\partial T}\right)_a (= -\Delta \bar{S})$

are related by equation 6.3(5).

$$\left(\frac{\partial \Delta \bar{G}}{\partial T}\right)_a = \left(\frac{\partial \Delta \bar{G}}{\partial T}\right)_W + \left(\frac{\partial \ln V^*}{\partial T}\right)_{\Delta \bar{G}} \left(\frac{\partial \Delta \bar{G}}{\partial \ln a}\right)_T \quad \text{Equation 6.3(5)}$$

where a = mass adsorbate adsorbed

W = volume of adsorption space

V* = molar volume of adsorbate.

The quantity $\left(\frac{\partial \ln V^*}{\partial T}\right)_{\Delta \bar{G}}$ represents the change in molar volume of adsorbate with change in temperature. It would therefore be expected to be positive in sign. The quantity $\left(\frac{\partial \Delta \bar{G}}{\partial \ln a}\right)_T$ has been found by Dovaston¹¹⁶ to be positive.

Thus for the condition of temperature independence of the characteristic curve and hence the D-R Type I plot as required by Dubin⁹⁹ equation 6.3(5) indicates the $\left(\frac{\partial \Delta \bar{G}}{\partial T}\right)_a$ should be positive and hence through equation 6.3(3) $\Delta \bar{S}$ be negative.

Dovaston et al¹¹⁶ have published the full form of equation 6.3(5) utilising the assumptions embodied in equations 6.3(6), 6.3(7) and 6.3(8). The full form of equation 6.3(5) is written as equation 6.3(9).

$$\left(\frac{\partial \Delta \bar{G}}{\partial T}\right)_a = -\left(\frac{\partial \Delta \bar{G}}{\partial a}\right)_T \left(\frac{\partial a}{\partial T}\right)_{\Delta \bar{G}} \quad \text{Equation 6.3(6)}$$

$$\left(\frac{\partial \Delta \bar{G}}{\partial T}\right)_W = -\left(\frac{\partial \Delta \bar{G}}{\partial W}\right)_T \left(\frac{\partial W}{\partial T}\right)_{\Delta \bar{G}} \quad \text{Equation 6.3(7)}$$

$$W = aV^* \quad \text{Equation 6.3(8)}$$

where W = volume of adsorption space filled

a = mass adsorbed

V* = molar volume of adsorbate.

$$\left(\frac{\partial \Delta \bar{G}}{\partial T}\right)_a = \left(\frac{\partial \Delta \bar{G}}{\partial T}\right)_W \left[1 + \left(\frac{\partial \ln V^*}{\partial \ln a}\right)_T\right] + \left(\frac{\partial \ln V^*}{\partial T}\right)_{\Delta \bar{G}} \left(\frac{\partial \Delta \bar{G}}{\partial \ln a}\right)_T \quad \text{Equation 6.3(9)}$$

It is apparent that equation 6.3(9) will only reduce to equation 6.3(5) if it is assumed that $\left(\frac{\partial \ln V^*}{\partial \ln a}\right)_T = 0$. In more practical terms this assumption requires that the density of the adsorbed phase should be independent of the mass adsorbed.

As Dovaston et al¹¹⁶ point out this assumption does not have general validity although it does appear also as an assumption adopted by Polanyi in describing adsorption at $T < T_c$.

Dovaston et al¹¹⁶ have reported the variation of q_{st} and $\bar{\Delta S}$ with a from measurements of adsorption of carbon dioxide on activated cellulose and cellulose triacetate carbons at 195K and 228K respectively (figures 6.3(1) and 6.3(2)).

From this data it is apparent that $\bar{\Delta S} < 0$ when q_{st} has reached an approximately constant value. Thus Dovaston et al¹¹⁶ suggested that as a consequence of the requirement $\bar{\Delta S} < 0$ the applicability of the D-R Type I equation is limited to adsorption values where the isosteric heat is approximately independent of the mass adsorbed.

Based on the approach of Bering and Serpinsky,¹¹⁷ Dovaston¹¹⁶ has derived an equation expressing the minimum relative pressure for applicability of the D-R Type I equation. This equation assumes that the required temperature independence is governed solely by the requirement $\bar{\Delta S} \leq 0$.

$$\left(\frac{p}{p_0}\right)_{\text{minimum}} = \exp[(\lambda_v - q_{st})/RT] \quad \text{Equation 6.3(10)}$$

where q_{st} = isosteric heat of adsorption

λ_v = latent heat of vapourisation of liquid adsorbate.

The application of equation 6.3(10) is illustrated in figure 6.3(3) for a range of adsorption temperatures.

For the activated and unactivated cellulose and cellulose triacetate carbons examined by Dovaston et al¹¹⁶ the lower pressure limit for the applicability of the D-R Type I equation was found to be about $\left(\frac{p}{p_0}\right) = 10^{-3}$ for adsorption at 195K.

An assessment of this lower pressure limit is important for as both Dovaston et al¹¹⁶ and Bering et al¹⁰⁰ have found that deviations from linearity are not necessarily observed at relative pressures lower than the calculated limit when plotted in the coordinates $\log W$ against $(\log \frac{p}{p_0})^2$.

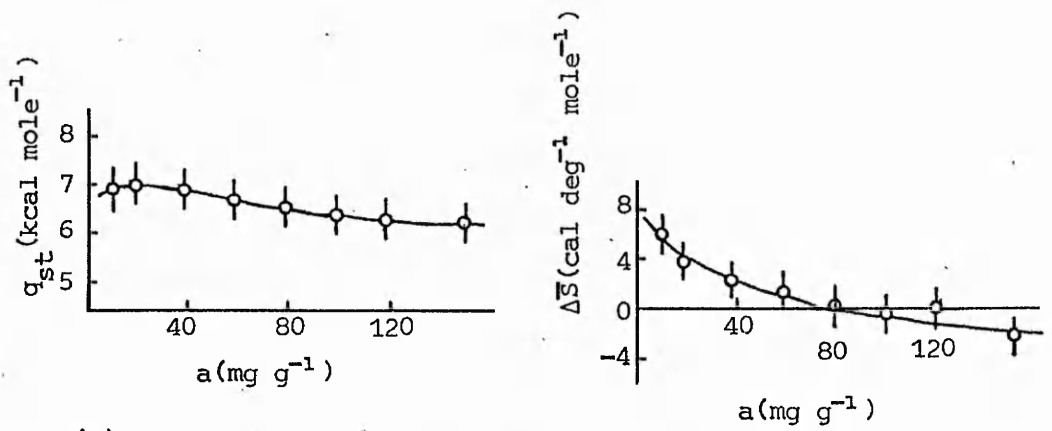


Figure 6.3(1)
 Isotheric heats and entropies of adsorption of carbon dioxide at 195K on cellulose carbon activated to 35% burn-out⁽¹¹⁶⁾

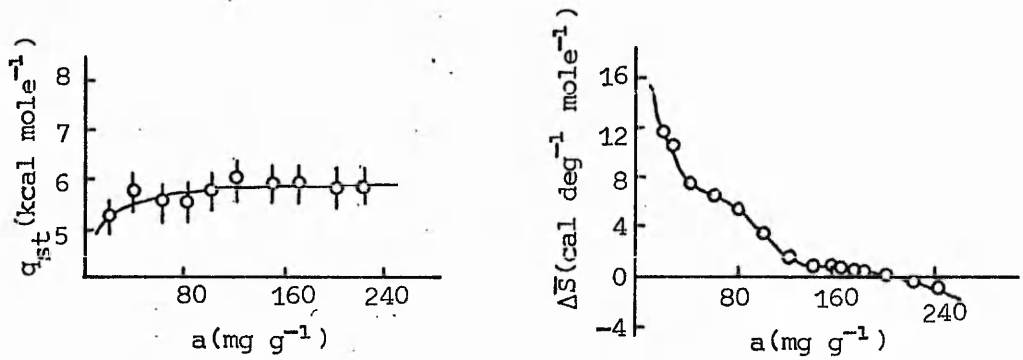


Figure 6.3(2)
 Isotheric heats and entropies of adsorption of carbon dioxide at 228K on cellulose carbon activated to 30% burn-out⁽¹¹⁶⁾

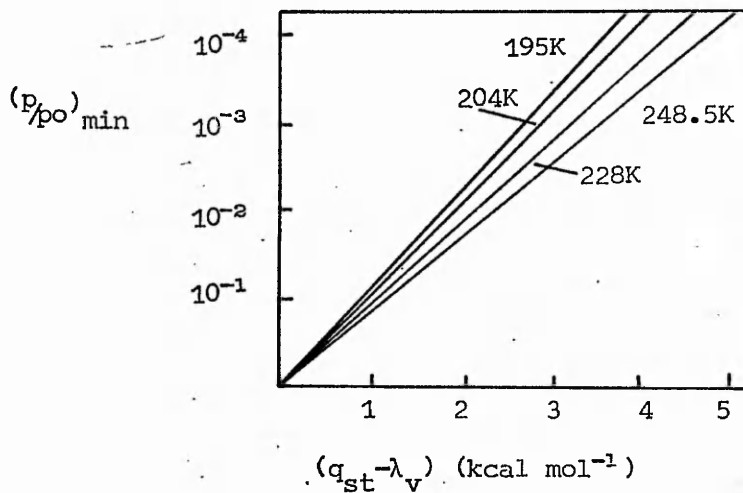


Figure 6.3(3)
 Variation of $(p/p_o)_{min}$ with $(q_{st} - \lambda_v)$ ⁽¹¹⁶⁾

Dovaston et al¹¹⁶ considered that the lower pressure limit for the temperature independence of the characteristic curve arises through the limitations of equation 6.1(3) as a description of the adsorption potential in the early stages of adsorption.

It may not however be possible at low relative pressures to regard the adsorbate as a liquid. Hence the temperature dependence of the characteristic curve at low relative pressures may reflect the adoption of an incorrect bulk liquid molar volume for the adsorbate.

Dovaston et al¹¹⁶ postulated that unless the adsorbent surface is extremely heterogeneous, initial adsorption whether considered as mobile or localised, provides a positive contribution to the adsorbate entropy ($\bar{S}_{\text{adsorbed}}$).

This postulate therefore provides a practical explanation for the positive entropy change observed in the initial stages of adsorption (see figures 6.3(1) and 6.3(2)).

It has already been pointed out that Marsh and Rand¹⁰³ in considering the applicability of the D-R Type I plot suggested that the relative pressure range encompassing the whole range of the distribution of change in partial molar free energy with adsorption volume should be investigated. Only if complete linearity in the D-R Type I plot is then observed, can the existence of a complete Rayleigh distribution, implied by the use of the equation be claimed.

Whilst such an exercise represents an attempt to fully justify the suitability of the D-R Type I equation it is doubtful if this is realistic in view of the inapplicability of Dubinin's basic condition at low relative pressures (i.e. equation 6.3(2)).

$$\left(\frac{\partial \Delta \bar{G}}{\partial T} \right)_W = 0$$

Equation 6.3(2)

6.4 Deviations observed in D-R Type I Plots

Several workers have noted deviations from linearity in D-R Type I plots.^{99,102,104,105,106,118,119}

As previously discussed there is a low relative pressure limit below which the D-R Type I plot is inapplicable. This low relative pressure limit varies with the type of adsorbate-adsorbent system under consideration.¹¹⁶

Caution is necessary in the interpretation of D-R Type I plots for whilst deviations from linearity are sometimes observed below this low pressure limit, in some systems linearity of the plot is maintained at such pressures.^{100,116}

The various types of deviations observed in D-R Type I plots will be discussed here in terms of the Marsh and Rand classification¹⁰² Marsh and Rand noted three general types of deviation and these are illustrated in figure 6.4(1).

Dubinin and Zaverina¹⁰⁶ measured adsorption isotherms of benzene vapour (293K) on a series of sugar cokes progressively activated by reaction with carbon dioxide at 1273K. The corresponding D-R Type I plots are illustrated in figure 6.4(2) together with the degrees of activation and the relative pressure ranges of linearity observed for the D-R Type I equation. Deviations from linearity are observed for the more highly activated samples at higher relative pressures.

Thus at high degrees of activation i.e. 95.5% burn-out, the plot is a curve which Dubinin¹⁰⁶ states can be linearised using the D-R Type II equation, indicating a complete lack of microporosity.

A further example of type B deviation has been reported by Marsh and Rand¹⁰² for the adsorption of carbon dioxide at 195K on polyfurfuryl alcohol carbon activated to 71.5% burn-out. [Figure 6.4(3)].

Marsh¹⁰² has stated that the distribution of adsorption volume with change in partial molar free energy on adsorption, found for the adsorption data of figure 6.4(3) approximates to a log normal form.

This statement correlates with the straight line obtained on application of the D-R Type II equation to the adsorption data for the sugar charcoal [95.5% burn-out, figure 6.4(2)] as the D-R Type II equation does in fact represent a log-normal distribution of

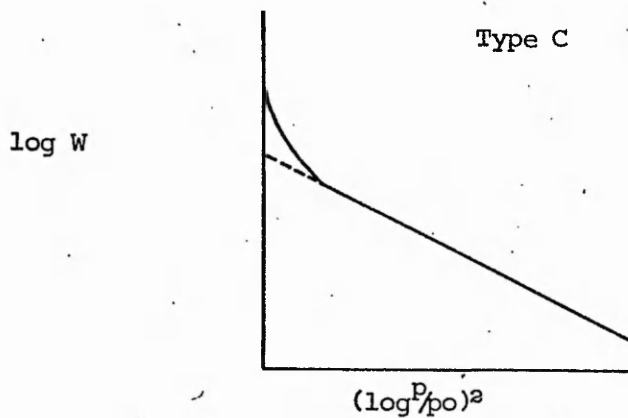
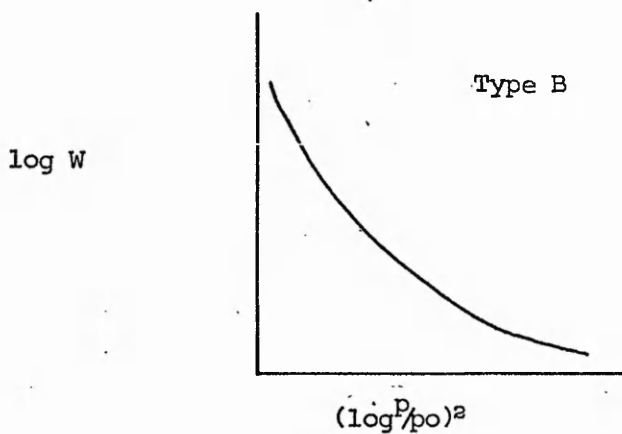
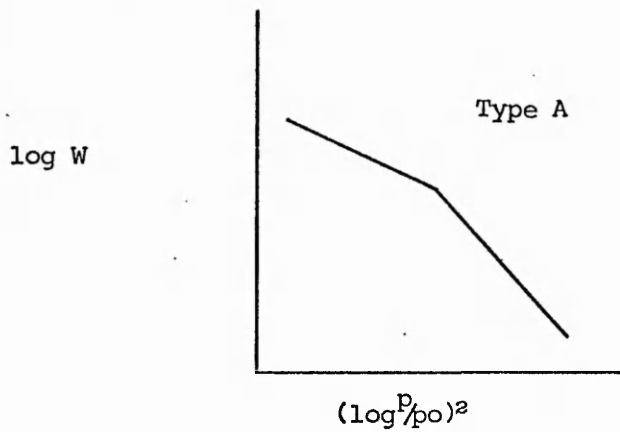


Figure 6.4(1)

Deviations observed in D-R type I plots according to the Marsh and Rand classification¹⁰²

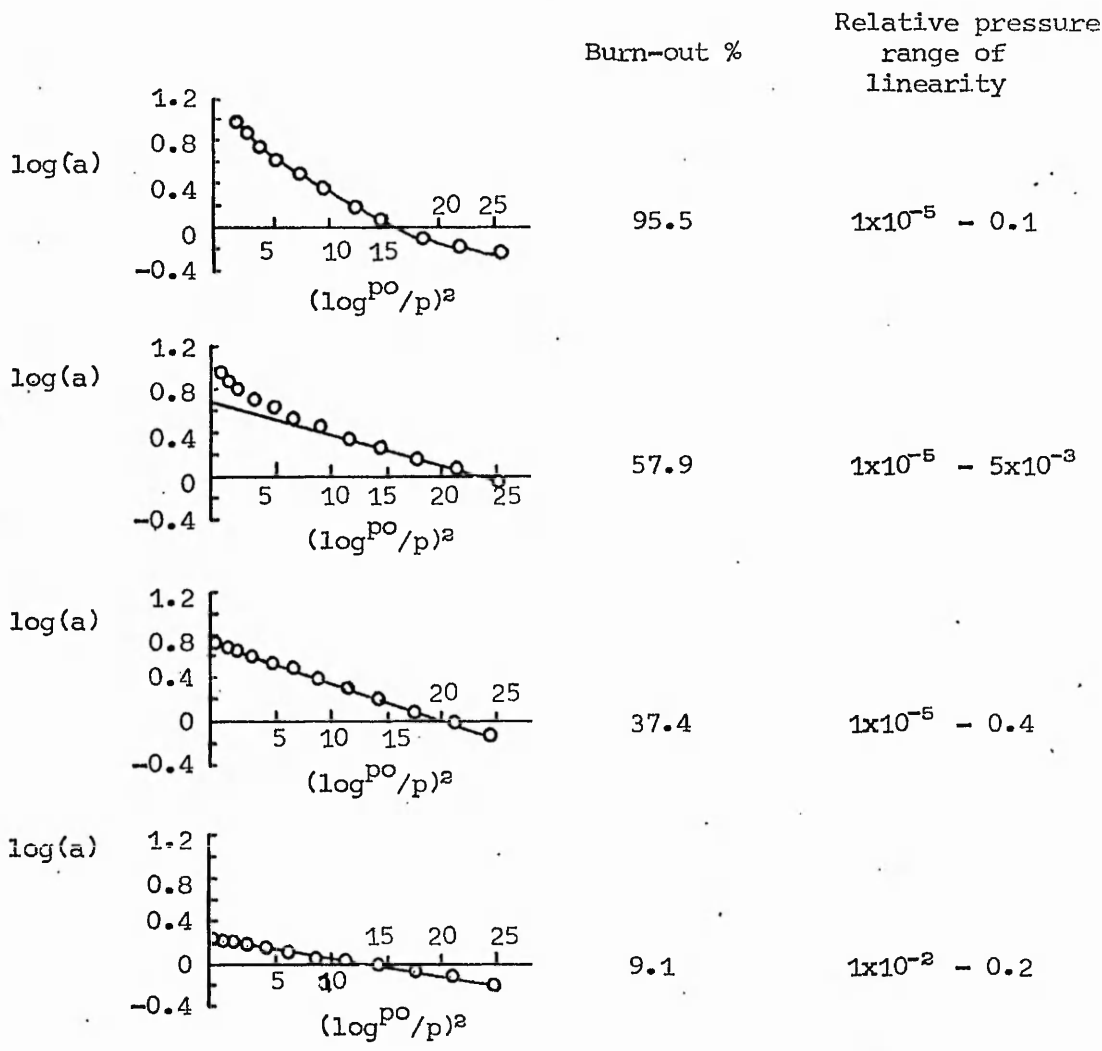


Figure 6.4(2)

D-R type I plots for the adsorption of benzene vapour at 293K on activated sugar charcoals. (106)

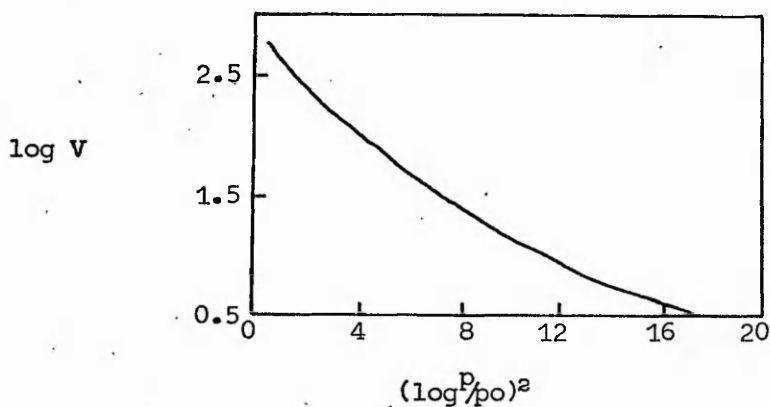


Figure 6.4(3)

D-R type I plot for the adsorption of carbon dioxide at 195K on 1123K poly-furfuryl alcohol carbon activated to 71.5% burn-out ($V =$ volume of adsorbate expressed as vapour at S.T.P. $\text{cm}^3 \text{g}^{-1}$). (102)

adsorption volume with change in partial molar free energy.

At intermediate degrees of activation of the sugar charcoal [57.9% burn-out, figure 6.4(2)] type C deviation is observed. Dubinin¹⁰⁶ postulated that in this carbon there exists both microporous and non-microporous structures.

An adsorption isotherm equation was therefore formulated¹⁰⁶ containing both D-R Type I and D-R Type II terms [equation 6.4(1)].

$$a = \frac{\alpha W_{\epsilon}}{V^*} \exp[-D(\ln P/p_0)^2] + \frac{(1-\alpha)W_{\epsilon}}{V^*} \exp[-D' \ln P/p_0] \quad \text{Equation 6.4(1)}$$

where a = mass of adsorbate

W_{ϵ} = total adsorption volume

α = fraction of total adsorption volume contained within micropores

V^* = molar volume of adsorbate.

It should be noted that the particular type C deviation discussed above is observed at values of $(\log^2 P/p_0)^2$ of approximately less than 10.

Further type C deviations have been observed by Dubinin for the adsorption of benzene at 293K on a series of progressively activated coals¹²⁰ (activating gas steam, temperature 1073-1173K, figure 6.4(4)) and by Marsh and Rand¹⁰² for the adsorption of nitrogen at 77K on activated polyfurfuryl alcohol carbon (71.5% burn-out, carbon prepared to a final heat treatment temperature of 1123K, figure 6.4(5)).

In figure 6.4(5) deviation from linearity in the D-R Type I plot occurs at $(\log^2 P/p_0)^2 < 3$, in figure 6.4(4) this deviation is observed in the range $10 < (\log^2 P/p_0)^2 < 15$.

In order to explain the type of deviations illustrated in figure 6.4(4) Dubinin^{105,120} postulated the presence of two independent microporous structures. An equation for the adsorption isotherm was therefore formulated containing two D-R Type I terms, each representing one of the microporous structures. [Equation 6.4(2)]

$$a = \frac{W_{01}}{V^*} \exp[-D(\ln P/p_0)^2] + \frac{W_{02}}{V^*} \exp[-D'(\ln P/p_0)^2] \quad \text{Equation 6.4(2)}$$

where a = mass of adsorbate

W_{01} = adsorption volume of first microporous structure

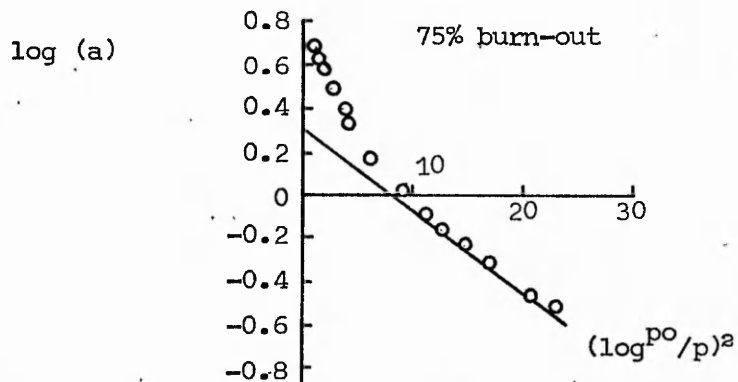
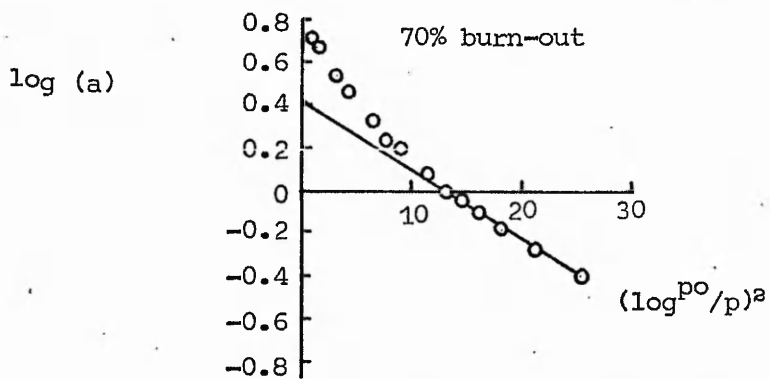
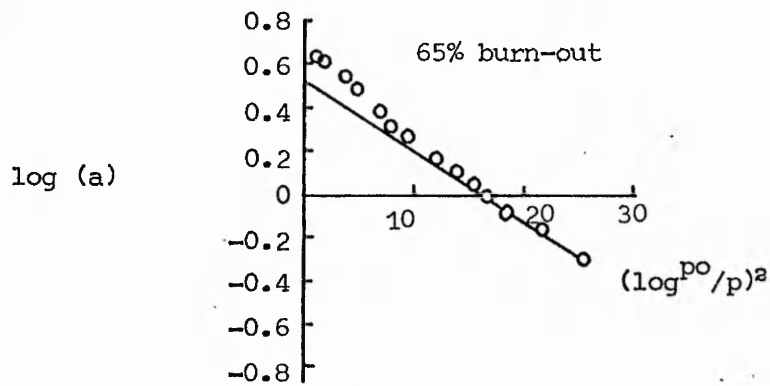


Figure 6.4(4)

D-R type I plots for the adsorption of benzene vapour at 293K on coals activated to various degrees of burn-out (\underline{a} = extent of adsorption, m mole g^{-1}) (120)

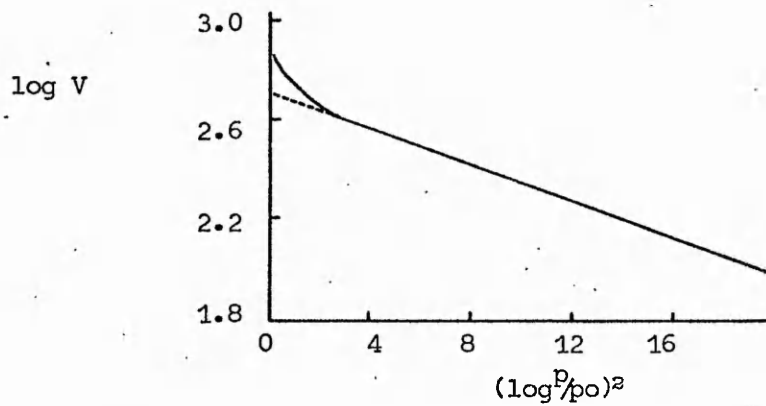


Figure 6.4(5)

D-R type I plot for the adsorption of nitrogen at 77K on 1123K polyfurfuryl alcohol carbon activated to 71.5% burn-out (V = volume of adsorbate expressed as vapour at S.T.P. $\text{cm}^3 \text{g}^{-1}$)

W_{02} = adsorption volume of second microporous structure

$$D = k \left(\frac{RT}{\beta} \right)^2$$

$$D' = k' \left(\frac{RT}{\beta} \right)^2$$

k = constant, possibly characterising first microporous structure

k' = constant, possibly characterising second microporous structure.

Thus by reference to figure 6.4(4), plotting the difference between the experimental adsorption values at low $(\log \frac{P}{p_0})^2$ values and the extrapolation of the linear portion of the plot at high $(\log \frac{P}{p_0})^2$ values a further linear plot representing the second microporous structure may be obtained [figure 6.4(6)]. The D-R Type I plots representing the first and second microporous structures are denoted by the nomenclature I and II respectively.

It has however been observed that for some results, to which the above treatment has been applied,^{102,119} the resultant D-R Type I plot at low $(\log \frac{P}{p_0})^2$ values is not linear but consists of two linear portions. [Figures 6.4(7), 6.4(8) and 6.4(9), 6.4(10)]

In these cases Marsh and Rand¹⁰² consider that whilst the whole distribution of W with $\Delta \bar{G}$ for one microporous structure may not be accurately represented by the D-R Type I equation, each half of the distribution can be so represented but by different slopes. It should however be noted that the adsorption data presented in figures 6.4(7) and 6.4(9) are for adsorption of nitrogen at 77K. Therefore some doubt may exist as to whether these data refer to equilibrium conditions, particularly at low relative pressures because of the possibility of activated diffusion effects. Type C deviation has also been observed for the adsorption of carbon dioxide at 195K on active carbons type 207C and 112C.¹¹⁸ [Figures 6.4(11) and 6.4(12)]. It is reported that active carbon 207C is coal-based and possesses narrower pores than 112C which is derived from coconut charcoal.

The deviations from linearity for adsorption at 195K in figures 6.4(11) and 6.4(12) are both observed at approximately $(\log \frac{P}{p_0})^2 < 3$. No corresponding deviations were observed however for the same adsorbate-adsorbent system at adsorption temperatures of 273K, 293K, 323K, 343K.

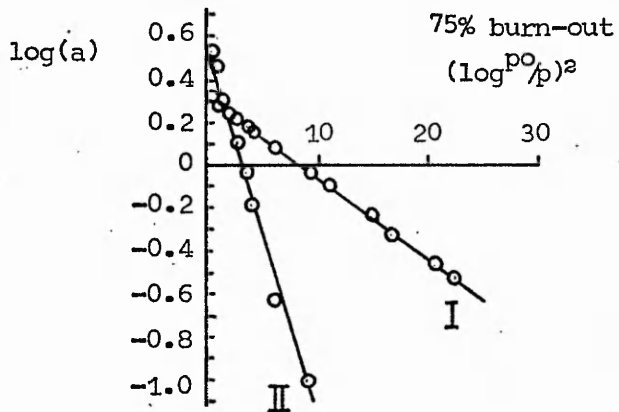
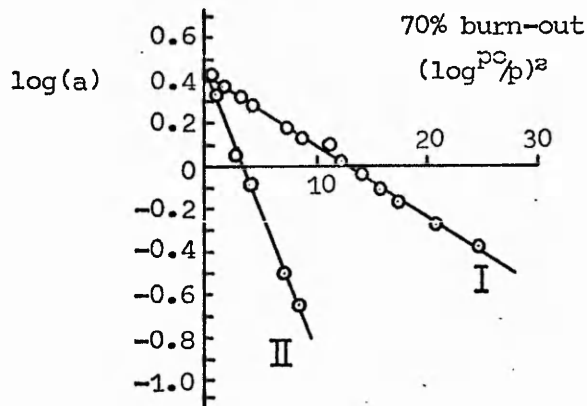
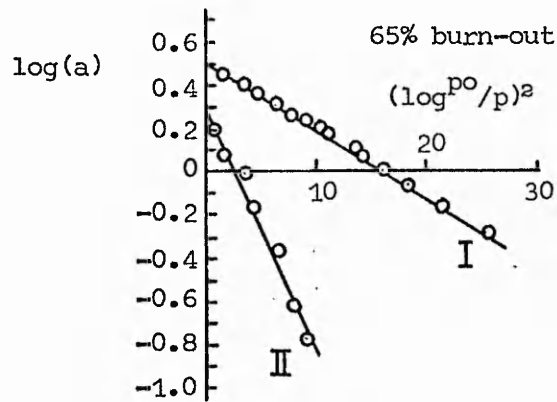


Figure 6.4(6)

Adsorption of benzene vapour at 293K on steam activated coal, plotted according to equation 6.4(2) (a = extent of adsorption m mole g^{-1}) (120)

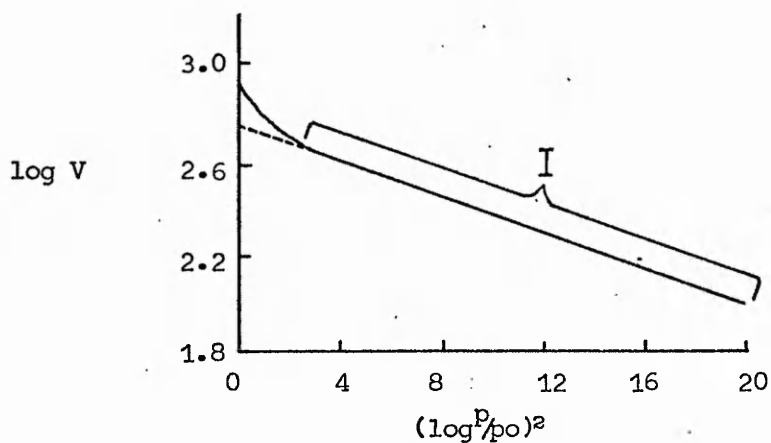


Figure 6.4(7)

D-R type I plot for the adsorption of nitrogen at 77K on 1123K polyfurfuryl alcohol carbon activated to 71.5% burn-out ($V =$ volume of adsorbate expressed as vapour at S.T.P., $\text{cm}^3 \text{g}^{-1}$). (102)

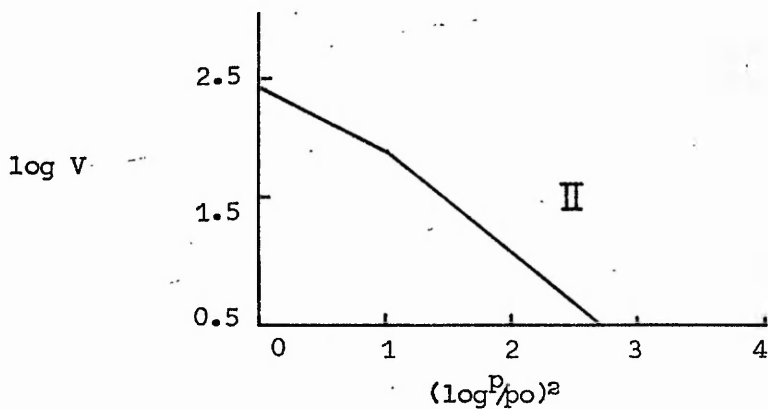


Figure 6.4(8)

D-R type I plot for the adsorption of nitrogen at 77K on 1123K polyfurfuryl alcohol carbon activated to 71.5% burn-out ($V =$ volume of adsorbate expressed as vapour at S.T.P., $\text{cm}^3 \text{g}^{-1}$). (102)

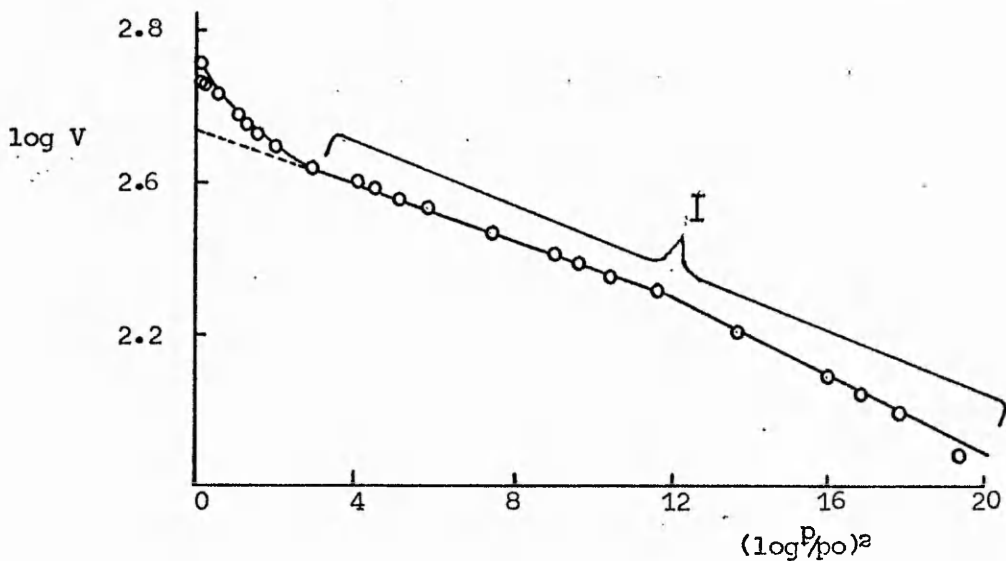


Figure 6.4(9)
 D-R type I plot for the adsorption of nitrogen at 77K on 1123K polyfurfuryl alcohol carbon containing nickel (Ni:C=1:1000) and activated to 89% burn-out ($V = \text{volume of adsorbate expressed as vapour at S.T.P., cm}^3 \text{ g}^{-1}$). (119)

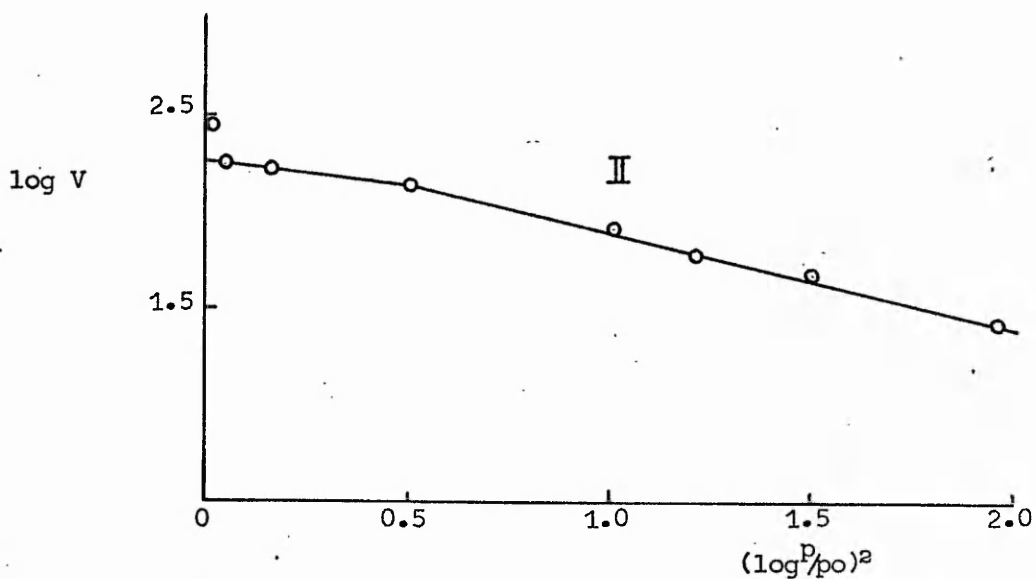


Figure 6.4(10)
 D-R type I plot for the adsorption of nitrogen at 77K on 1123K polyfurfuryl alcohol carbon containing nickel (Ni:C=1:1000) and activated to 89% burn-out ($V = \text{volume of adsorbate expressed as vapour at S.T.P., cm}^3 \text{ g}^{-1}$). (119)

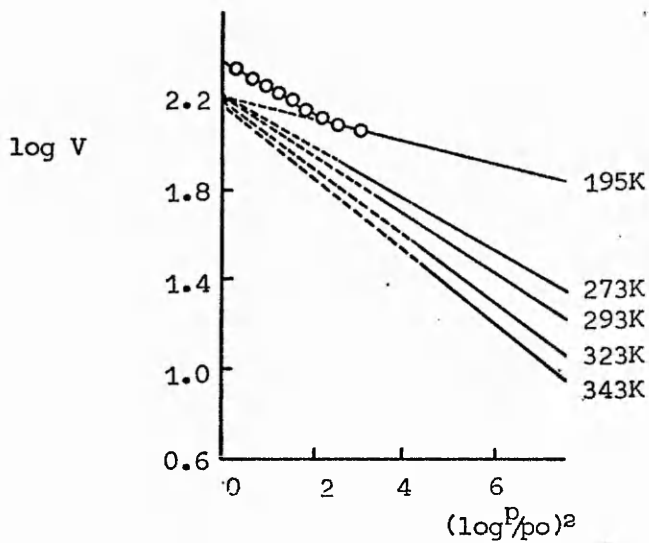


Figure 6.4(11)

D-R type I plots for the adsorption of carbon dioxide (195-343K) on active carbon (type 207C). (V = volume of adsorbate expressed as vapour at S.T.P., $\text{cm}^3 \text{g}^{-1}$) (118)

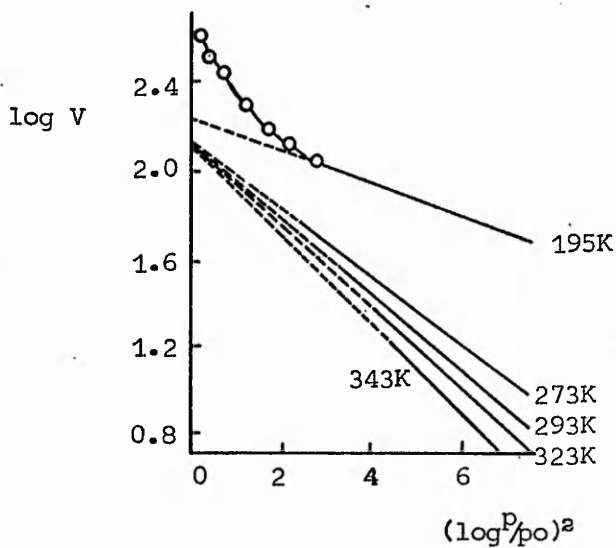


Figure 6.4(12)

D-R type I plots for the adsorption of carbon dioxide (195-343K) on active carbon (type 112C). (V = volume of adsorbate expressed as vapour at S.T.P., $\text{cm}^3 \text{g}^{-1}$) (118)

Marsh¹¹⁸ in this particular case attributed the deviations observed for adsorption at 195K to reversible filling processes in transitional porosity. In a more general comment Freeman et al¹⁰⁴ consider the presence of conical pores as a possible reason for type C deviation.

The third type of deviation, type A, of the Marsh and Rand classification must now be considered.

This type of deviation has been observed by Marsh and Rand¹⁰³ for the adsorption of carbon dioxide at 195K on polyfurfuryl alcohol carbons heat treated to various temperatures [figure 6.4(13)] and lowly activated polyfurfuryl carbons [figure 6.4(14)]. It is considered to arise where the entry of the adsorbate molecules is restricted^{104,105}, possibly through the presence of slit-shaped pores.¹⁰⁵

Chiche et al¹³⁸ have also observed type A deviations for the adsorption of carbon dioxide at 273K on heat treated Dourges coal [figure 6.4(15)].

Illustrated in figure 6.4(16) is the characteristic curve for the Dourges coal. Also illustrated in figure 6.4(16) are separate characteristic curves constructed for each of the linear portions of the D-R Type I plot of the 873K coke. From these characteristic curves are constructed the distributions of change in partial molar free energy with adsorption volume illustrated in figure 6.4(17). Also included in figure 6.4(17) is the observed distribution curve (solid line).

Chiche et al¹³⁸ considered that the change in the gradient observed in the D-R Type I plots may be interpreted in terms of a change in the mechanism of adsorption from an initial distribution of partial molar free energy change to a second distribution, as illustrated by the solid line in figure 6.4(17).

As is clear from figure 6.4(17) the Dourges coal has a continuous distribution of partial molar free energy change on adsorption with adsorption volume. On pyrolysis to temperatures between 873K and 1023K this distribution is extended to higher values of $\Delta\bar{G}$ i.e. to narrower pores. However pyrolysis also results in the creation of a number of pores of a particular size in excess of that number predicted

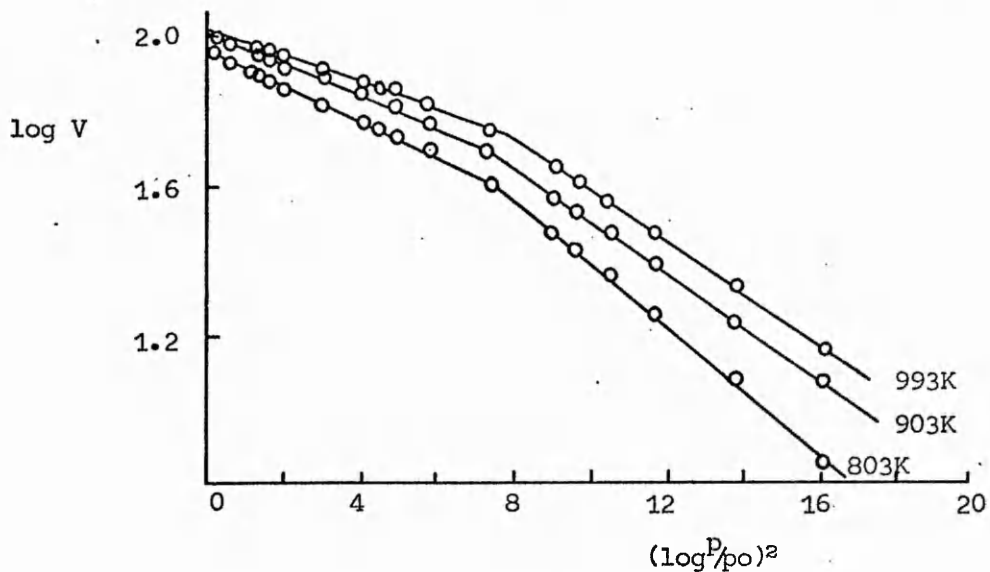


Figure 6.4(13)
 D-R type I plots for the adsorption of carbon dioxide at 195K on polyfurfuryl alcohol carbons heat treated to various temperatures (V = volume of adsorbate expressed as a vapour at S.T.P., $\text{cm}^3 \text{g}^{-1}$). (103)

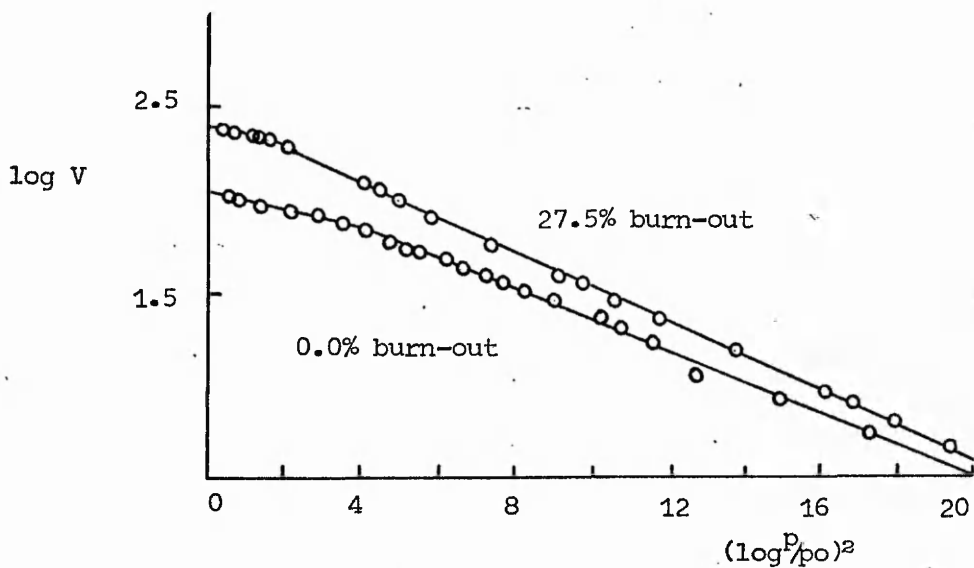


Figure 6.4(14)
 D-R type I plots for the adsorption of carbon dioxide at 195K on lowly activated 1123K polyfurfuryl alcohol carbons (V = volume of adsorbate expressed as a vapour at S.T.P., $\text{cm}^3 \text{g}^{-1}$). (103)

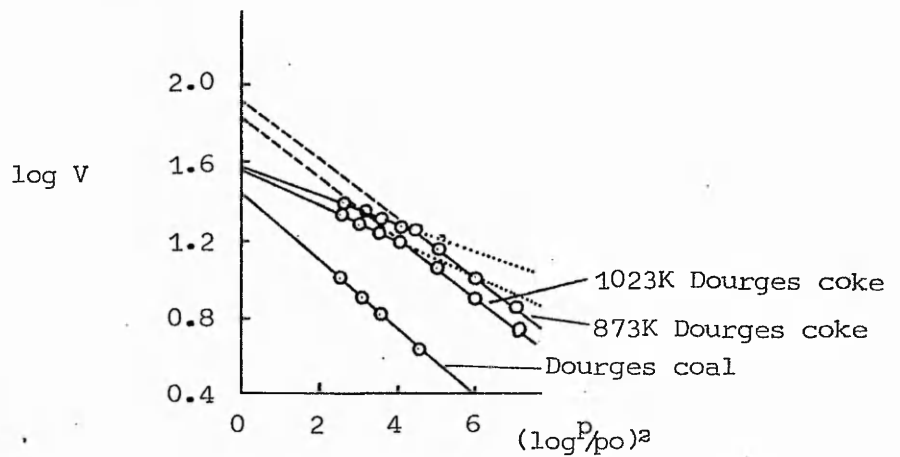


Figure 6.4(15)

D-R type I plots for the adsorption of carbon dioxide at 273K on Dourges coal, 873K Dourges coke and 1023K Dourges coke. (V = volume adsorbed expressed as a vapour at S.T.P., $\text{cm}^3 \text{g}^{-1}$). (138)

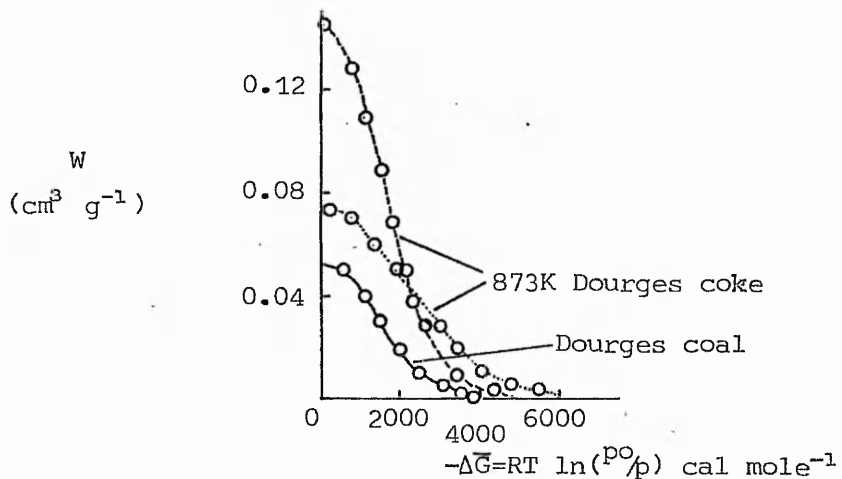


Figure 6.4(16)

Characteristic curves for Dourges coal and the 873K Dourges coke. (W = volume of adsorption space filled with liquid carbon dioxide per unit mass of adsorbent, $\text{cm}^3 \text{g}^{-1}$). (138)

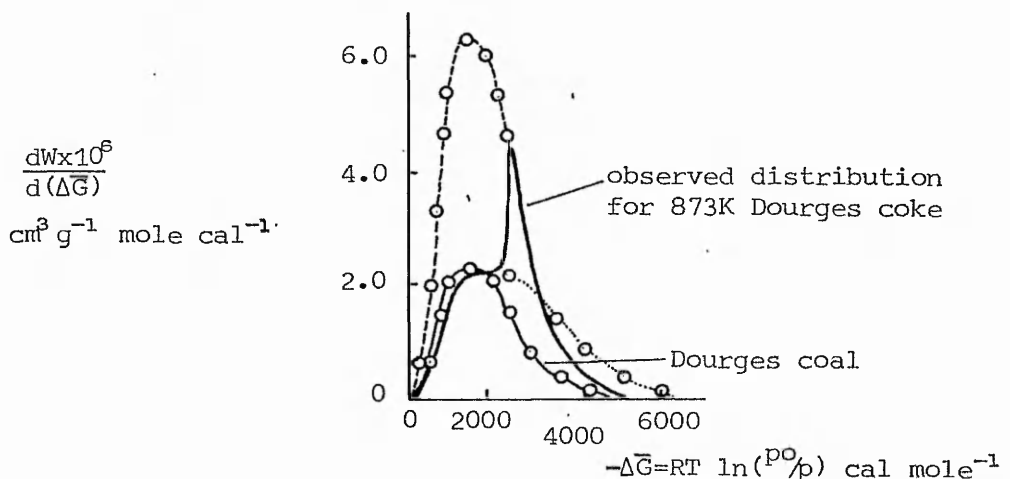


Figure 6.4(17)

Distribution of change in partial molar free energy on adsorption with adsorption volume for Dourges coal and 873K Dourges coke. (138)

by the distribution associated with the low intercept plot of figure 6.4(15) for the 873K coke.

In addition Chiche¹³⁸ notes that from a comparison of the observed distribution curve with that constructed for the low intercept D-R Type I plot it would appear that pores of very small size do not adsorb carbon dioxide to the predicted extent. Chiche¹³⁸ considers that this may indicate removal of some micropores on heat treatment by a widening rather than a narrowing mechanism.

An additional type of deviation from linearity of the D-R Type I plot, apparently not described in the Marsh and Rand¹⁰² classification has been reported by Marsh¹¹⁹. At very low values of $(\log \frac{p}{p_0})^2$ (i.e. very high relative pressures) Marsh¹¹⁹ has observed an upturn in the D-R Type I plot for the adsorption of nitrogen at 77K on polyfurfuryl alcohol carbon (95.5% burn-out) containing iron as an added impurity [figure 6.4(18)].

Whilst Marsh¹¹⁹ attributed this sudden upturn to the filling of transitional porosity some doubt must exist as to the accuracy and reproducibility of the corresponding data especially as these are very close to relative pressures at which bulk condensation of the adsorbate is to be expected.

Most of the deductions concerning the structure of microporous materials are based of necessity on adsorption data. However until an alternative experimental technique is available to verify these deductions any statements concerning microporosity and in particular the dimensions of microporosity must be viewed with extreme caution.

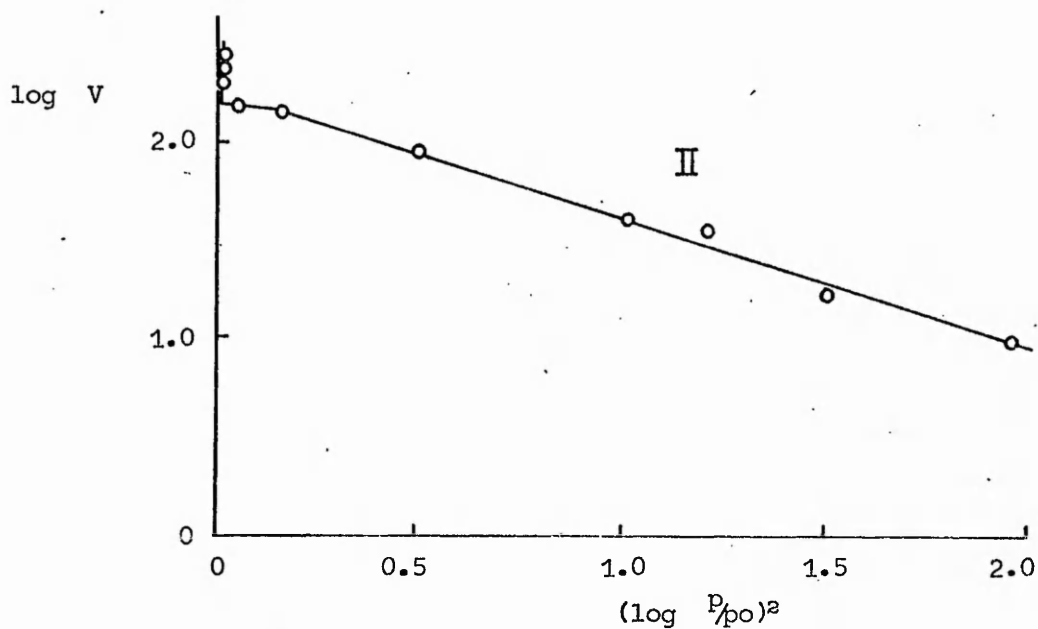


Figure 6.4(18)

D-R type I plot constructed according to equation 6.4(2) for the adsorption of nitrogen at 77K on 1023K polyfurfuryl alcohol carbon containing iron impurity (Fe:C=1:1000) activated to 95.5% burn-out ($V =$ volume of adsorbate expressed as a vapour at S.T.P., $\text{cm}^3 \text{g}^{-1}$). (119)

CHAPTER 7

Experimental Methods

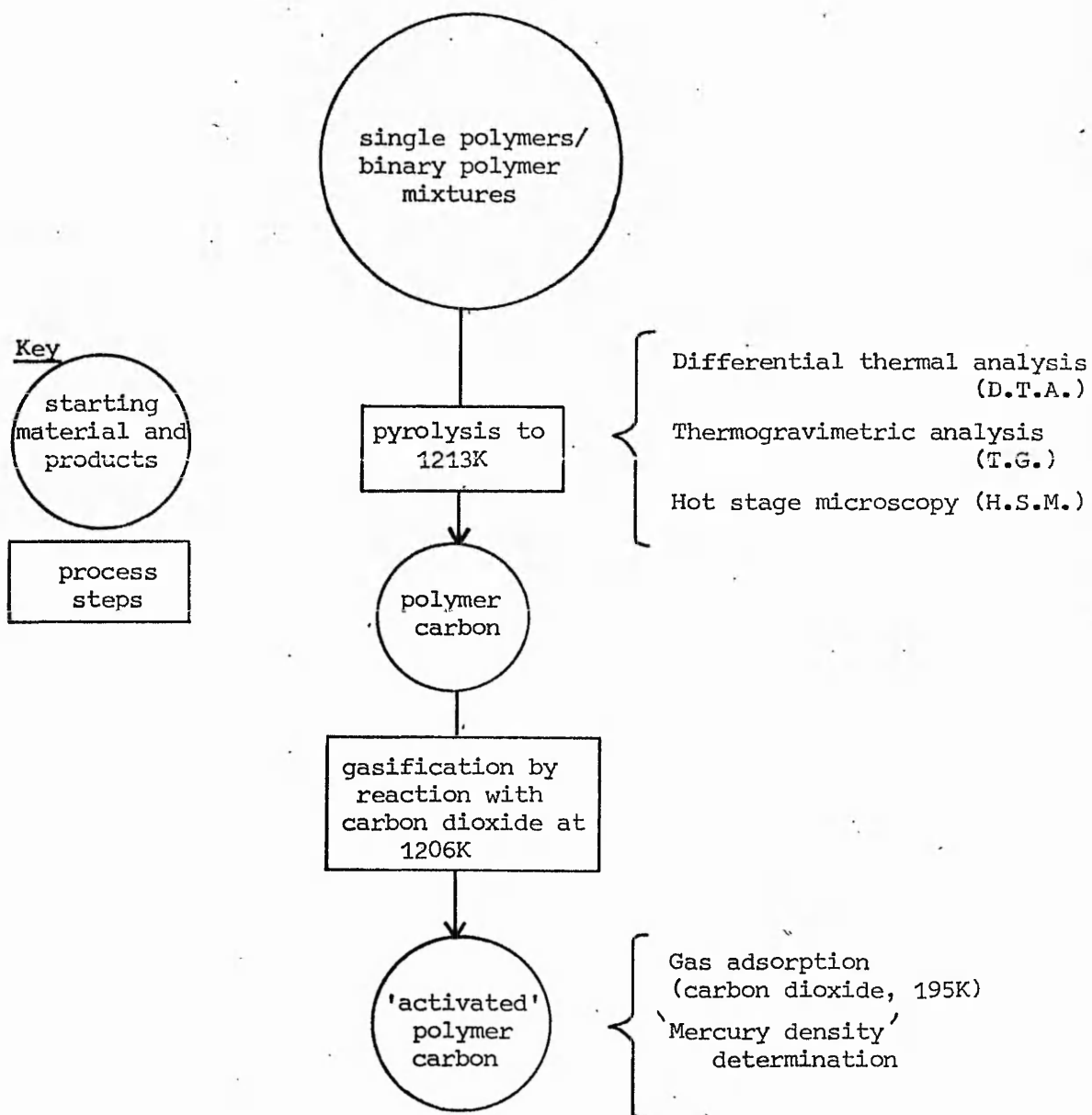
7.1 Introduction

The experimental techniques employed in this study are displayed schematically in figure 7.1(1).

A large scale pyrolysis procedure was adopted to produce carbon in sufficient quantities for gasification and thence the gas adsorption and mercury density studies.

Figure 7.1(1)

Schematic representation of the analytical techniques employed.



7.2 Textile fibres and their preparation

Merino Top 64 wool (mean fibre diameter 23.1×10^{-6} m) was supplied by the Wool Industries Research Association (W.I.R.A.), Leeds. Terylene staple (mean fibre diameter 18.3×10^{-6} m) and Courtelle filament yarn (mean fibre diameter 20.5×10^{-6} m) were supplied by Imperial Chemical Industries, Harrogate and Courtaulds Ltd., Spondon respectively. Mean fibre diameters were determined by the I.W.T.O. standard method¹³⁰ at W.I.R.A., Leeds.

The fibres were cut commercially to a length of 7.5×10^{-4} m and soxhlet extracted with petroleum ether (boiling point range 313-333K) for a period of four hours to remove grease and commercial additives. The wool was additionally extracted with methanol over a four hour period to remove soaps and suint.

The cut and solvent extracted fibres were then air dried at 323K for four hours and then left for twelve hours in the atmosphere to regain their normal moisture content.

Binary mixtures of the fibres were made up to various compositions by mass. A particular fibre mixture is therefore denoted by the two component fibres and their relative proportions expressed as a percentage by mass, e.g. wool 25/Terylene 75 or more briefly W25/T75. Homogeneity of a fibre mixture was achieved by double passage through a British Standard (B.S.) 12 mesh sieve.

All samples for large scale pyrolysis were pyrolysed in pellet form. The pellets were prepared in a die (Research and Industrial Instruments Co Ltd., Mark 3 die) under an applied load of 10,000 lbs (Blackhawk Ltd. hydraulic press). The pellet size range was 0.5 - 0.8 g.

For D.T.A. studies samples of binary polymer mixtures were prepared on a small scale (mass c.a. 0.040 g). The compositions of binary polymer mixtures employed in H.S.M. studies were not determined quantitatively. For T.G. studies a standardised sample mass of 0.1 g was adopted. Samples of binary polymer mixtures for T.G. were specially prepared in these 0.1 g portions.

7.3 Large Scale Pyrolysis

Large scale pyrolysis was carried out in a horizontal tube furnace (Amalgams Ltd., type HT2). The mullite furnace tube had an internal diameter of 4.0×10^{-2} m, and a length of 0.9 m.

The furnace operation was controlled through a temperature controller (Eurotherm type 072) linked to temperature programmer (Eurotherm type LP96/RG) and a process timer (Eurotherm type 200). All samples were subjected to a constant rate of temperature increase ($10 \text{ degrees min}^{-1}$) from ambient to 1213K. The maximum heat treatment temperature (1213K) was maintained for one hour before 'natural' cooling to complete the pyrolysis cycle.

A nitrogen atmosphere was maintained over the sample throughout pyrolysis. A nitrogen flow rate of $1.05 \text{ dm}^3 \text{ min}^{-1}$ through the furnace tube was adopted as standard for all pyrolyses.

All gases employed in this project were high purity grade (Air Products Ltd). Prior to use all gases were dried by passage over activated silica gel.

The textile polymer pellets were pyrolysed in nickel crucibles (internal diameter 2×10^{-2} m, height 2.5×10^{-2} m). The yield of polymer carbon expressed as a percentage of the initial mass of the textile polymer pellets was recorded for each separate pyrolysis experiment.

The values of carbon yield reported in this study represent the arithmetic mean from a minimum of six separate pyrolysis experiments. Reported with each yield is an indication of the range of yield values observed for that particular polymer carbon.

Each polymer carbon product was broken down and graded by sieving. That portion of the product between the sieve sizes B.S.8 and B.S.30 was selected for gasification.

7.4 Thermogravimetric analysis and gasification

Both thermogravimetric analysis (T.G.) of the textile fibres and gasification of the polymer carbon were carried out in a thermobalance (Stanton Instruments type TR-02) modified for operation in a controlled atmosphere. The thermobalance modification and the basic gasification procedure have been described by McEnaney and Rowan.¹²¹

Standardised gas flow rates (entry $1.58 \text{ dm}^3 \text{ min}^{-1}$, exit $1.63 \text{ dm}^3 \text{ min}^{-1}$) were adopted for all gas atmospheres required in both the T.G. and gasification experiments.

A methylated spirit/solid carbon dioxide cold trap was employed in the exhaust line during T.G. experiments to prevent entry of degradation products into the flow-meters.

Details of sample preparation for T.G. are described in section 7.2. In both T.G. and gasification experiments the sample was contained in a circular silica crucible (internal diameter $1.9 \times 10^{-2} \text{ m}$, internal height $1.2 \times 10^{-2} \text{ m}$). A nitrogen atmosphere and an average rate of temperature increase of $9 \text{ degrees min}^{-1}$ over the temperature range ambient -1213K were adopted as standard for the T.G. studies.

An apparent increase in weight or 'buoyancy effect' was observed when an empty silica crucible was heated under the conditions adopted for the T.G. study.

The precise variation of this apparent increase in weight has been postulated as the result of the interplay of several factors.¹²⁵ In this study the 'buoyancy effect' was found to be an approximately linear function of temperature and amounted to $4 \times 10^{-3} \text{ g}$ for an empty silica crucible at 1213K.

The presence of a fibre sample within the silica crucible will add to the 'buoyancy effect' observed for the crucible alone. However as pyrolysis proceeds the volume of this sample will change as the various degradation reactions occur. It was therefore considered impractical to correct for 'buoyancy effects' associated with the volume of the fibre sample. These sample volumes were however assessed to be small in comparison with the volume of the silica crucible-itself. Thus since similar 'buoyancy effects' were operative for successive T.G. experiments it is considered that these effects

cancel when mass loss data over similar temperature ranges are compared. Any differences observed reflecting real variations in actual mass loss behaviour. On this basis no buoyancy corrections have been applied to the T.G. curves included in this study. The residual yields at 1213K observed from T.G. experiments have however been corrected using the 'buoyancy effect' observed for an empty crucible at 1213K.

In the gasification experiments the polymer carbon was heated from ambient to the gasification temperature of 1213±3K in a nitrogen atmosphere. Carbon dioxide was selected as the reactant for the gasification of the carbon samples.

The extent of gasification is termed the burn-out and consists of the mass loss during gasification expressed as a percentage of the original mass of polymer carbon present in the nitrogen atmosphere of the thermobalance at 1213K prior to the commencement of the gasification reaction.

7.5 Gas adsorption

Gas adsorption studies on the activated polymer carbons were carried out using conventional McBain silica spring balances. The experimental technique for the determination of adsorption isotherms using a McBain system is well established. Illustrated in figure 7.5(1) is a schematic representation of the McBain system used in this study.

The silica spring sensitivities were 0.740 m g^{-1} and 0.983 m g^{-1} and the sample mass employed was in the range $0.1 - 0.2 \text{ g}$.

Adsorption isotherms were determined at a temperature of 195K (methylated spirit/solid carbon dioxide bath) using carbon dioxide as the adsorbate. Adsorption measurements were made in the pressure range $6.6 \text{ Nm}^{-2} - 5.7 \times 10^4 \text{ Nm}^{-2}$.

Dovaston et al¹¹⁶ consider that carbon dioxide (195K) is a satisfactory adsorbate for adsorption studies on polymer carbons. They¹¹⁶ do however consider that in some unactivated polymer carbon samples entry of the adsorbate molecules into adsorbent pores may be restricted.

Whilst the equilibration time observed for the polymer carbons in this study was relatively short (0.5-1.0 hours) it is possible that restricted entry effects may be operative in some of the unactivated and lowly activated samples. No evidence was found however to indicate that such effects were in fact operative.

It has been postulated by both Spencer¹²⁶ and Dubinin¹²⁷ that carbon dioxide is adsorbed at 195K as a supercooled liquid, although Dubinin¹²⁷ has postulated that the first layer of carbon dioxide next to the adsorbent surface may be considered as a two-dimensional solid.

Lamond and Marsh¹²⁸ therefore extrapolated the vapour pressure data for liquid carbon dioxide¹²⁹ and obtained a value of $1.89 \times 10^5 \text{ Nm}^{-2}$ for the saturation vapour pressure at a temperature of 195K. This value has been employed in the current study.

Dubinin¹²⁷ measured the variation with temperature of the mass of carbon dioxide required to fill a particular adsorption volume in a small pore silica gel. From these data Dubinin¹²⁷ calculated the density of carbon dioxide at 195K and obtained a value of 1.36 g cm^{-3} . However this density value represents an extrapolation of the available

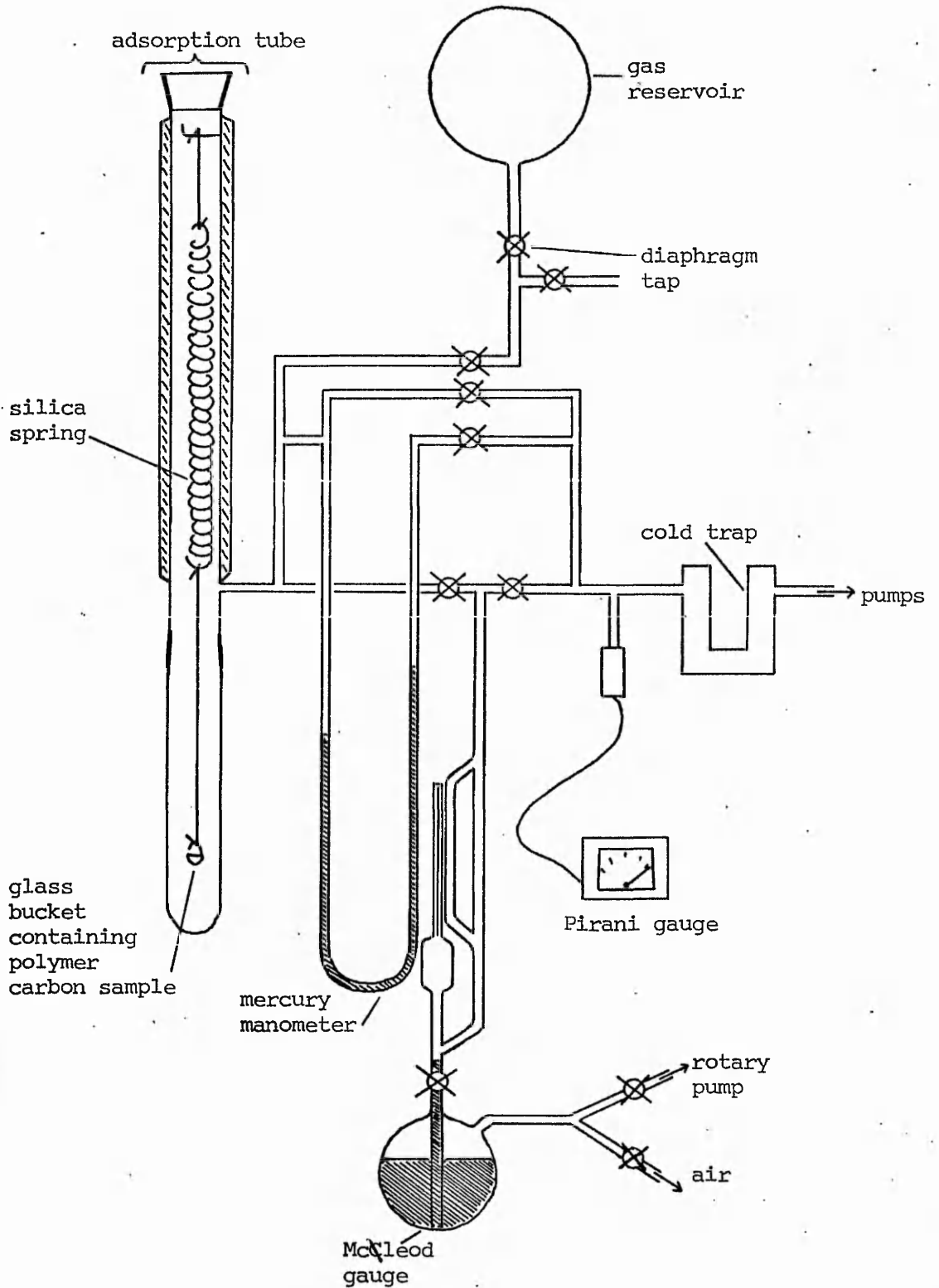


Figure 7.5(1)
 Schematic representation of McBain system employed in this study.
 (The second adsorption tube is omitted from the diagram)

data and is not therefore entirely satisfactory.

In order to examine the adsorptive behaviour of individual polymer carbons the D-R type I equation was employed. It was considered more realistic in applying the D-R type I equation to plot $\log \underline{a}$ against $(\log \frac{P}{P_0})^2$ rather than $\log W$ against $(\log \frac{P}{P_0})^2$ where \underline{a} represents the mass of adsorbate adsorbed at pressure \underline{P} and \underline{W} the volume of adsorption space filled at pressure \underline{P} .

As discussed in section 6.1 both these approaches assume a constant density of adsorbate with increasing extent of adsorption. In view of Dubinin's postulate¹²⁷ that the first layer of carbon dioxide adsorbed may be considered as a two-dimensional solid with subsequent adsorption as a supercooled liquid this latter assumption may indeed be questionable.

As will be discussed in a later section it was considered unsound to apply the D-R type I equation to data obtained at a pressure below 12.8 Nm^{-2} . In view of this lower pressure limit it was considered unnecessary to correct measured pressures for thermal transpiration effects. Further spurious mass changes due to the effect of thermal transpiration at low relative pressures were found to be negligible in comparison with the mass changes accompanying adsorption in the large majority of polymer carbons.

The measurement of a range of adsorption isotherms was repeated to check the reproducibility of the overall adsorption technique. It was found that for the arbitrarily adopted standard - adsorption uptake (mg g^{-1}) at a relative pressure of 0.3, the results could be reproduced to $\pm 5 \text{ mg g}^{-1}$. This figure was therefore adopted to describe the accuracy of all the adsorption results.

The effect of buoyancy on the adsorption data of all carbons with an uptake greater than 30 mg g^{-1} was estimated as approximately $\leq 1\%$. This effect was considered negligible and no buoyance corrections have been made to the adsorption data presented.

In view of the overall accuracy adopted to describe the adsorption data any adsorption measurements of $\leq 10 \text{ mg g}^{-1}$ are considered negligible. Further any discussion of adsorption data or derived D-R type I plots where the adsorption uptake is less than 40 mg g^{-1} must be considered in the light of the accuracy describing adsorption

measurements i.e. $\pm 5 \text{ mg g}^{-1}$. Thus for measured uptakes of less than 40 mg g^{-1} the possible error is $\geq 25\%$.

Whilst the buoyancy correction for uptakes of less than 30 mg g^{-1} was determined to be between 1% and 5% of that uptake it was considered to lie within the error range of the adsorption measurements and was also neglected.

Listed in table 7.5(1) are the individual polymers and binary polymer mixtures pyrolysed and activated by the techniques described in sections 7.3 and 7.4 respectively. Adsorption isotherms were determined for all the activated polymer carbon prepared from the samples listed in table 7.5(1).

Table 7.5(1)

Single polymers

Wool (W)

Courtelle (C)

Terylene (T)

Binary polymer mixtures

Wool/Courtelle

Wool/Terylene

Courtelle/Terylene

Compositions (mass %)

W90/C10

W90/T10

C90/T10

W75/C25

W75/T25

C85/T15

W60/C40

W60/T40

C75/T25

W50/C50

W50/T50

C65/T35

W35/C65

W40/T60

C55/T45

W25/C75

W25/T75

C50/T50

W15/C85

C25/T75

7.6 Mercury density determination

The 'mercury densities' of selected polymer carbons were determined employing the apparatus and experimental procedure developed by Dollimore et al.¹²² The density bottle and vacuum jacket within which this density bottle is located are illustrated in figures 7.6(1) and 7.6(2) respectively.

The practical technique of density determination was developed using Sutcliffe Speakman carbon (type 203B). A sample size of 0.080 g was adopted as standard for the technique and an average value for the 'mercury density' of the type 203B carbon was determined as $1.05 \pm 0.03 \text{ g cm}^{-3}$.

As only a limited quantity (0.2 g) of each activated polymer carbon was available from the adsorption studies, each 'mercury density' value determined for these carbons was taken as the mean of two separate density determinations.

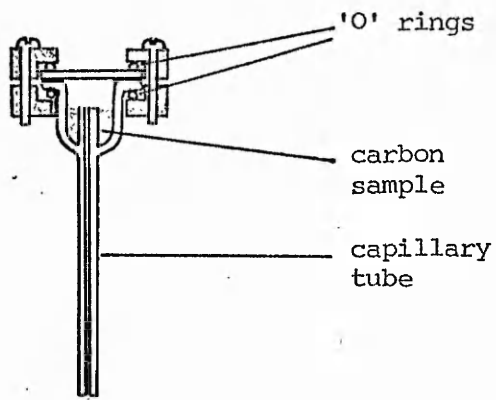


Figure 7.6(1)
Cross section of density bottle

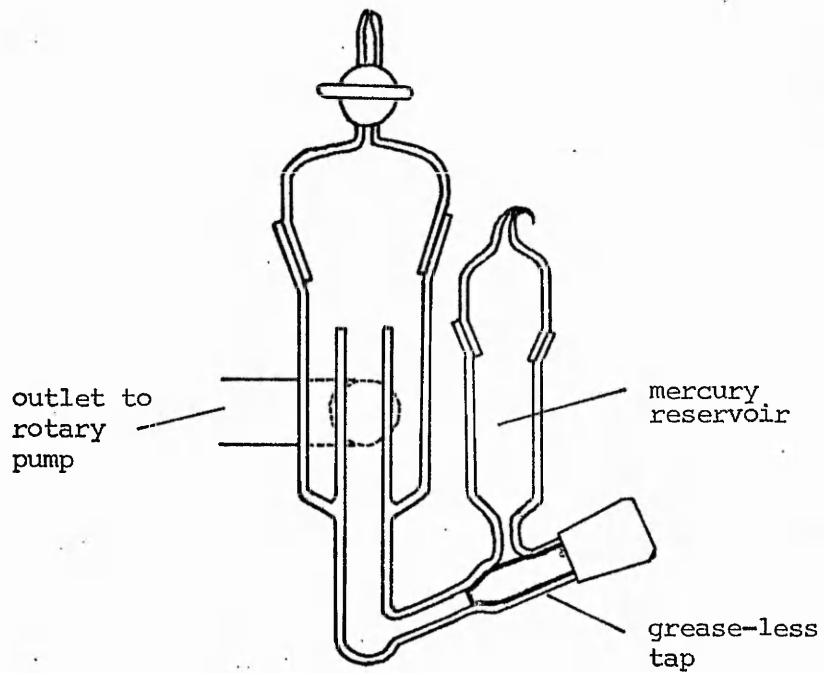


Figure 7.6(2)
Density system as developed by Dollimore et al.¹²²

7.7. Differential Thermal Analysis

The D.T.A. apparatus employed in this study (Stanton Redcroft 67 system fitted with a standard IB module) operated over the temperature range 123K-773K. The D.T.A. cell assembly is illustrated in cross-section in figure 7.7(1). The thermocouple junctions were welded to the bases of the two metal platforms which in turn are mounted symmetrically in the base of the furnace cup.

The difference in temperature (ΔT) between the sample and the reference material and the sample temperature (T_{sample}) were both recorded (ordinate) against time (abscissa) on a two channel recorder (Smiths Industries Servoscribe type RE 520.20).

The fibres were washed and mixed as described in section 7.2. A sample size of 3×10^{-3} - 4×10^{-3} g was adopted as standard. Sample dilution was considered unnecessary.

Kieselguhr (BDH) was selected as the most suitable reference material, one criterion being the base-line stability achieved. Prior to use the kieselguhr was maintained at a temperature of 1173K over a period of 24 hours.

Work by Yariv et al¹²³ has indicated that interaction of the sample material or its decomposition products with the reference material and diluent (if employed) may take place giving rise to spurious peaks in the D.T.A. curve. Yariv et al¹²³ consider that interaction may take place through the mechanism of physical or chemical adsorption. They did however produce evidence which indicated that little interaction took place between kieselguhr and benzoic acid or its decomposition products.

However Manley¹²⁴ investigating the reactions occurring between alkyd and melamine resins in surface coatings observed spurious peaks in the D.T.A. curve. The alkyd and melamine resins were deposited on kieselguhr using a xylene based solvent.

Further investigation indicated that the spurious D.T.A. peaks were related to oxidation of residual solvent absorbed in the kieselguhr. However continuous vacuum drying at an unspecified temperature for a period of 24 hours was found to be ineffective in removing this adsorbed solvent.

In the present study where kieselguhr was employed mainly as a reference material and only occasionally as an inert support it was

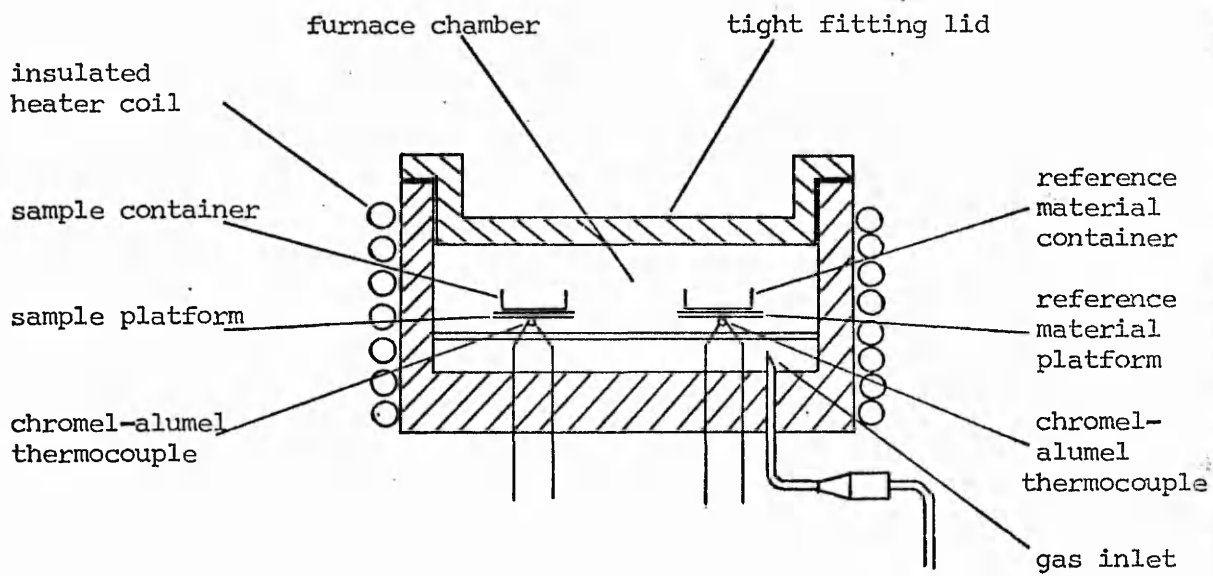


Figure 7.7(1)
 Cross-section of D.T.A. cell assembly.

considered that interactions involving a solvent as observed by Manley¹²⁴ were unlikely to occur. Further no evidence was found to suggest the occurrence of interactions between the sample or its degradation products and kieselguhr when the latter was employed either as a reference material or as a diluent. Kieselguhr was therefore considered satisfactory as both a reference material and as an inert support.

The sample and reference materials were placed in circular flat bottom aluminium dishes (diameter 0.5×10^{-2} m, height 0.2×10^{-2} m) which were sited on the platforms illustrated in figure 7.7(1). The addition of loose fitting lids to these dishes was found to improve peak definition. This was presumably as a result of a reduction in heat loss by convection.

A flowing nitrogen atmosphere was adopted as standard to preclude oxidative peaks from the D.T.A. curve. Prior to each heating cycle the cell assembly (total volume 5×10^{-3} dm³) was purged with nitrogen for a period of five minutes at a flow rate of 4×10^{-2} dm³ min⁻¹. This was considered sufficient to completely replace all air in the sample and reference dishes with nitrogen. Immediately before the commencement of the actual heating cycle the nitrogen flow rate was reduced to 1×10^{-2} dm³ min⁻¹.

In the type of D.T.A. apparatus employed in this study the gas flow passes over rather than through the sample material as in some types of apparatus. Thus the entry of nitrogen into and the escape of volatile and gaseous decomposition products from the sample dish depend on the process of diffusion.

Wool/Terylene, wool/Courtelle, Terylene/Courtelle and Terylene/kieselguhr mixtures of various compositions were examined by D.T.A. All samples were heated at a constant rate of temperature increase of 10 degrees min⁻¹.

It was decided to study in detail only those peaks which in the D.T.A. curves of the single components were clearly defined and exhibited peak temperatures reproducible to ± 6 degrees.

Each D.T.A. experiment on a particular sample was repeated at least five times and thus quoted peak temperatures are the arithmetic mean (rounded to the nearest degree) of at least five separate

determinations. Following each quoted peak temperature is a temperature range representing the maximum observed variation in that particular peak temperature.

With the type of D.T.A. cell assembly illustrated in figure 7.7(1) the initial point of departure from the base-line for a particular peak represents the sample temperature at the initiation of the particular change reflected by the occurrence of the peak. However with the occurrence of overlapping peaks in the D.T.A. curves of binary mixtures the sample temperature at the peak maxima itself was adopted as characteristic of the peak. It is acknowledged that the sample temperature at the peak maxima does not correspond to either the temperature of initiation nor the temperature of termination of the process reflected by the particular D.T.A. peak.

7.8 Hot-Stage Microscopy (H.S.M.)

Physical changes occurring in fibre samples during pyrolysis were recorded photographically using a hot-stage microscope (Reichert type M.E.F. fitted with a Vacutherm micro-furnace).

The fibre specimen was observed through an observation window sited beneath the sample.

Observations were made in the temperature range from ambient to 773K.

During all observations a nitrogen atmosphere was maintained in the micro-furnace (flow rate $1.2 \text{ dm}^3 \text{ min}^{-1}$).

Fibre samples were observed, mounted between glass microscope slides positioned on a specially constructed stainless steel sample platform [see figure 7.8(1)].

The sample temperature was measured using an electronic thermometer (Comark type 1602) incorporating a chromel-alumel thermocouple. The thermocouple tip was located between the microscope slides adjacent to the sample.

The furnace was heated by two platinum elements positioned above the sample platform. The heater control unit consisted of a variable regulating transformer requiring manual operation.

Photographs of the sample at various stages of pyrolysis were recorded using a single plate camera attached to the main microscope. The film type employed was Kodak Commercial Ortho (Estar, thick base type 4180).

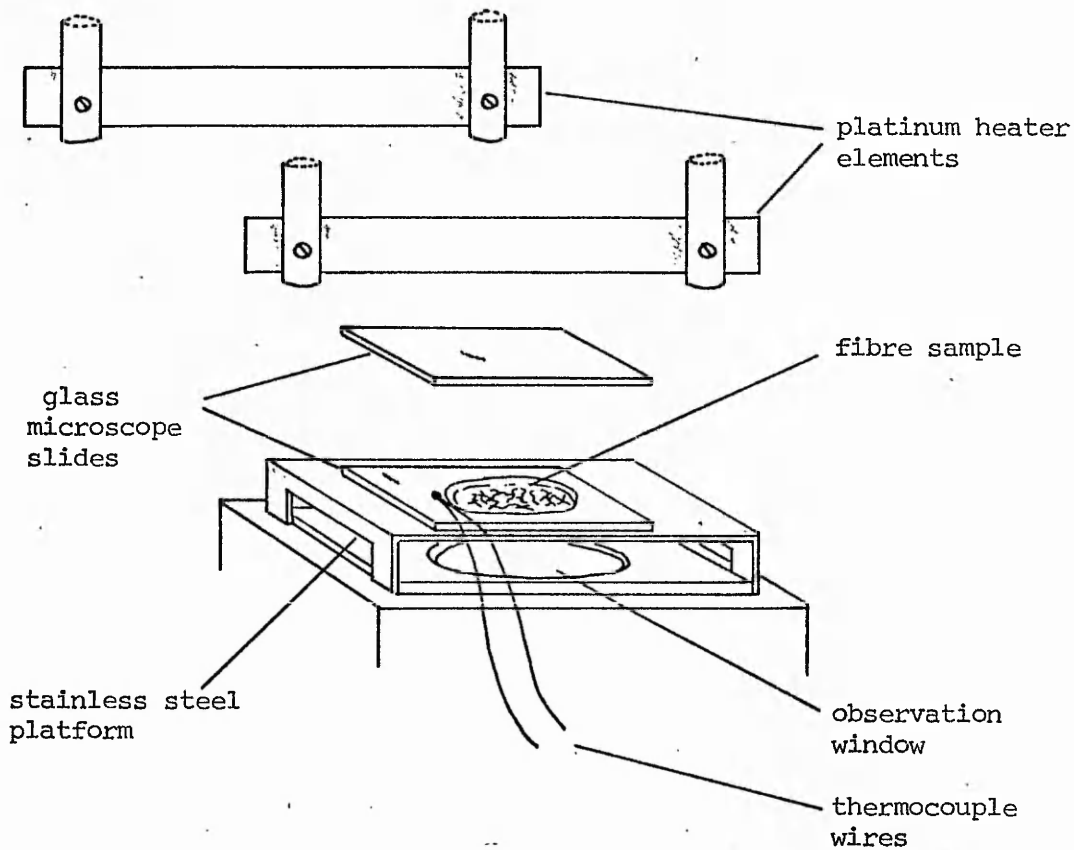


Figure 7.8(1)
Sample presentation for hot-stage microscopy.

CHAPTER 8

Results and discussion of the pyrolysis studies on single polymers

8.1 Introduction

In this chapter and the following chapter the results of the pyrolysis studies on the single polymers and the binary polymer mixtures are presented and discussed.

The pyrolysis behaviour observed for the single polymers using D.T.A., T.G. and H.S.M. is presented separately in this chapter.

In chapter 9 the pyrolysis behaviour observed for the binary polymer mixtures is presented and discussed in the light of the previous observations of the single polymers.

8.2 Merino Top 64 wool

The D.T.A. curve obtained for Merino Top 64 wool is illustrated in figure 8.2(1). Illustrated in figure 8.2(2) is the D.T.A. curve of Merino Top 64 wool obtained after an initial heat treatment. In this heat treatment the wool was heated to a temperature of 421K at 10 degrees min^{-1} and after a hold period of 1 hour at 421K cooled to ambient. The wool was then heated to 773K at 10 degrees min^{-1} and the D.T.A. curve recorded.

In all the D.T.A. curves obtained from this study the differential temperature ΔT (degrees, ordinate) is plotted against sample temperature T_{sample} (degrees, abscissa). By convention endothermic peaks are drawn on the abscissa side of the base-line.

The T.G. curve obtained for Merino Top 64 wool is illustrated in figure 8.2(3). As with all the T.G. data reported in this study, mass loss as a percentage of polymer mass at ambient (ordinate) is plotted against sample temperature T_{sample} (degrees, abscissa).

Illustrated in plates 8.2(1), 8.2(2), 8.2(3) and 8.2(4) are hot-stage microscope photographs of Merino Top 64 wool. Plate 8.2(1) illustrates the appearance of the fibres prior to pyrolysis. Plates 8.2(2), 8.2(3) and 8.2(4) illustrate the appearance of the wool at temperatures of 508K, 583K and 598K respectively during pyrolysis.

In table 8.2(1) are recorded the residual yields of wool carbon observed at 1213K from T.G. and large scale pyrolysis. (L.S.P.)

Schwenker and Dusenbury³⁹ have reported the D.T.A. curve for IWS wool C in a nitrogen atmosphere up to a temperature of 773K. Although substantially similar to the D.T.A. curve illustrated in figure 8.2(1), peak temperatures for the endotherms occurring in the temperature range 473-573K are slightly different. This may reflect the different types of wool fibre employed.

Crighton and Happey³⁵ have reported a D.T.A. curve for Merino 70 wool run under a nitrogen atmosphere.

In a second experiment they isothermed a Merino 70 wool sample at 421K for three hours under continuous evacuation before cooling to ambient. The D.T.A. curve for this wool sample was then determined under conditions of continuous evacuation.³⁵

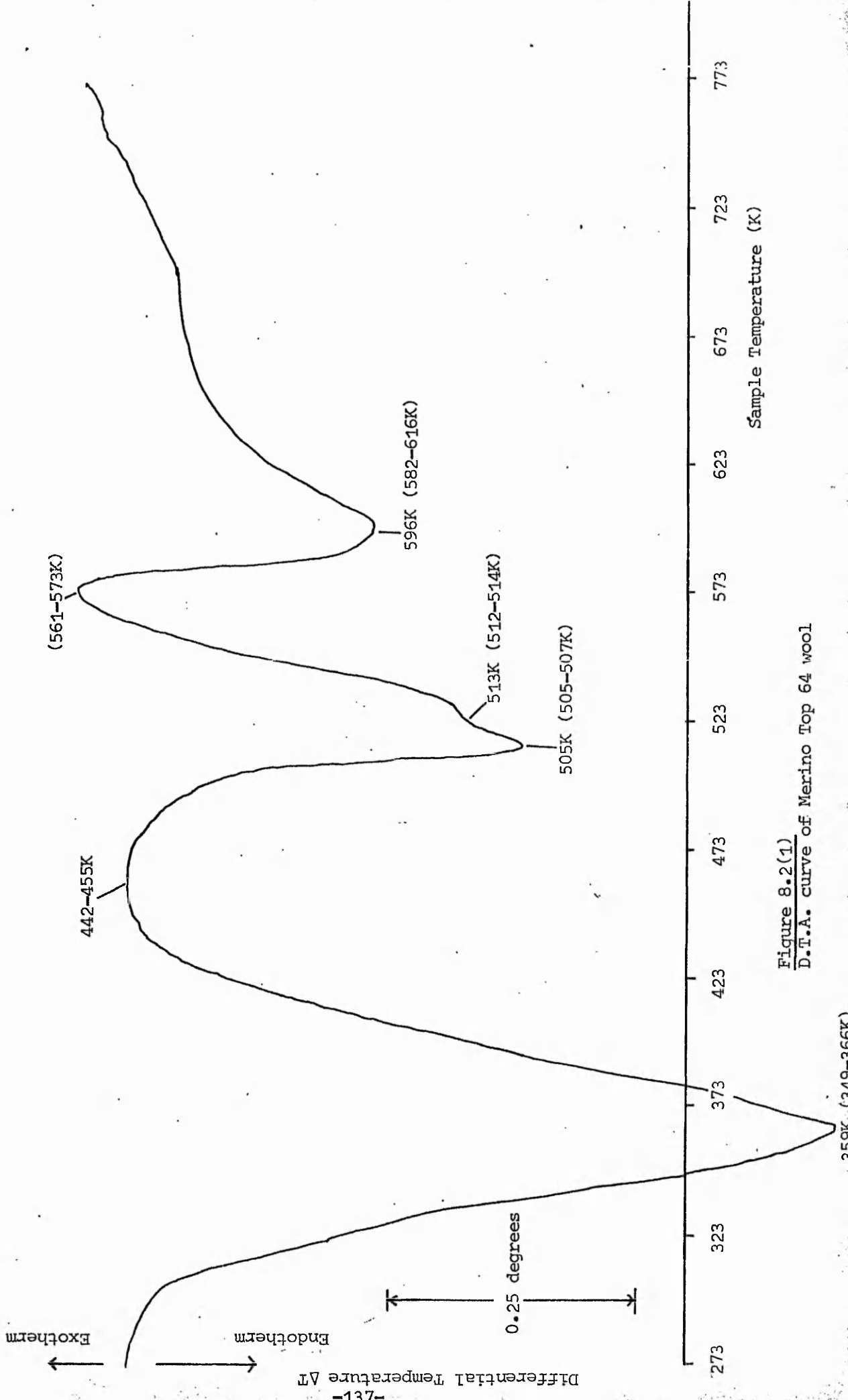


Figure 8.2(1)
D.T.A. curve of Merino Top 64 wool

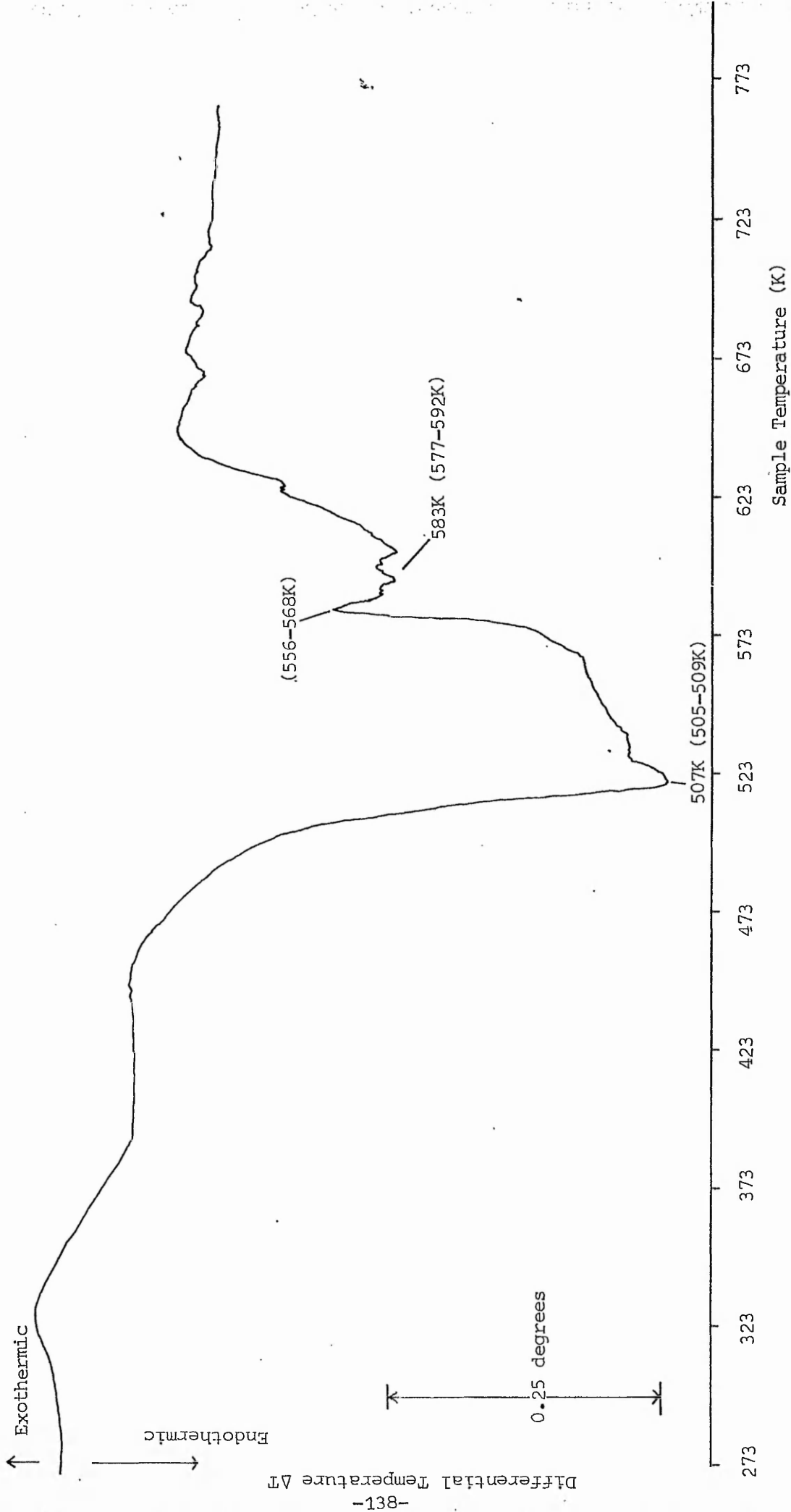


Figure 8.2(2)
 D.T.A. curve of heat treated Merino Top 64 wool.

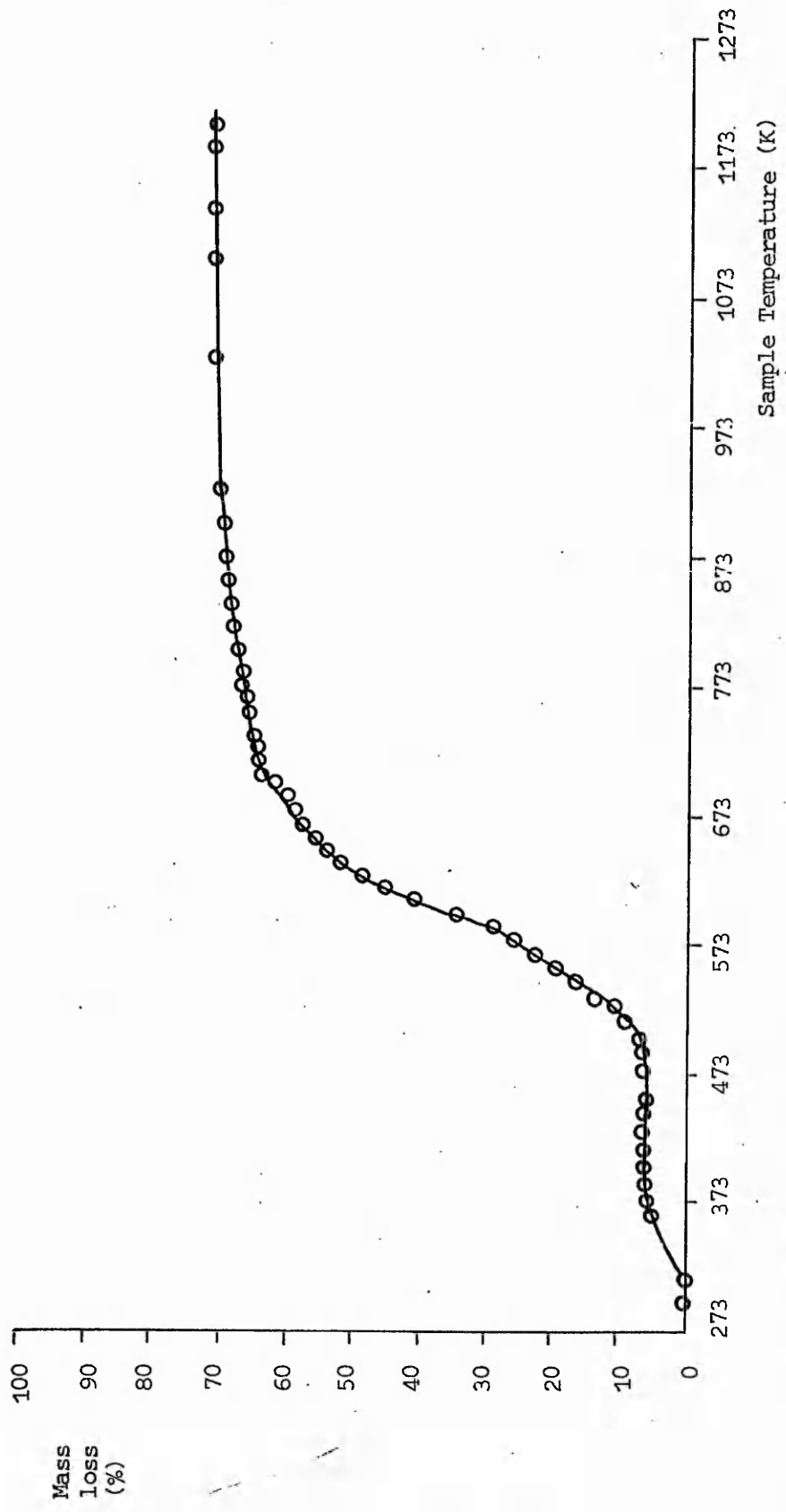


Figure 8.2(3)
T.G. curve of Merino Top 64 Wool.



plate 8.2(1)
Wool fibres at room temperature (294K)



plate 8.2(2)
Wool fibres at 508K

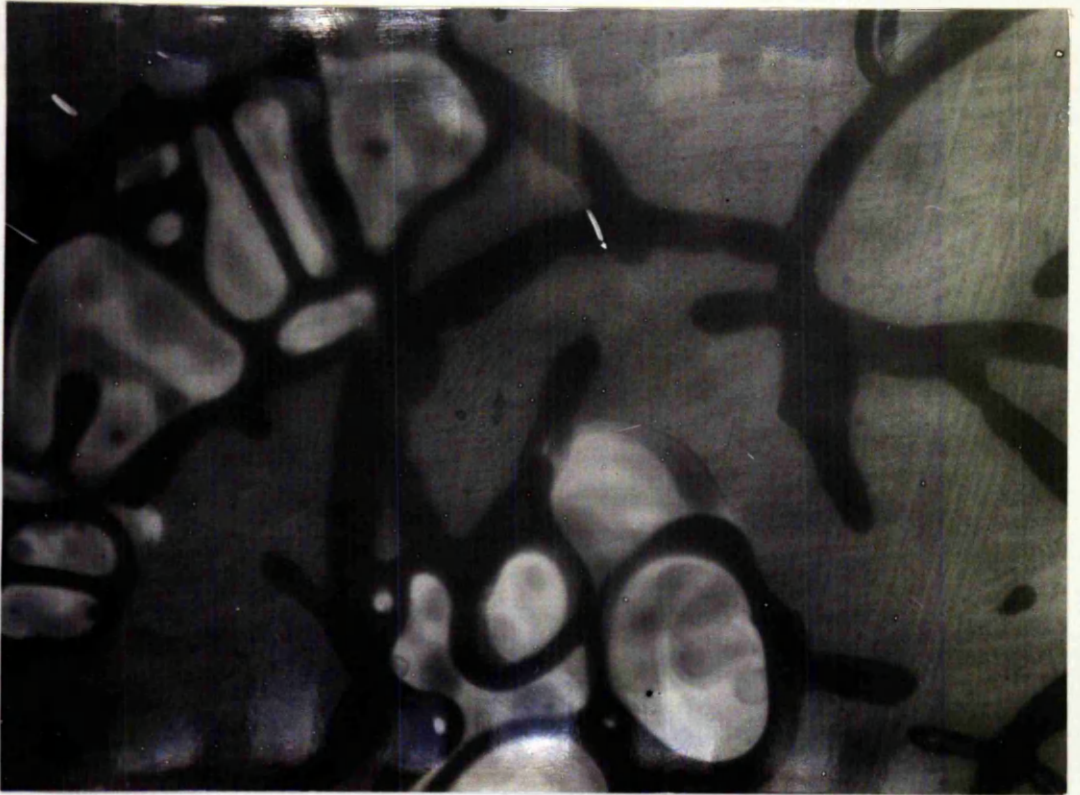


plate 8.2(3)
Wool fibres at 583K

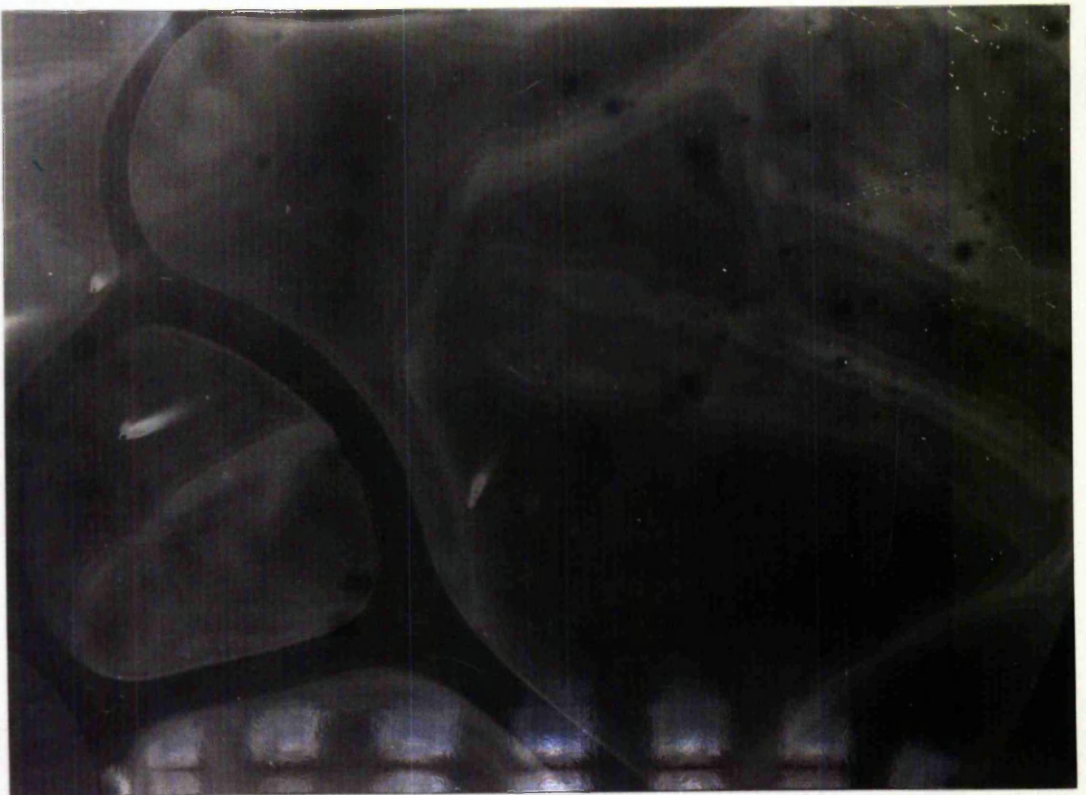


plate 8.2(4)
Wool at 598K

Table 8.2(1)

Residual yield of wool carbon at 1213K from T.G. and large scale
pyrolysis (L.S.P.)

T.G.	L.S.P.
23.5%	20.6%
	(observed range 18.7-22.5%)

Crichton and Happey³⁵ considered that this isothermal heat treatment removed water from the fibre thus eliminating the large low temperature endotherm from the D.T.A. curve. They have suggested that the elimination of this endotherm helps to give a more detailed D.T.A. curve at higher temperatures.

Certainly marked differences in the D.T.A. curves in the temperature range 473-573K were observed from heat treated and non-heat treated wool samples.³⁵

Following a somewhat similar heat treatment applied to the wool samples in this study noticeable changes were observed in the D.T.A. curve (compare figures 8.2(1) and 8.2(2)). Notably the large low temperature endotherm 359K (349-366K) reflecting water loss was eliminated. The endothermic peaks in the temperature range 473-573K appeared broader and the high temperature endotherm was more jagged in appearance.

Direct comparison of the D.T.A. curves obtained for wool after isothermal heat treatment by Crichton and Happey³⁵ and those obtained in this study are not strictly valid in view of the difference in the atmospheres adopted.

As a general comment however it would seem possible that the isothermal heat treatment not only removes water from the fibre but also results in chemical and structural changes within the fibre. It may thus follow that changes of this type account for the differences observed in the D.T.A. curves illustrated in figures 8.2(1) and 8.2(2).

As discussed in the preceding paragraphs the endotherm observed at 359K (349-366K) in figure 8.2(1) represents the loss of loosely bound water. The loss of more strongly bound water reported for wool³⁷ was not resolved, in this study, as a separate peak under a nitrogen atmosphere.

Both the endothermic peak and shoulder which occurred at 505K (505-507K) and 513K (512-514K) respectively (figure 8.2(1)) were reproducible. These endothermic changes were followed by a return to the base-line at 561-573K.

In figure 8.2(2) an endothermic peak was observed at 507K(505-509K) followed by, initially a gradual return to the base-line at 556-568K. Various shoulders were observed in this region of base-line return. They proved however to be unreproducible.

In figure 8.2(1) a further endotherm was observed at 596K (582-616K). The peak was somewhat jagged in appearance and the peak temperature was found to be somewhat variable. These factors indicated that the sample may be melting and/or bubbling.

If indeed fusion and degradation reactions occurred then changes may be expected in the thermal contact between sample and sample dish together with variations in the thermal parameters of the sample itself.

The endotherm observed at 583K (577-592K) in figure 8.2(2) also exhibited a variable peak temperature and was jagged in appearance. The same comments may therefore be applied to this endothermic peak.

Following the endotherms observed at 596K (582-616K) and 583K (577-592K) in figures 8.2(1) and 8.2(2) respectively a gradual movement of the curve in the exothermic direction was observed.

The T.G. data illustrated in figure 8.2(3) showed an initial mass loss of 6% reflecting water loss. The sample mass then stabilised until the temperature reached 483K.

Mass loss recommenced above 483K reaching a constant rate in the temperature range 503-583K. Above 583K the rate increased somewhat until at 633K the rate of mass loss began to decrease. A slow reduction in the rate was then observed up to the final heat treatment temperature of 1213K.

Using H.S.M. the wool fibres were observed to curl above 508K (see plate 8.2(2)) forming a tangled mass. At temperatures above 513K the fibres began to grow darker in appearance. At approximately 583K bubble formation was observed within individual fibres (see plate 8.2(3)). The fibres fused gradually and eventually the whole field of vision was filled with a dark fused mass (see plate 8.2(4)). Solidification of this fused mass appeared to take place at temperatures above 613K.

In order to assess the significance of peaks observed in the D.T.A. curve of Merino Top 64 wool it is necessary to relate the observed peaks to data provided by both T.G. and H.S.M. employed as complementary techniques.

In the temperature range 503-583K corresponding to the endothermic peak in the D.T.A. curve at 505K (505-507K) (Figure 8.2(1)) a mass

loss of 22% was observed.

Similarly in the temperature range of the endotherm observed at 596K (582-616K) (figure 8.2(1)) a mass loss of 23% was observed. The rate of mass loss decreased above 633K and in the temperature range 633-1213K amounted to a further 21.5%.

This T.G. data is in broad agreement with that reported by Schwenker et al⁴⁷ for wool fibre of an unspecified type.

It would appear from the results of this study that the endothermic peaks observed in the D.T.A. curve at 505K (505-507K) and 596K (582-616K), (figure 8.2(1)), both reflect the occurrence of fairly extensive degradative processes.

In consideration of previous work^{39,41,42,44} it would seem probable that the endotherm at 505K (505-507K) represents disordering or melting of α -keratin together with the occurrence of degradation reactions including disulphide bond cleavage particularly in the amorphous matrix material where these linkages appear to be concentrated.

In view of the large mass loss observed in the temperature range of the endothermic peak observed at 596K (582-616K) it would appear that this peak reflects the occurrence of further, more extensive degradation reactions.

It would seem therefore unlikely that this endotherm solely reflects disordering of β -keratin as previously proposed.³⁹

H.S.M. indicated that fusion of Merino Top 64 wool fibre began at approximately 583K. This contrasts with fusion temperatures of 523-533K and 533K recorded by Felix et al³⁶ and Haly⁴¹ respectively.

It would therefore seem that the endothermic peak at 596K (582-616K) may be attributed to the combined effects of sample fusion and general degradative processes occurring above 583K. Its jagged appearance and variable position are attributable to changing thermal contact and thermal parameters of the sample as previously discussed in this section.

The general exothermic behaviour observed at higher temperatures may reflect the occurrence of cross-linking reactions within the solid pyrolysis residues.

As table 8.2(1) indicates, an approximate residual yield of 20% was obtained after pyrolysis to 1213K. The difference between recorded residual yields from T.G. and L.S.P. will be discussed later.

8.3 Terylene

The D.T.A. and T.G. curves obtained for Terylene are illustrated in figures 8.3(1) and 8.3(2) respectively.

Illustrated in plates 8.3(1), 8.3(2) and 8.3(3) are hot-stage microscope photographs of Terylene. Plate 8.3(1) illustrates the appearance of the fibres prior to pyrolysis. Plates 8.3(2) and 8.3(3) illustrate the appearance of the Terylene at 530K and 698K respectively during pyrolysis.

Recorded in table 8.3(1) are the residual yields observed at 1213K from T.G. and large scale pyrolysis.

The endothermic peak occurring in the D.T.A. curve (figure 8.3(1)) at 325K (320-329K) probably represents the loss of water from the fibre.

A displacement of the base-line in the exothermic direction was observed at 417K (415-419K). This may reflect the remnants of an exothermic crystallisation process observed by Scott¹³² at 413K in amorphous PET.

The prominent endothermic peak observed at 530K (529-531K) reflects the occurrence of fusion and corresponds to that observed by Schwenker and Beck⁵¹ at 535K for Dacron run under a nitrogen atmosphere.

Plate 8.3(2), a hot-stage microscope photograph taken at 530K illustrates the fusion of the Terylene fibres.

At temperatures between 653K and 673K an exothermic peak was observed in the D.T.A. curve. The peak itself was however jagged and variable in shape possibly reflecting bubbling within the sample. Indeed hot-stage microscopic observations indicated bubbling within the fused Terylene at approximately 673K. No attempt has been made to assign a peak temperature to this exotherm.

This exotherm corresponds to exothermic peaks observed in drawn Dacron fibre (nitrogen atmosphere) by Gillham and Schwenker⁴⁹ and Schwenker and Beck⁵¹ at 653K and 662K respectively.

Following this exothermic activity an endothermic peak [peak temperature 710K (702-712K)] followed by an exothermic peak [peak temperature 745K(741-746K)] were observed (see figure 8.3(1)).

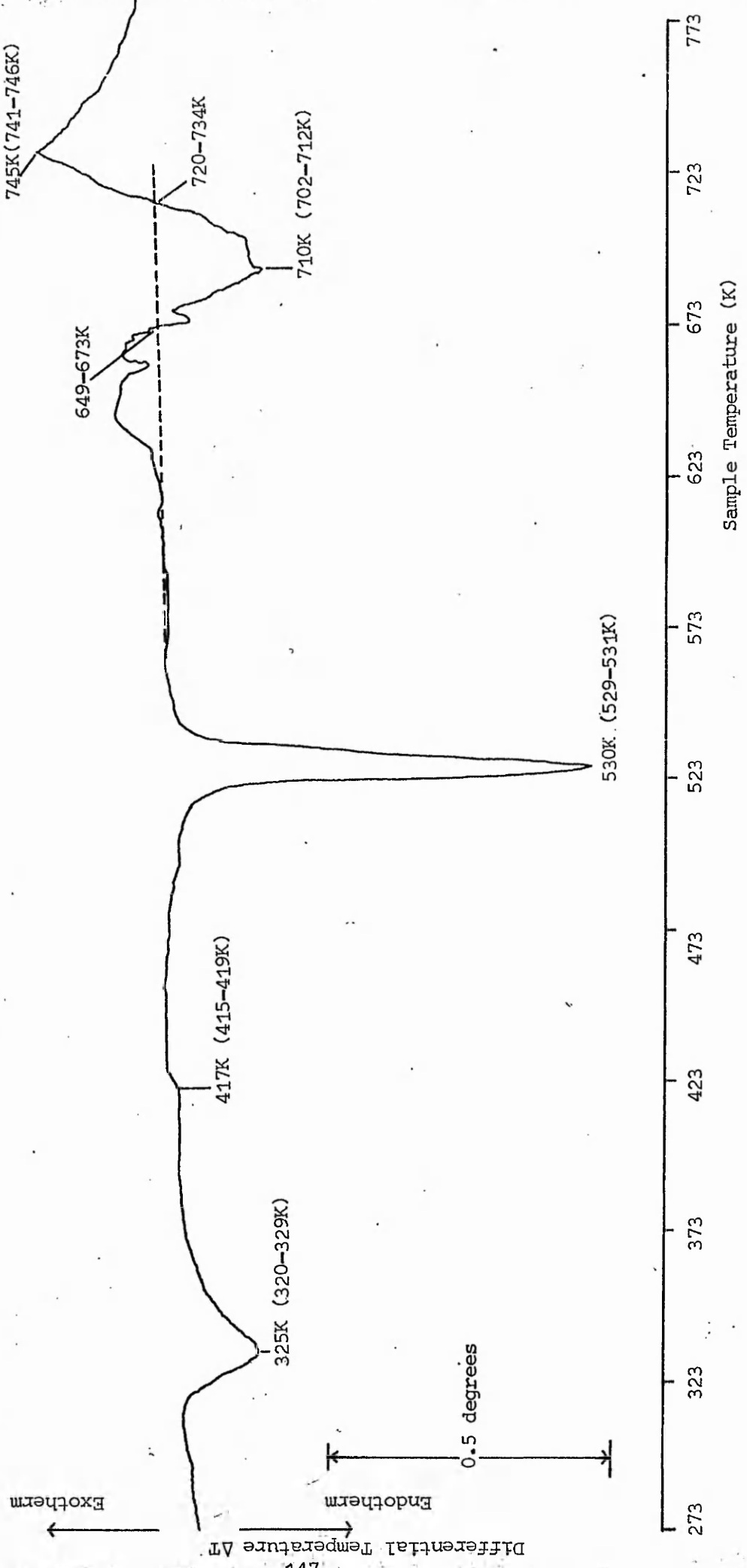


Figure 8.3(1)
D.T.A. curve of Terylene

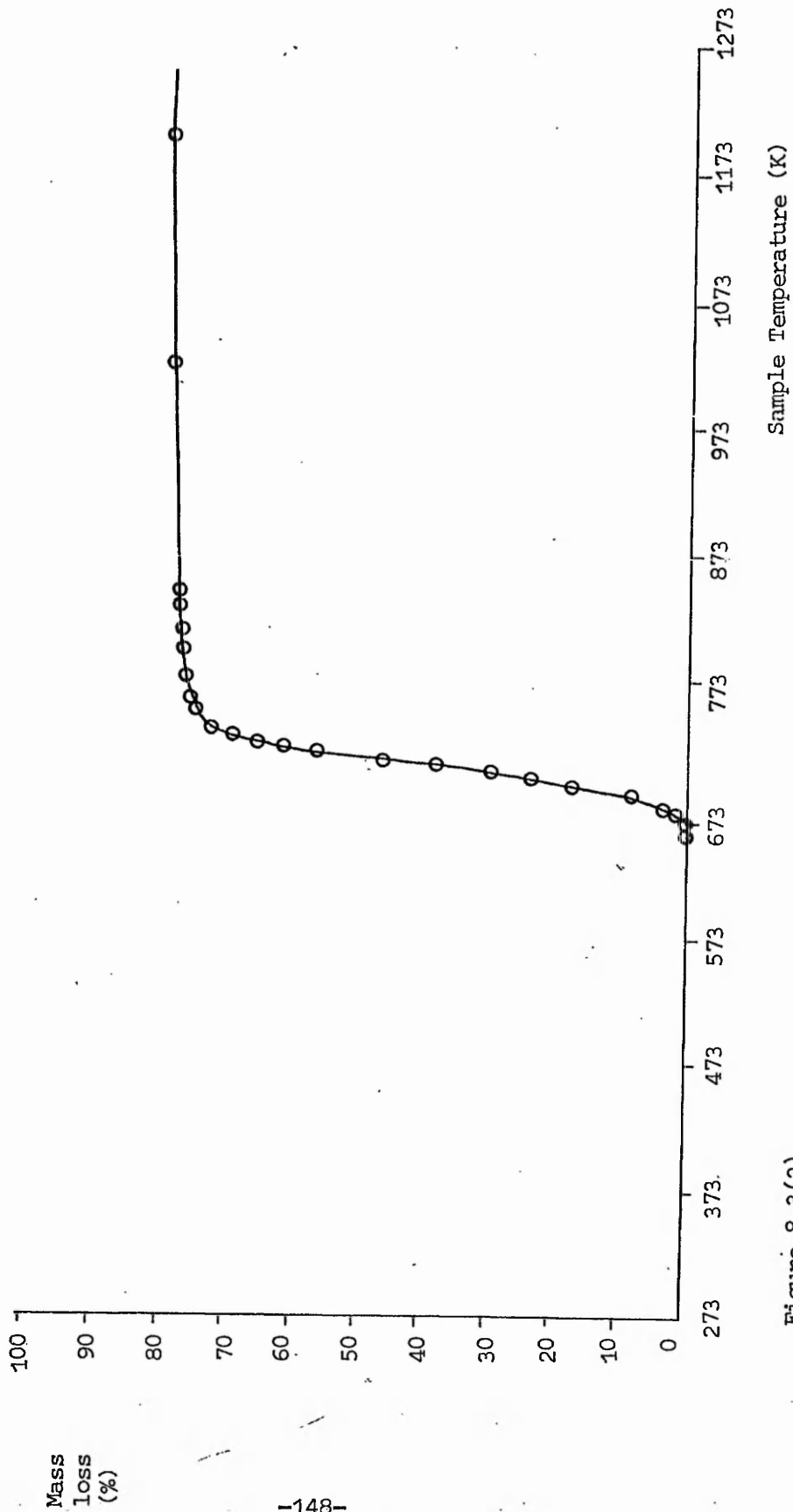


Figure 8.3(2)
T.G. curve for Terylene

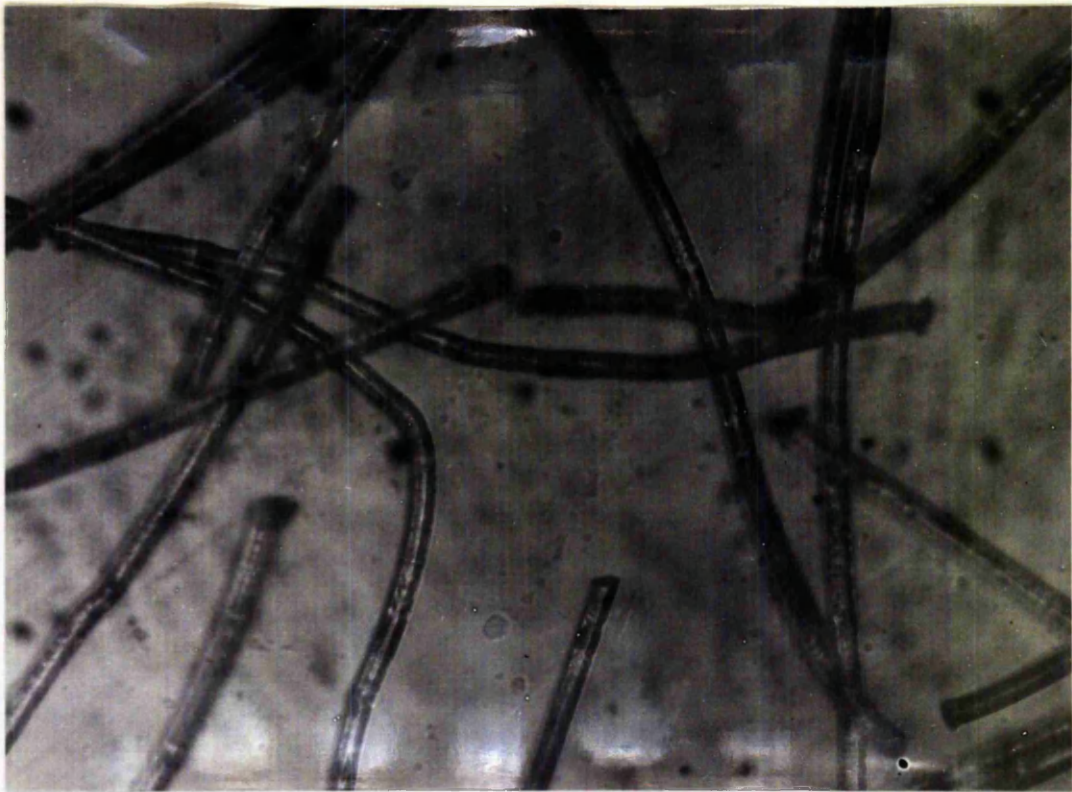


plate 8.3(1)
Terylene fibres at room temperature (294K)



plate 8.3(2)
Terylene fibres at 530K

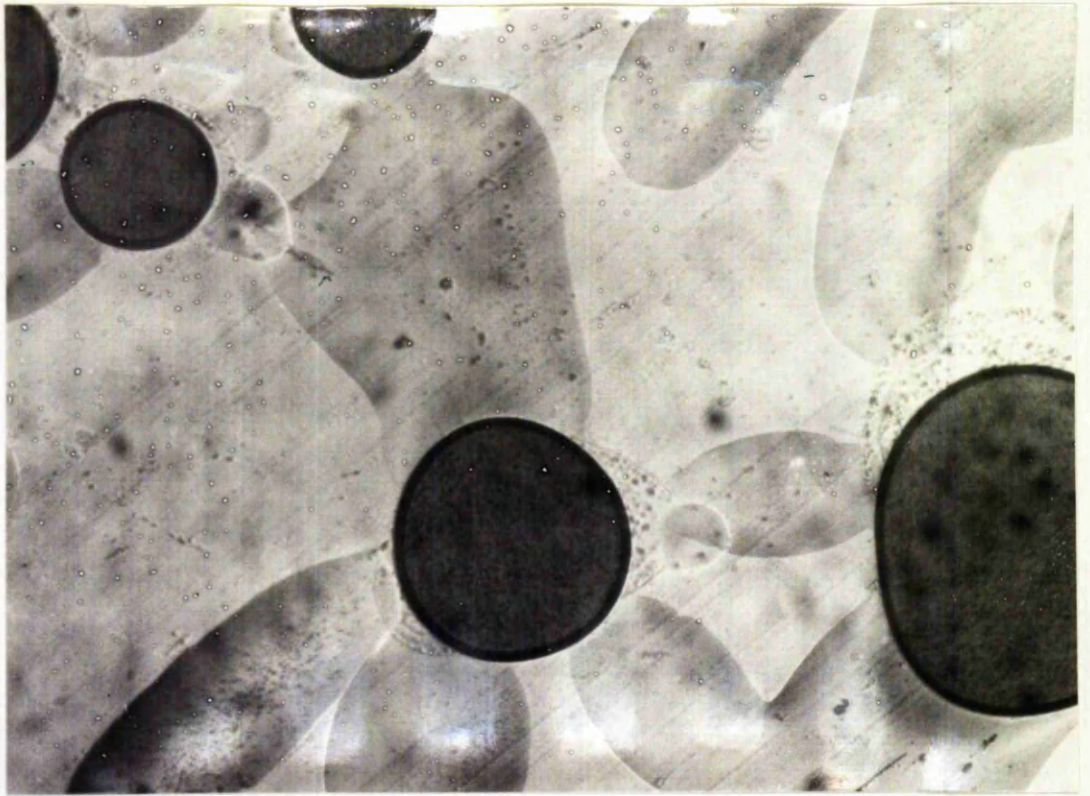


plate 8.3(3)
Terylene at 698K

Table 8.3(1)

Residual yield of Terylene carbon at 1213K from T.G. and large scale pyrolysis (L.S.P.).

T.G.	L.S.P.
16.5%	18.4% (17.9-19.3%)

Again these peaks correspond to the endothermic peak (peak temperature 701K) and exothermic peak (peak temperature 748K) observed by Gillham and Schwenker⁴⁹ for Dacron (nitrogen atmosphere).

The T.G. data illustrated in figure 8.3(2) indicate that significant mass loss commenced at 653K, a mass loss of 7% being recorded between 663K and 683K.

Above 683K the rate of mass loss increased significantly and between 683K and 728K the mass loss amounted to 58%.

At temperatures between 728K and 1213K a gradual decrease in the rate of mass loss was observed. The mass loss recorded in this temperature range amounted to a further 14.5%.

The mechanism of the pyrolytic breakdown of PET as proposed by Buxbaum⁵³ is initiated through main chain breakdown at ester linkages [see figure 3.3(1)]. Various cross-linking reactions involving the products from this breakdown were postulated to take place.

In addition if 2-hydroxy-ethyl end groups are present in the polymer chain these may break down to form acetaldehyde [figure 3.3(2)] or alternatively react with products of degradation [figure 3.3(3)].

In view of these latter reactions of the 2-hydroxy-ethyl end groups Buxbaum⁵³ postulated that no significant decrease in molecular weight should be observed until all the 2-hydroxy-ethyl end groups have been consumed.

It seems reasonable to assume that these recombination reactions involving 2-hydroxy-ethyl end groups constitute an exothermic process where only small concurrent mass losses will be observed. These small mass losses represent evolution of acetaldehyde and other relatively small molecules.

Thus this postulated exothermic reaction accompanied by little mass loss correlates with the exothermic peak observed in the D.T.A. curve in the temperature range 653-683K which was associated with a mass loss of 7% [see figures 8.3(1) and 8.3(2)]. The bubbling observed in the fused Terylene at 673K may therefore reflect evolution of volatile products including acetaldehyde from the pyrolysis residue.

If Buxbaum's postulate⁵³ is correct then once all the 2-hydroxy-ethyl end groups have been consumed the occurrence of chain scission

reactions will result in an effective decrease in the molecular weight of the polymer. The more volatile fragments formed, escape from the residue.

Thus an endothermic process accompanied by considerable mass loss might be expected to follow the previously discussed exotherm. Again this suggestion correlates with the observed D.T.A. and T.G. data, for an endothermic peak was observed in the D.T.A. curve at 710K (702-712K) accompanied by a mass loss of 58%. [See figures 8.3(1) and 8.3(2)].

Schwenker and Beck⁵¹ have observed an endotherm in the D.T.A. curve of Dacron at 720K and both they and Pande⁵² have postulated that this reflects depolymerisation of the polymer.

Following this endotherm, movement of the D.T.A. curve in the exothermic direction was observed with an exothermic peak occurring at 745K (741-746K) [figure 8.3(1)]. Corresponding peaks have been recorded for Dacron run in a nitrogen atmosphere by Gillham⁴⁹ at 748K and at 723K by Schwenker.¹³³

It must be stressed that gross changes in both sample mass and thermal characteristics must occur in the temperature range of the endothermic peak at 710K (702-712K).

Both the endotherm at 710K (702-712K) and the exotherm at 745K (741-746K) were reproducible. It is however possible that whilst exothermic reactions are occurring following the endotherm at 710K (702-712K), the exothermic peak at 745K (741-746K) may be misleading and could be the result of the gross changes in both sample mass and thermal characteristics.

The occurrence of these high temperature exothermic reactions would correlate with the formation of a highly cross-linked residue from PET pyrolysis observed at 773K by Gillham and Schwenker⁴⁹ using Torsional Braid Analysis (T.B.A.).

8.4 Courtelle

The D.T.A. and T.G. curves obtained for Courtelle in this study are illustrated in figures 8.4(1) and 8.4(2). These curves correspond fairly closely with those reported by Turner and Johnson⁵⁷ up to 773K for Courtelle heated in a nitrogen atmosphere at 6 degrees min^{-1} .

Illustrated in plate 8.4(1) is a hot-stage microscope photograph of Courtelle taken at a pyrolysis temperature of 773K. It is clear from the appearance of the fibres that fusion has not taken place. As previously discussed fusion of PAN is only apparently observed⁸⁴ at very high rates of temperature increase, greatly in excess of those employed in this study.

The initial endotherm observed in the D.T.A. curve at 341K (337-344K) probably represents the loss of water from the fibre.

A major exothermic peak was then observed with a peak temperature of 568K (568-570K). The initiation temperature of this peak being observed in the temperature range 465-472K and the base-line return in the temperature range 634-654K.

As the temperature was further increased a second exothermic peak was observed at 689K (676-704K). It is however clear from the quoted temperature range that the actual peak temperature was somewhat variable.

The T.G. data [figure 8.4(2)] indicated that significant mass loss commenced at 543K. A rapid initial mass loss of 10% was observed to 573K.

The rate of mass loss decreased above 573K and by 648K a further mass loss of 11.5% was observed.

Above 648K the rate of mass loss increased and by 738K an additional mass loss of 19.5% was recorded.

From 738K to 1213K the rate of mass loss decreased, and in this temperature range a further mass loss of 12% was observed.

The large exothermic peak observed at 568K (568-570K) in this study corresponds to that observed by Turner⁵⁷ for Courtelle (nitrogen atmosphere) at approximately 533K and 563K (rates of temperature increase of 1 degree min^{-1} and 6 degrees min^{-1} respectively). As previously discussed this exotherm has been considered^{57,58} to reflect the occurrence of the reaction leading to the formation of the ladder

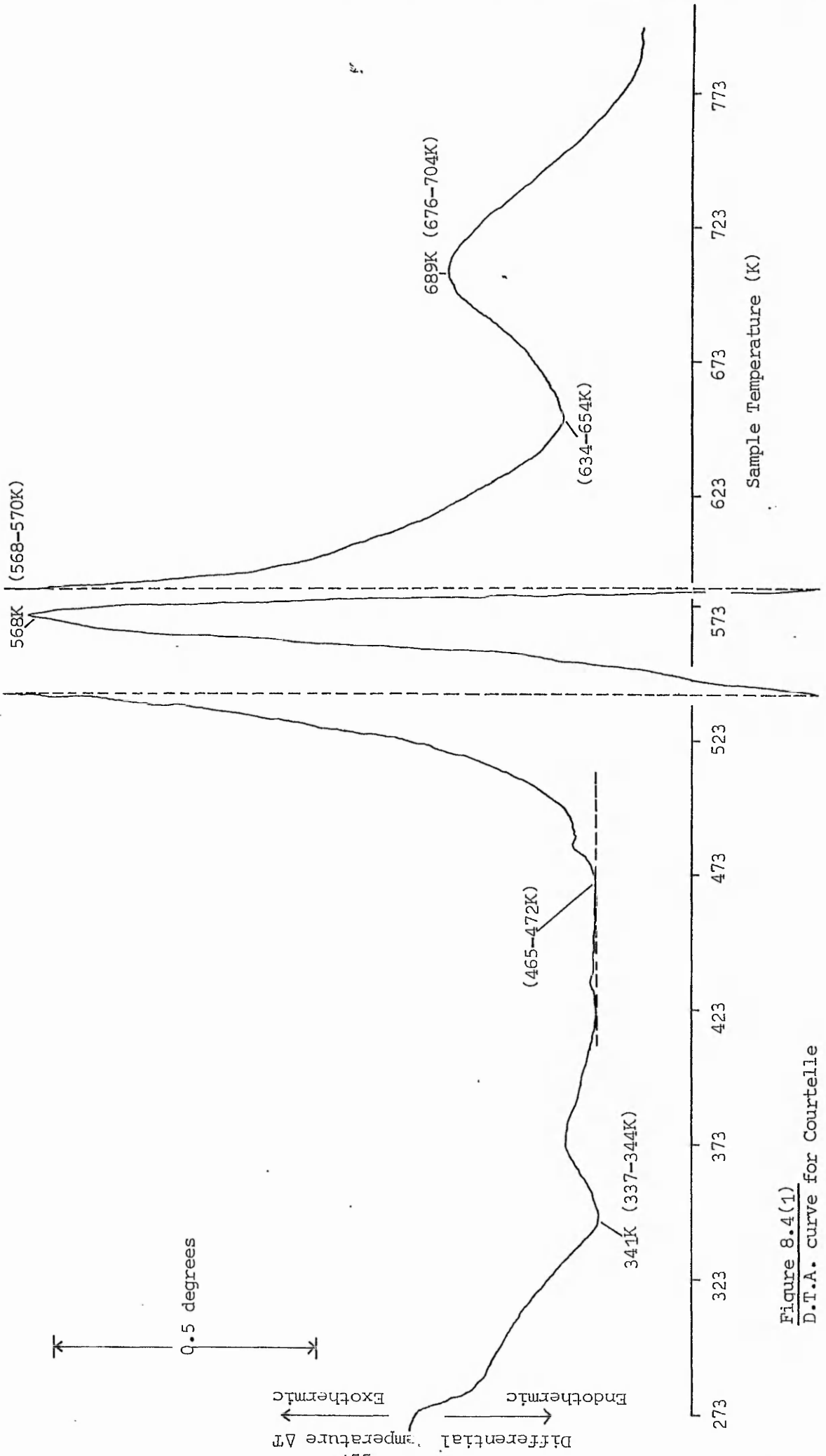


Figure 8.4(1)
D.T.A. curve for Courtelle

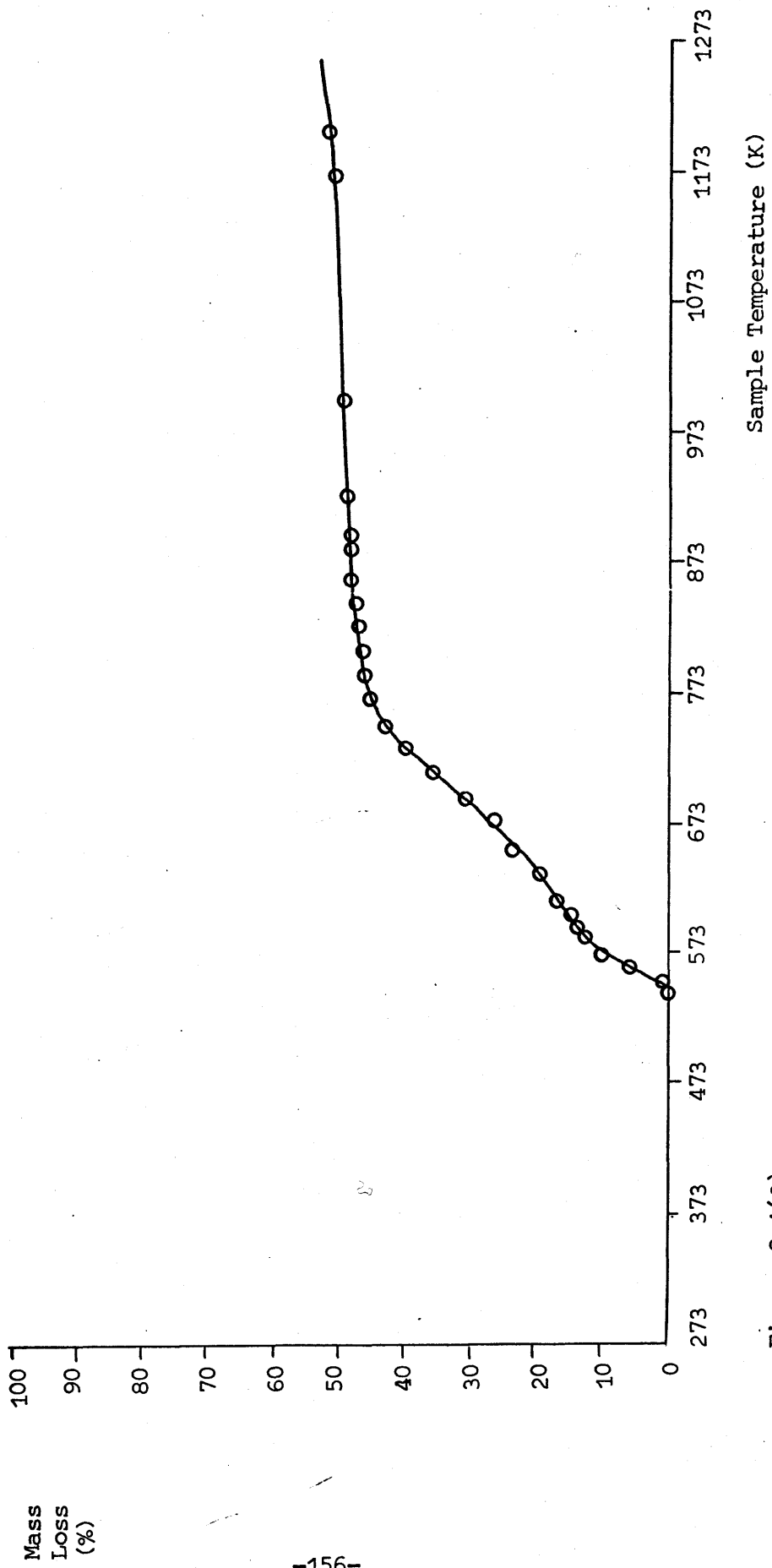


Figure 8.4(2)
T.G. curve for Courtelle

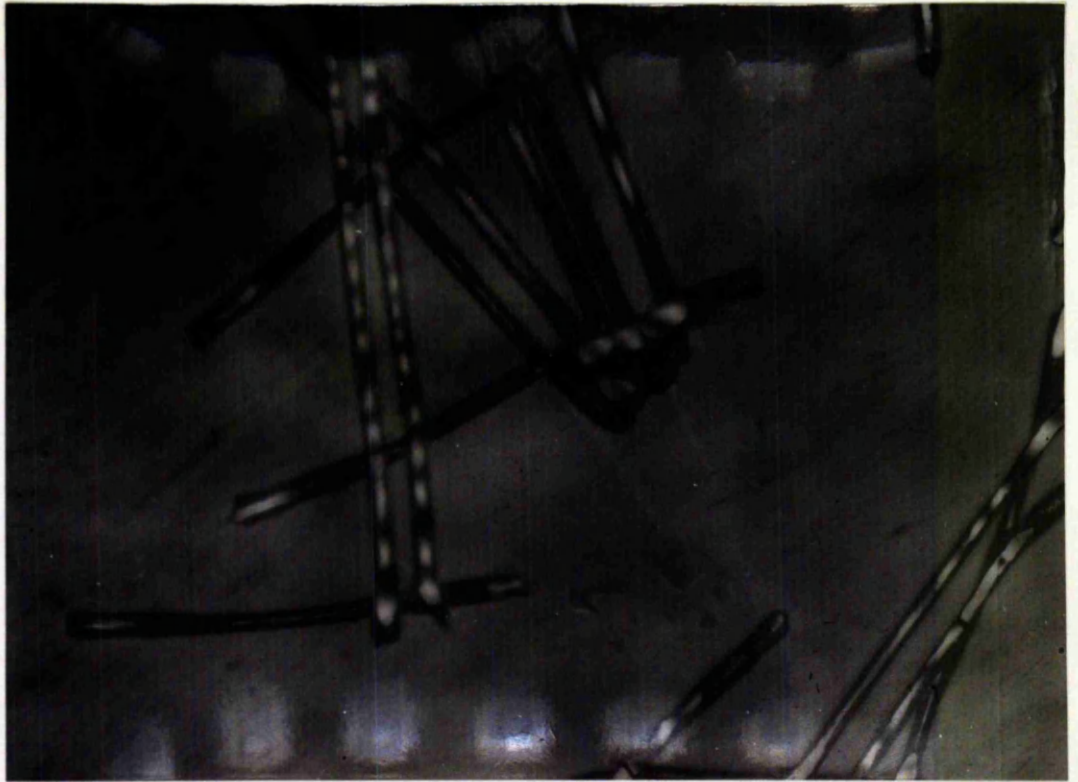


plate 8.4(1)
Courteille fibres at 773K

Table 8.4(1)

Residual yield of Courtelle carbon at 1213K from T.G. and large scale pyrolysis (L.S.P.)

T.G.	L.S.P.
43.0%	43.9% (43.2-44.9%)

polymer structure [see figure 4.2(2)]. The peak temperatures observed for this exothermic peak would seem to be markedly dependent on the rate of temperature increase adopted.

From a comparison of the D.T.A. and T.G. data [figure 8.4(1), figure 8.4(2)] initial mass loss at 543K was observed somewhat after the initiation temperature 465-472K of the large exothermic peak at 568K (568-570K).

The rate of mass loss was observed to increase and then decrease with the observed increase and decrease of the differential temperature in the D.T.A. curve of the exothermic peak at 568K (568-570K).

These observations would correlate with the postulate discussed previously⁶¹ that the magnitude of the differential temperature associated with this exotherm determined the extent of occurrence of chain scission reactions and therefore the extent of mass loss observed.

The rate of mass loss was then observed to increase in the temperature range 648-738K which corresponds approximately with the temperature range observed for the exotherm in the D.T.A. curve, peak temperature 689K (676-704K).

As previously discussed the thermal behaviour of PAN in this temperature range is not firmly established. Indeed the observations of Schwenker⁵¹ suggest that the exotherm observed in this temperature range is associated with an oxidation reaction. Further Turner⁵⁷ has not resolved a discrete exothermic peak in this temperature range from Courtelle (nitrogen atmosphere).

It is however considered that the exothermic peak observed in this study at 689K (676-704K) corresponds with that observed by Gillham and Schwenker⁴⁹ for a PAN film (nitrogen atmosphere) at 703K.

The extent of mass loss observed in the temperature range of this exotherm (19.5%) presumably reflects the continued occurrence of chain scission reactions. Turner and Johnson⁸ have suggested that chain scission reactions make a significant contribution to mass losses observed for Courtelle up to a temperature of 723K. The type of degradation products detected by Watt⁷⁸ in this temperature region would seem to confirm this suggestion.

Whilst chain scission reactions might be expected to be endothermic in nature, the peak observed is in fact exothermic [689K (676-704K)]. Whilst the chemistry of the pyrolysis reactions in this

temperature region is complex the occurrence of cross-linking reactions detected by Watt⁷⁸ in the range 673-773K in PAN fibre may account for the observed exothermic peak [689K (676-704K)] in the D.T.A. curve.

Such cross-linking reactions might be expected to stabilise the pyrolysis residue and indeed the mass losses observed above 738K are in fact relatively small.

The small but continuing mass loss observed in the temperature range 738-1213K presumably reflects mainly hydrogen and nitrogen evolution from the pyrolysis residue possibly through the mechanisms proposed by Turner.⁸

CHAPTER 9

Results and preliminary discussion of the pyrolysis studies on binary polymer mixtures

9.1 Wool/Terylene

Illustrated in figure 9.1(1) are the D.T.A. curves for Merino Top 64 Wool and Terylene together with an example of a D.T.A. curve for a mixture of the two polymers (Wool 25/Terylene 75).

D.T.A. curves were obtained for three wool/Terylene mixtures of composition 25/75, 50/50 and 75/25 (mass %). Further curves were obtained for kieselguhr/Terylene mixtures of composition 25/75, 50/50 and 75/25 (mass %).

Tables 9.1(1), 9.1(2) and 9.1(3) indicate the peak temperatures of the Terylene peaks 530K (529-531K, endotherm), 710K (702-712K, endotherm) and 745K (741-746K, exotherm) in the various wool/Terylene mixtures examined.

In table 9.1(4) are listed the peak temperatures of these Terylene peaks in the D.T.A. curves of the kieselguhr/Terylene mixtures.

Table 9.1(5) indicates the peak temperatures observed for the wool endotherm [505K (505-507K)] in the various wool/Terylene mixtures examined.

Illustrated in figures 9.1(2), 9.1(3) and 9.1(4) are the T.G. curves observed for wool/Terylene mixtures of composition 75/25, 50/50 and 25/75 (mass %) respectively. Superimposed on each curve is the T.G. curve predicted on the basis of the mass loss characteristics of the individual polymers.

The residual yields at 1213K from the large scale pyrolysis of wool/Terylene mixtures are recorded in figure 9.1(5). The maximum observed variation is included for each yield determined.

Table 9.1(6) indicates the residual yield of carbon at 1213K observed by T.G. and large scale pyrolysis from wool/Terylene mixtures.

Illustrated in plates 9.1(1), 9.1(2) and 9.1(3) are hot-stage microscope photographs of a wool/Terylene mixture at various stages during pyrolysis. The exact composition of this mixture was not determined.

Plate 9.1(1) illustrates the appearance of the mixture prior to pyrolysis. Plates 9.1(2) and 9.1(3) illustrate the appearance of the

mixture at temperatures of approximately 508K and 538K respectively.

The D.T.A. curves illustrated in figure 9.1(1) have been displaced relative to each other in the direction of the differential temperature axis to simplify their examination.

As previously discussed only those D.T.A. peaks which were clearly defined and with peak temperatures reproducible to within ± 6 degrees were considered for study.

Most features observed in the D.T.A. curves of the single polymers were also present in the D.T.A. curves of the wool/Terylene mixtures. One major exception was the wool endothermic peak [596K (582-616K), figure 8.2(1)]. This endotherm was observed at 589K (577-606K) in the wool 75/Terylene 25 mixture.

However in both 50/50 and 25/75 wool/Terylene mixtures this endothermic peak was not resolved and was presumably contained within a broad endotherm observed in the temperature range 473-623K.

Tables 9.1(2) and 9.1(3) indicate that considerable displacement of the Terylene endotherm [710K (702-712K)] and exotherm [745K (741-746K)] was observed in the wool/Terylene mixtures. As previously discussed these two peaks observed in the D.T.A. curve of Terylene are associated with polymer degradation reactions.

Tarim and Cates⁴⁶ however could not resolve the corresponding degradative peaks in the D.T.A. curve of a wool 65/Dacron 35 (mass %) mixture (static air atmosphere).

Using the wool 65/Dacron 35 mixture in a cross-differential experiment with a wool 65/asbestos 35 mixture Tarim and Cates⁴⁶ observed the Dacron peaks - exotherm (695K), endotherm (720K) and exotherm (753K) at temperatures of 623K, 673K and 743K respectively.

As previously discussed each D.T.A. peak temperature obtained in this study is reported as a mean of at least six experiments. Each peak temperature is reported with the experimentally observed range of peak temperatures from which this mean value has been derived.

A criterion has been adopted in order to assess the significance of any observed displacement of peak temperature. Only those displacements, where the experimentally observed peak temperature range of adjacent members of the composition range do not overlap, are

considered to be significant.

The composition range consisted of the following:-
e.g. Terylene, T75/W25, T50/W50, T25/W75, Wool.

Employing this criterion the observed displacement of the Terylene endotherm [710K (702-712K)] and exotherm [745K (741-746K)] recorded in tables 9.1(2) and 9.1(3) respectively may be regarded as significant.

It is however clear from table 9.1(1) that no significant displacement of the Terylene endotherm [530K (529-531K)] was observed.

Table 9.1(5) indicates that a small but significant displacement was observed for the wool endotherm [505K (505-507K)] between wool and the wool 75/Terylene 25 mixture. No further significant displacement of this peak was however observed.

The T.G. curves illustrated in figures 9.1(2), 9.1(3) and 9.1(4) indicate that the rapid mass losses observed in the mixtures and possibly reflecting the occurrence of Terylene degradation reactions were observed at lower temperatures than would be predicted from a consideration of the T.G. curves of the single polymers.

Somewhat similar mass loss behaviour has been observed for a wool 50/Dacron 50 (mass %) mixture. Tarim and Cates⁴⁶ consider that this behaviour is due to the occurrence of Dacron mass loss at a temperature approximately 50 degrees below that expected from the T.G. curve for Dacron alone.

An analysis of the T.G. curves illustrated in figures 9.1(2), 9.1(3) and 9.1(4) indicates that no simple relationship exists between mixture composition and the temperature at which deviations from predicted mass loss behaviour occur.

Previous workers^{51,52} have suggested that the peak observed in the D.T.A. curve for Terylene at 710K [(702-712K), endotherm][figure 8.3(1)] probably represents depolymerisation. Further it has been suggested in this study that the exothermic peak 745K (741-746K) is related to the occurrence of cross-linking reactions in the pyrolysis residues of Terylene.

Thus since these two Terylene D.T.A. peaks were observed at lower temperatures in the wool/Terylene mixtures, and mass losses possibly characteristic of Terylene were observed at lower temperatures

in these mixtures, it is considered that the thermal depolymerisation and cross-linking reactions of Terylene occur at lower temperatures in the presence of wool or its degradation products.

Hot-stage microscopic observations of wool and Terylene have indicated that both polymers fuse, wool above 583K and Terylene at 530K. From visual observation of the pyrolysis behaviour of a wool/Terylene mixture it appeared that fused Terylene coated the wool fibres prior to their own fusion above 583K [figure 9.1(3)].

It was therefore considered that the wool in some form may act as a physical support facilitating the degradation of Terylene at lower temperatures.

In order to test this theory, D.T.A. curves were obtained for a series of kieselguhr/Terylene mixtures. The kieselguhr was chosen as a substitute for wool. Whilst kieselguhr does not fuse it was considered chemically and thermally inert and therefore suitable as a purely physical support for the Terylene once Terylene fusion had taken place.

Table 9.1(4), parts (a), (b) and (c) records the peak temperatures observed in the D.T.A. curves of the kieselguhr/Terylene mixtures of the Terylene peaks - endotherm [530K (529-531K)], endotherm [710K (702-712K)] and exotherm [745K (741-746K)] respectively.

It is clear from this data that no significant displacement of these Terylene peaks was observed in the D.T.A. curves of the kieselguhr/Terylene mixtures.

Whilst kieselguhr may have limitations as a substitute for wool in testing the physical support theory, the results obtained using kieselguhr show no evidence to support this theory.

Thus it would appear that wool does not act as a physical support in reducing the temperatures at which Terylene depolymerisation and cross-linking reactions are observed. It would seem therefore that some other form of interaction occurred. Other possible types of interaction will be considered in a later section.

The residual yields at 1213K for the large scale pyrolysis of wool/Terylene mixtures are illustrated in figure 9.1(5) and listed in table 9.1(6). These yields are the arithmetic mean of six or more separate pyrolyses.

From a consideration of figure 9.1(5) it would appear that the residual yields observed for the wool/Terylene mixtures are within the ranges expected on the basis of the yield behaviour of the single polymers.

A fairly wide yield range was observed for the yields of the single polymers and the wool/Terylene mixtures. This observation is worthy of further consideration.

Both wool and Terylene fuse and bubble extensively during pyrolysis as observed by hot-stage microscopy and produce soft coking carbons. This type of pyrolysis behaviour tends to result in the loss of material by overflow from the pyrolysis crucible and hence introduces errors into the recorded yields. A further factor in reducing accuracy is that overall the pyrolysis yields for the wool/Terylene system are low when compared with e.g. the Terylene/Courtelle system.

The residual yields derived from T.G. are the results from single experiments, and hence no estimate of possible errors has been included.

Table 9.1(6) lists the residual yields at 1213K obtained from T.G. and large scale pyrolysis.

For the large scale pyrolysis experiments compressed textile pellets (sample mass 0.5 - 0.8 g) were employed. Samples prepared for T.G. experiments were however uncompressed (sample size standardised at 0.1 g).

These differences in sample presentation together with the inherent differences in furnace geometry between the T.G. and large scale pyrolysis apparatus may account for differences in the residual yields observed by the two techniques. Similar experimental differences are presumably a factor preventing more extensive correlation of D.T.A. and T.G. data.

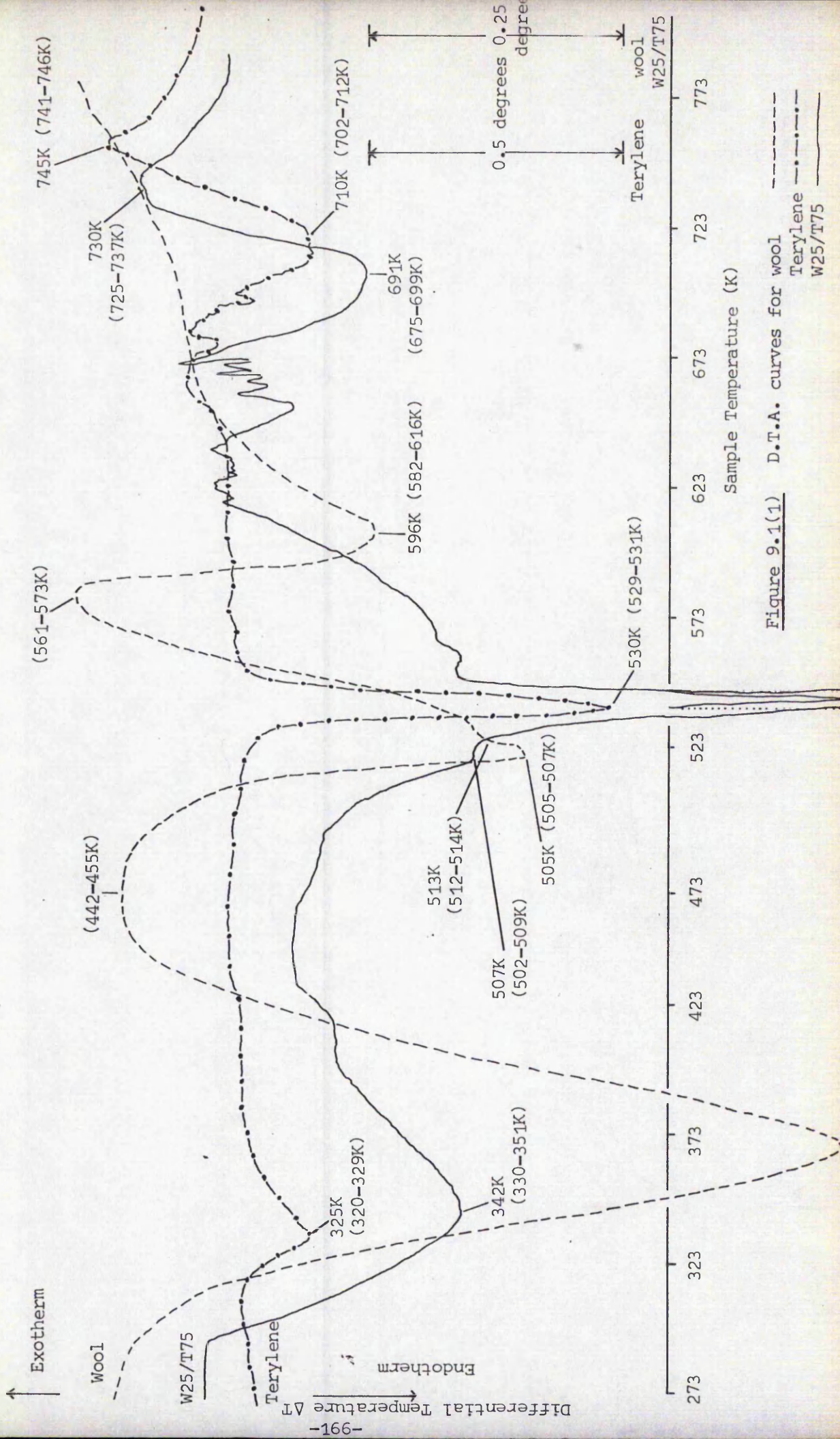


Figure 9.1(1) D.T.A. curves for wool

Terylene
 Terylene W25/T75

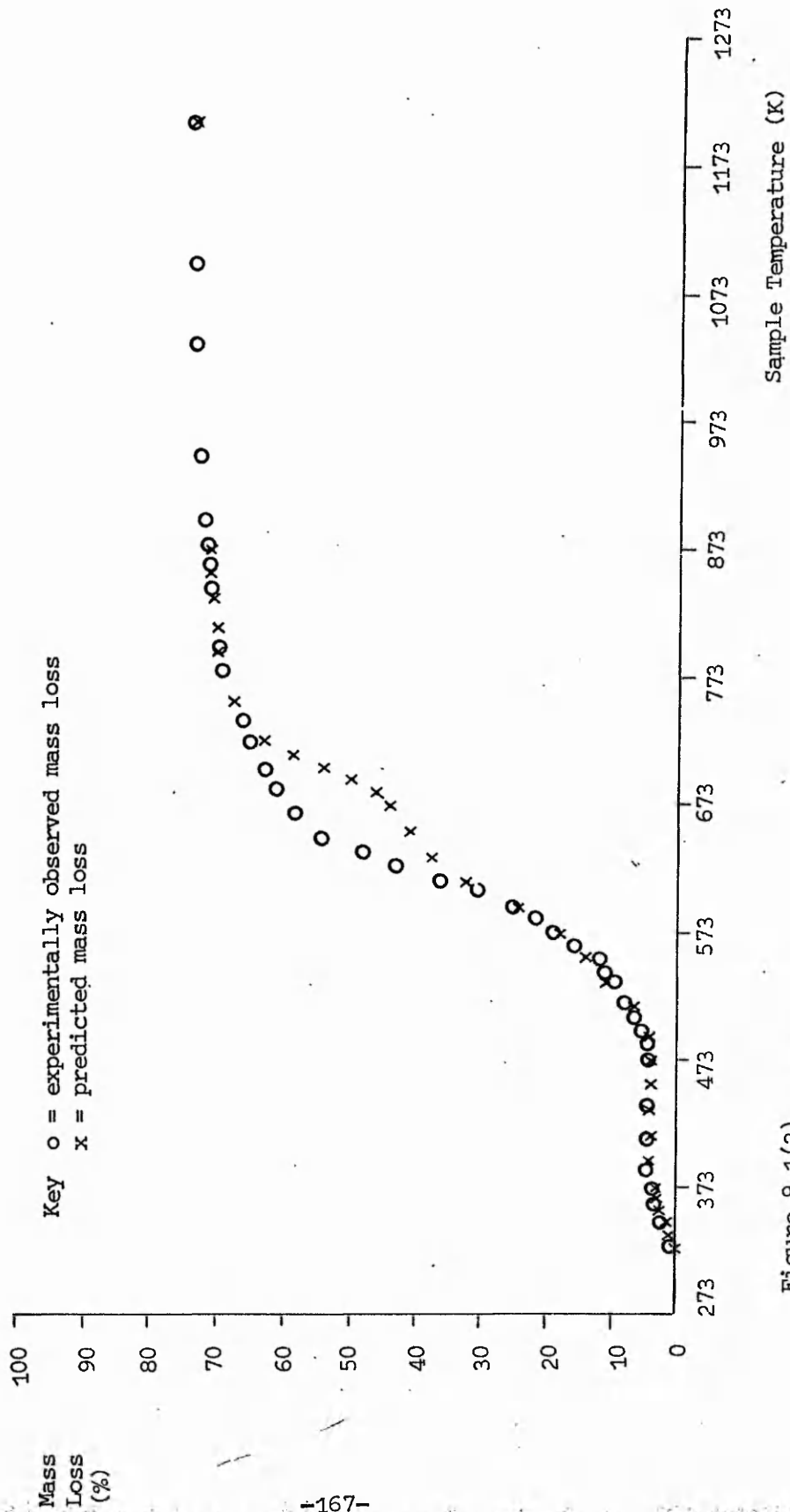


Figure 9.1(2)
 T.G. curve for W75/T25

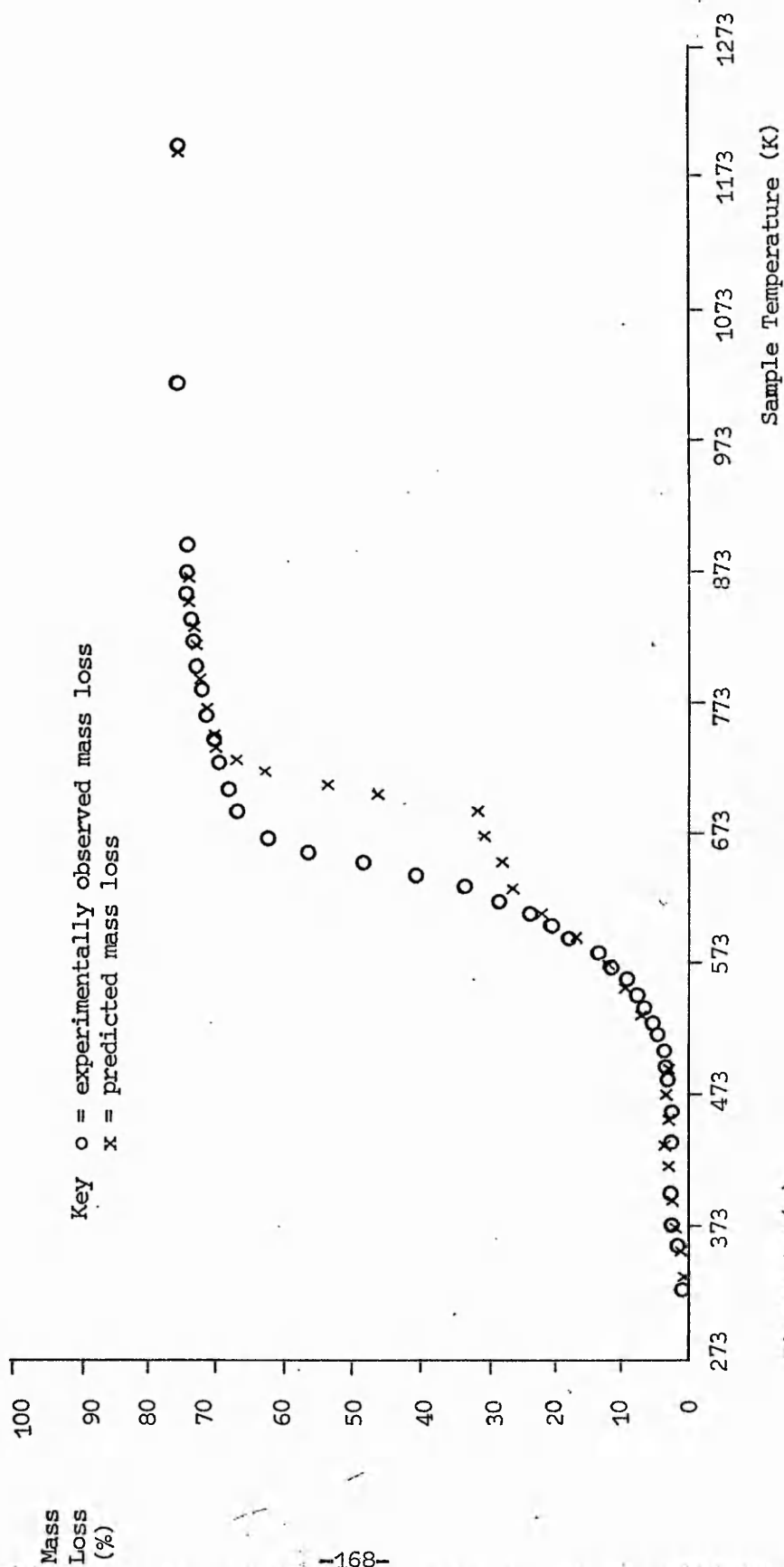


Figure 9.1(3)
 T.G. curve for W50/T50

Mass
Loss
(%)

-169-

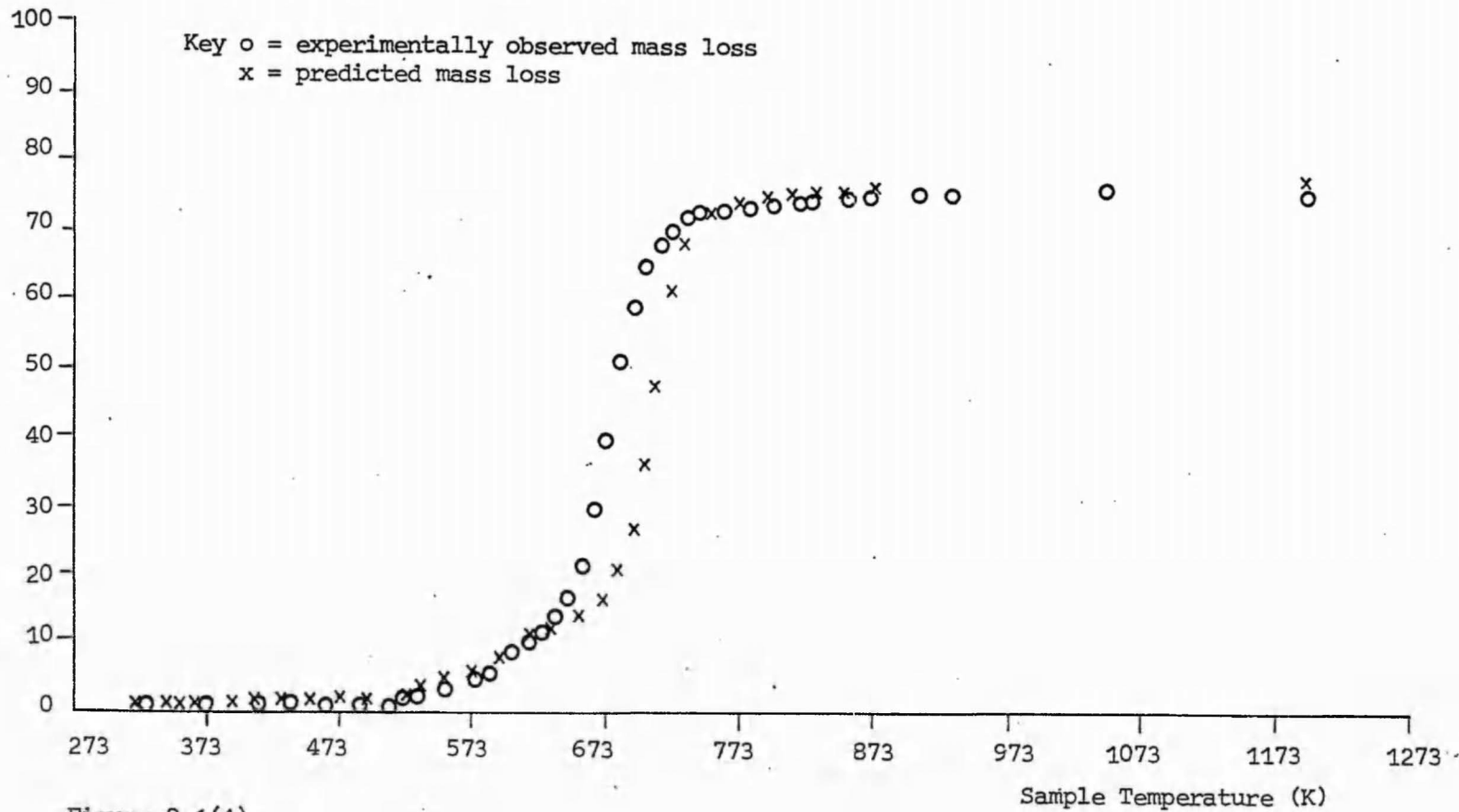


Figure 9.1(4)
T.G. curve for W25/T75

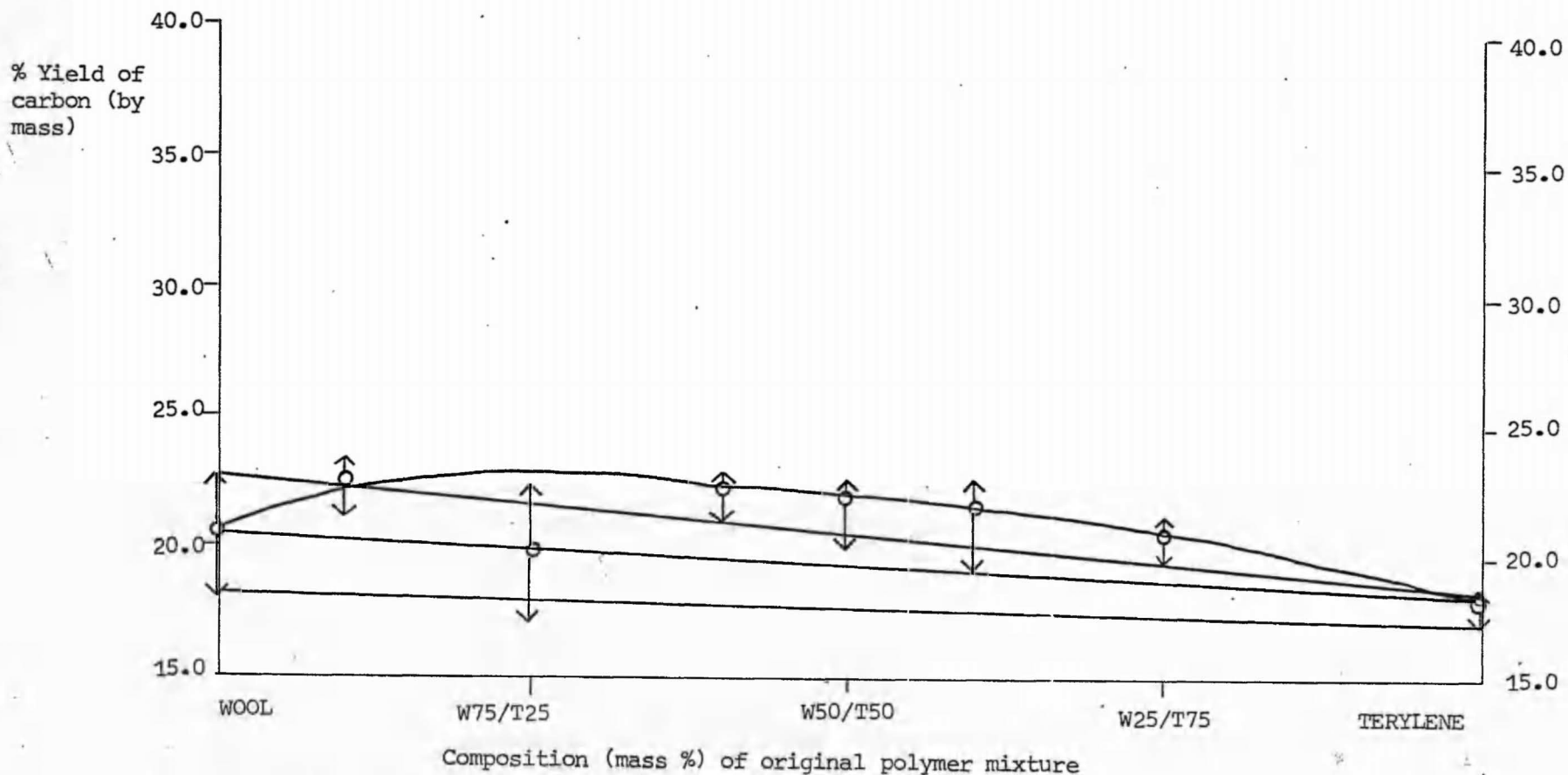


Figure 9.1(5) Variation of the yield of carbon obtained at 1213K from large scale pyrolysis with original mixture composition for the Wool/Terylene system.

Table 9.1(1)

Position of Terylene endotherm [530K (529-531K)] in the D.T.A. curves of wool/Terylene mixtures.

Mixture (mass %)	Peak temperature (K)
Wool (W)	-
W75/T25	529K (529K)
W50/T50	529K (529-530K)
W25/T75	529K (527-531K)
Terylene (T)	530K (529-531K)

Table 9.1(2)

Position of Terylene endotherm [710K (702-712K) in the D.T.A. curves of wool/Terylene mixtures.

Mixture (mass %)	Peak temperature (K)
Wool (W)	-
W75/T25	653K (647-656K)
W50/T50	676K (673-679K)
W25/T75	693K (687-699K)
Terylene (T)	710K (702-712K)

Table 9.1(3)

Position of the Terylene exotherm [745K (741-746K)] in the D.T.A. curves of wool/Terylene mixtures.

Mixture (mass %)	Peak temperature (K)
Wool (W)	-
W75/T25	Not resolved
W50/T50	713K (711-716K)
W25/T75	730K (725-737K)
Terylene (T)	745K (741-746K)

Table 9.1(4)

Position of (a) Terylene endotherm [530K (529-531K)]

(b) Terylene endotherm [710K (702-712K)]

(c) Terylene exotherm [745K (741-746K)]

in the D.T.A. curves of kieselguhr/Terylene mixtures.

	Mixture (mass %)	Peak temperature (K)
(a)	kieselguhr (K)	-
	K75/T25	531K (530-534K)
	K50/T50	532K (531-534K)
	K25/T75	533K (531-534K)
	Terylene (T)	530K (529-531K)
(b)	kieselguhr (K)	-
	K75/T25	711K (706-716K)
	K50/T50	712K (707-713K)
	K25/T75	714K (711-716K)
	Terylene (T)	710K (702-712K)
(c)	kieselguhr (K)	-
	K75/T25	738K (734-741K)
	K50/T50	741K (737-748K)
	K25/T75	741K (740-741K)
	Terylene (T)	745K (741-746K)

Table 9.1(5)

Position of the Merino Top 64 wool endotherm [505K (505-507K)] in the D.T.A. curves of wool/Terylene mixtures.

Mixture (mass %)	Peak temperature
Wool (W)	505K (505-507K)
W75/T25	509K (509-511K)
W50/T50	511K (509-512K)
W25/T75	507K (502-509K)
Terylene (T)	-

Table 9.1(6)

Residual yield of carbon at 1213K from the pyrolysis of wool/Terylene mixtures. Data from T.G. and large scale pyrolysis (L.S.P.)

Mixture (mass %)	Residual Yield (%)	
	T.G.	L.S.P.
Wool (W)	23.5	20.6
W90/T10	-	22.5
W75/T25	21.5	19.9
W60/T40	-	22.4
W50/T50	20.0	22.0
W40/T60	-	21.8
W25/T75	20.0	20.7
Terylene (T)	16.5	18.4

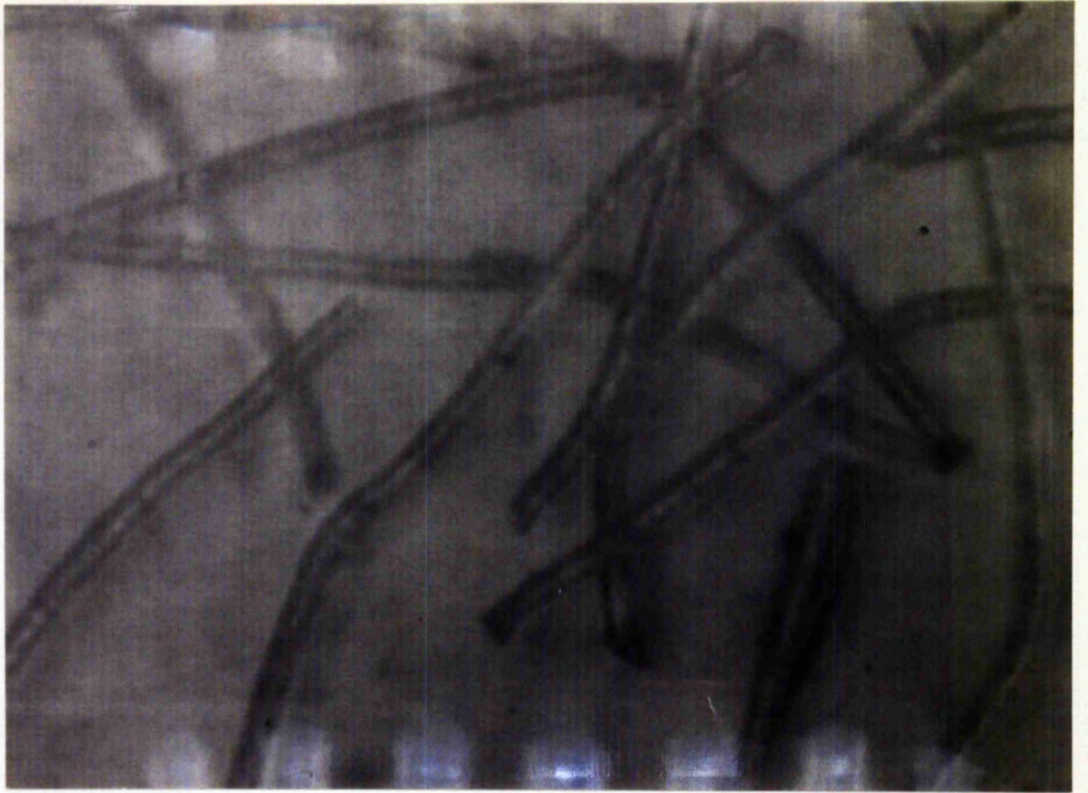


plate 9.1(1)
Wool/Terylene fibre mixture at room temperature (294K)



plate 9.1(2)
Wool/Terylene fibre mixture at 508K



plate 9.1(3)
Wool/Terylene fibre mixture at 538K

9.2 Wool/Courtelle

Illustrated in figure 9.2(1) are the D.T.A. curves for Merino Top 64 wool and Courtelle together with an example of a D.T.A. curve for a mixture of the two polymers (wool 75/Courtelle 25).

D.T.A. curves were obtained for three wool/Courtelle mixtures of composition 25/75, 50/50 and 75/25 (mass %).

Tables 9.2(1) and 9.2(2) indicate the peak temperatures of the Courtelle exotherm [568K (568-570K)] and wool endotherm [505K (505-507K)] in the D.T.A. curves of the various wool/Courtelle mixtures examined.

Illustrated in figures 9.2(2), 9.2(3) and 9.2(4) are the T.G. curves observed for the wool/Courtelle mixtures of composition 75/25, 50/50 and 25/75 (mass %). Superimposed on each curve is the T.G. curve predicted on the basis of the mass loss characteristics of the individual polymers.

The residual yields at 1213K from the large scale pyrolysis of wool/Courtelle mixtures are recorded in figure 9.2(5). The maximum observed variation is included for each yield determined.

Table 9.2(3) indicates the residual yield of carbon at 1213K observed by T.G. and large scale pyrolysis from wool/Courtelle mixtures.

Illustrated in plates 9.2(1), 9.2(2) and 9.2(3) are hot-stage microscope photographs of a wool/Courtelle mixture at various stages during pyrolysis. The exact composition of this mixture was not determined.

Plate 9.2(1) illustrates the appearance of the mixture prior to pyrolysis. Plates 9.2(2) and 9.2(3) illustrate the appearance of the mixture at temperatures of approximately 513K and 623K respectively.

The D.T.A. curves illustrated in figure 9.2(1) have been displaced relative to each other in the direction of the differential temperature axis to simplify analysis.

The D.T.A. curves of all the wool/Courtelle mixtures examined exhibited two readily identified peaks in addition to the endotherm reflecting water loss. These peaks were the Courtelle exotherm [568K (568-570K)] and the wool endotherm [505K (505-507K)].

The Courtelle exotherm [568K (568-570K)] exhibited a small but significant displacement to lower temperatures between Courtelle and

the wool 25/Courtelle 75 mixture [table 9.2(1)]. This would seem to correspond to the observation by Tarim and Cates⁴⁶ that the large Orlon exotherm (peak temperature 581K) occurred with a peak temperature of 571K in the D.T.A. curve of a wool 50/Orlon 50 (mass %) mixture run in a static air atmosphere.

The wool endotherm [596K (582-616K)] was not resolved in the D.T.A. curves of any of the wool/Courtelle mixtures. It is probable that this peak distinct in the D.T.A. curve of wool alone was masked by the exothermic effects of the preceding Courtelle peak, observed in the D.T.A. curve of Courtelle alone at 568K (568-570K).

The Courtelle exotherm [689K (676-704K)] was observed in the wool 50/Courtelle 50 and wool 25/Courtelle 75 mixtures with peak temperatures of 705K (698-718K) and 698K (685-704K) respectively. In view of the overlap of the temperature ranges observed for this peak it is considered that no significance can be attached to any apparent peak displacement in this case.

Grassie and McGuchan⁶¹ utilised both peak initiation temperature (T_I) and peak heights (ΔT) observed for the large exotherm occurring in the D.T.A. curve of PAN to assess changes in the characteristics of the reaction leading to formation of the ladder polymer structure brought about by the presence of additives.

In the current study where the D.T.A. curves are derived from binary polymer mixtures such an analysis of the large Courtelle exotherm [568K (568-570K)] was considered.

However in the case of wool/Courtelle mixtures the occurrence of the wool endothermic peaks at 505K (505-507K) and 596K (582-616K) served to modify the shape of the Courtelle exothermic peak at 568K (568-570K).

Thus possible changes in T_I and ΔT corresponding to those observed by Grassie and McGuchan⁶¹ in the presence of additives are masked by thermal changes in the additive itself.

Further the considerable changes in sample mass and thermal characteristics above 473K render inappropriate any attempt at a more quantitative treatment of the D.T.A. curves.

The T.G. curves presented in figures 9.2(2), 9.2(3) and 9.2(4) indicate that slightly higher residual yields than predicted, were

observed at 1213K for both the wool 75/Courtelle 25 and wool 25/Courtelle 75 mixtures. The wool 50/Courtelle 50 mixture exhibited a somewhat larger difference between the observed and predicted residual yields at 1213K. This residual yield behaviour corresponds to that observed at 1213K from the large scale pyrolyses. [See figure 9.2(5)]. Thus significantly higher residual yields than would be predicted were observed for mixtures of compositions intermediate between wool 75/Courtelle 25 and wool 25/Courtelle 75.

The T.G. curve for the mixture wool 75/Courtelle 25 is illustrated in figure 9.2(2). Apart from mass loss differences related to water loss, observed and predicted mass loss curves coincide up to a temperature of 773K. Above this temperature slightly lower than predicted mass losses were observed.

In the T.G. curves of mixtures of higher Courtelle content [i.e. wool 50/Courtelle 50, figure 9.2(3) and wool 25/Courtelle 75 figure 9.2(4)] the observed and predicted mass losses coincided up to a temperature of 573K. Again above this temperature somewhat lower than predicted mass losses were observed. This mass loss behaviour will be further discussed in a later chapter.

The possible effects of thermal run-away occurring in Courtelle must be considered when correlating results derived from D.T.A., T.G. and large scale pyrolysis.

Work by Bromley¹³⁴ has shown that the pyrolysis behaviour (inert atmosphere) of pre-oxidised PAN fibres was a function of sample size. Bromley¹³⁴ found that in large samples of pre-oxidised PAN fibres (12 kg) heated to temperatures above the initiation temperature of the large PAN exotherm (corresponding to the Courtelle exotherm observed at 568K (568-570K) in this study) extensive thermal run-away was observed within the sample.

Thus at a fibre temperature of 423K during pyrolysis at a constant rate of temperature increase a sharp temperature rise to about 673K was recorded. The temperature then fell back to 598K.

It is thus possible that in Courtelle samples above a certain critical sample mass thermal run-away effects may occur following the initiation of the large exothermic peak observed at 568K (568-570K).

In large PAN samples this thermal run-away may lead to more extensive chain scission reactions and changes in the type and relative

quantities of volatile degradation products.

Thermal run-away effects in Courtelle samples have not been detected in this study by D.T.A. or T.G.

However the technique of large scale pyrolysis utilised larger samples and through lack of temperature measurement within the sample itself, the effect if operative was undetected.

It is therefore considered that whilst thermal run-away effects may have been operative during the large scale pyrolysis of binary polymer mixtures containing Courtelle, no reduction in residual yield was observed for samples of high Courtelle content. On the contrary the majority of polymer mixtures containing Courtelle (i.e. wool/Courtelle and in section 9.3, Terylene/Courtelle) exhibited significantly higher than predicted residual yields at 1213K under the conditions of large scale pyrolysis.

Plate 9.2(1) illustrates the similarity in appearance of wool and Courtelle fibres at room temperature.

In plate 9.2(2) taken at 513K the darker, curled wool fibres are easily distinguished from the lighter, straight Courtelle fibres.

In plate 9.2(3) the wool fibres are observed to have broadened and presumably fused although no evidence of actual flow of the fused wool can be detected.

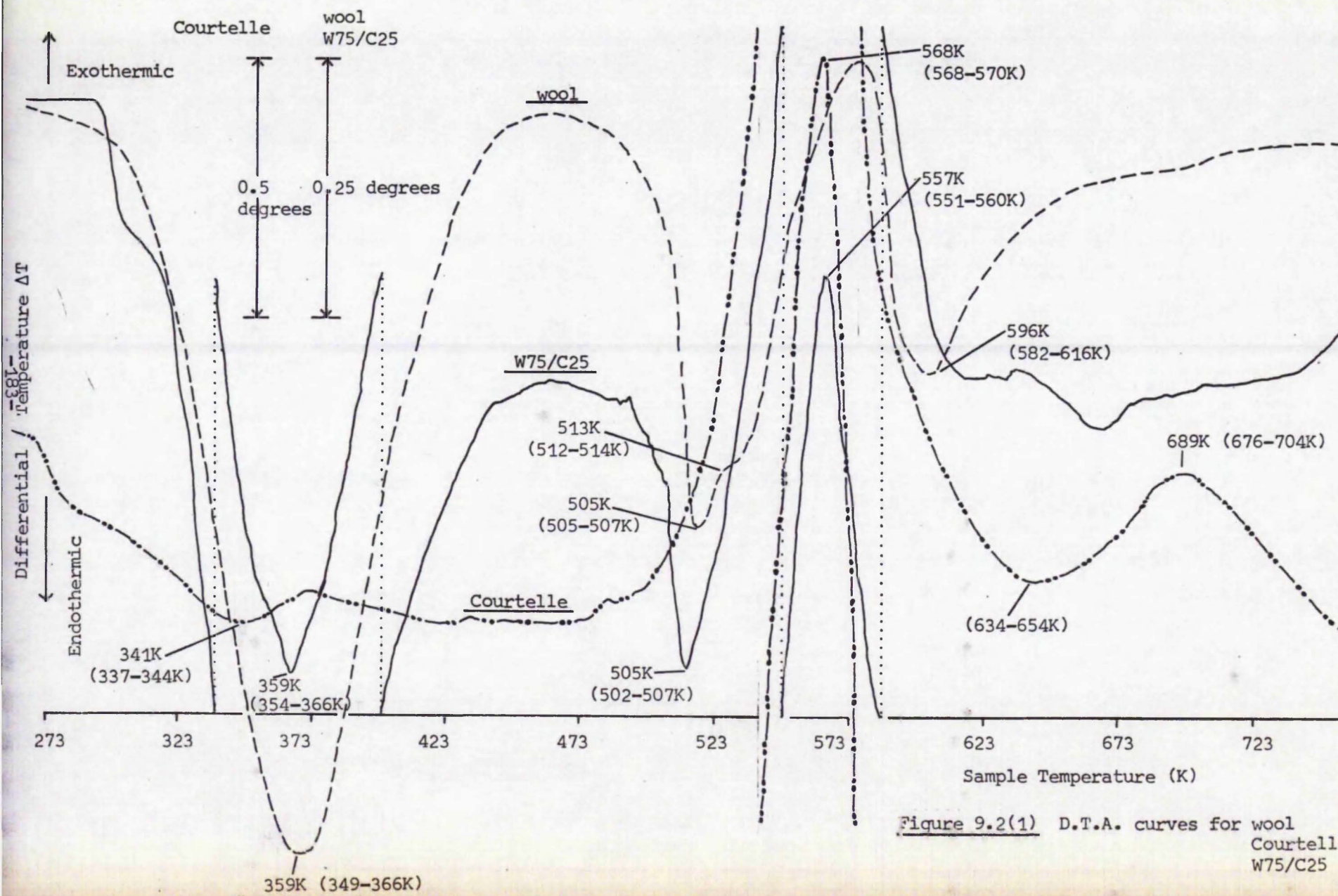


Figure 9.2(1) D.T.A. curves for wool
 Courtelle
 W75/C25

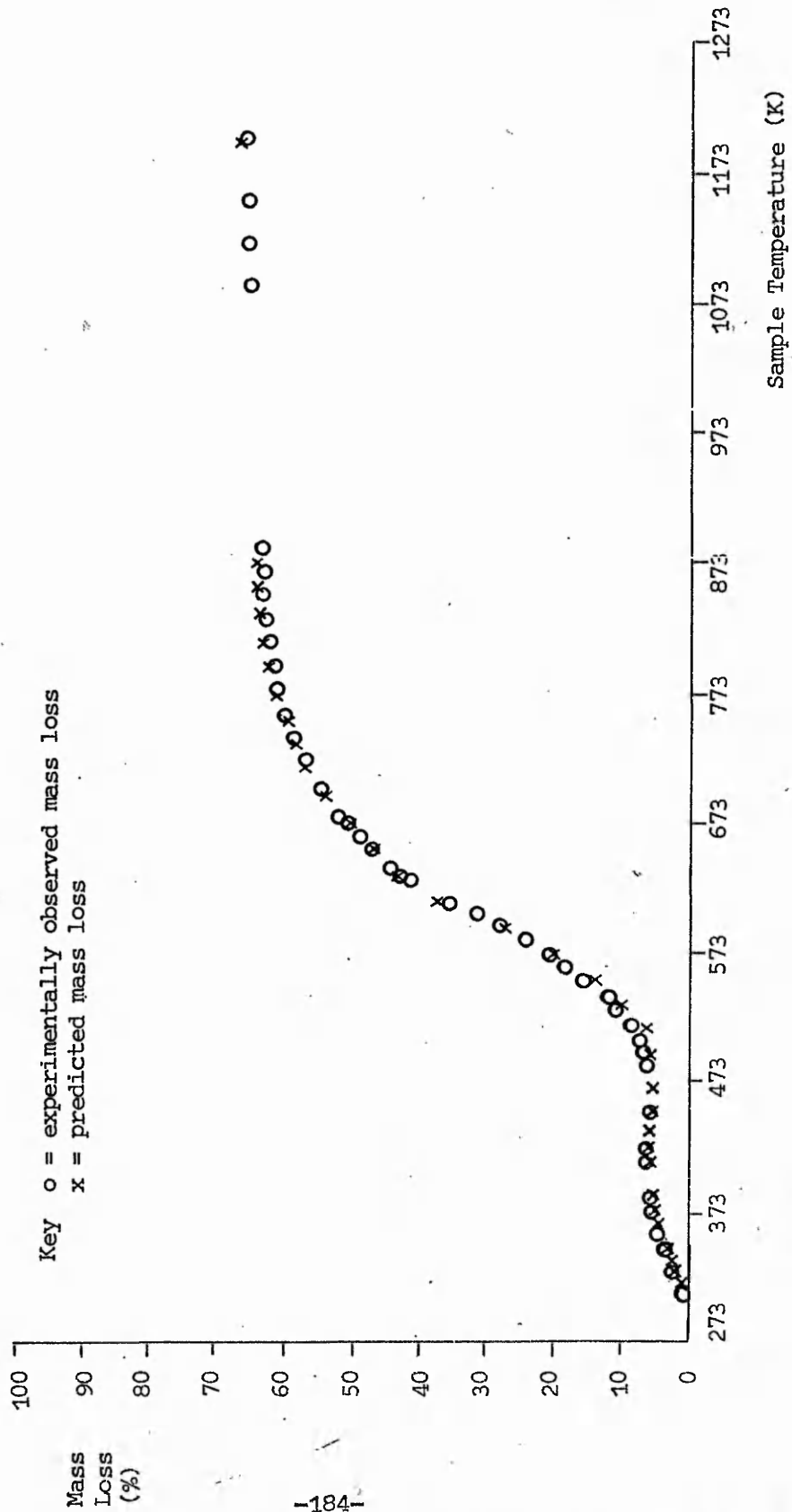


Figure 9.2(2)
T.G. curve for W75/C25

-185-

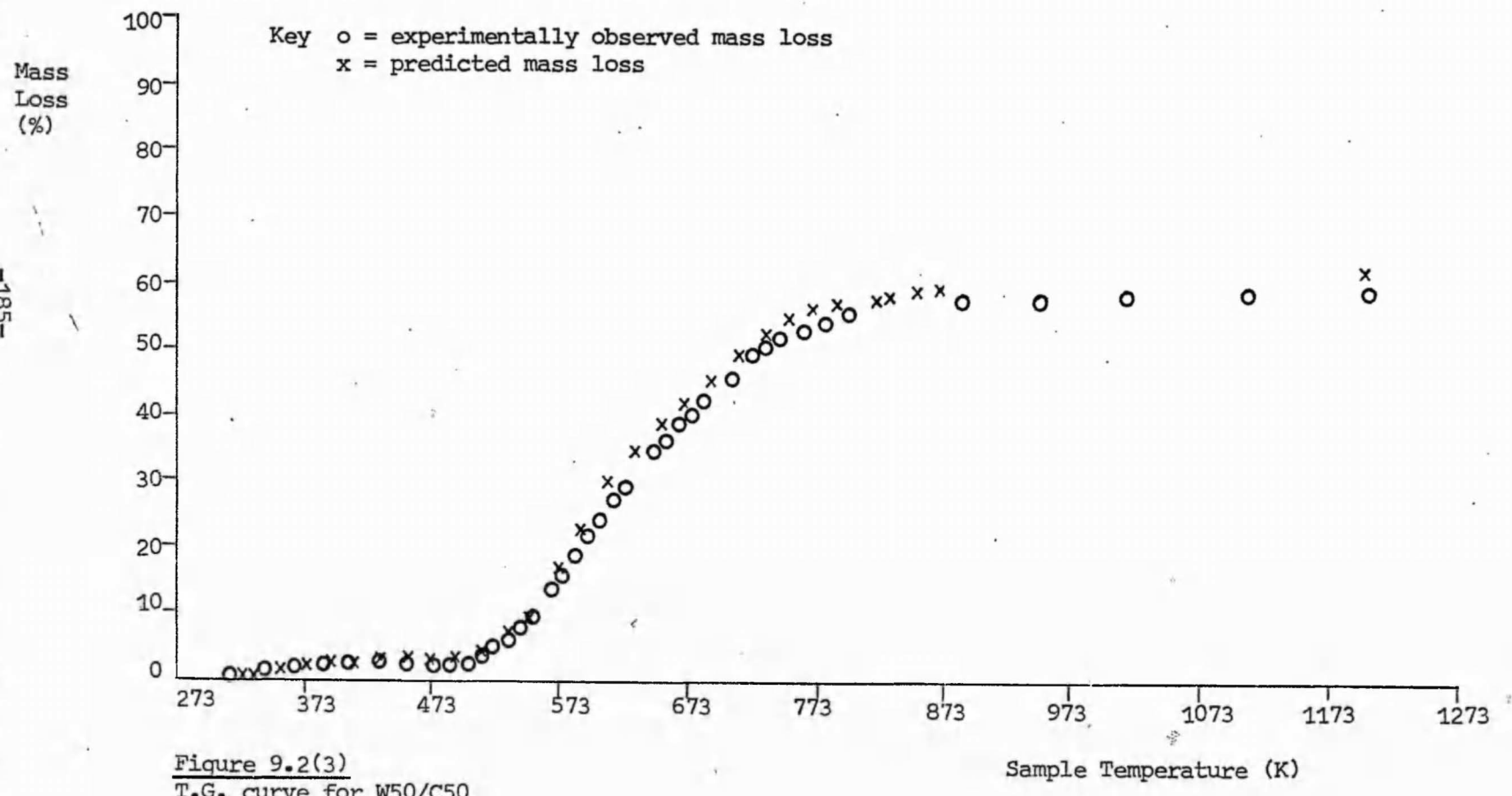


Figure 9.2(3)
T.G. curve for W50/C50

Sample Temperature (K)

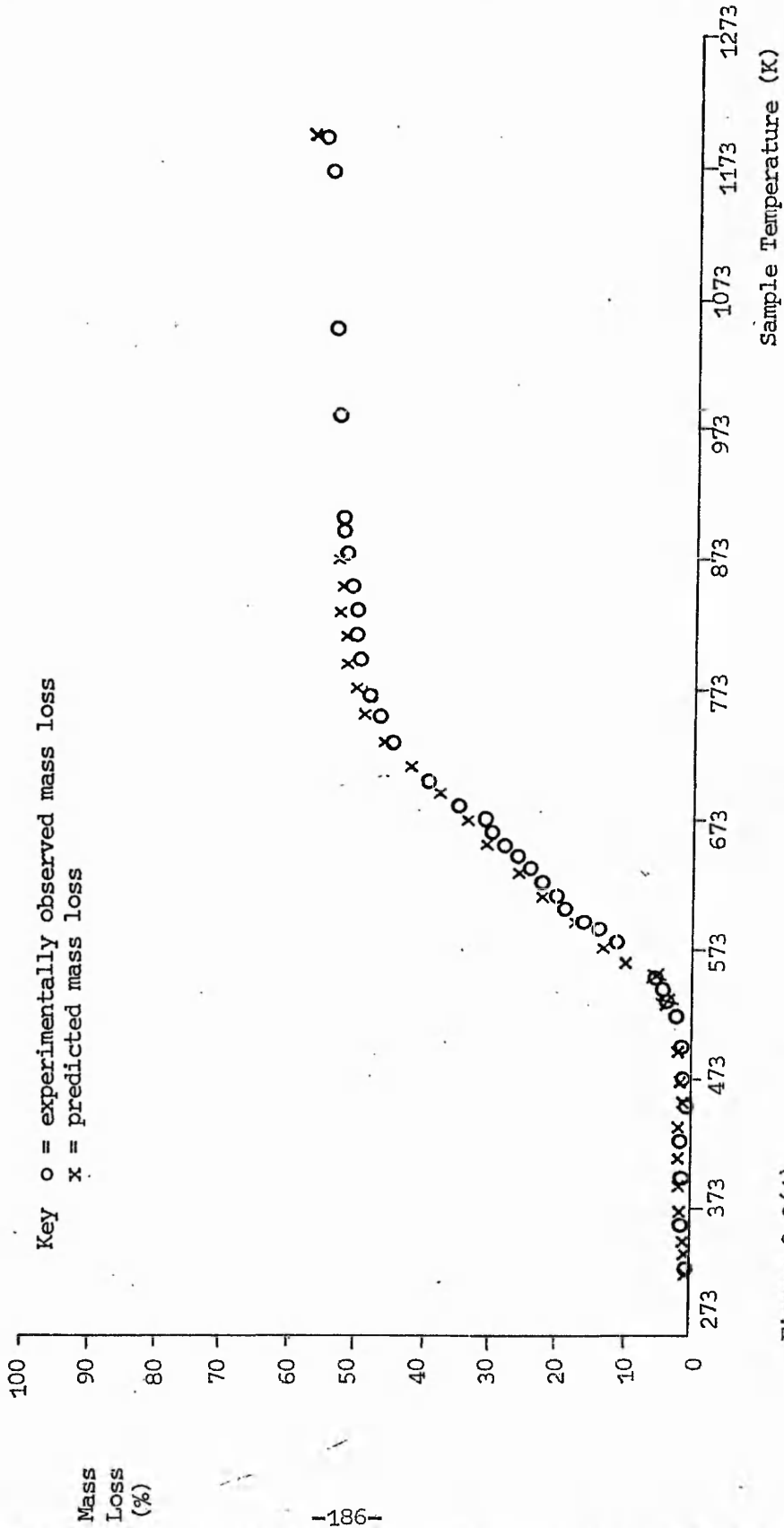


Figure 9.2(4)
 T.G. curve for W25/C75

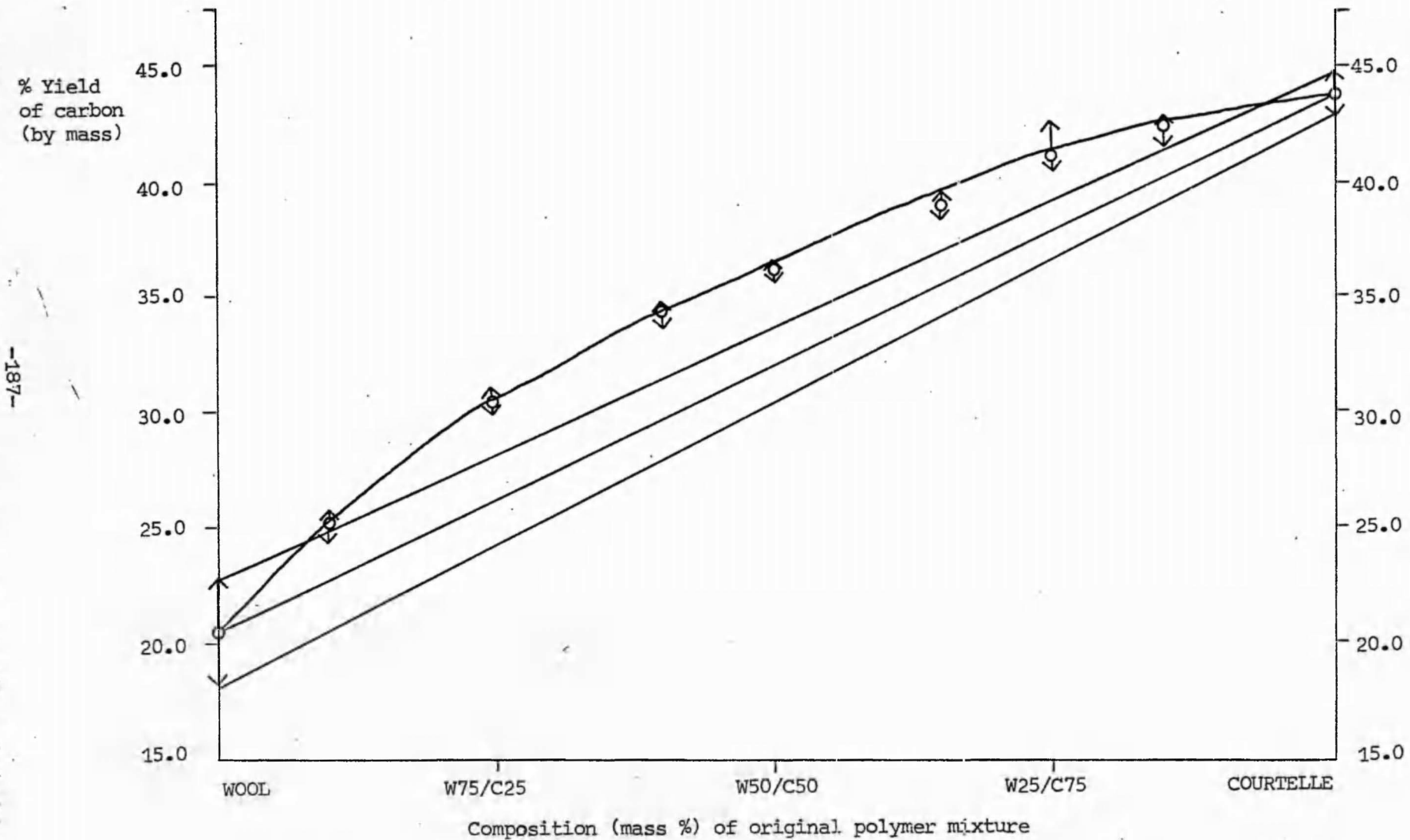


Figure 9.2(5) Variation of the yield of carbon at 1213K from large scale pyrolysis with original mixture composition for the Wool/Courtelle system.

Table 9.2(1)

Position of the Courtelle exotherm [568K(568-570K)] in the D.T.A. curves of wool/Courtelle mixtures.

Mixture (mass %)	Peak temperature (K)
Wool (W)	-
W75/C25	557K (551-560K)
W50/C50	561K (558-563K)
W25/C75	566K (558-568K)
Courtelle (C)	568K (568-570K)

Table 9.2(2)

Position of the wool endotherm [505K (505-507K)] in the D.T.A. curves of wool/Courtelle mixtures.

Mixture (mass%)	Peak temperature (K)
Wool (W)	505K (505-507K)
W75/C25	505K (502-507K)
W50/C50	505K (505-508K)
W25/C75	507K (507K)
Courtelle (C)	-

Table 9.2(3)

Residual yield of carbon at 1213K from the pyrolysis of wool/Courtelle mixtures. Data from T.G. and large scale pyrolysis (L.S.P.).

Mixture (mass %)	Residual yield (%)	
	T.G.	L.S.P.
Wool (W)	23.5	20.6
W90/C10	-	25.1
W75/C25	29.5	30.4
W60/C40	-	34.6
W50/C50	36.5	36.5
W35/C65	-	39.1
W25/C75	40.0	41.3
W15/C85	-	42.8
Courtelle (C)	43.0	43.9

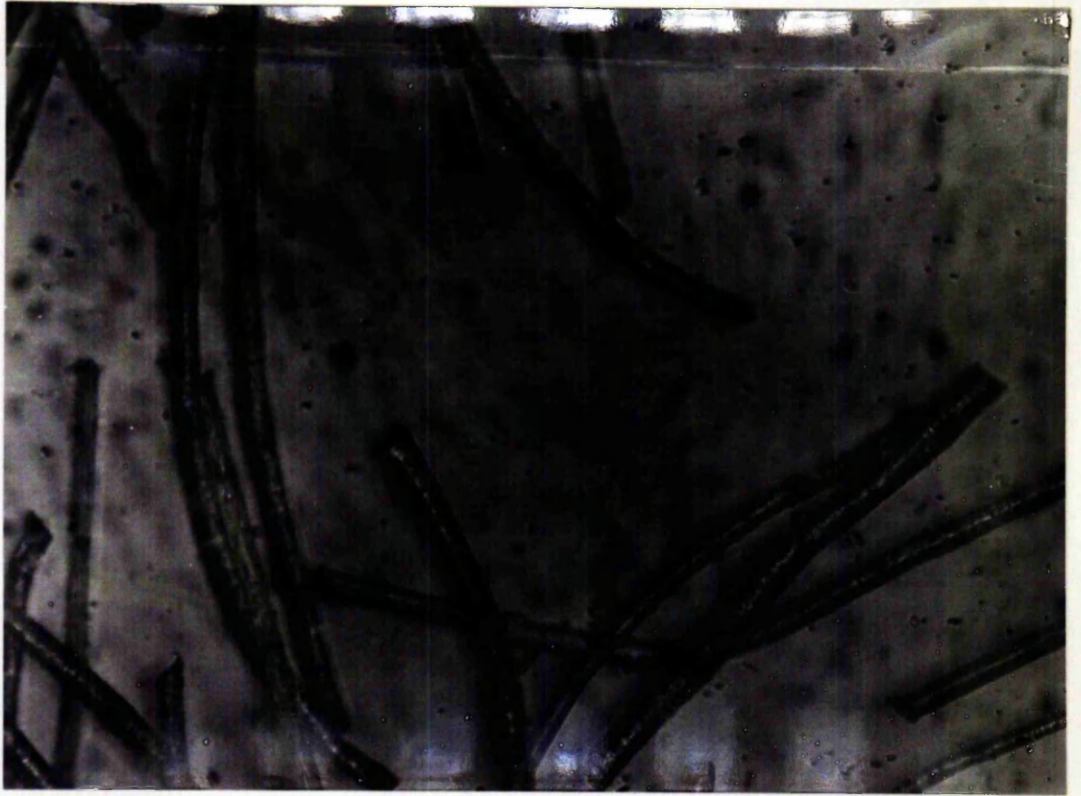


plate 9.2(1)
Wool/Courtelle fibre mixture at room temperature (294K)

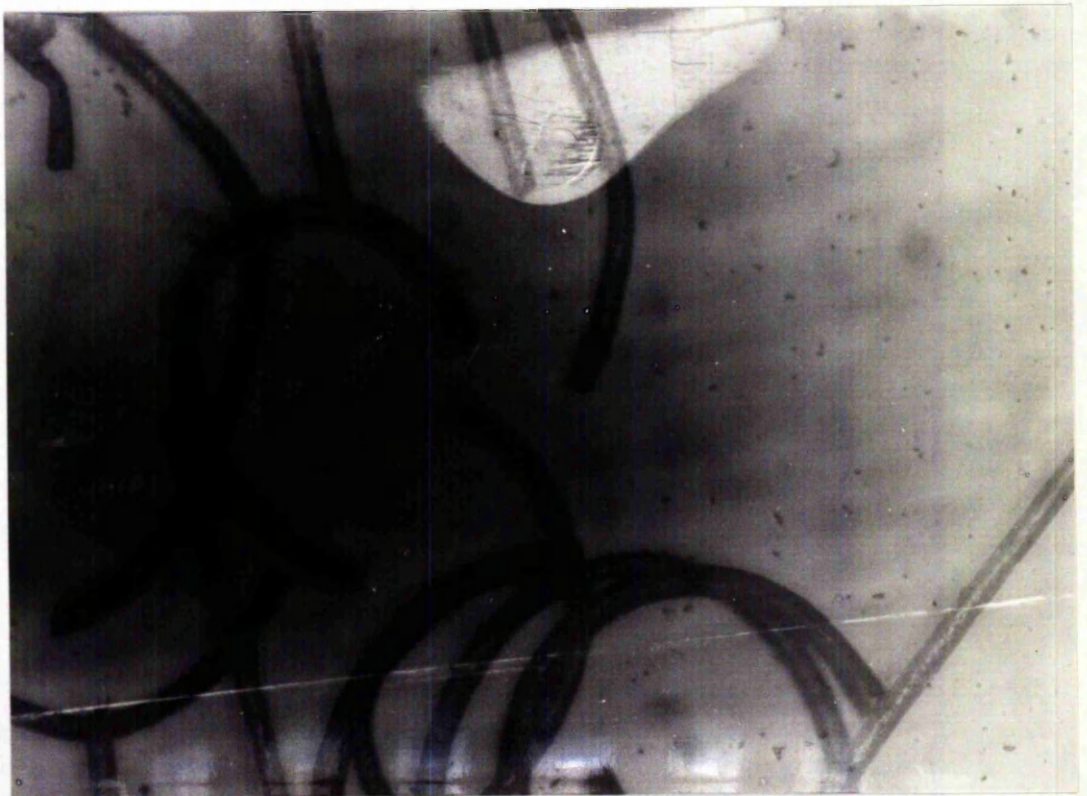


plate 9.2(2)
Wool/Courtelle fibre mixture at 513K

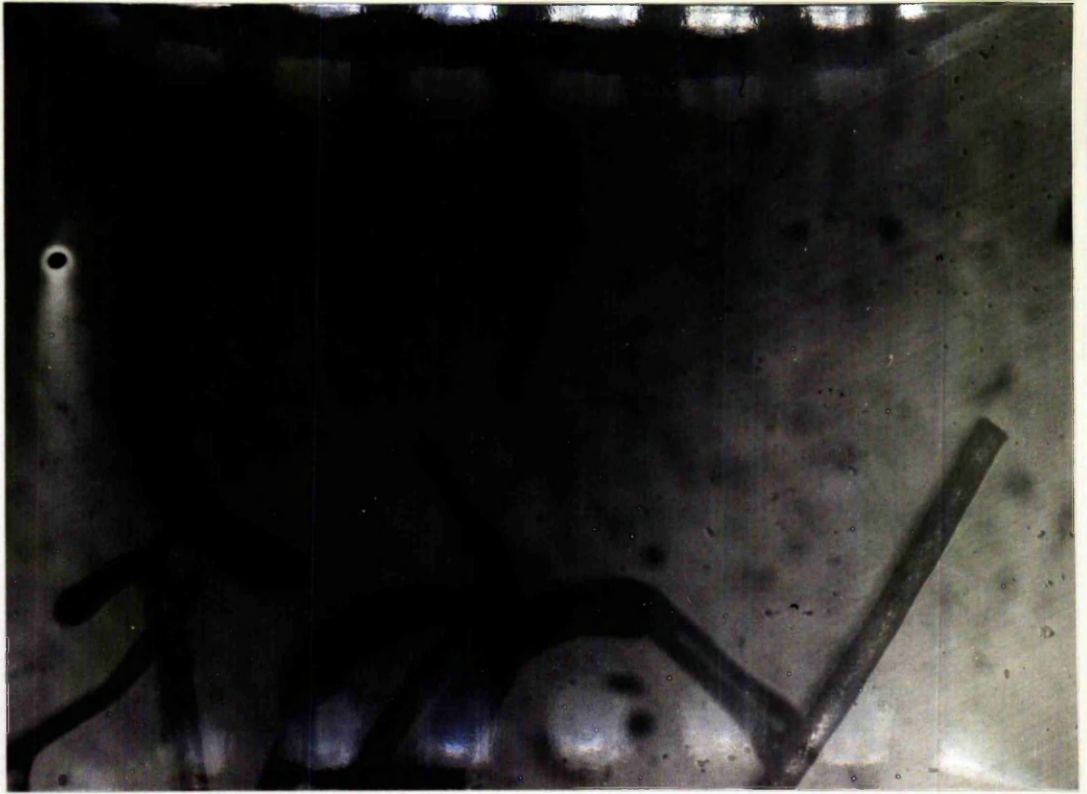


plate 9.2(3)
Wool/Courtelle fibre mixture at 623K

9.3 Terylene/Courtelle

Illustrated in figure 9.3(1) are the D.T.A. curves for Terylene and Courtelle together with an example of a D.T.A. curve for a mixture of the two polymers (Terylene 75/Courtelle 25).

D.T.A. curves were obtained for eight Terylene/Courtelle mixtures of composition 75/25, 60/40, 50/50, 40/60, 32.5/67.5, 25/75, 15/85 and 7.5/92.5 (mass %). As previously reported in section 9.1, D.T.A. curves for various kieselguhr/Terylene mixtures were also recorded [table 9.1(4)].

Table 9.3(1) indicates the peak temperatures observed for the Terylene endotherm [710K (702-712K)] and exotherm [745K (741-746K)] in the D.T.A. curves of the various Terylene/Courtelle mixtures examined.

Recorded in table 9.3(2) parts (a) and (b) are the peak temperatures observed in the D.T.A. curves of the mixtures for the Courtelle exotherm [568K (568-570K)] and Terylene endotherm [530K (529-531K)] respectively.

Table 9.3(4) contains the peak temperature, from the D.T.A. curves of the various mixtures of an unassigned exothermic peak. This exotherm is believed to arise as the result of the combined effects of the Courtelle exotherm [689K (676-704K)] and Terylene exotherm (not resolved in this study, literature values of peak temperature 653K,⁴⁹ 662K⁵¹).

Illustrated in figures 9.3(2), 9.3(3) and 9.3(4) are the T.G. curves observed for Terylene/Courtelle mixtures of composition 25/75, 50/50 and 75/25 (mass %) respectively. Superimposed on each curve is the T.G. curve predicted on the basis of the mass loss characteristics of the individual polymers.

The residual yields at 1213K from the large scale pyrolysis of Terylene/Courtelle mixtures are recorded in figure 9.3(5). The maximum observed variation is included for each yield determined.

Table 9.3(3) indicates the residual yield of carbon at 1213K observed by T.G. and large scale pyrolysis for Terylene/Courtelle mixtures.

Illustrated in plates 9.3(1), 9.3(2), 9.3(3) and 9.3(4) are hot-stage microscope photographs of a Terylene/Courtelle mixture

at various stages during pyrolysis. The exact composition of this mixture was not determined. Plate 9.3(1) illustrates the appearance of the mixture prior to pyrolysis. Plates 9.3(2) and 9.3(3) illustrate the appearance of the mixture at temperatures of 529K and 623K respectively. Plate 9.3(4) was taken at approximately 710K.

From the D.T.A. curves of the single polymers illustrated in figure 9.3(1) the Courtelle exotherm [568K (568-570K)] and Terylene endotherm [530K (529-531K)], each characteristic of the individual polymers, would be expected to appear in the D.T.A. curves of the mixtures. This was found to be the case except for the mixture Terylene 7.5/Courtelle 92.5 where the Terylene endotherm [530K (529-531K)] was unresolved.

As previously discussed in section 9.1 the displacement of a peak in the D.T.A. curves of a binary polymer system is only regarded as significant when the experimentally observed peak temperature ranges of adjacent members of the composition range do not overlap. Whilst a considerable range of Terylene/Courtelle mixtures have been examined by D.T.A. the composition range described above in relation to 'significant peak displacement' is considered to be Terylene, T75/C25, T50/C50, T25/C75 and Courtelle.

From table 9.3(2) (a) and (b) it is clear that no significant displacement of either the Courtelle exotherm [568K (568-570K)] or the Terylene endotherm [530K (529-531K)] was observed throughout the entire composition range.

Above a temperature of 573K the interpretation of the D.T.A. curves for the Terylene/Courtelle polymer mixtures is somewhat more difficult.

As previously discussed an exothermic peak has been observed in the D.T.A. curve of Dacron (nitrogen atmosphere) at 653K and 662K by Gillham⁴⁹ and Schwenker⁵¹ respectively.

Whilst exothermic activity was detected at these temperatures in the Terylene D.T.A. curves reported in this study the peak itself was not clearly resolved.

As previously discussed little has been reported concerning the appearance of the PAN D.T.A. curve above 573K. However the D.T.A. curve of Courtelle reported in this study appeared to exhibit base-line return in the temperature range 634-654K followed by an exothermic

peak at 689K (676-704K).

In an attempt to clarify the thermal changes observed above 573K in the Terylene/Courtelle system additional mixtures were prepared and examined by D.T.A.

In the D.T.A. curve of the mixture Terylene 75/Courtelle 25 illustrated in figure 9.3(1) an exotherm was observed at 662K (645-680K) followed by a possible endotherm [710K (697-706K)] and then an exotherm [734K (730-741K)].

One explanation of this peak sequence is that the exothermic peak reported in the D.T.A. curve of Dacron at 653K⁴⁹ and 662K⁵¹ and the exothermic activity in Courtelle at 689K (676-704K) may combine in the mixture Terylene 75/Courtelle 25, resulting in the exothermic peak observed at 662K (645-680K), neither peak being individually resolved.

The proposed endotherm observed at 701K (697-706K) and exotherm at 734K (730-741K) may then correspond to the endothermic and exothermic peaks observed in the D.T.A. curve of Terylene at 710K (702-712K) and 745K (741-746K) respectively.

The peak sequence above 573K observed for the mixture Terylene 75/Courtelle 25 was repeated throughout the range of composition. That is, following the large Courtelle exotherm [568K (568-570K)] was observed the sequence exotherm, endotherm (postulated), exotherm.

The latter endotherm and exotherm are thus tentatively assigned to the Terylene endothermic and exothermic peaks observed at 710K (702-712K) and 745K (741-746K) respectively in the D.T.A. curve of Terylene alone.

Table 9.3(1) (b) indicates that if this peak assignment is correct considerable displacement of the Terylene exotherm [745K (741-746K)] is observed.

Tarim and Cates⁴⁶ have reported the D.T.A. curve (static air atmosphere) of a Dacron 75/Orlon 25 mixture. The Dacron fusion endotherm (535K) and degradative exotherm (753K) together with the major Orlon exotherm (581K) were observed. However the Dacron exotherm (695K) and endotherm (720K) together with the Orlon exotherm (693K) were not resolved.

In a D.T.A. experiment employing the cross-differential technique [Dacron 75/Orlon 25 (mass %) - sample against asbestos 75/Orlon 25 (mass %) -reference] the Dacron peaks, exotherm (695K),

endotherm (720K) and exotherm (753K) were observed at 653K, 698K and 743K respectively.⁴⁶

Table 9.3(4) indicates the peak position observed in the mixtures of the exotherm which may arise as a result of the Courtelle exotherm at 689K (676-704K) and reported Dacron exotherm at 653K⁴⁹ and 662K.⁵¹ No significant displacement of this peak was observed and the temperature ranges of observation for this peak were large. The observation of Tarim and Cates⁴⁶ concerning apparent displacement of the Dacron exotherm (695K) tend to support the postulate that the exotherm reported in table 9.3(4) arises from the superposition of the two exotherms as previously discussed.

Figure 9.3(5) indicates that the residual yields observed at 1213K from the large scale pyrolysis of all Terylene/Courtelle mixtures examined were significantly higher than predicted. Figures 9.3(2), 9.3(3) and 9.3(4) indicate that this is also true for the T.G. yields observed at 1213K from the three mixtures examined.

Figures 9.3(2), 9.3(3) and 9.3(4) also indicate that the initial mass losses probably associated with the Courtelle portion of the polymer mixtures were reduced in the presence of Terylene.

The T.G. data for all three mixtures examined indicated that the sharp mass losses observed for the mixtures and possibly reflecting Terylene degradative reactions occurred at lower temperatures than would have been predicted from a consideration of the T.G. data for Terylene alone.

A correlation would therefore appear to exist between the T.G. data observed for both Terylene/Courtelle and wool/Terylene systems. In both the sharp mass losses in the mixtures possibly reflecting Terylene degradative reactions were observed to occur at lower temperatures than would have been predicted.

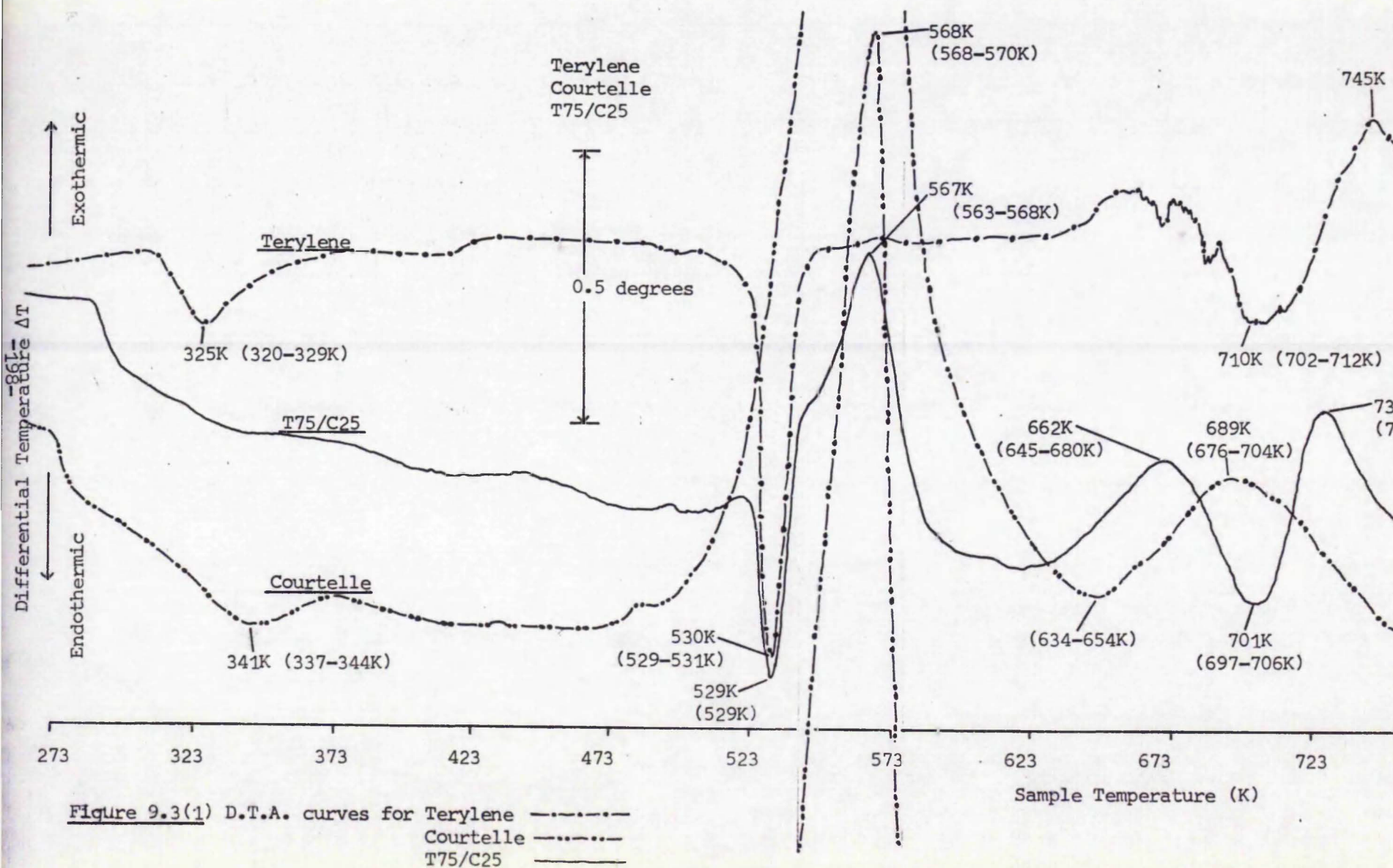
The Terylene endothermic peak [710K (702-712K)] associated with sharp mass loss in Terylene might on the basis of the T.G. data be expected to occur at lower temperatures in the D.T.A. curves of both Terylene/Courtelle and wool/Terylene systems.

For the wool/Terylene system this would appear to be the case [see table 9.1(2)]. Whilst the endotherm observed in the D.T.A. curve

of Terylene/Courtelle mixtures and attributed to the Terylene endotherm [710K (702-712K)], (table 9.3(1), (a)) was also displaced to lower temperatures this displacement was not significant.

In plate 9.3(2) taken at 529K fusion of the Terylene fibres is apparent. Further some of the Courtelle fibres appear to be partially coated with fused Terylene.

From plate 9.3(3) it would appear that further coating of the Courtelle fibres has taken place. At approximately 710K [plate 9.3(4)] the Courtelle fibres are observed in a mass of fused and degrading Terylene.



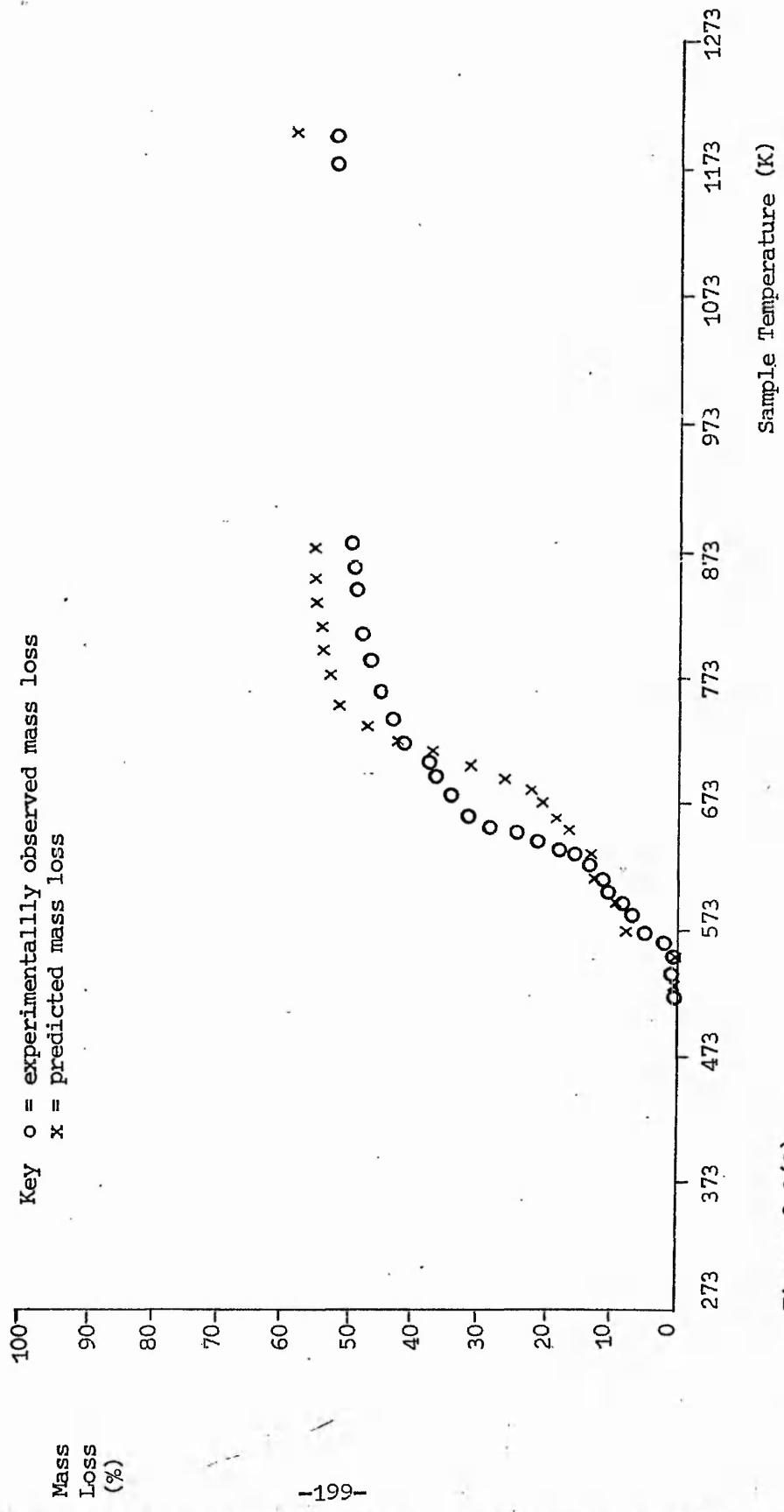


Figure 9.3(2)
 T.G. curve for C75/T25

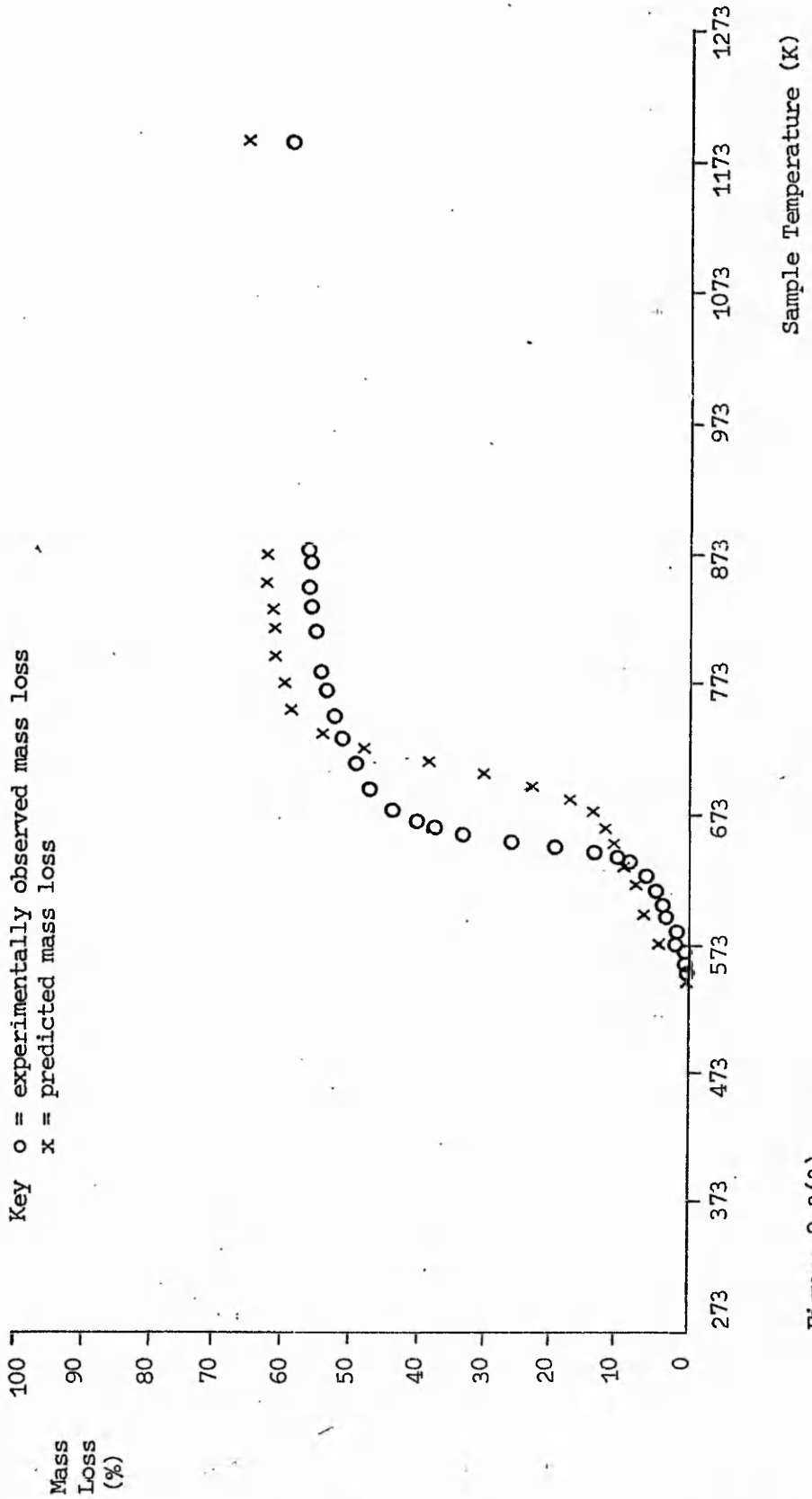
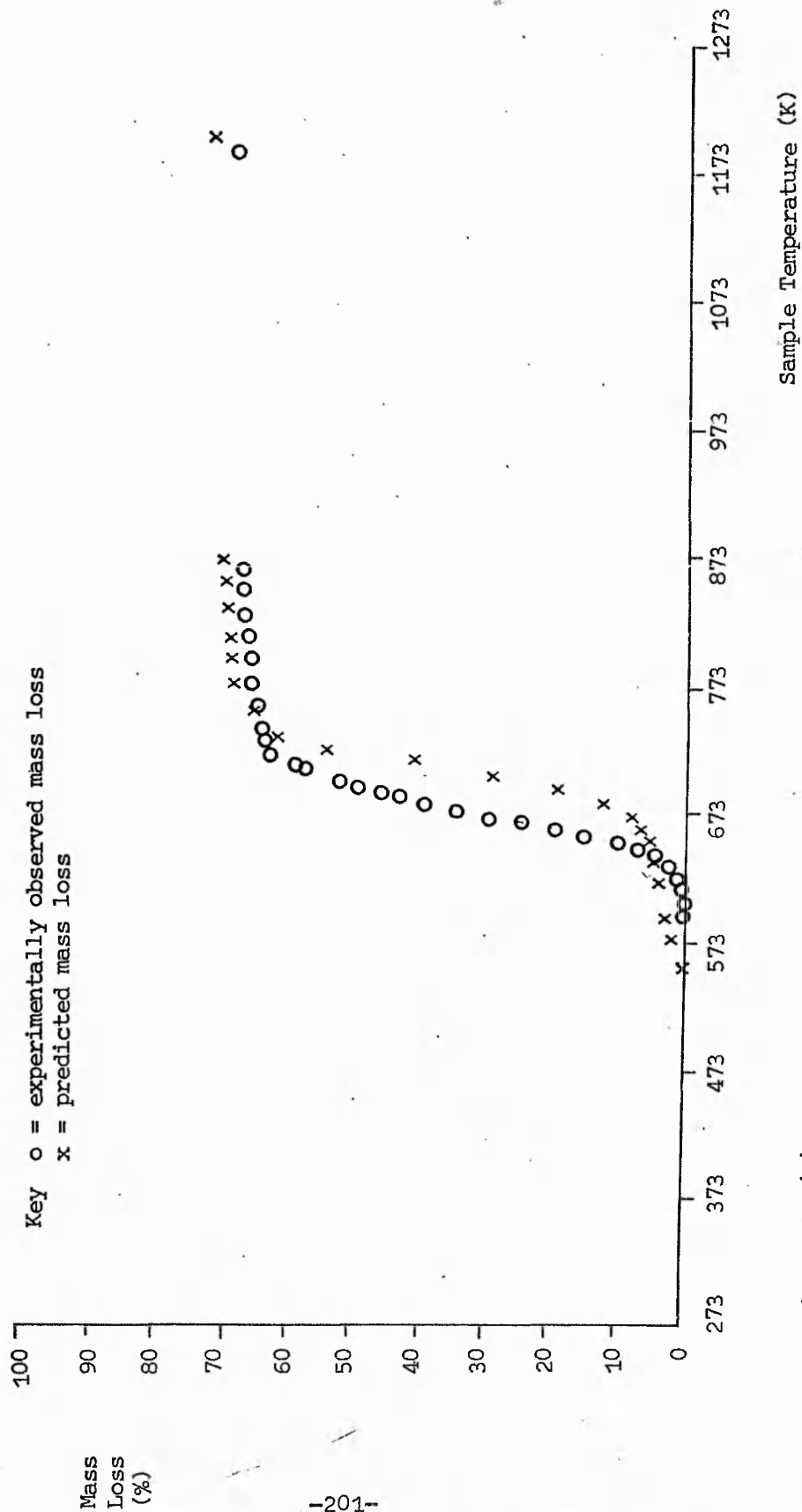
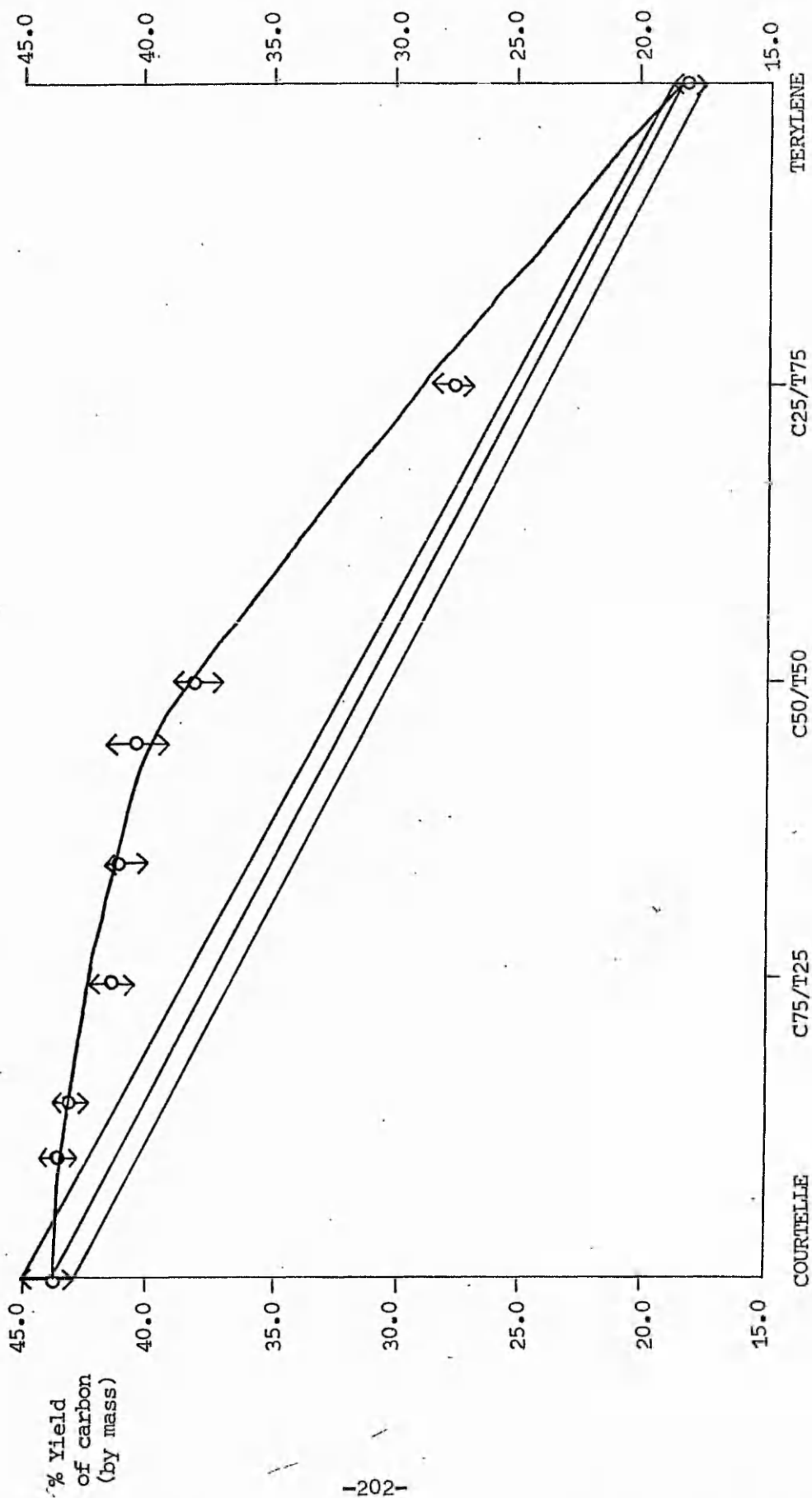


Figure 9.3(3)
 T.G. curve for C50/T50





Composition (mass %) of original polymer mixture

Figure 9.3(5) Variation of the yield of carbon at 1213K from large scale pyrolysis with original mixture composition for the Courtelle/Terylene system.

Table 9.3(1)

Position of (a) Terylene endotherm [710K (702-712K)]

(b) Terylene exotherm [745K (741-746K)]

in the D.T.A. curves of Terylene/Courtelle mixtures.

	Mixture (mass %)	Peak temperature (K)
(a)	<u>Courtelle (C)</u>	-
	C92.5/T7.5	681K (678-685K)
	C85/T15	688K (685-697K)
	C75/T25	689K (666-697K)
	C67.5/T32.5	692K (668-699K)
	C60/T40	693K (666-706K)
	C50/T50	695K (682-706K)
	C40/T60	697K (692-711K)
	C25/T75	701K (697-706K)
	<u>Terylene (T)</u>	<u>710K (702-712K)</u>
(b)	<u>Courtelle (C)</u>	-
	C92.5/T7.5	693K (687-699K)
	C85/T15	698K (694-706K)
	C75/T25	706K (701-711K)
	C67.5/T32.5	709K (699-713K)
	C60/T40	713K (704-718K)
	C50/T50	724K (720-725K)
	C40/T60	728K (726 -730K)
	C25/T75	734K (730 -741K)
	<u>Terylene (T)</u>	<u>745K (741-746K)</u>

Table 9.3(2)

Position of (a) Courtelle exotherm [568K (568-570K)]
 (b) Terylene endotherm [530K (529-531K)]
 in the D.T.A. curves of Terylene/Courtelle mixtures.

	Mixture (mass %)	Peak temperature (K)
(a)	<u>Courtelle (C)</u>	<u>568K (568-570K)</u>
	C92.5/T7.5	568K (565-570K)
	C85/T15	568K (568-569K)
	<u>C75/T25</u>	<u>568K (565-570K)</u>
	C67.5/T32.5	568K (565-569K)
	C60/T40	568K (565-570K)
	C50/T50	568K (565-570K)
	C40/T60	567K (565-568K)
	C25/T75	567K (563-568K)
	<u>Terylene (T)</u>	<u>-</u>
(b)	<u>Courtelle (C)</u>	<u>-</u>
	C92.5/T7.5	-
	C85/T15	526K (526-529K)
	<u>C75/T25</u>	<u>528K (526-529K)</u>
	C67.5/T32.5	528K (526-529K)
	C60/T40	529K (526-531K)
	C50/T50	529K (526-531K)
	C40/T60	529K (529-530K)
	C25/T75	529K (529K)
	<u>Terylene (T)</u>	<u>530K (529-531K)</u>

Table 9.3(3)

Residual yield of carbon at 1213K from the pyrolysis of Terylene/
Courtelle mixtures. Data from T.G. and large scale pyrolyses.

Mixture (mass %)	Residual Yield (mass %)	
	T.G.	Large Scale Pyrolysis
Courtelle (C)	43.0	43.9
C90/T10	-	43.7
C85/T15	-	43.2
C75/T25	43.0	41.6
C65/T35	-	41.1
C55/T45	-	40.5
C50/T50	36.0	38.2
C25/T75	27.0	27.6
Terylene (T)	16.5	18.4

Table 9.3(4)

Position of unassigned exothermic peak in D.T.A. curves of Terylene/Courtelle mixtures. Possibly arising from the superposition of the Courtelle exotherm 689K (676-704K) and Terylene exotherm. Whilst this latter peak was not resolved in this study other workers have reported peak temperatures of 653K⁴⁹ and 662K.⁵¹

Mixture (mass %)	Peak temperature (K)
Courtelle (C)	689K (676-704K)
C92.5/T7.5	667K (664-671K)
C85/T15	670K (661-680K)
C75/T25	677K (666-685K)
C67.5/T32.5	669K (646-685K)
C60/T40	666K (647-692K)
C50/T50	666K (649-680K)
C40/T60	662K (649-679K)
C25/T75	662K (645-680K)
Terylene (T)	653K, ⁴⁹ 662K ⁵¹ (literature values)

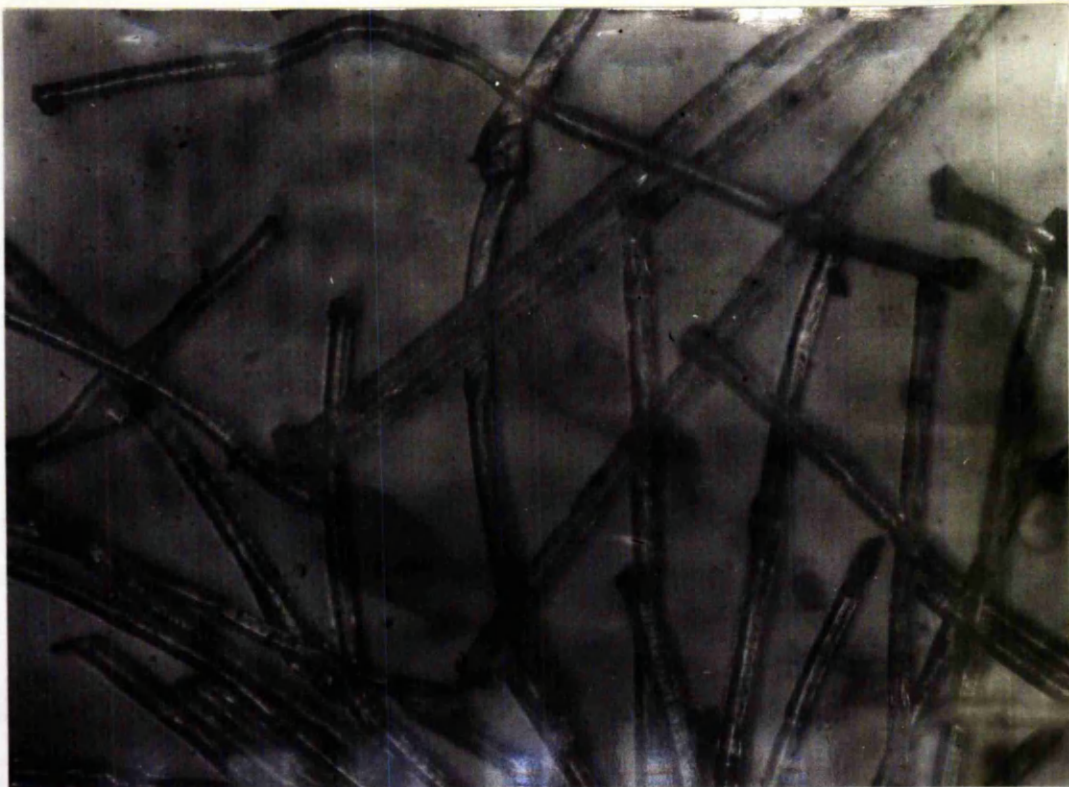


plate 9.3(1)
Terylene/Courtelle fibre mixture at room temperature (294K)

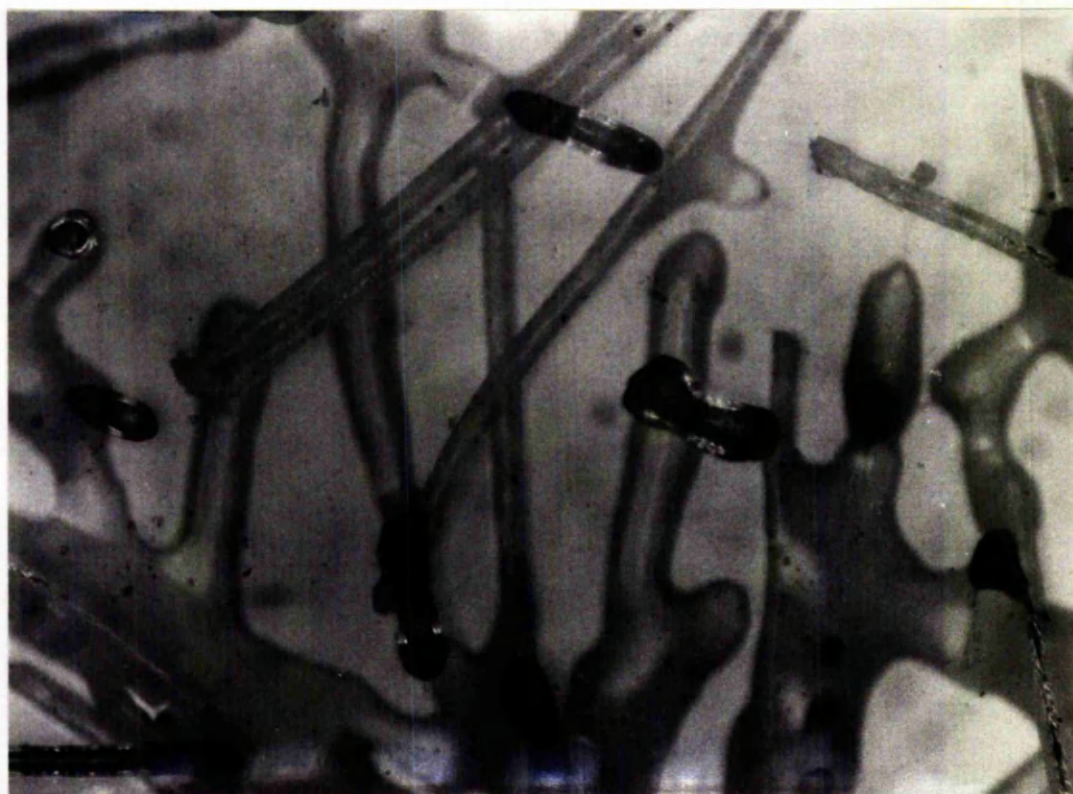


plate 9.3(2)
Terylene/Courtelle fibre mixture at 529K

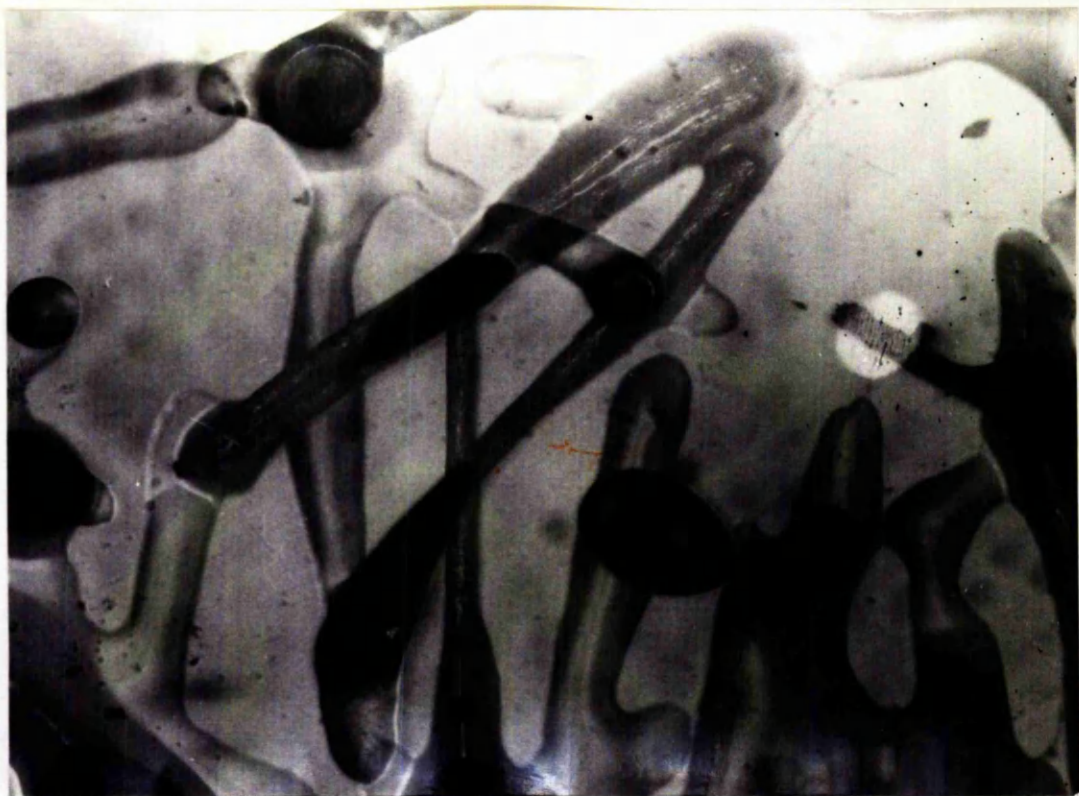


plate 9.3(3)
Terylene/Courtelle fibre mixture at 623K

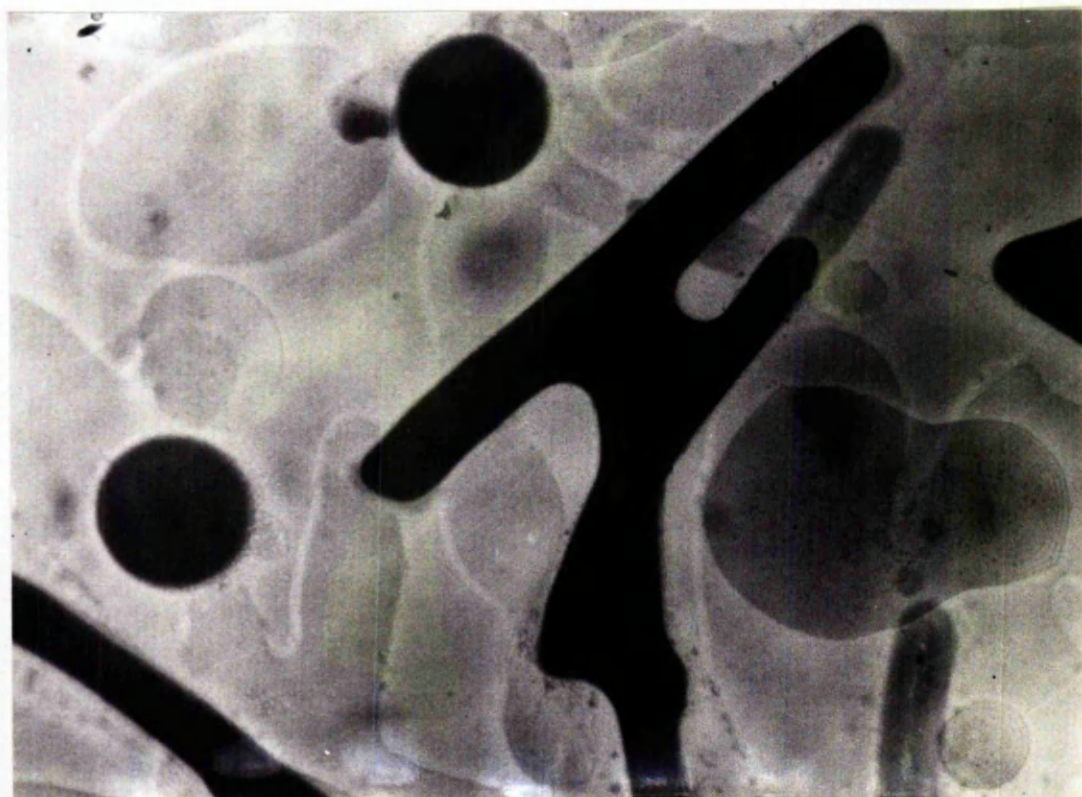


plate 9.3(4)
Terylene/Courtelle fibre mixture at approximately 710K

CHAPTER 10

Introduction to adsorption results and discussion

10.1 A criterion for comparison of adsorption results

It is clear from an examination of the appropriate figures in chapter 11 that relatively few of the D-R type I plots for the polymer carbons examined were in fact linear.

As discussed in chapter 6 it is clear that any attempt to determine values for the constants \underline{W}_0 and \underline{k} arising from application of the D-R type I equation can only be considered successful where complete linearity is observed.

In examples where only partial linearity of the D-R type I plot was observed, \underline{W}_0 and \underline{k} values may be obtained from the linear portion.

However as the D-R type I equation in these cases is only apparently applicable over a limited part of the relative pressure range, the values derived for \underline{W}_0 and \underline{k} may not be directly comparable with those obtained from a completely linear plot. In those cases where complete non-linearity of the D-R type I plot was observed it is obviously impossible to derive any values for the constants \underline{W}_0 and \underline{k} .

An alternative approach has therefore been sought to compare the adsorption data obtained from the various activated samples. By inspection it is evident that in the majority of cases adsorption isotherms of type I character as defined in the B.D.D.T. classification³⁵ were observed.

It was observed in some isotherms however that adsorption continued to occur at relative pressures larger than $P/p_0 = 0.3$.

It is believed in such cases that the amount of carbon dioxide adsorbed would reach a constant value at higher relative pressures on the grounds of recent and as yet unpublished work completed in this laboratory. In this work nitrogen adsorption isotherms (77K) were measured to saturation pressures for carbons prepared from Terylene and PAN homopolymer. In all cases the amount of nitrogen adsorbed eventually became constant, hence the isotherms approximate in character to type I.

For the great majority of isotherms examined in this study the adsorption reached a constant value at a relative pressure of c.a. $P/p_0 = 0.3$. It was therefore decided arbitrarily to adopt the

adsorption of carbon dioxide at 195K expressed in milligrams per gram of adsorbent at $P/p_0 = 0.3$ for the purposes of comparing the adsorption behaviour of carbon samples. Hereafter this adsorption parameter is referred to as the x_c value.

10.2 Format and treatment of adsorption results

Adsorption isotherms were determined for each activated polymer carbon sample. Thus from each polymer carbon a family of isotherms is presented and these isotherms reflect the adsorptive behaviour of the various activated samples over the relative pressure range investigated.

The burn-outs produced by carbon dioxide gasification were all determined exactly, however the individual burn-outs obtained differed slightly from the planned values of 0, 10, 20, 30, 40 and 50%. Thus the adsorption at $P/p_0 = 0.3$ for these latter planned burn-outs was interpolated from a plot of x_c against experimentally observed burn-out.

The x_c values for all polymer carbon samples investigated are listed in table 10.2(1). As previously discussed x_c values $\leq 10 \text{ mg g}^{-1}$ must be regarded as negligible. Further adsorption data where the x_c value lies in the range $10 \text{ mg g}^{-1} < x_c < 40 \text{ mg g}^{-1}$ must be regarded with caution in view of the considered accuracy of $\pm 5 \text{ mg g}^{-1}$.

As discussed in chapter 6 the D-R type I equation may be written in the linear form of equation 6.1(12).

$$\text{Log}W = \text{log}W_0 - D(\text{log}P/p_0)^2 \quad \text{Equation 6.1(12)}$$

The activated polymer carbon samples examined in this study are generally regarded as microporous adsorbents and therefore the D-R type I equation has been applied to the adsorption data.

As discussed in section 7.5 the D-R type I equation was plotted as $\text{log}a$ against $(\text{log}P/p_0)^2$ rather than $\text{log}W$ against $(\text{log}P/p_0)^2$.

Whilst it is believed¹¹⁶ that activated diffusion effects may be operative in polymer carbon samples activated to 0% no evidence for such effects has been found in this study. D-R type I plots have therefore been constructed for all 0% burn-out polymer carbons where a significant x_c value was recorded.

Observed deviations from linearity in D-R type I plots are discussed in terms of the classification of Marsh and Rand¹⁰² as previously discussed [see figure 6.4(1)].

In order to simplify the illustration of D-R type I plots, only representative plots are illustrated for the activated series derived

Table 10.2(1)

\underline{x}_c values for all polymer carbon samples investigated.

Single Polymers	\underline{x}_c mg g ⁻¹					
	Burn-out %					
	0	10	20	30	40	50
Wool	⑩	100	165	238	305	328
Terylene	255	300	360	442	538	645
Courtelle	∞	81	154	221	269	298
Polymer Mixtures						
W90/C10	⑫	90	152	208	246	237
W75/C25	∞	90	151	192	206	207
W60/C40	∞	75	146	190	196	182
W50/C50	∞	78	149	210	262	285
W35/C65	∞	78	145	200	240	258
W25/C75	∞	72	130	162	164	137
W15/C85	9	72	110	118	72	∞
W90/T10	⑫	114	192	268	330	373
W75/T25	43	135	235	303	381	449
W60/T40	⑩	132	214	290	352	402
W50/T50	⑩	126	198	256	300	330
W40/T60	⑪	128	205	272	335	391
W25/T75	105	151	250	311	369	420
C90/T10	1.5	⑬	⑭	⑮	∞	∞
C85/T15	∞	47.5	55.5	47.5	∞	∞
C75/T25	∞	70	114	134	127	105
C65/T35	∞	76	128	158	157	141
C55/T45	⑮	93	170	245	323	397
C50/T50	10	113	208	308	393	455
C25/T75	80	85	290	397	505	610

Key ∞ = negligible \underline{x}_c value i.e. ≤ 10 mg g⁻¹

⑪ = significant \underline{x}_c value, however error range $\geq 25\%$ of \underline{x}_c .

from each polymer carbon.

Whilst the Marsh and Rand classification¹⁰² is useful in terms of a general study of observed D-R type I deviations certain limitations are found in practice.

First, due to the thermodynamic limitations of the Potential theory as previously discussed and in view of Dovaston's findings¹¹⁶ concerning cellulose carbons only the portion of the D-R type I plot at $(\log P/P_0)^2 \leq 10$ has been considered for analysis. Whilst it is true this limit will probably vary from one system to another, the limit determined by Dovaston¹¹⁶ will be applied to the systems examined in this study in view of the lack of further thermodynamic data.

A second point concerning the Marsh and Rand classification¹⁰² is that in many cases where non-linearity was observed exact classification of the type of deviation was difficult.

Thus the Marsh and Rand type A deviation¹⁰² [see figure 6.4(1)] was reported to consist of two linear portions. Whilst the general shape of this deviation was observed in certain cases in this study, it was often found that the plot consisted in practice of a linear portion at high values of $(\log P/P_0)^2$ and a curved portion at low $(\log P/P_0)^2$ values.

The adsorption results from this study are presented in four sections. The first section (11.1) contains adsorption data for the polymer carbons derived from wool, Terylene and Courtelle. The following three sections (11.2, 11.3, 11.4) contain the adsorption data for the three binary textile polymer systems - wool/Terylene, wool/Courtelle and Terylene/Courtelle. For each of the carbons derived from the single polymers and from the binary polymer mixtures three diagrams are presented. The first illustrates the adsorption isotherms for each burn-out. The second shows the change in the observed \underline{x}_c value with burn-out and the third illustrates the D-R type I plots for representative burn-outs.

Included at the end of each section dealing with a particular binary mixture there is a master diagram illustrating the change in the \underline{x}_c value for each burn-out over the complete composition range.

Each isotherm and D-R type I plot presented is designated by the number of the isotherm from which the data is derived (e.g. I29) and the exact burn-out (%) of the particular polymer carbon (e.g. 29.7%).

Further, in order to facilitate analysis of the adsorption isotherms and D-R type I plots presented the data for the different planned burn-outs are plotted according to the key presented below.

Burn-out (%)	data point
50	—□—
40	—△—
30	—○—
20	—×—
10	—=—
0	—▽—

CHAPTER 11

Results and preliminary discussion of the adsorption studies on polymer carbons

11.1(a) Wool carbon

The adsorption isotherms obtained for activated wool carbon samples [see figure 11.1(1)] indicated that with increasing degree of activation the value of x_c reaches a maximum at c.a. 40-50% burn-out. This behaviour is clearly illustrated in figure 11.1(2).

The adsorption isotherm for 0% burn-out indicated that little accessible porosity was present in the carbon formed by pyrolysis. However gasification was effective in initially increasing the adsorptive capacity.

D-R type I plots for three representative activated wool carbon samples are illustrated in figure 11.1(3).

In discussing these plots the planned burn-out value will be utilised rather than the actual exact burn-out value (e.g. 10% rather than 8.3% in the case of I29).

For 10% burn-out, type A deviation was observed whilst the 20% burn-out plot was approximately linear. At burn-outs greater than 20% type B deviation was observed, the curvature increasing with increasing activation.

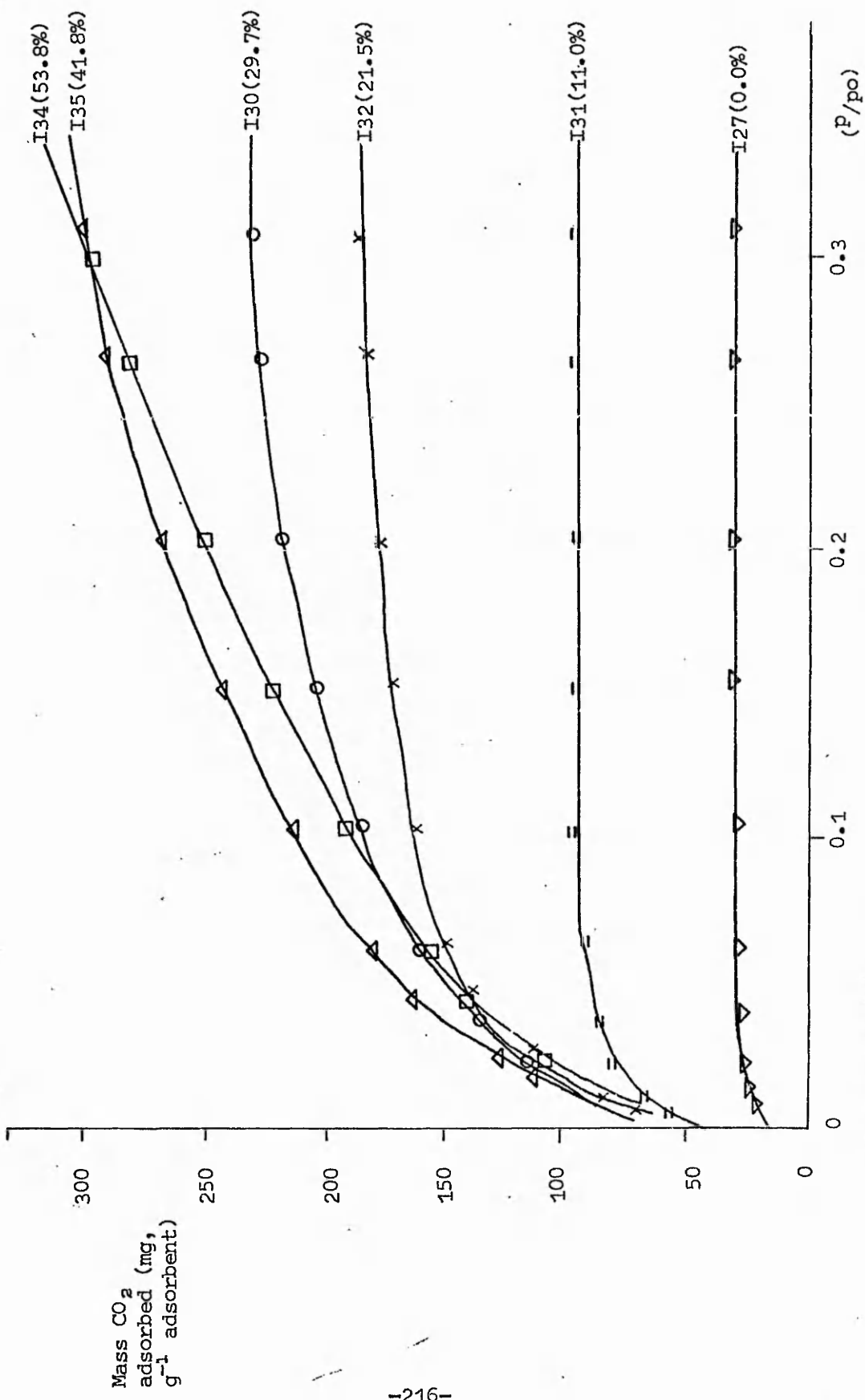


Figure 11.1(1)
 Adsorption of carbon dioxide at 195K on 1313K wool carbon activated by carbon dioxide at 1303K.

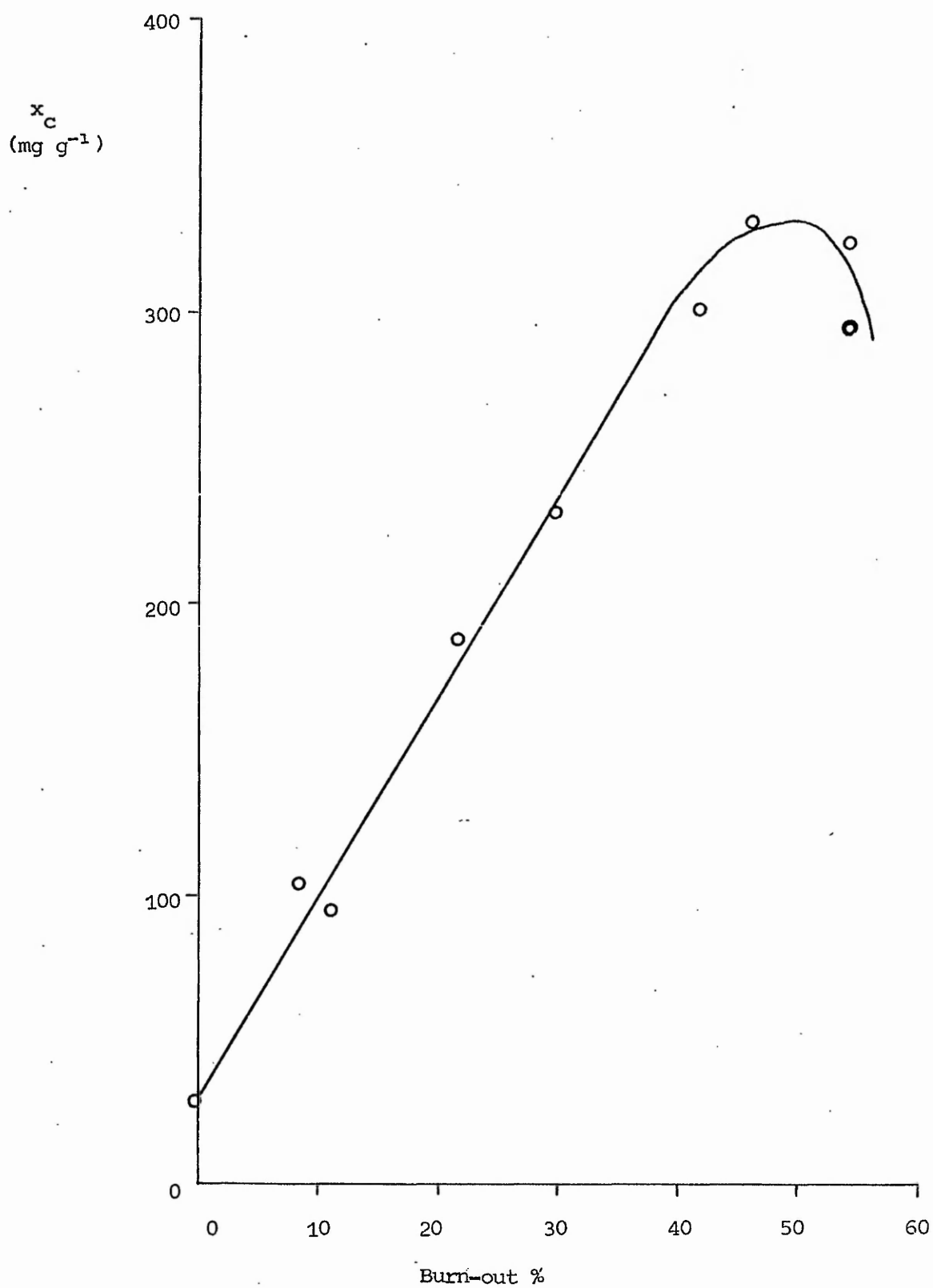


Figure 11.1(2)
 Variation of x_c (mg g^{-1}) with burn-out (%) for wool carbon.

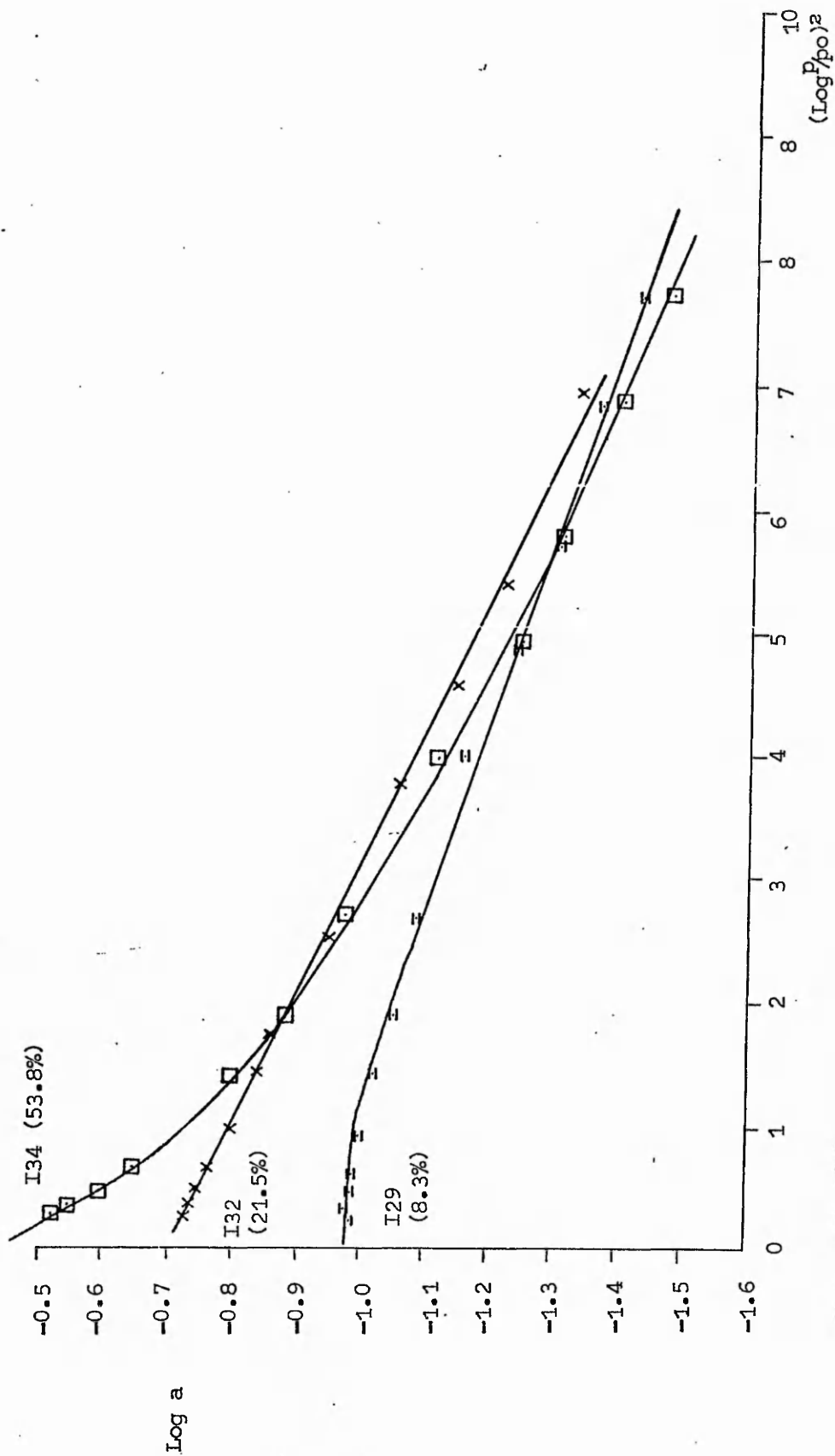


Figure 11.1(3)
Representative D-R type I plots for wool carbons.

11.1(b) Terylene carbon

From figures 11.1(4) and 11.1(5) it is clear that in the burn-out range 0-56% increasing activation of Terylene carbon produced corresponding increases in adsorption.

Both activated and unactivated Terylene carbons were characterised by a large adsorptive capacity for carbon dioxide (195K). Thus the samples activated to 0% and 50% burn-out had x_c values of approximately 250 mg g⁻¹ and 650 mg g⁻¹ respectively.

The D-R type I plots for all the Terylene carbon samples exhibited type A deviation. The slope of the linear portions of each plot both increased as the degree of activation increased [see figure 11.1(6)].

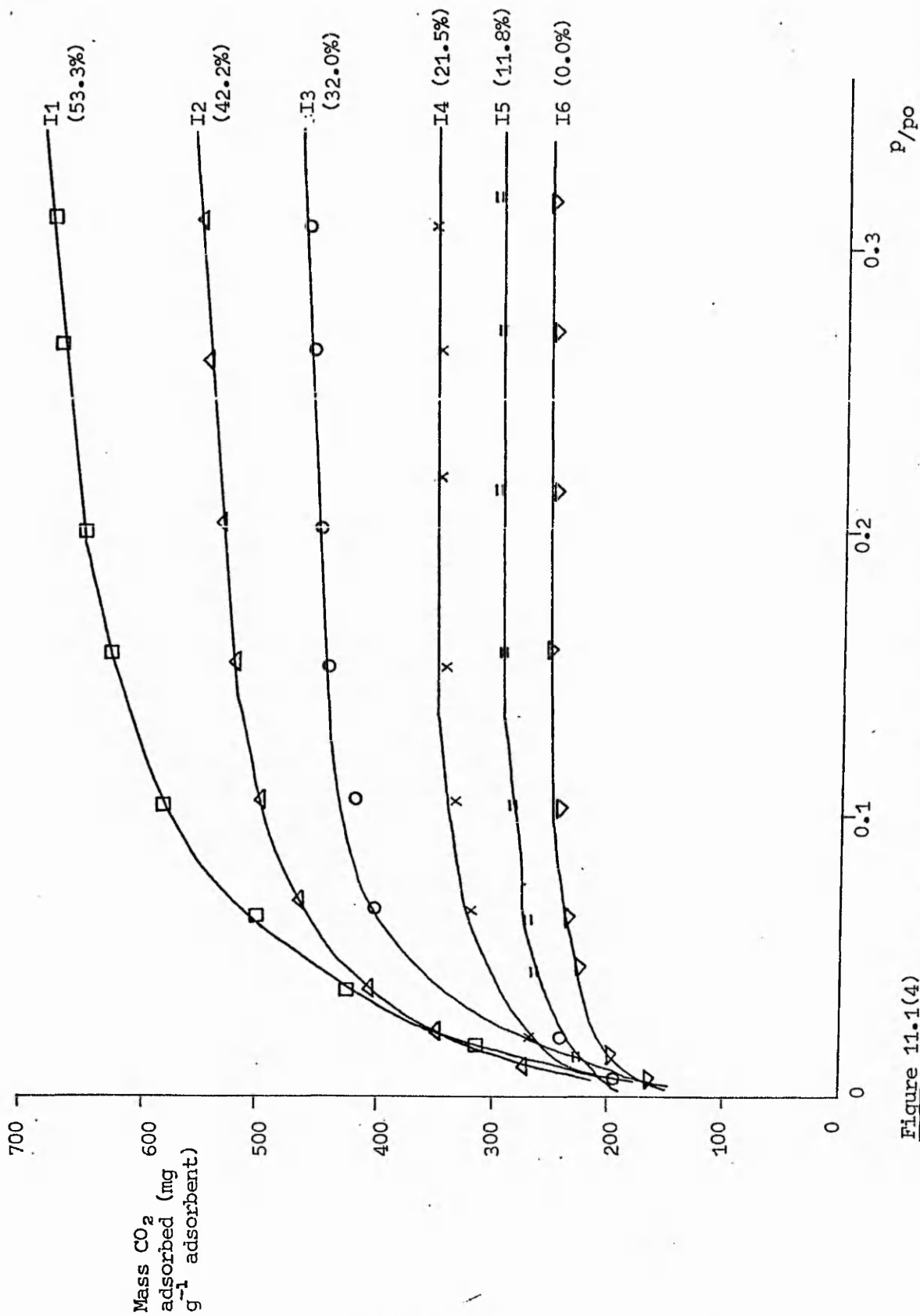


Figure 11.1(4)
 Adsorption of carbon dioxide at 195K on 1313K Terylene carbon activated by carbon dioxide at 1303K.

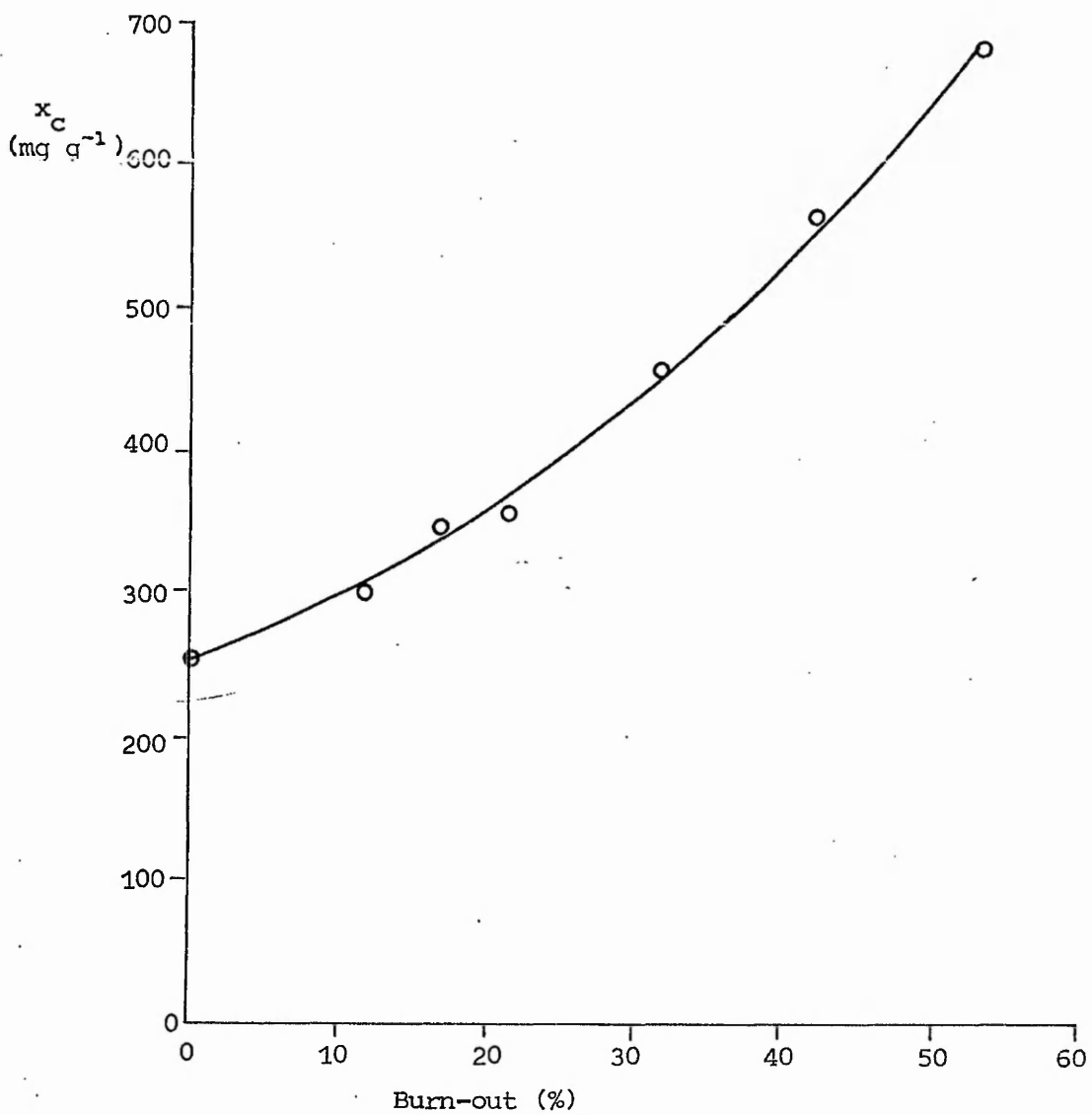


Figure 11.1(5)
 Variation of x_c (mg g^{-1}) with burn-out (%) for Terylene carbon.

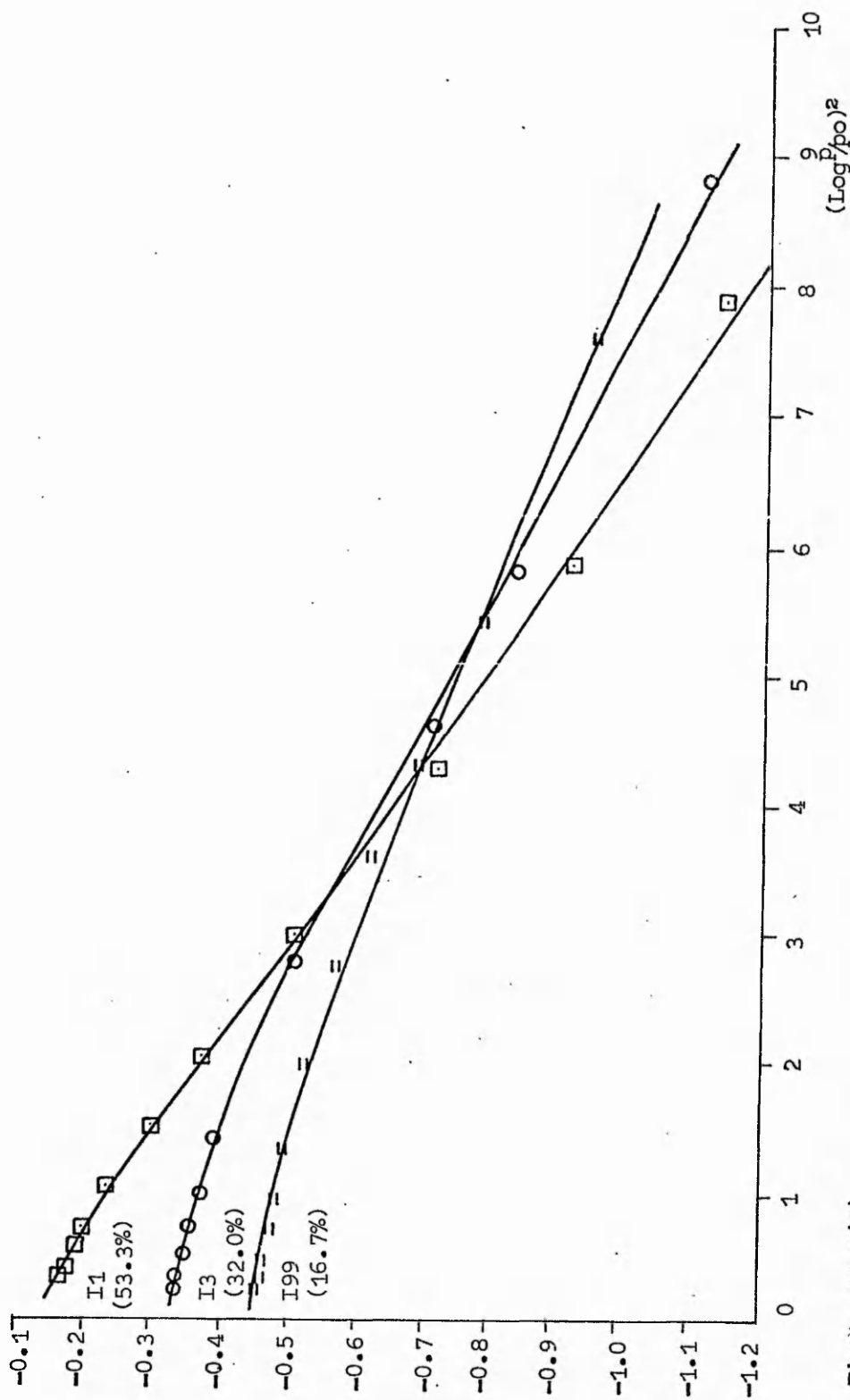


Figure 11.1(6)
Representative D-R type I plots for Terylene carbons.

11.1(c) Courtelle carbon

As illustrated in figures 11.1(7) and 11.1(8) the carbon produced by the pyrolysis of Courtelle contained little accessible porosity.

However it was apparent that adsorptive capacity increased considerably with increased activation.

Representative D-R type I plots are illustrated in figure 11.1(9). For both 10% and 20% burn-outs the D-R type I plot may be considered linear. However at higher degrees of activation type B deviation was observed, the curvature increasing with the degree of activation.

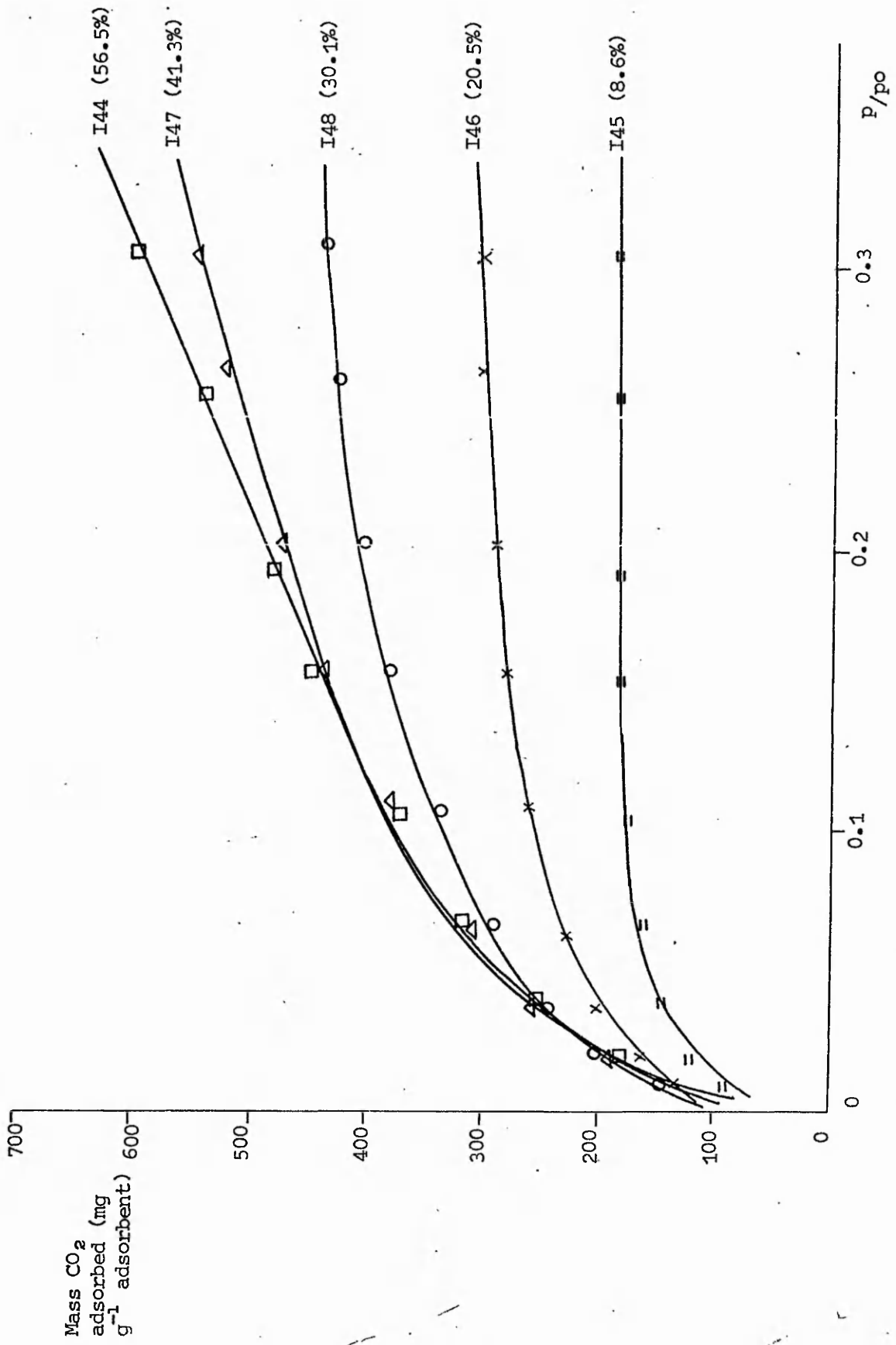


Figure 11.1(7)
 Adsorption of carbon dioxide at 195K on 1313K Courtelte carbon activated by carbon dioxide at 1303K.

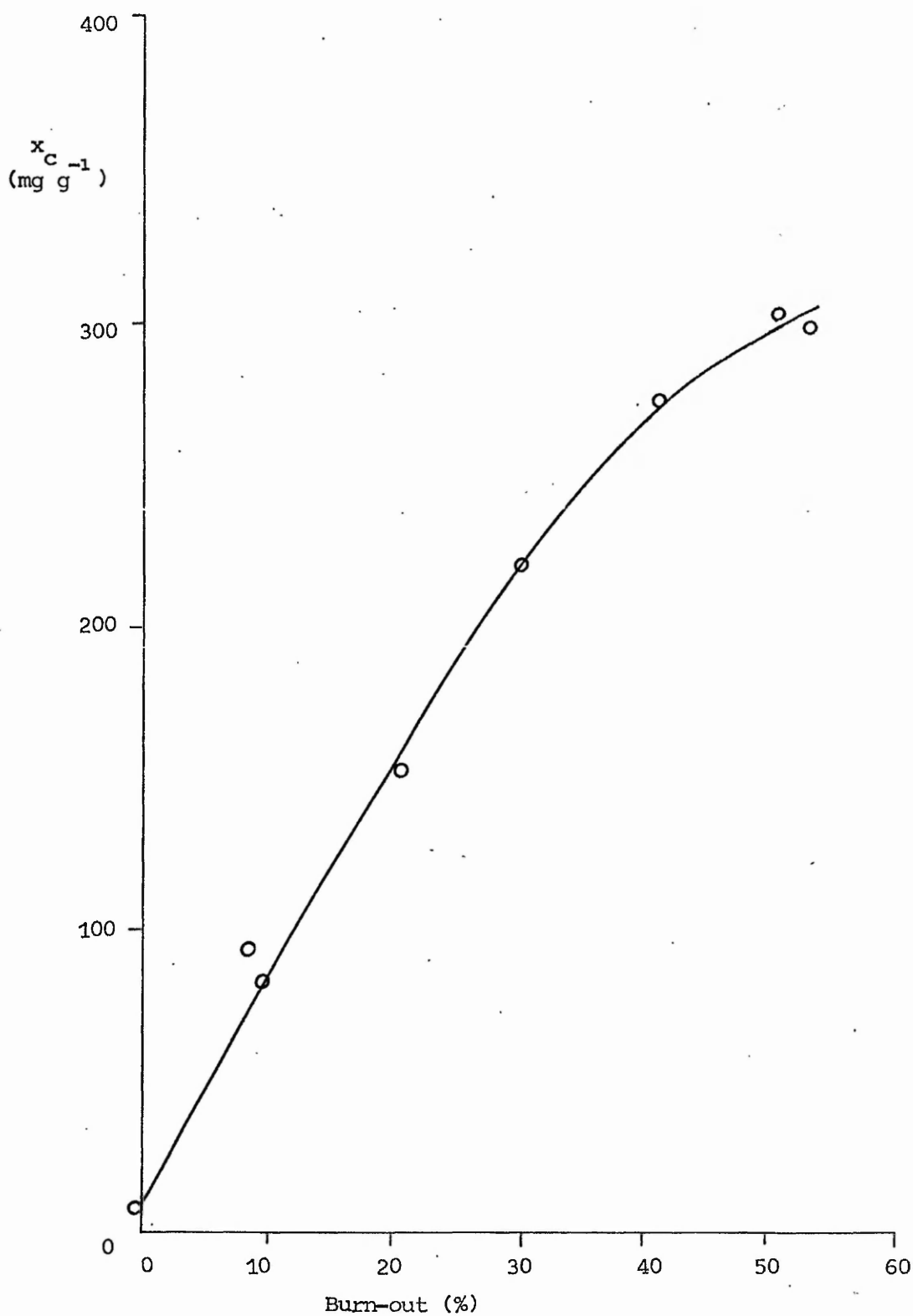


Figure 11.1(8)
Variation of x_c (mg g^{-1}) with burn-out (%) for Courtelle carbon.

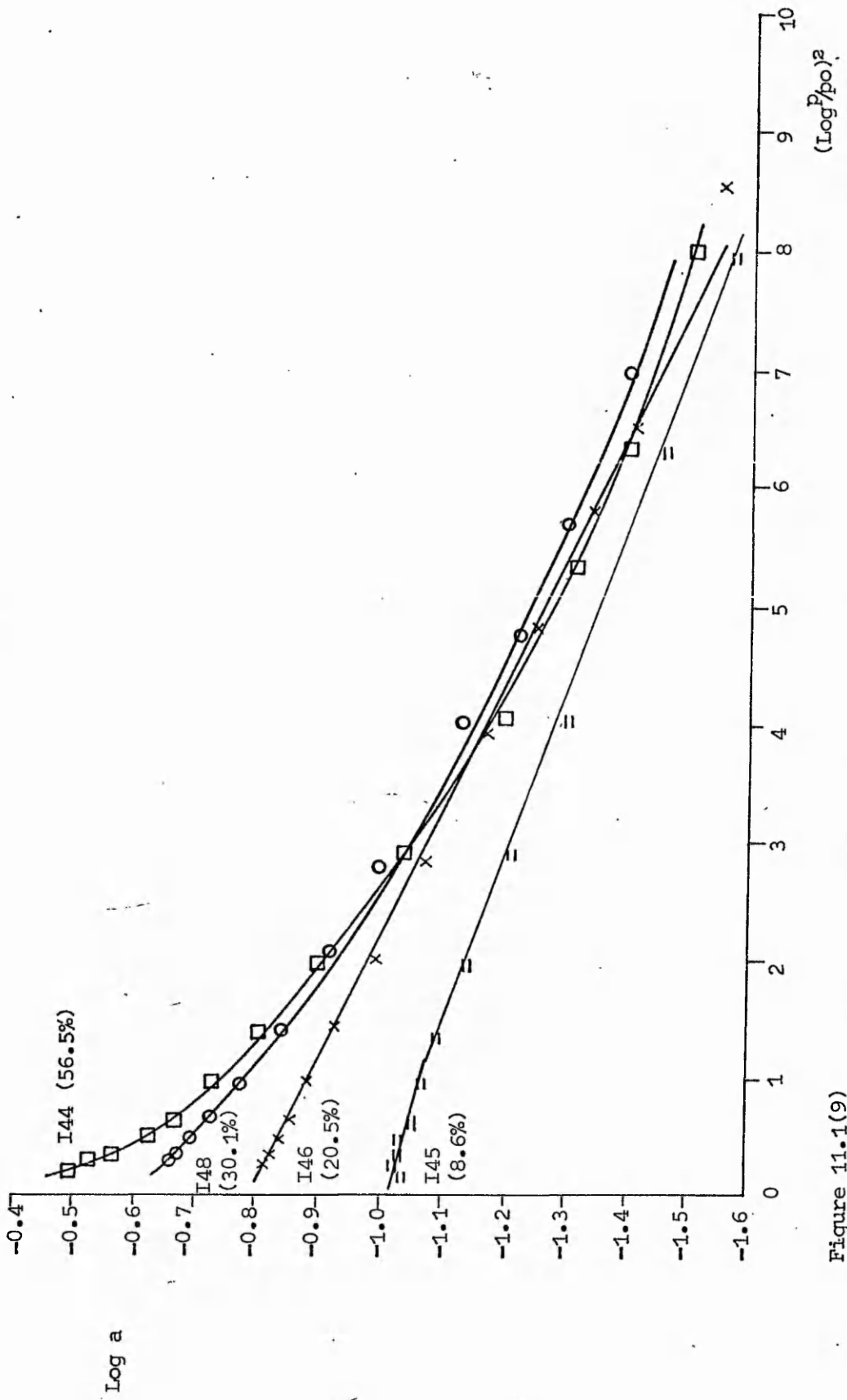


Figure 11.1(9)
 Representative D-R type I plots for Courtelle carbons.

11.2 Wool/Terylene carbon

The textile polymer mixtures from which the wool/Terylene carbons were produced are listed in table 11.2(1). This table also provides a key to the location of all the adsorption data presented for this system of carbons.

For each carbon the variation of \underline{x}_c with burn-out is summarised in table 11.2(2).

From table 11.2(2) it is clear that throughout the wool/Terylene system (with the exception of wool) over the burn-out range investigated, progressive activation resulted in a continuous increase in \underline{x}_c .

Representative D-R type I plots for the wool/Terylene system are located as indicated in table 11.2(1). The overall behaviour of the system in terms of the type of D-R type I plot observed is indicated in table 11.2(3).

From a consideration of both tables 11.2(2) and 11.2(3) few clear trends are apparent through the system.

Thus a continuous increase in \underline{x}_c was observed with burn-out for all except the carbon derived from wool. Further the maximum observed \underline{x}_c value decreased from Terylene to W50/T50, this decrease was however somewhat irregular.

Table 11.2(3) indicates that at low burn-out (i.e. 0%, 10%) type A deviation of the D-R type I plot was generally observed. At high burn-outs (i.e. 40%, 50%) with the exception of the carbon derived from Terylene, type B deviation was generally observed.

From table 11.2(3) it is clear that at intermediate burn-outs (i.e. 20%, 30%) linear D-R type I plots were observed together with examples of both type A and type B deviations.

The overall variation in \underline{x}_c with increasing degree of burn-out for all the carbons prepared from wool/Terylene mixtures is illustrated in figure 11.2(19). It is apparent from an examination of figure 11.2(19) that certain trends do exist in the variation of \underline{x}_c with both burn-out and composition of the original polymer mixture. The significance of these trends together with that of the trends observed in the corresponding figures for the wool/Courtelle and Terylene/Courtelle will be assessed in chapter 13.

Table 11.2(1)

Location of (a) adsorption isotherms

(b) $\frac{x_c}{c}$ /burn-out diagrams

(c) D-R type I plots.

for the wool/Terylene system.

Mixture (mass %)	(a) Adsorption Isotherms	(b) $\frac{x_c}{c}$ /burn-out diagrams	(c) D-R type I plots
Wool (W)	figure 11.1(1)	figure 11.1(2)	figure 11.1(3)
W90/T10	" 11.2(1)	" 11.2(2)	" 11.2(3)
W75/T25	" 11.2(4)	" 11.2(5)	" 11.2(6)
W60/T40	" 11.2(7)	" 11.2(8)	" 11.2(9)
W50/T50	" 11.2(10)	" 11.2(11)	" 11.2(12)
W40/T60	" 11.2(13)	" 11.2(14)	" 11.2(15)
W25/T75	" 11.2(16)	" 11.2(17)	" 11.2(18)
Terylene (T)	" 11.1(4)	" 11.1(5)	" 11.1(6)

Table 11.2(2)

Summary of the \bar{x}_C /burn-out diagrams for the carbons of the wool/Terylene system.

Mixture (mass %)	figure	behaviour observed	maximum \bar{x}_C value observed in the burn-out range 0-50%
Wool (W)	11.1(2)	maximum \bar{x}_C value occurs at 45-55% burn-out	330 mg g ⁻¹
W90/T10	11.2(2)	continuous increase in \bar{x}_C value with burn-out	370 mg g ⁻¹ (at 50% burn-out)
W75/T25	11.2(5)	———— " ————	475 ———— " ————
W60/T40	11.2(8)	———— " ————	400 ———— " ————
W50/T50	11.2(11)	———— " ————	330 ———— " ————
W40/T60	11.2(14)	———— " ————	390 ———— " ————
W25/T75	11.2(17)	———— " ————	420 ———— " ————
Terylene (T)	11.1(5)	———— " ————	650 ———— " ————

Table 11.2(3)

Applicability of the D-R type I equation to the wool/Terylene carbon system. Deviations from linearity are classified according to the notation of Marsh and Rand.¹⁰²

Mixture (mass %)	Burn-out (%)					
	0	10	20	30	40	50
Wool (W)	(A)	A	L	B	B	B
W90/T10	(A)	A	A	L	B	B
W75/T25	(A)	A	A	L	B	B
W60/T40	(A)	A	A	L	B	B
W50/T50	(B/L)	A	L	B	B	B
W40/T60	(L)	A	A	L	B	B
W25/T75	C	A	L	L	B	B
Terylene(T)	A	A	A	A	A	A

Key

A = Type A deviation (according to Marsh and Rand)¹⁰²

B = " B " " " " " "

C = " C " " " " " "

L = Linear plot

X = Not plotted, negligible gas uptake.

Where A, B, C, L ringed indicates possible error range $\geq 25\%$ of corresponding x_c value.

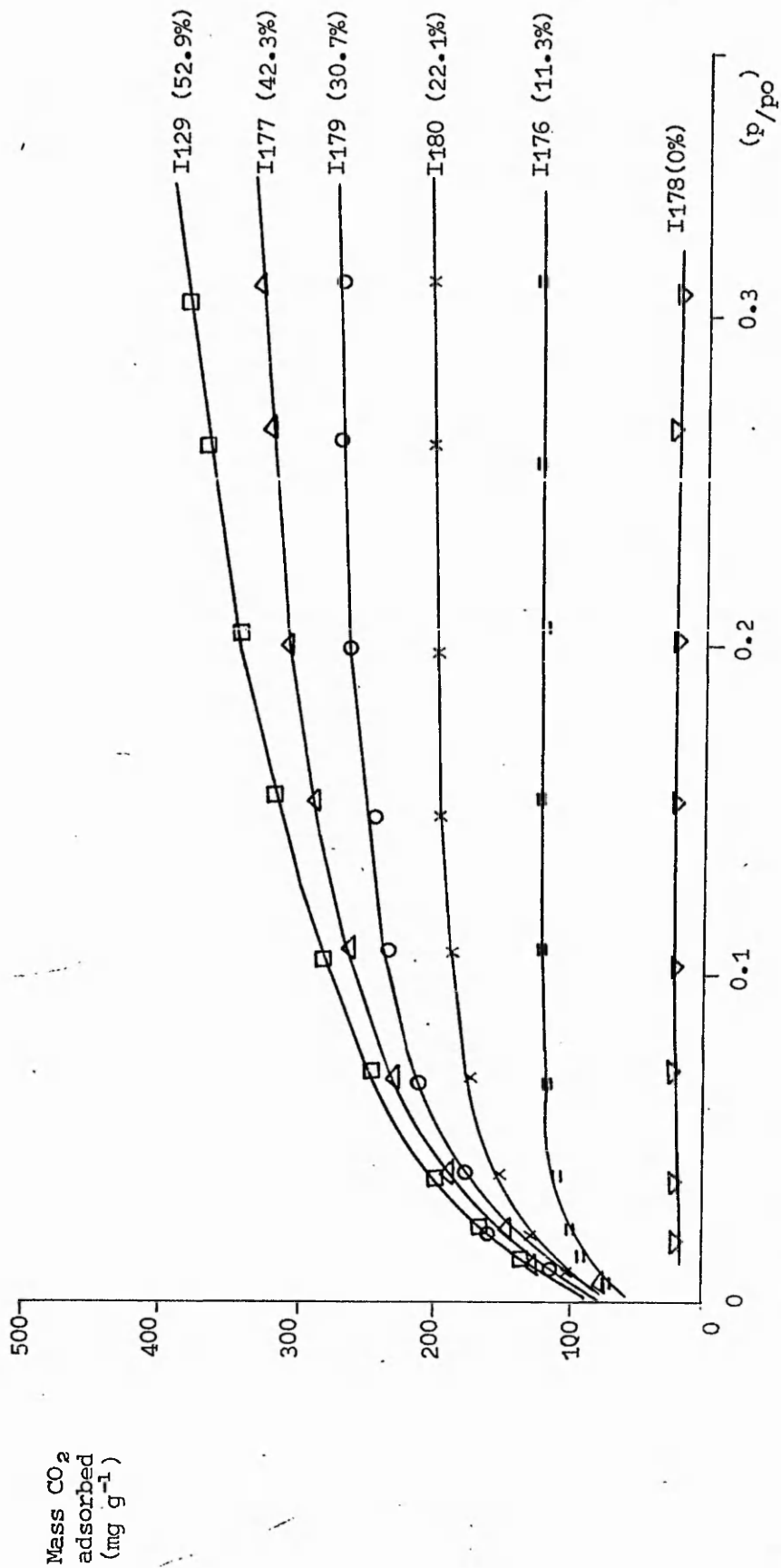


Figure 11.2(1)
Adsorption of carbon dioxide at 195K on 1313K W90/T10 carbon activated by carbon dioxide at 1303K.

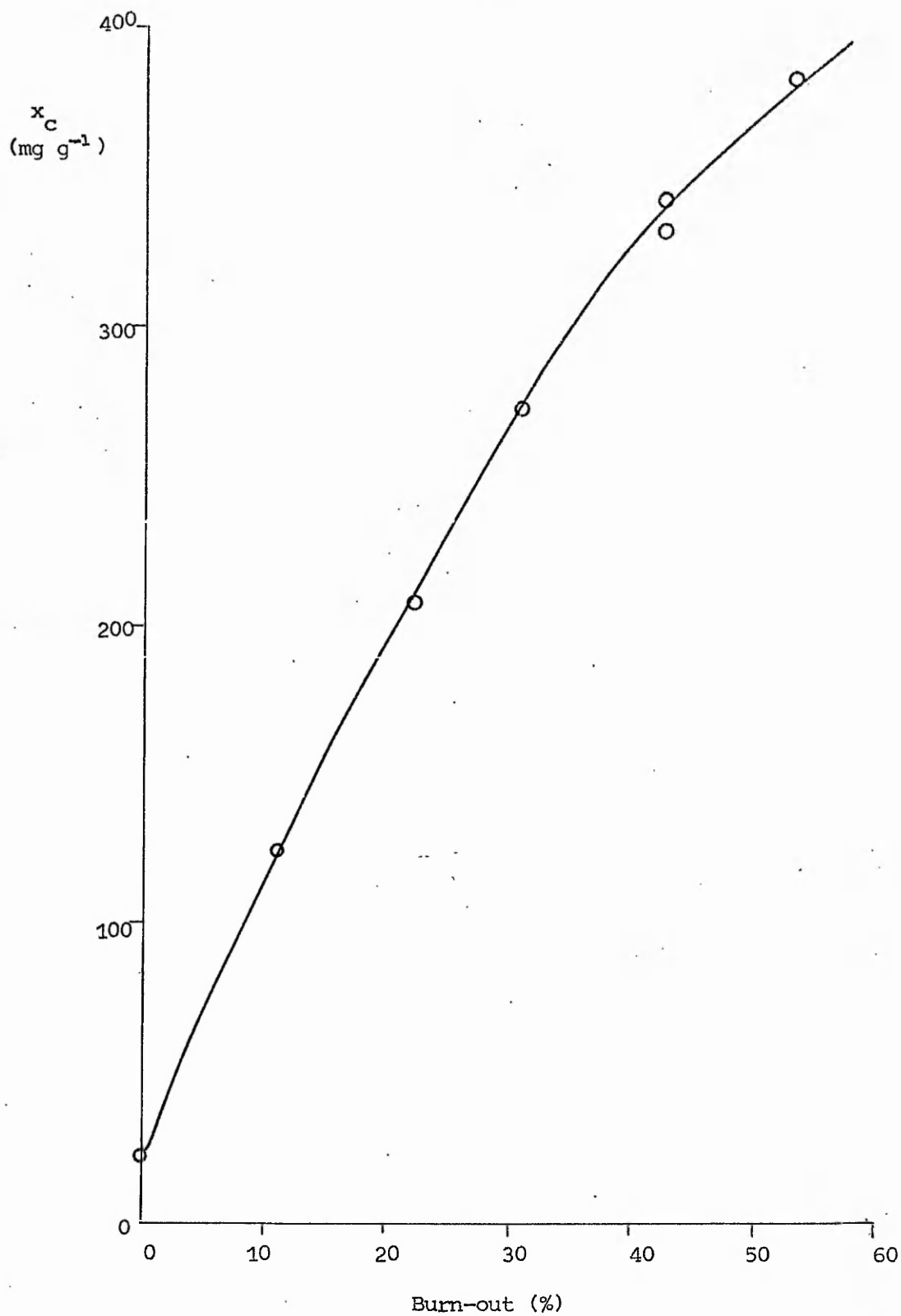


Figure 11.2(2)
 Variation of x_c (mg g^{-1}) with burn-out (%) for W90/T10 carbon.

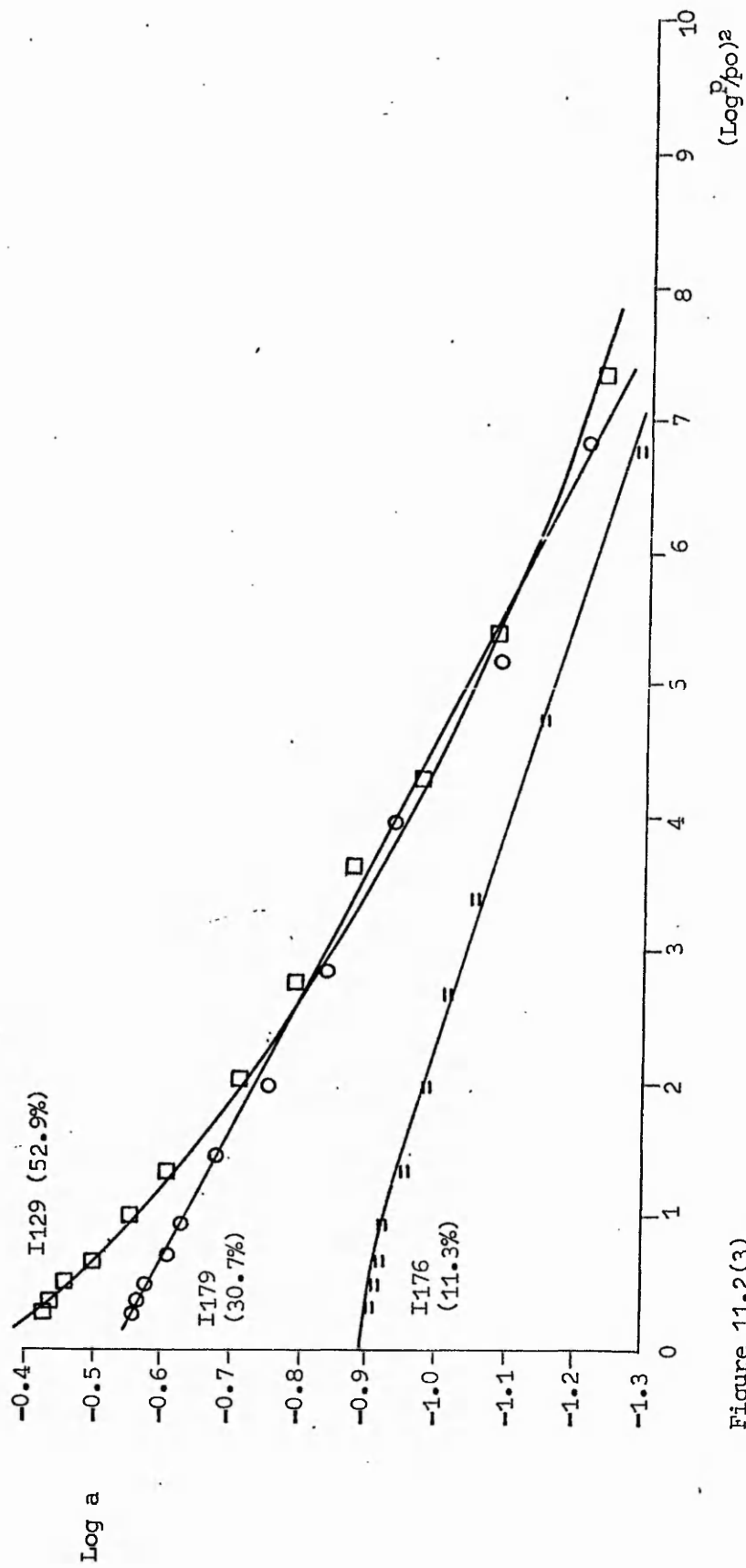


Figure 11.2(3)
 Representative D-R type I plots for W90/T10 carbons.

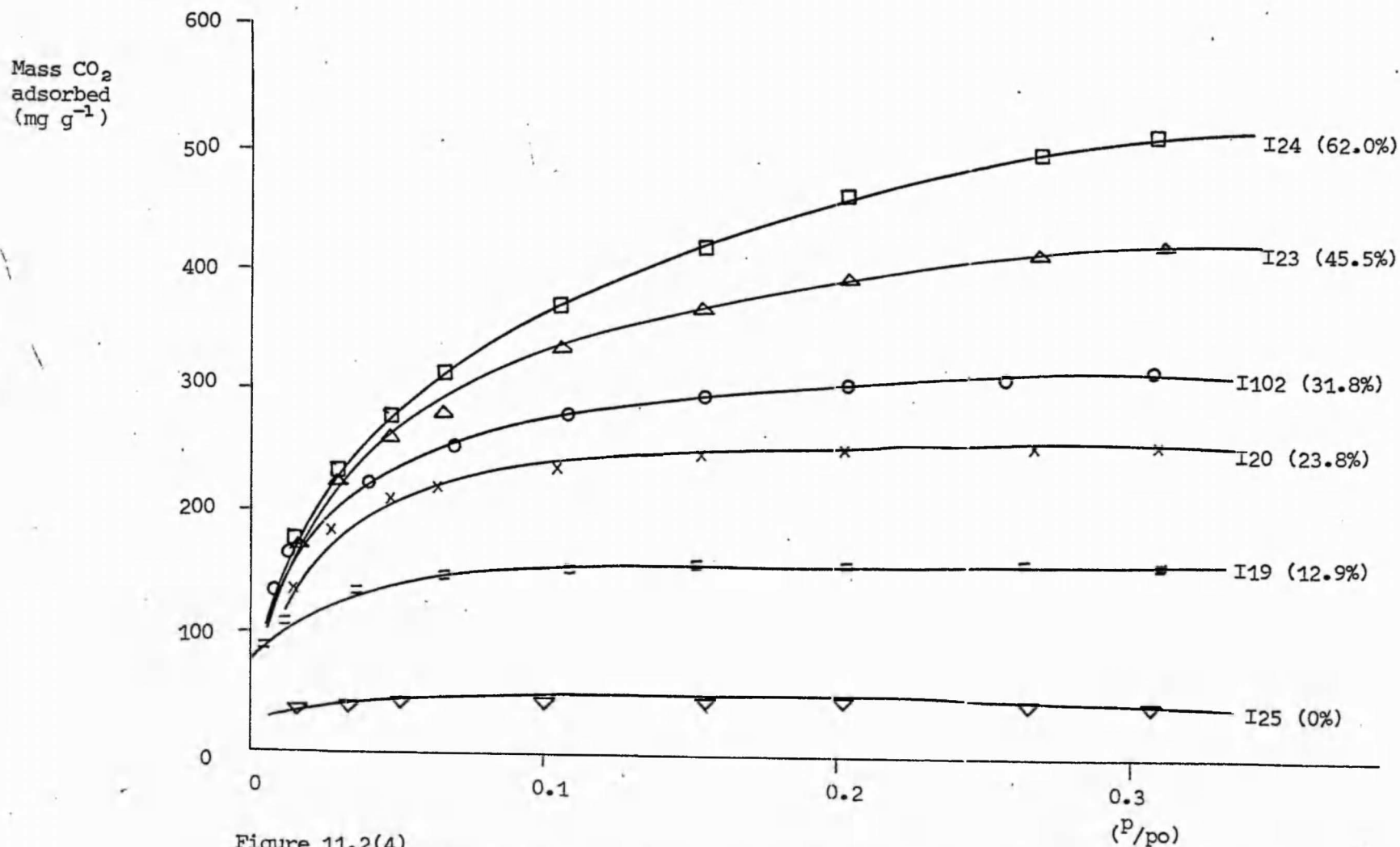


Figure 11.2(4)
Adsorption of carbon dioxide at 195K on 1313K W75/T25 carbon activated by carbon dioxide at 1303K

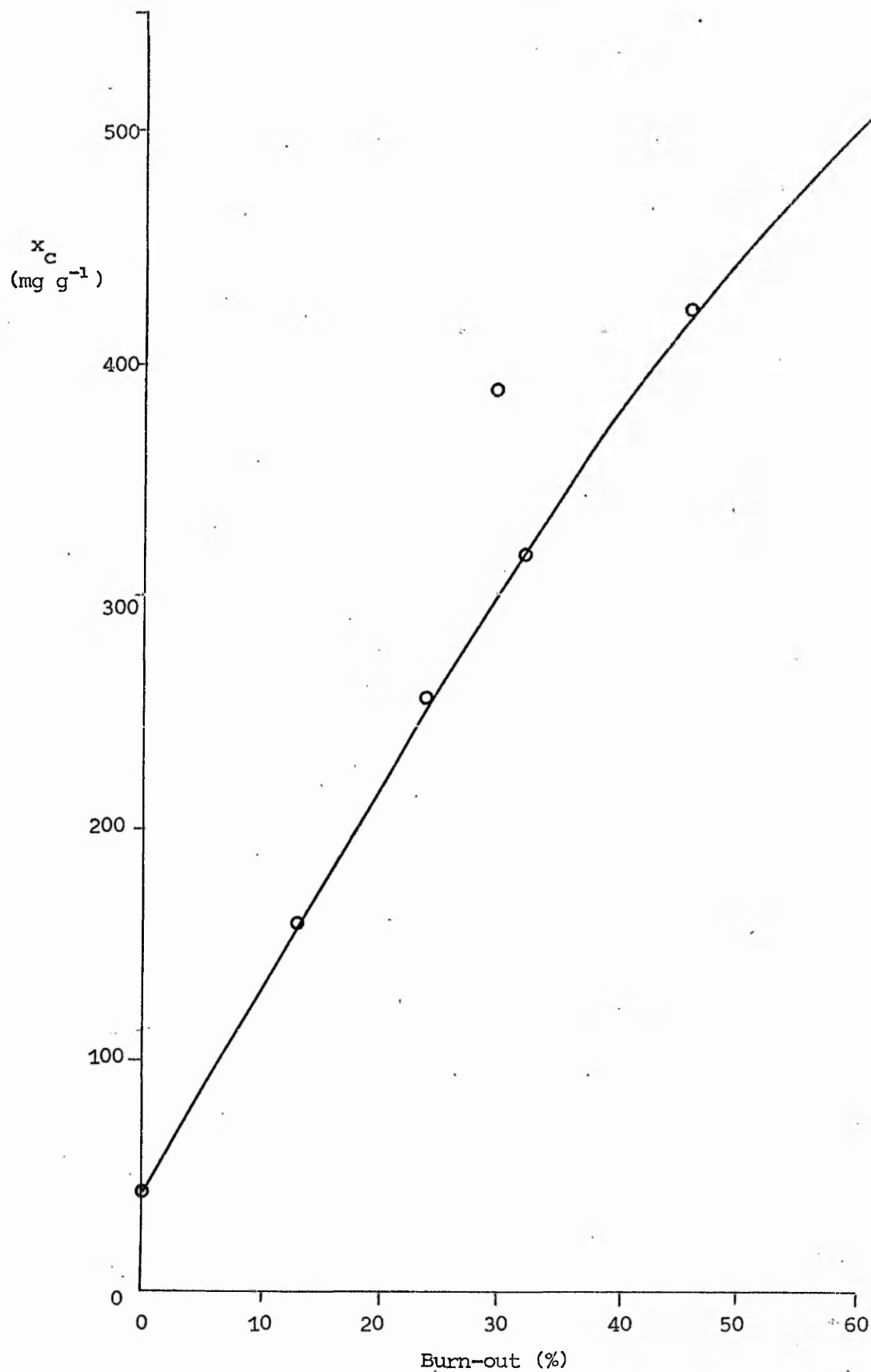


Figure 11.2(5)
Variation of x_c (mg g^{-1}) with burn-out (%) for W75/T25 carbon.

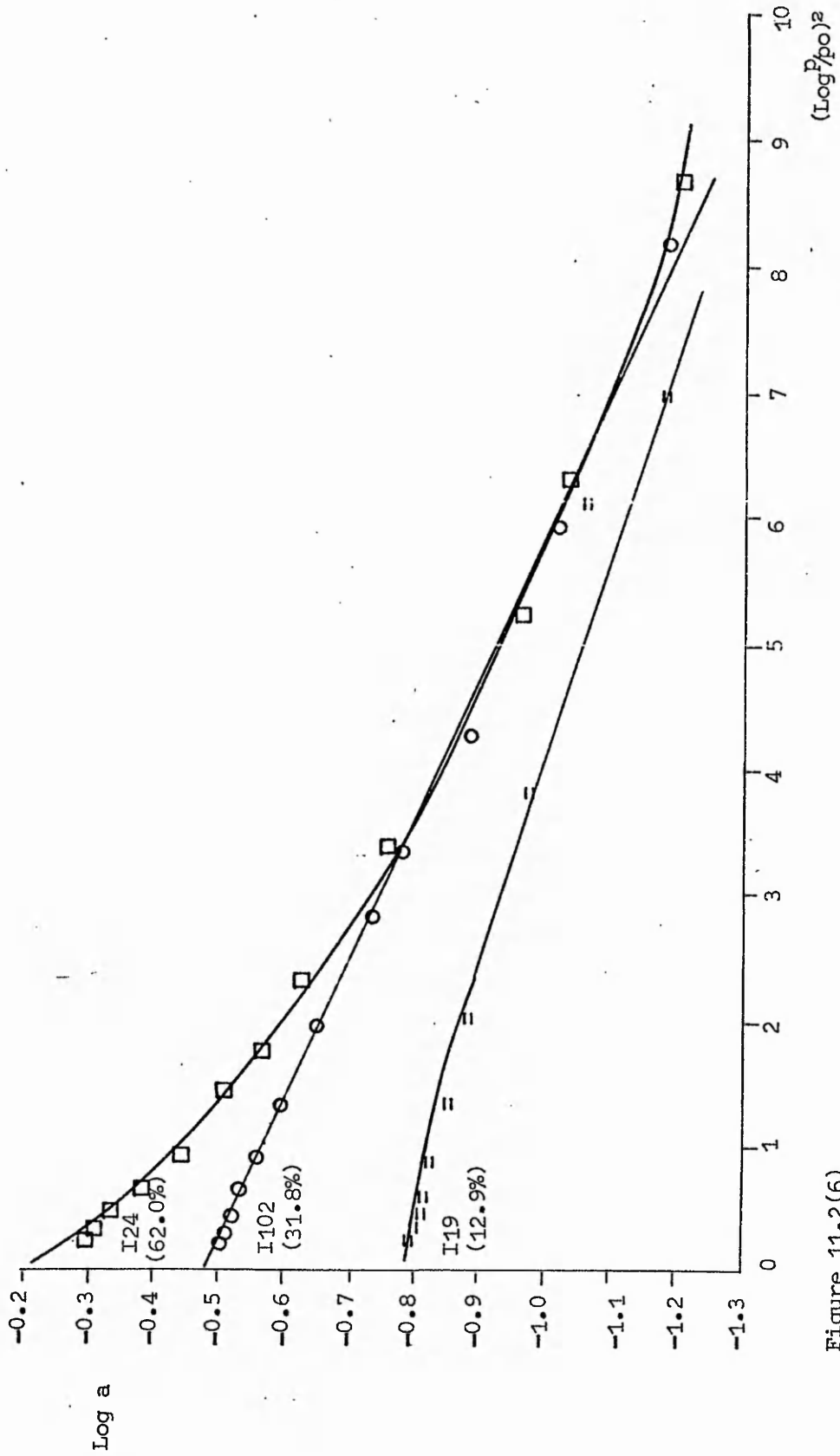


Figure 11.2(6)
 Representative D-R type I plots for W75/T25 carbon

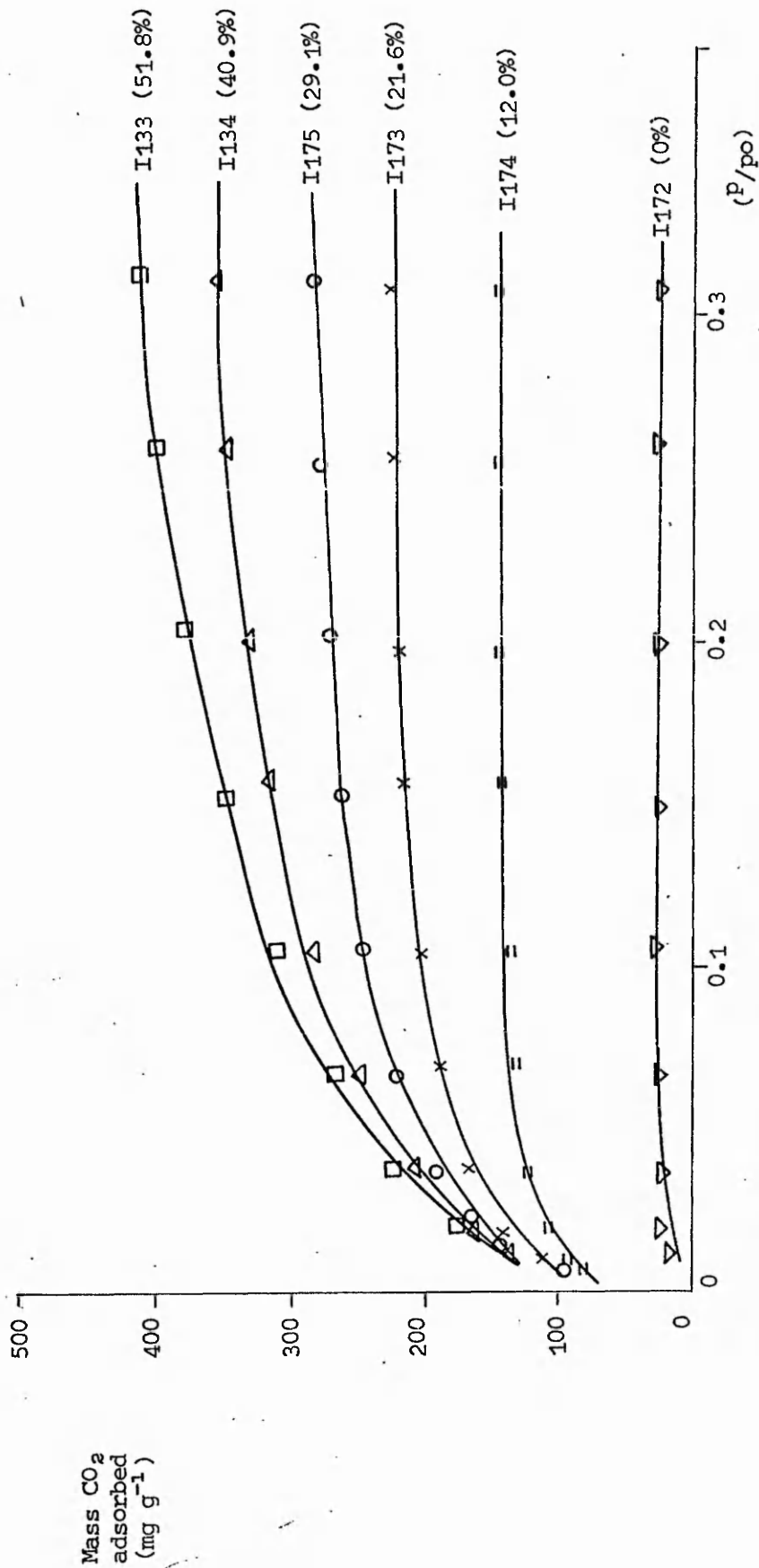


Figure 11.2(7)
 Adsorption of carbon dioxide at 195K on 1313K W60/T40 carbon activated by carbon dioxide at 1303K.

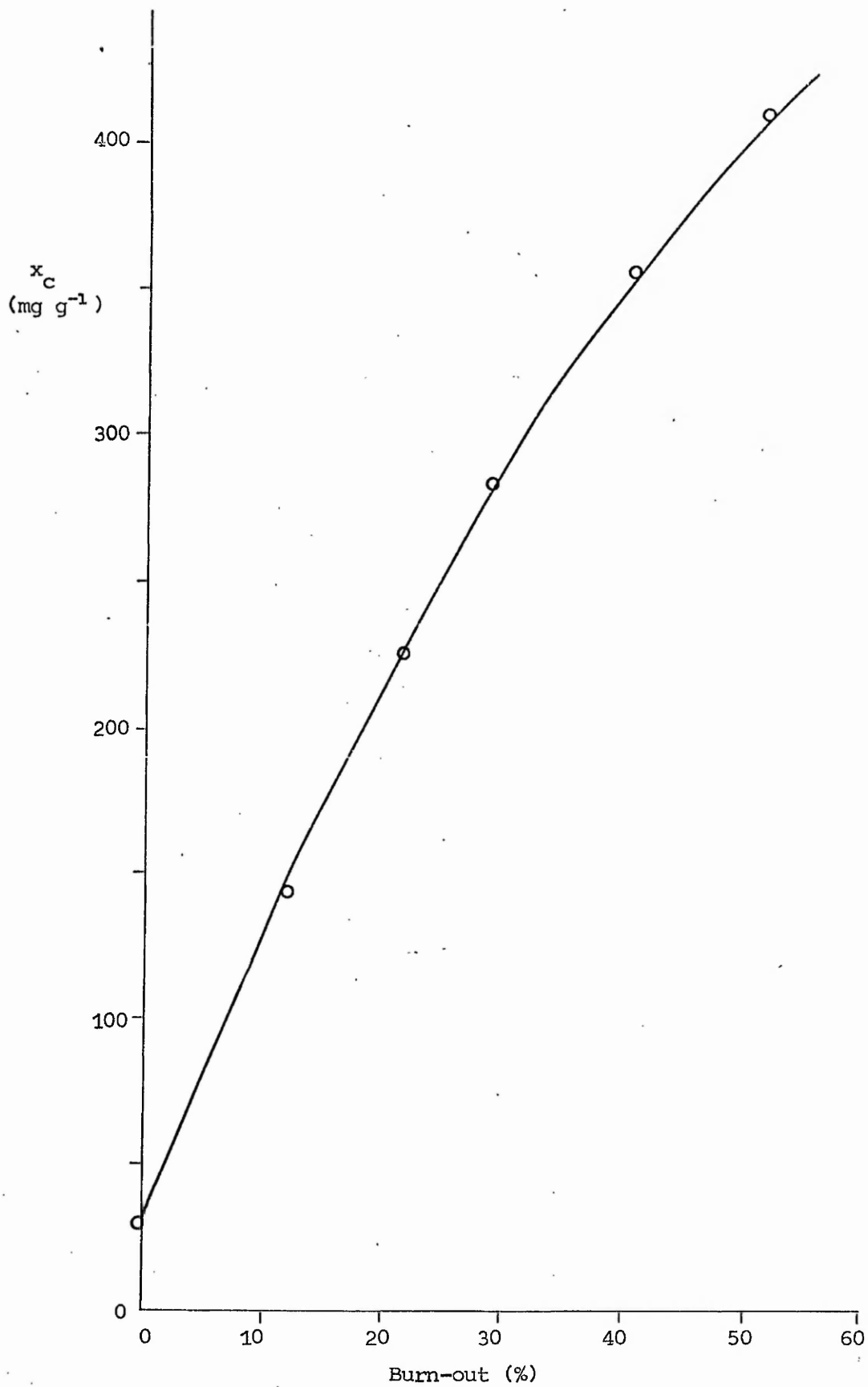


Figure 11.2(8)
Variation of x_C (mg g^{-1}) with burn-out (%) for W60/T40 carbon.

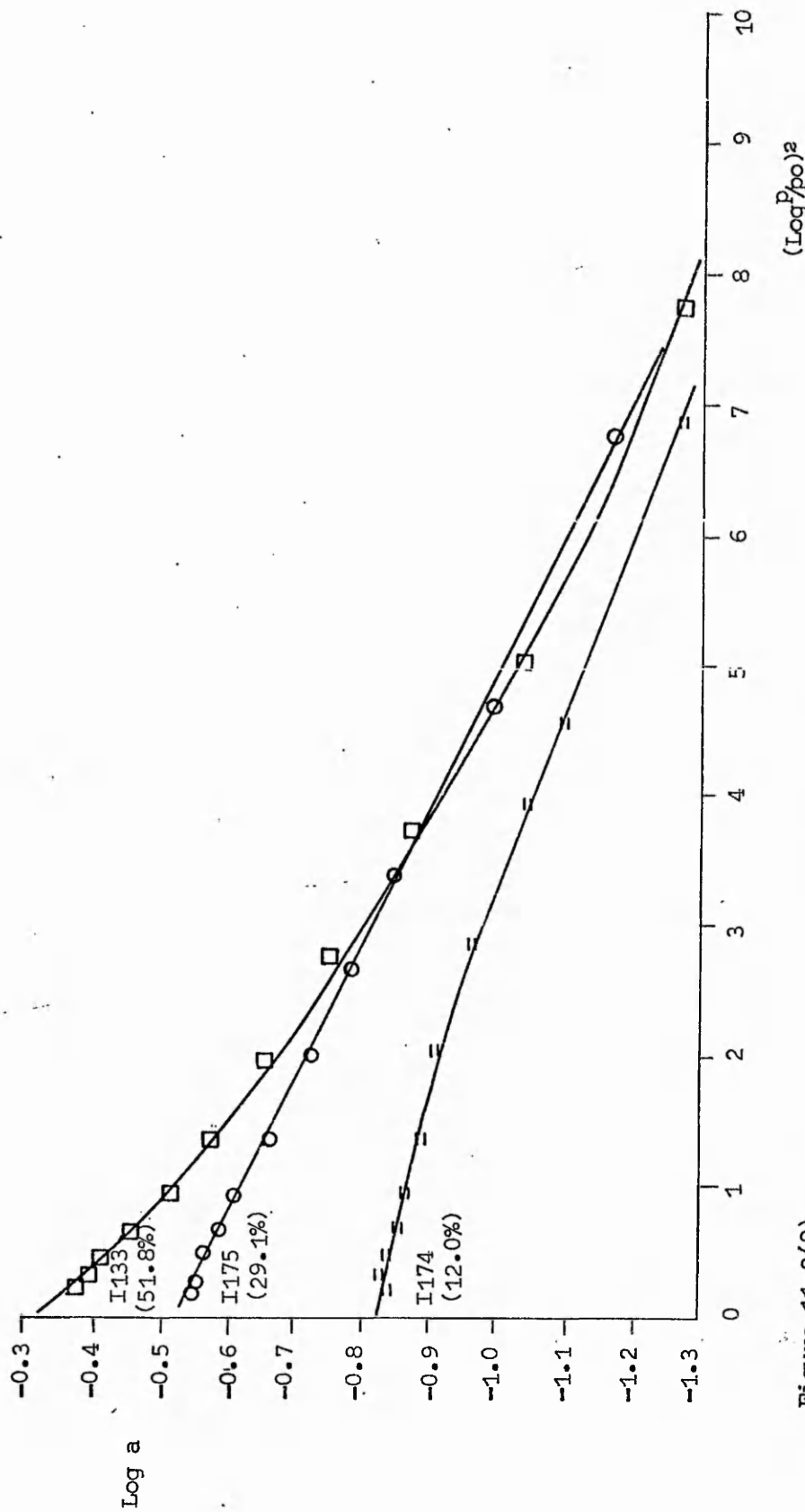


Figure 11.2(9)
 Representative D-R type I plots for W60/T40 carbons.

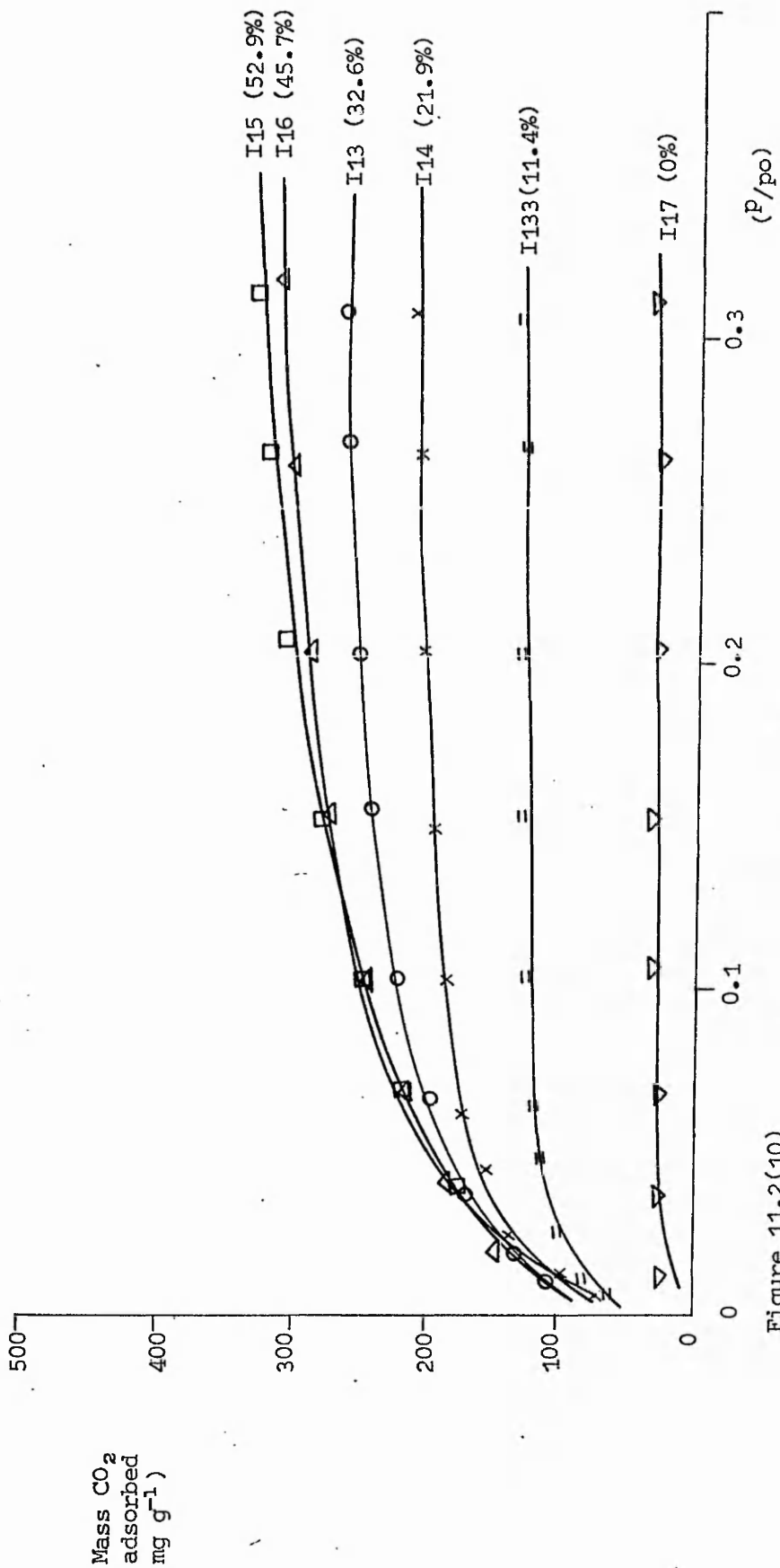


Figure 11.2(10)

Adsorption of carbon dioxide at 195K on 1313K W50/T50 carbon activated by carbon dioxide at 1303K.

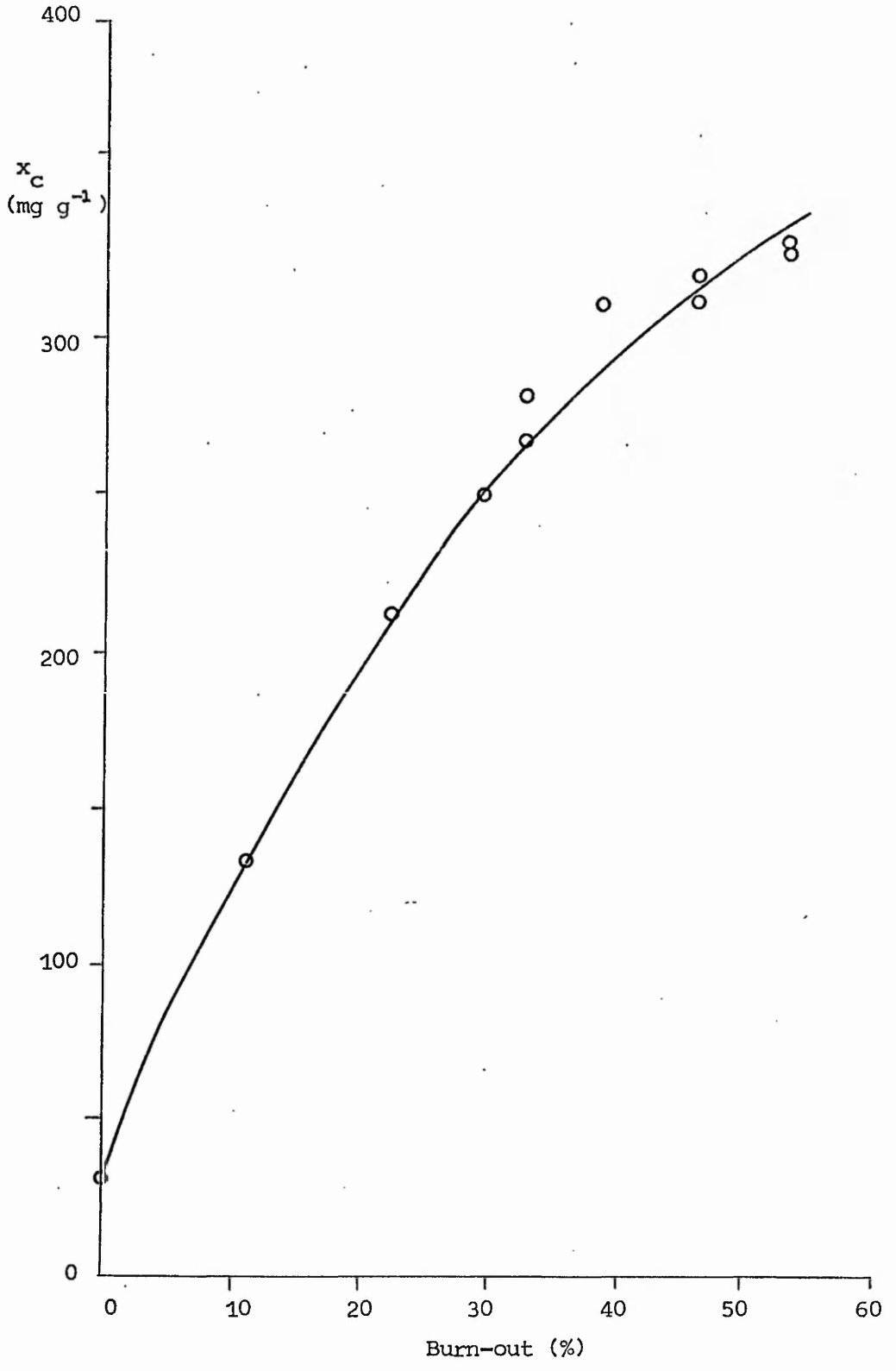


Figure 11.2(11)
Variation of x_c (mg g⁻¹) with burn-out (%) for W50/T50 carbon.

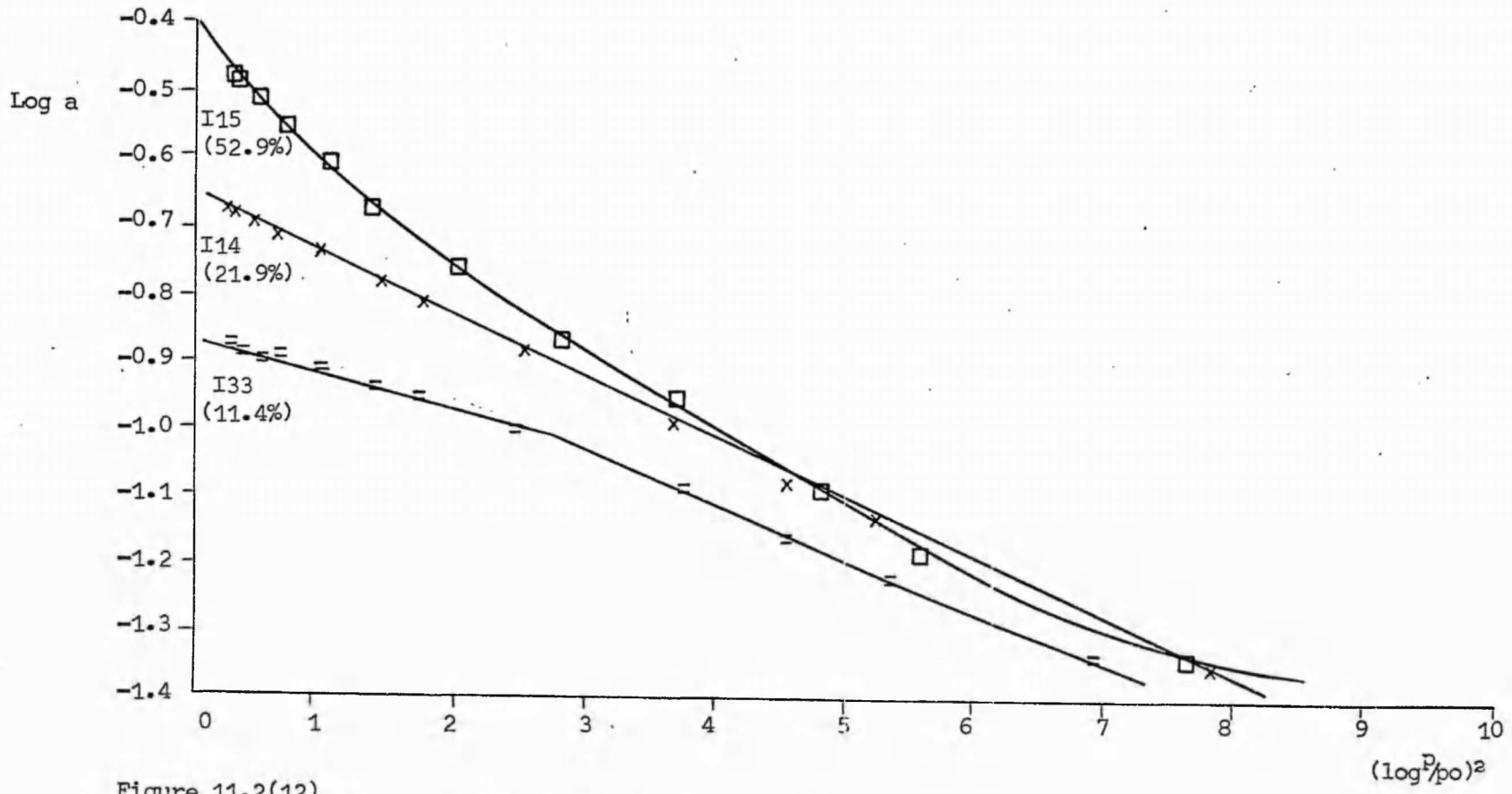


Figure 11.2(12)
Representative D-R type I plots for W50/T50 carbons.

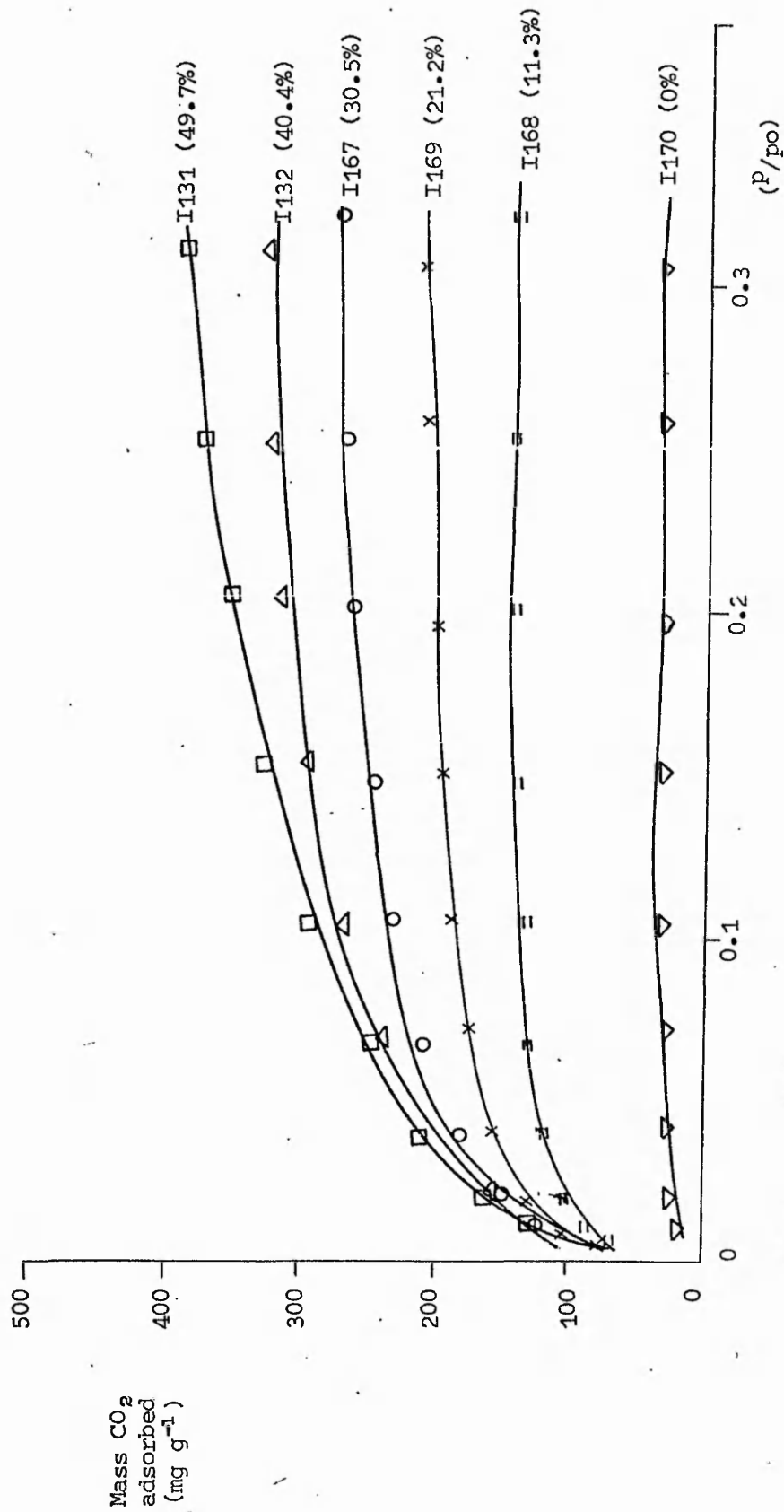


Figure 11.2(13)
Adsorption of carbon dioxide at 195K on 1313K W4C/T60 carbon activated by carbon dioxide at 1303K.

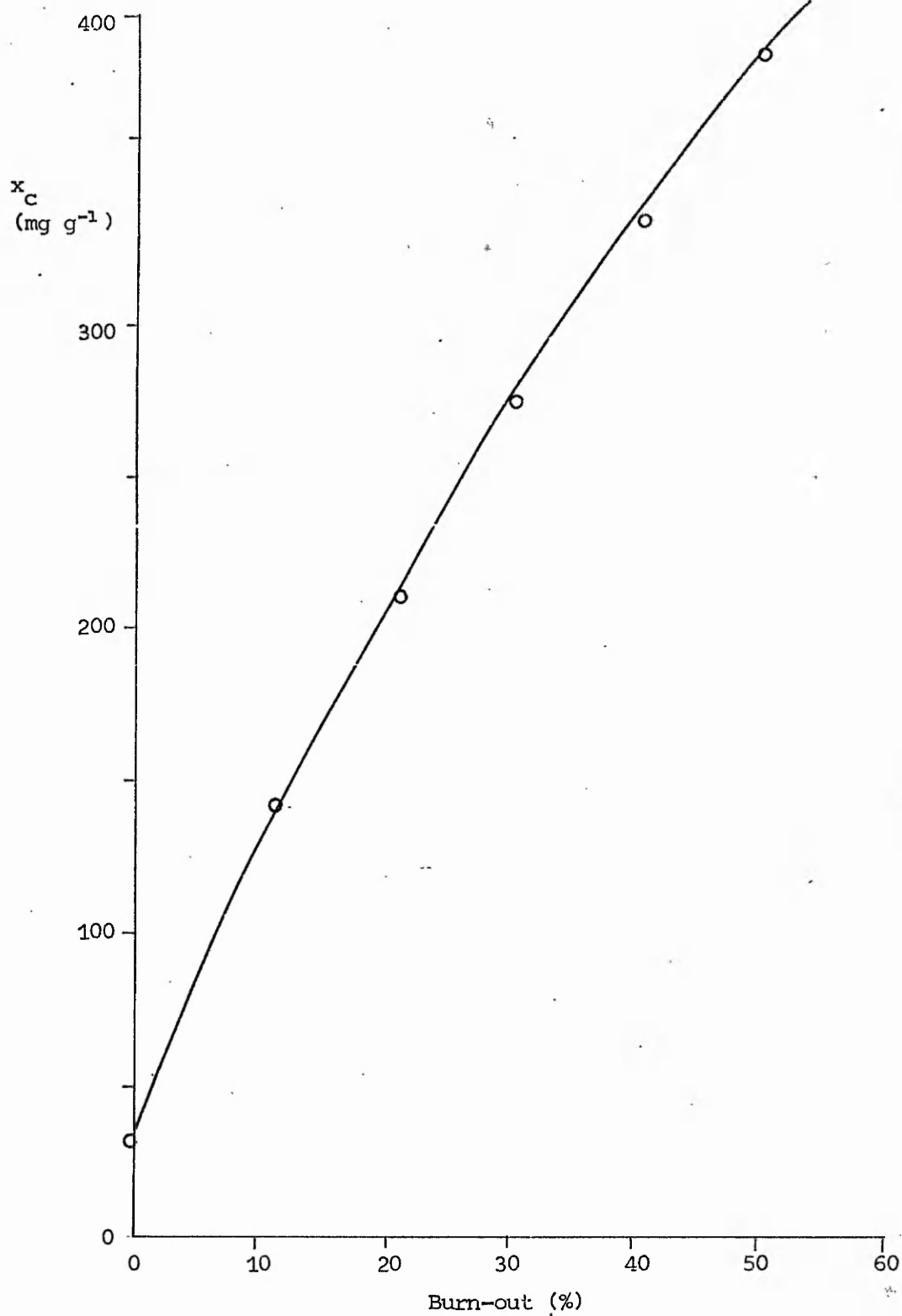


Figure 11.2(14)
Variation of x_c (mg g^{-1}) with burn-out (%) for W40/T60 carbon.

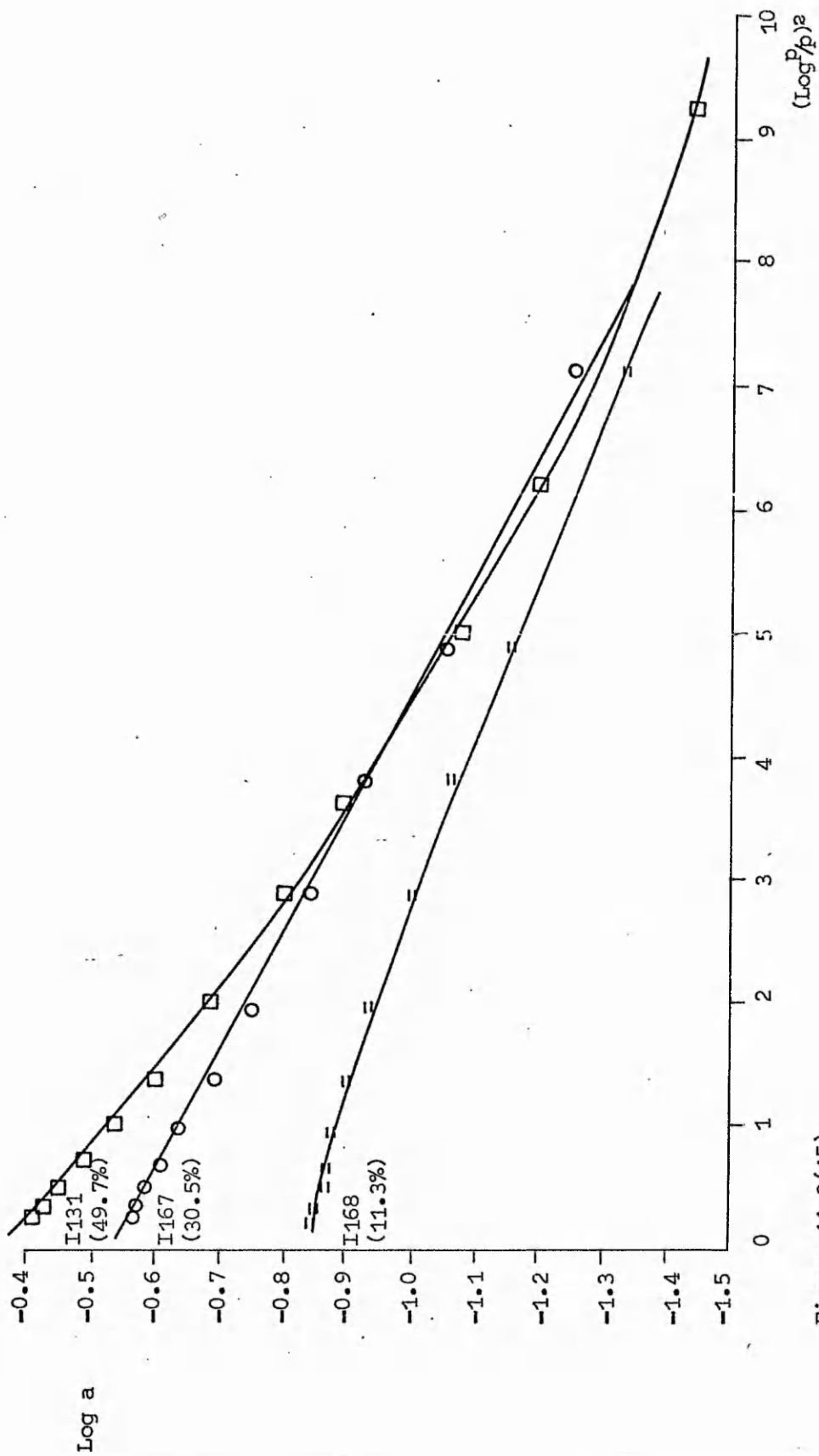


Figure 11.2(15)
Representative D-R type I plots for W40/T60 carbons.

-246-

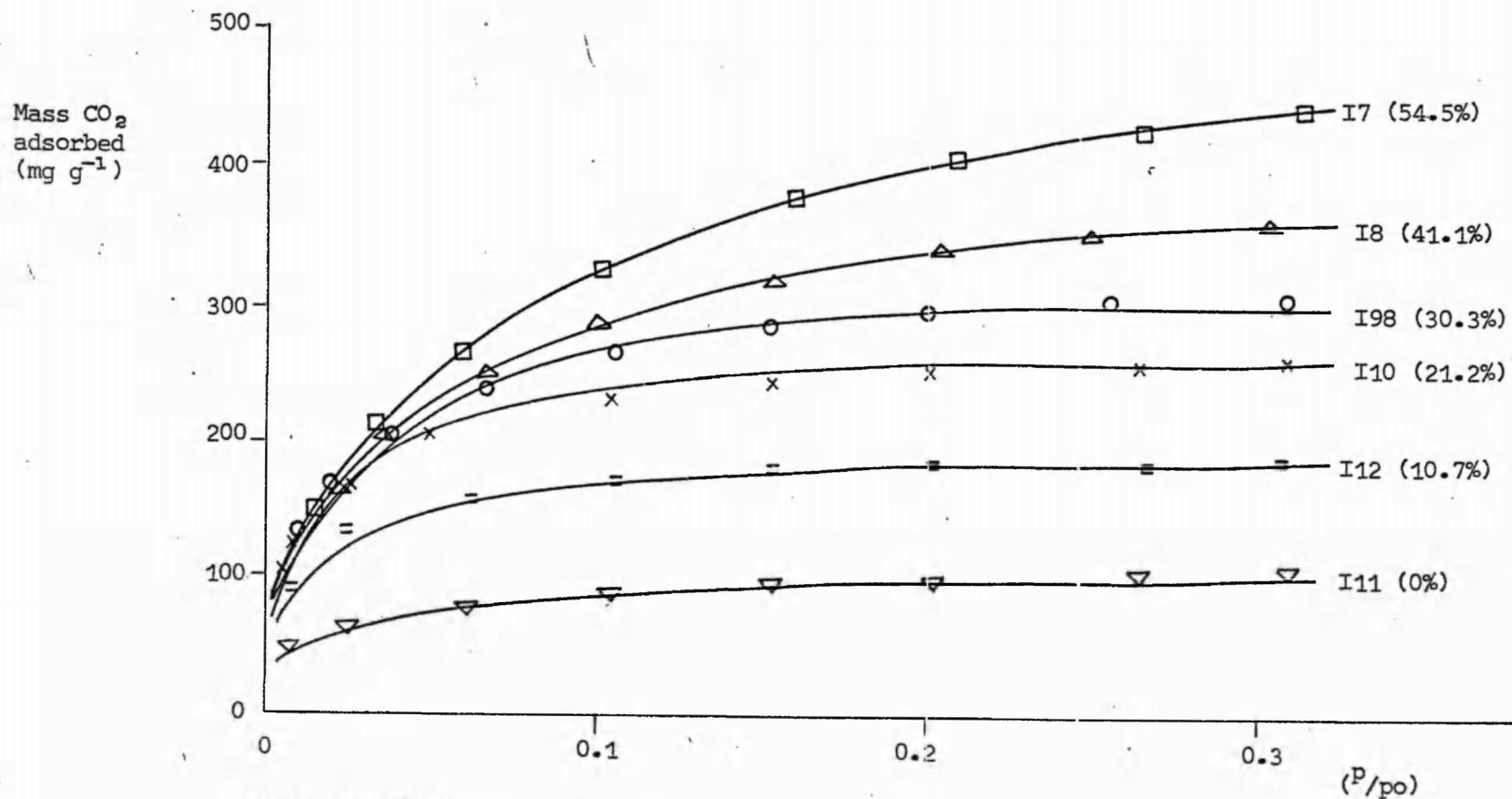


Figure 11.2(16)

Adsorption of carbon dioxide at 195K on 1313K W25/T75 carbon activated by carbon dioxide at 1303K.

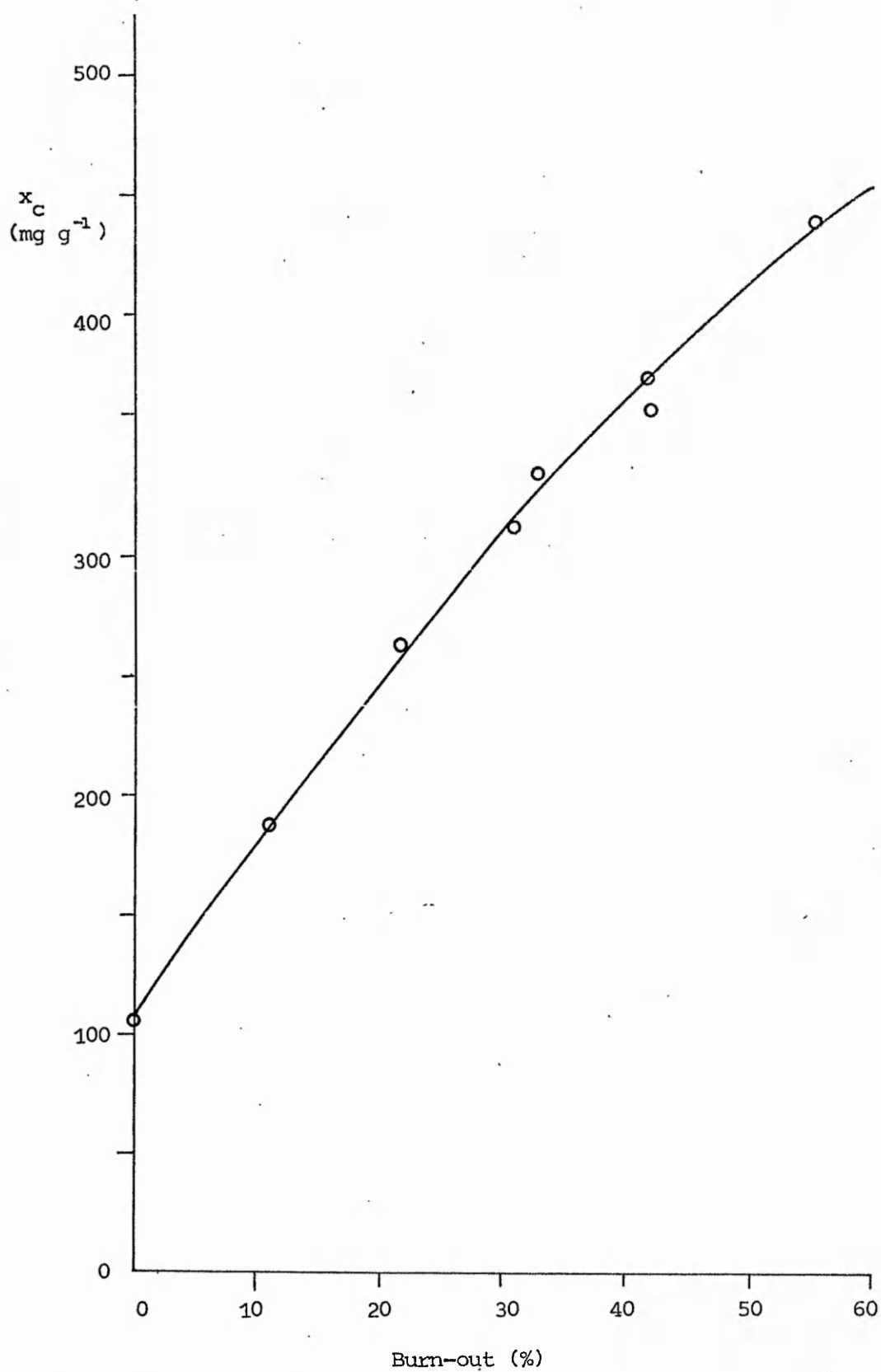


Figure 11.2(17)
Variation of x_c (mg g^{-1}) with burn-out (%) for W25/T75 carbon.

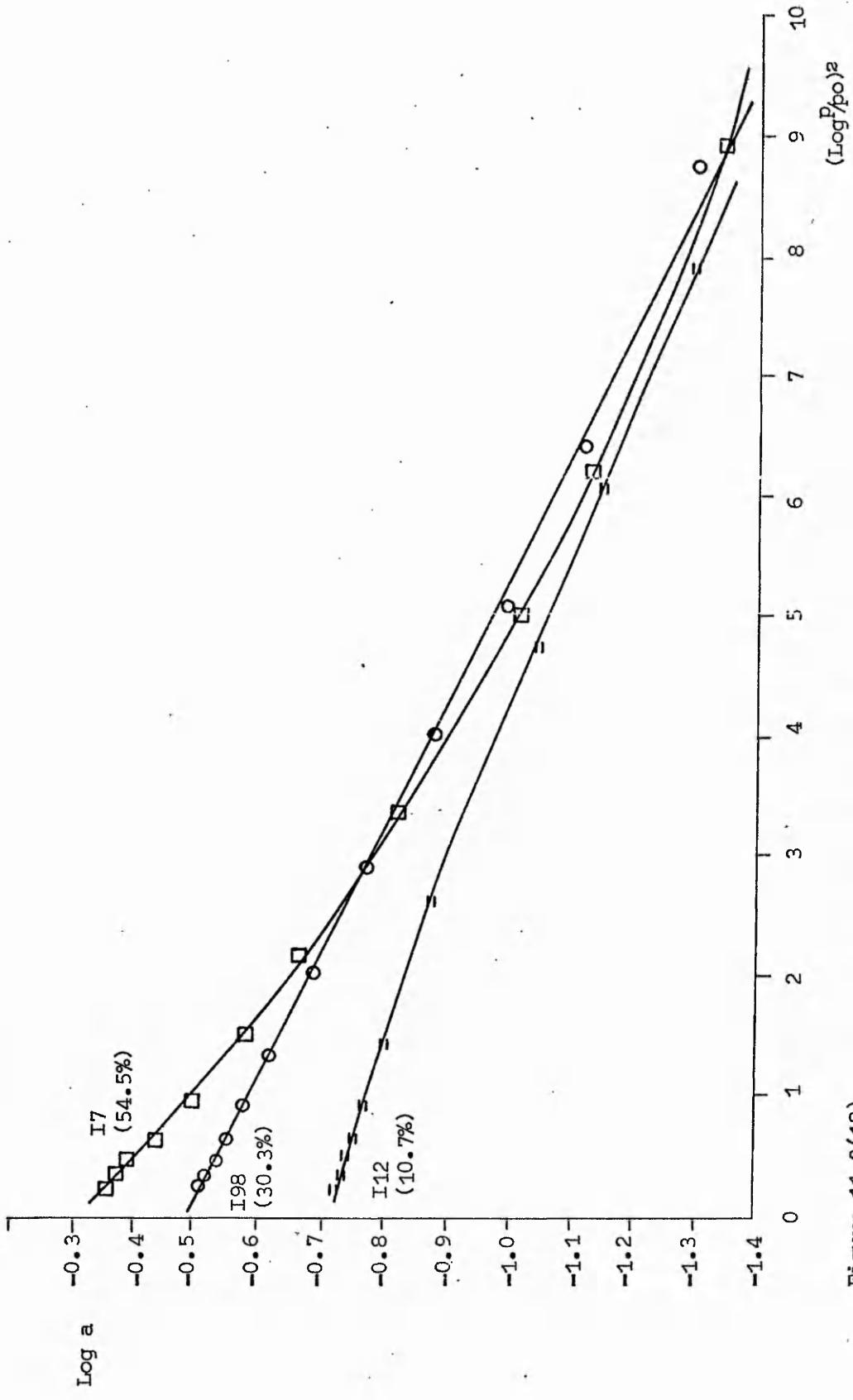


Figure 11.2(18)
Representative D-R type I plots for W25/T75 carbons

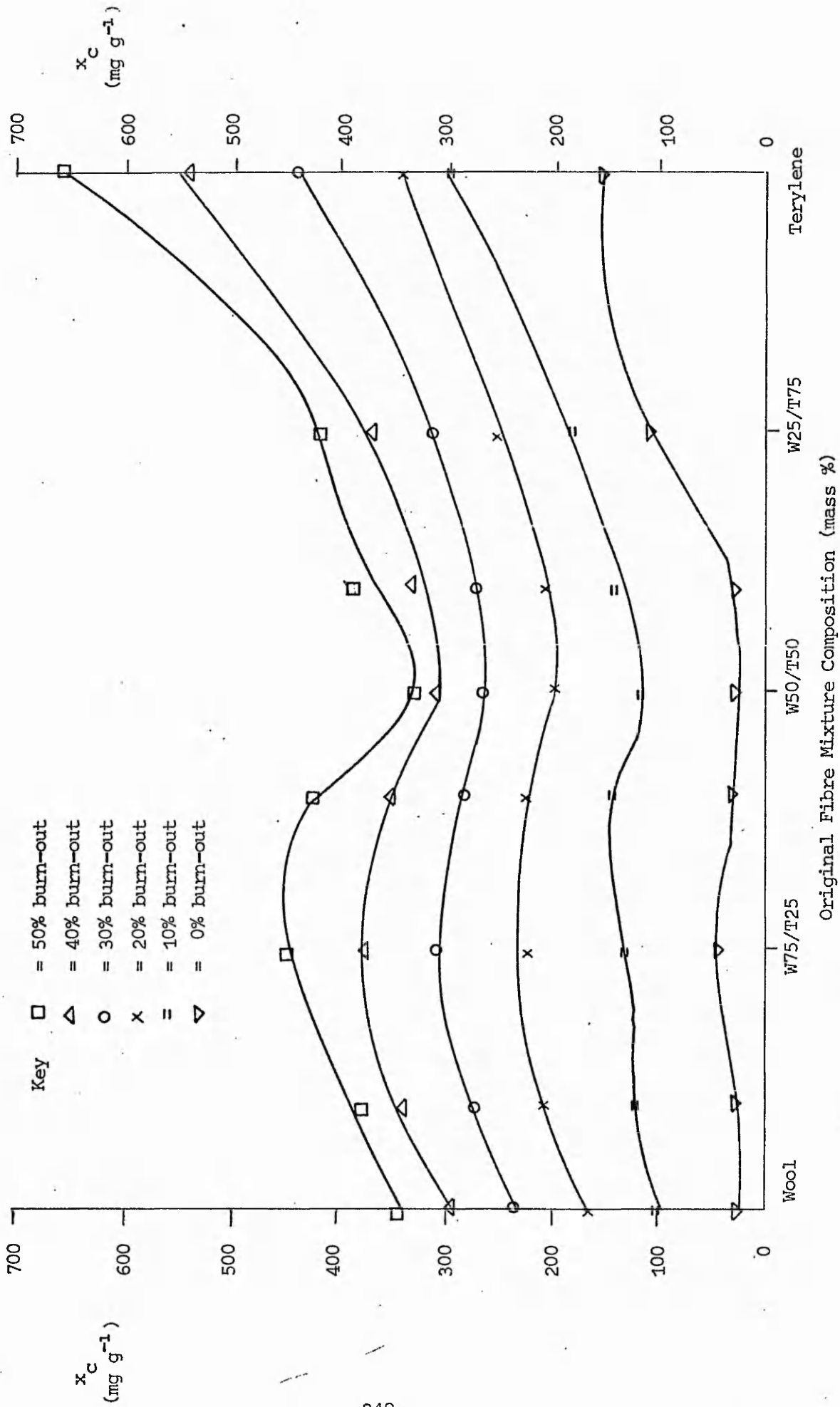


Figure 11.2(19)
Variation of x_C for burn-outs in range 0-50% over entire composition range for Wool/Terylene carbons.

11.3 Wool/Courtelle carbon

The textile polymer mixtures from which the wool/Courtelle carbons were produced are listed in table 11.3(1). This table also provides a key to the location of all the adsorption data presented for this system of carbons.

For each carbon of this system the variation of x_c with burn-out is summarised in table 11.3(2). With the exception of Courtelle all the carbons exhibited a maximum in this variation. For the Courtelle carbon a continuous increase in x_c with burn-out was observed [see figure 11.1(8)].

It is however apparent from figure 11.1(8) that for Courtelle carbon at burn-outs of greater than or equal to 35% the slope of the plot decreased possibly indicating a maximum at somewhat higher burn-outs than those investigated in this study.

The W15/C85 carbon was somewhat unusual in its behaviour. Relatively low x_c values were recorded for all the activated W15/C85 carbon samples particularly at 40% and 50% burn-outs [see figure 11.3(20)].

Representative D-R type I plots for all the wool/Courtelle system are located as indicated in table 11.3(1). The overall behaviour of the system in terms of the type of D-R type I plot observed is indicated in table 11.3(3).

It is clear from table 11.3(3) that at low burn-out (10%) a linear plot or type A deviation was generally observed. At 20% burn-out type B deviation together with some linear plots were found and at higher burn-outs (30%, 40%, 50%) type B deviation was observed.

Somewhat unusual behaviour was observed for the W15/C85 carbon. At burn-outs of 20%, 30% and 40% type C deviation was observed for this carbon. As previously discussed in section 6.4 the occurrence of type C deviation has been correlated with the presence of a bimodal distribution of adsorption volume with partial molar free energy change on adsorption.

For the W15/C85 carbon the variation of mercury density with burn-out has also been determined. These density data are presented and discussed in chapter 12.

The variation in x_c with increasing degree of burn-out for all the carbons prepared from wool/Courtelle mixtures is illustrated in figure 11.3(22).

Table 11.3(1)

Location of (a) adsorption isotherms
 (b) $\frac{x_c}{c}$ /burn-out diagrams
 (c) D-R type I plots
 for the wool/Courtelle system.

Mixture (mass %)	(a) Adsorption Isotherms	(b) $\frac{x_c}{c}$ /burn-out diagrams	(c) D-R type I plots
Wool (W)	figure 11.1(1)	figure 11.1(2)	figure 11.1(3)
W90/C10	" 11.3(1)	" 11.3(2)	" 11.3(3)
W75/C25	" 11.3(4)	" 11.3(5)	" 11.3(6)
W60/C40	" 11.3(7)	" 11.3(8)	" 11.3(9)
W50/C50	" 11.3(10)	" 11.3(11)	" 11.3(12)
W35/C65	" 11.3(13)	" 11.3(14)	" 11.3(15)
W25/C75	" 11.3(16)	" 11.3(17)	" 11.3(18)
W15/C85	" 11.3(19)	" 11.3(20)	" 11.3(21)
Courtelle (C)	" 11.1(7)	" 11.1(8)	" 11.1(9)

Table 11.3(2)

Summary of x_c /burn-out diagrams for the carbons of the wool/Courtelle system.

Mixture (mass %)	figure	behaviour observed	maximum x_c value observed in the burn-out range 0-50%
Wool (W)	11.1(2)	maximum x_c value occurs $\frac{x_c}{C}$ at 45-55% burn-out	330 (mg g ⁻¹)
W90/C10	11.3(2)	maximum x_c value occurs $\frac{x_c}{C}$ at 40-45% burn-out	250 "
W75/C25	11.3(5)	x_c value constant $\frac{x_c}{C}$ at >40% burn-out	210 "
W60/C40	11.3(8)	maximum x_c value at 35- $\frac{x_c}{C}$ 45% burn-out	195 "
W50/C50	11.3(11)	x_c value apparently $\frac{x_c}{C}$ constant at 50-55% burn-out	290 "
W35/C65	11.3(14)	x_c value apparently $\frac{x_c}{C}$ constant at 50% burn-out	260 "
W25/C75	11.3(17)	maximum x_c value at 30-40% $\frac{x_c}{C}$ burn-out	170 "
W15/C85	11.3(20)	maximum x_c value at 25-35% $\frac{x_c}{C}$ burn-out	120 "
Courtelle	11.1(8)	continuous increase in x_c value with burn-out	300 (at 50% burn-out)

Table 11.3(3)

Applicability of the D-R type I equation to the wool/Courtelle carbon system. Deviations from linearity are classified according to the notation of Marsh and Rand.¹⁰²

Mixture (mass %)	Burn-out (%)					
	0	10	20	30	40	50
Wool (W)	Ⓐ	A	L	B	B	B
W90/C10	Ⓐ	A	L	B	B	B
W75/C25	X	A	L	B	B	B
W60/C40	X	A	B	B	B	B
W50/C50	X	L/A	B	B	B	B
W35/C65	X	A	B	B	B	B
W25/C75	X	L	B	B	B	B
W15/C85	X	L	C	C	C	X
Courtelle (C)	X	A	L	B	B	B

Key

A = Type A deviation (according to Marsh and Rand)¹⁰²

B = " B " " " " " "

C = " C " " " " " "

L = Linear plot

X = Not plotted, negligible gas uptake.

Where A, B, C, L ringed indicates possible error range $\geq 25\%$ of corresponding x_c value.

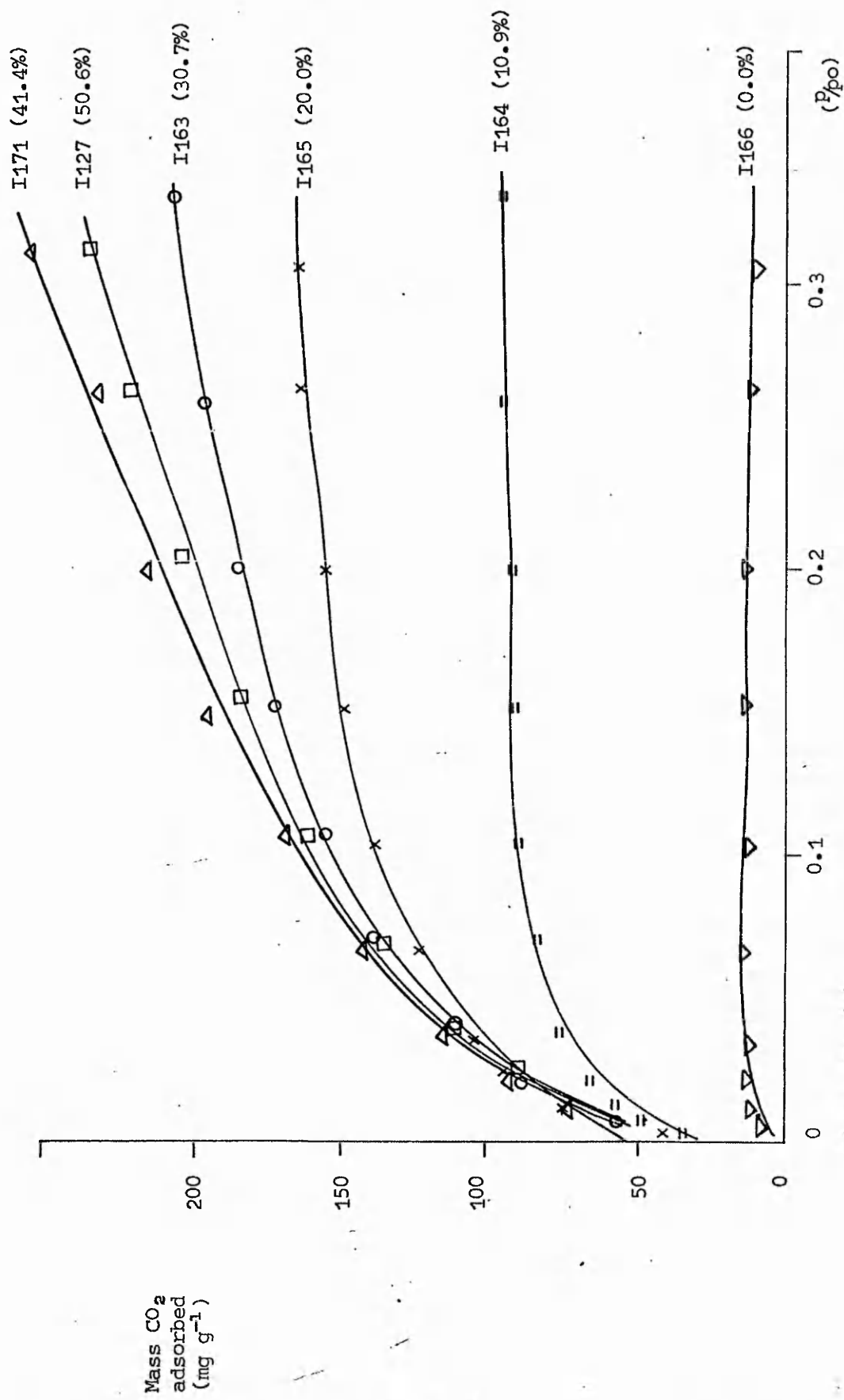


Figure 11.3(1)
Adsorption of carbon dioxide at 195K on 1313K W90/C10 carbon activated by carbon dioxide at 1303K.

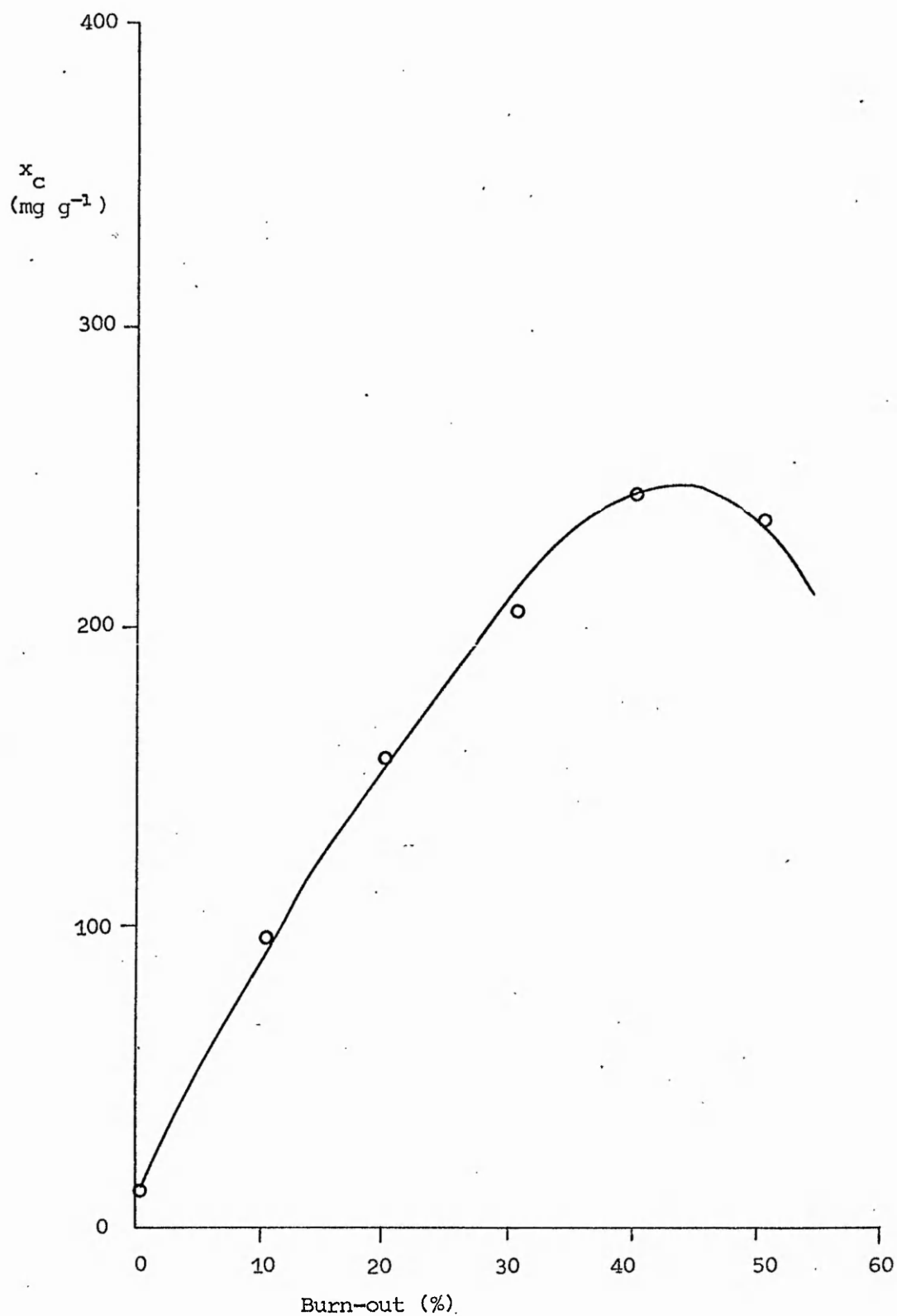


Figure 11.3(2)
Variation of x_c (mg g^{-1}) with burn-out (%) for W90/C10 carbon.

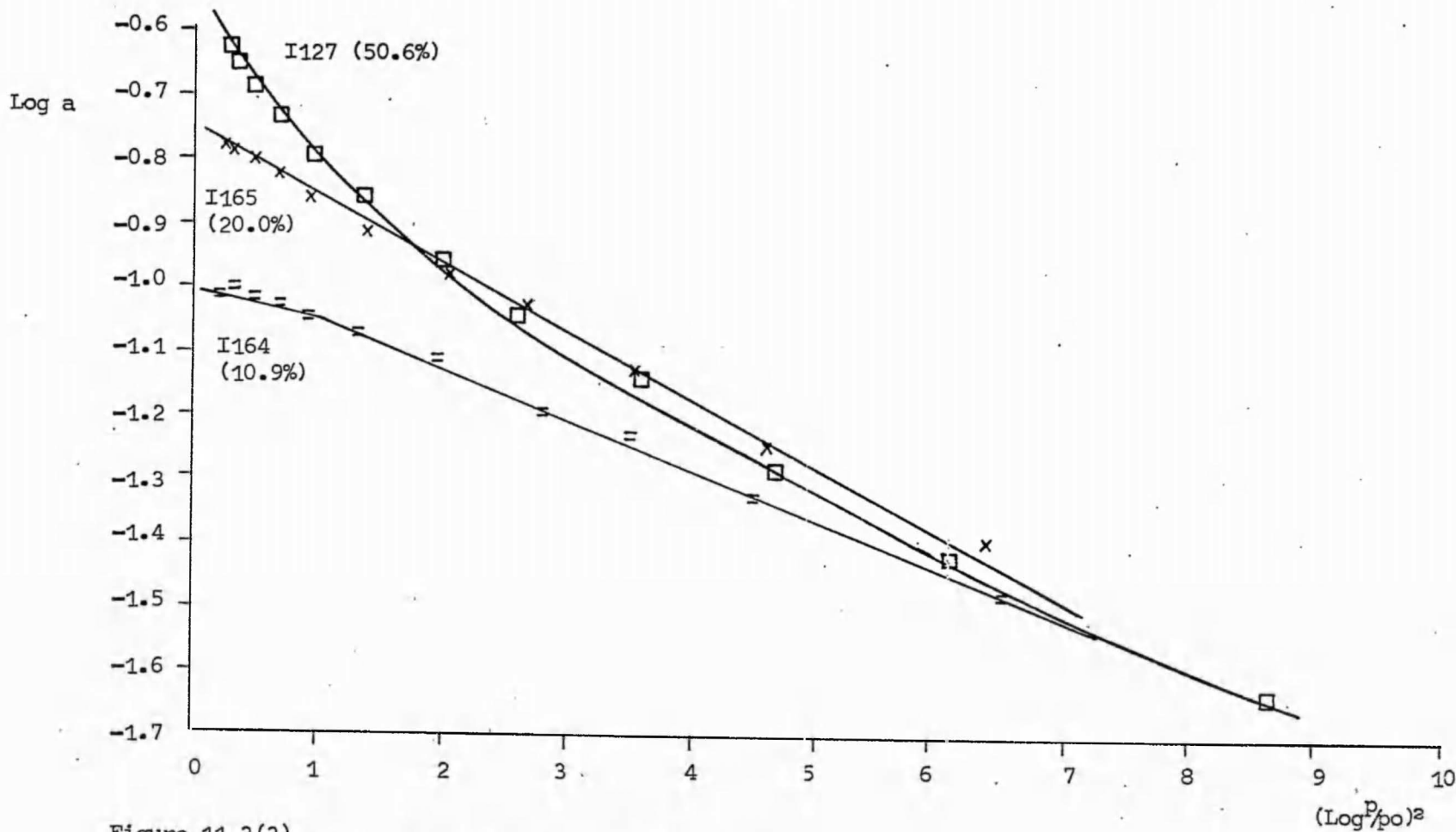


Figure 11.3(3)
Representative D-R type I plots for W90/C10 carbons

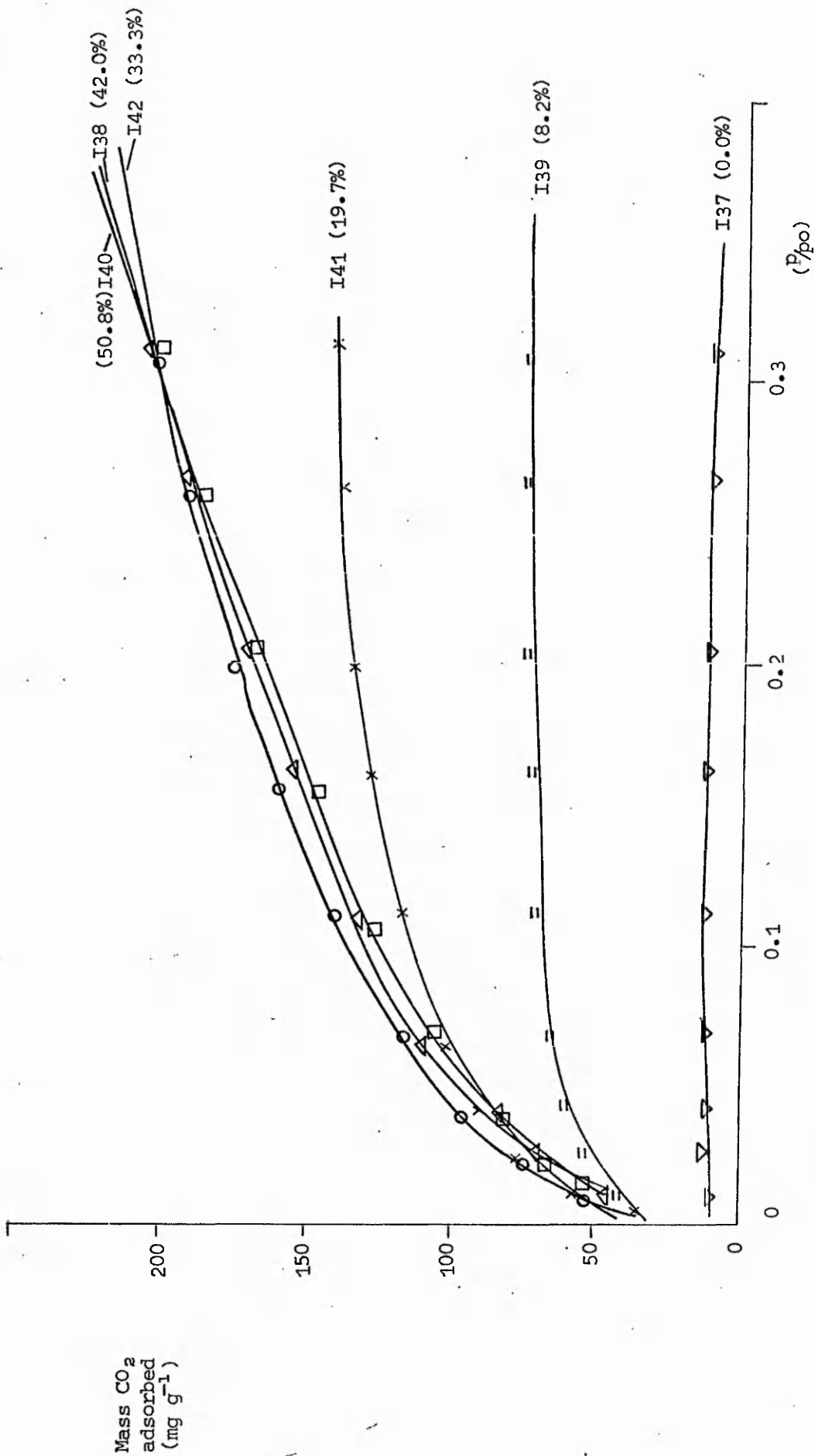


Figure 11.3(4)
Adsorption of carbon dioxide at 195K on 1313K W75/C25 carbon activated by carbon dioxide at 1303K.

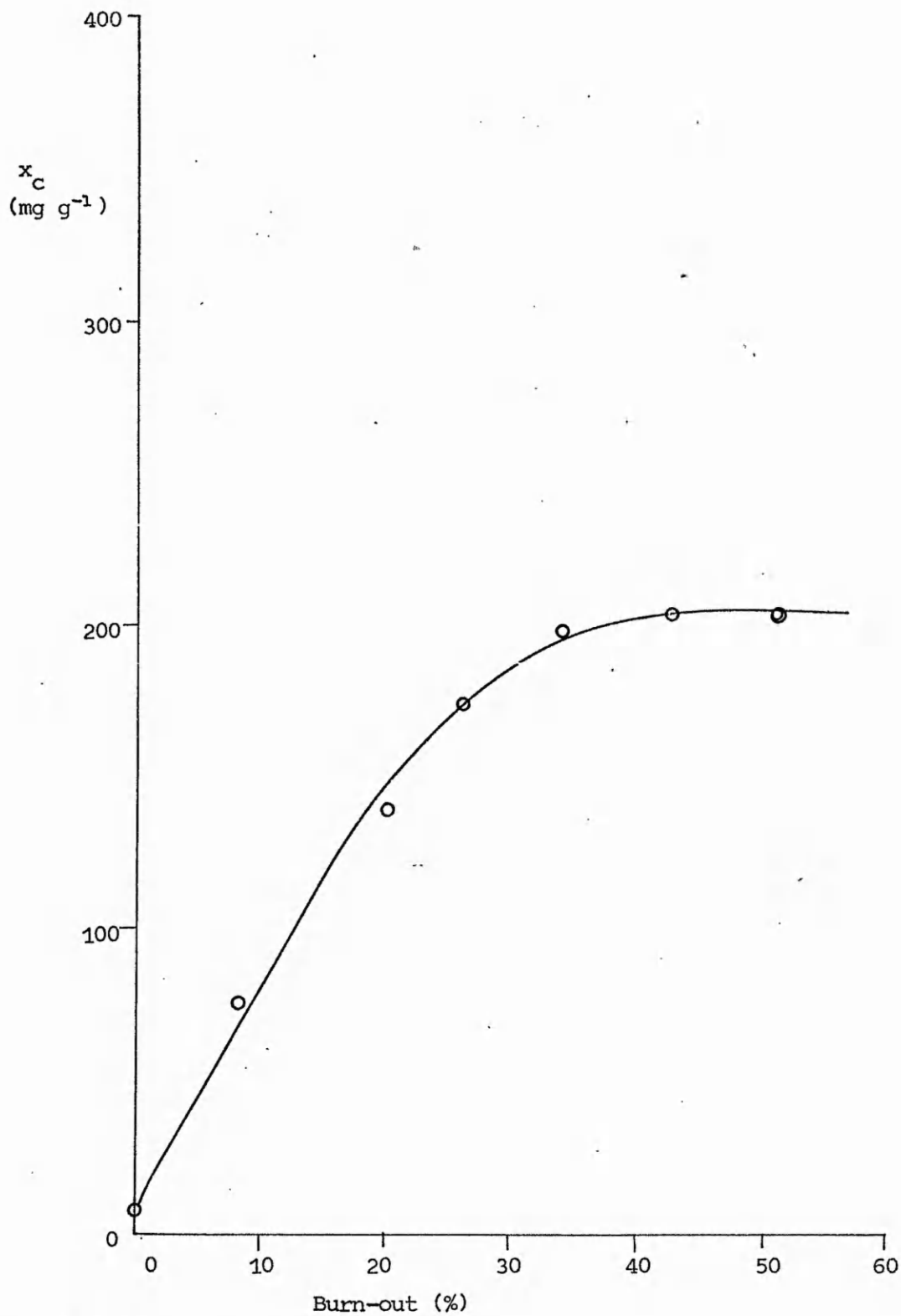


Figure 11.3(5)
Variation of x_c (mg g^{-1}) with burn-out (%) for W75/C25 carbon.

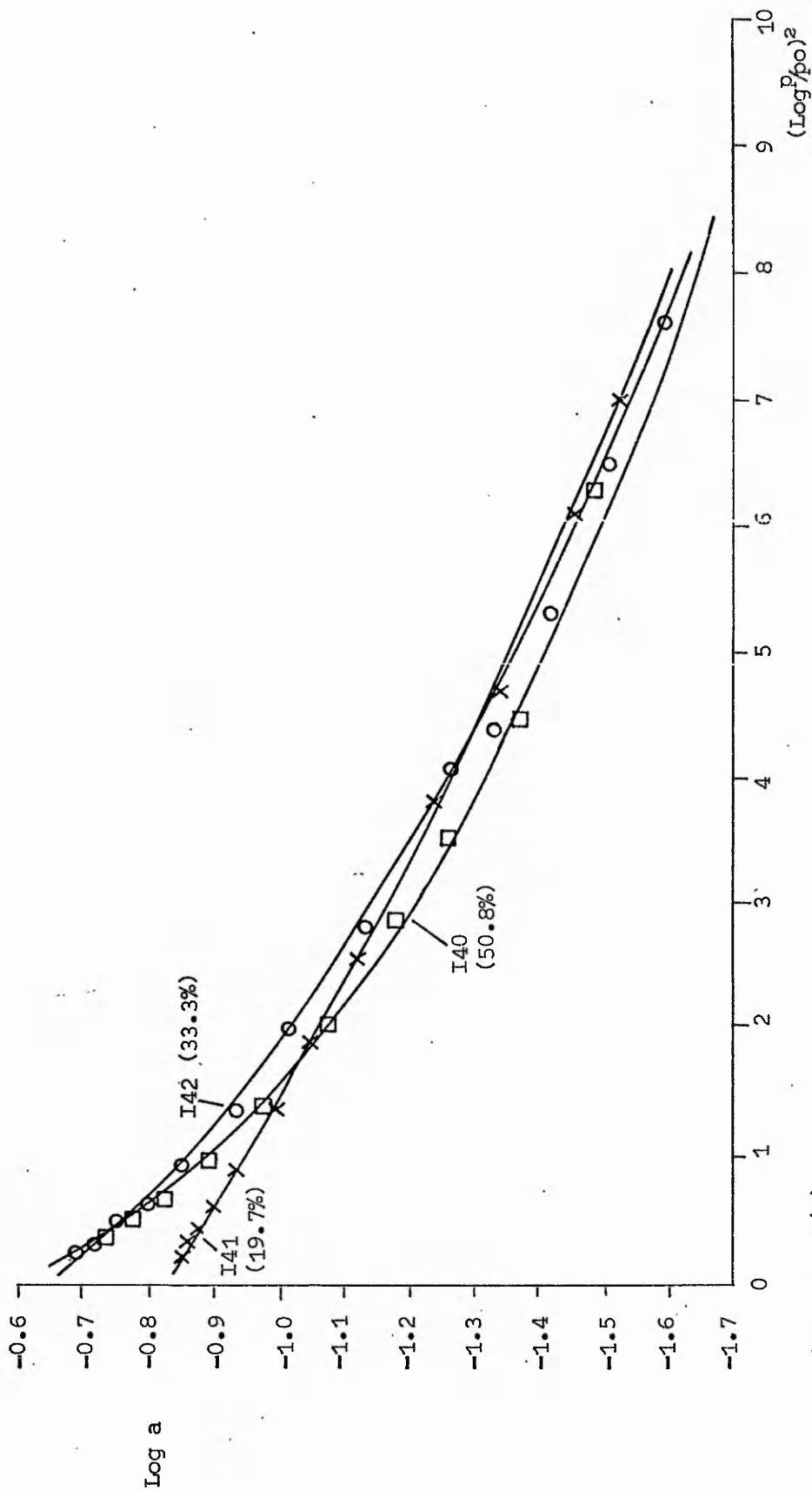


Figure 11.3(6)
Representative D-R type I plots for W75/C25 carbons.

Mass CO₂
adsorbed
(mg g⁻¹)

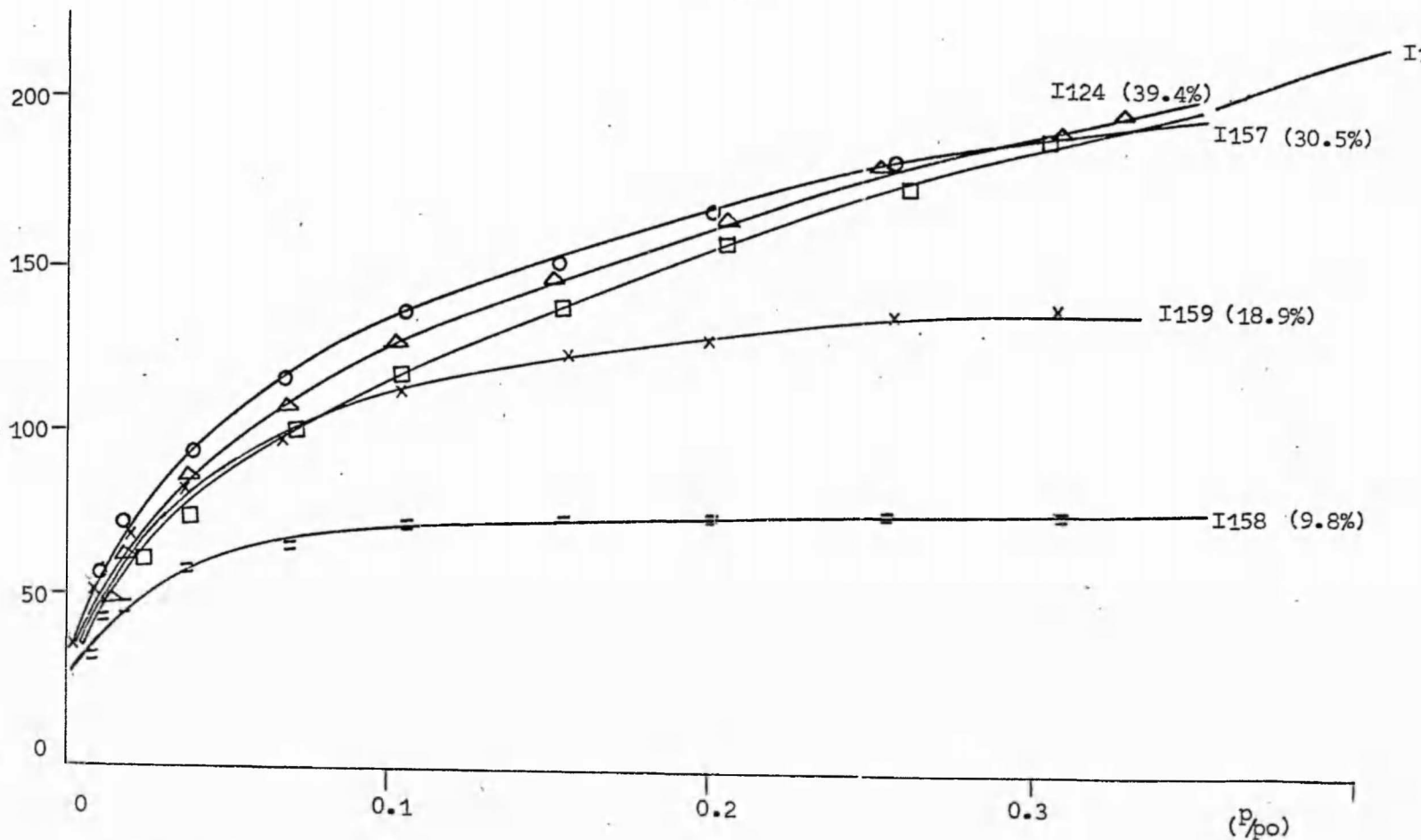


Figure 11.3(7)

Adsorption of carbon dioxide at 195K on 1313K W60/C40 carbon activated by carbon dioxide at 1303K.

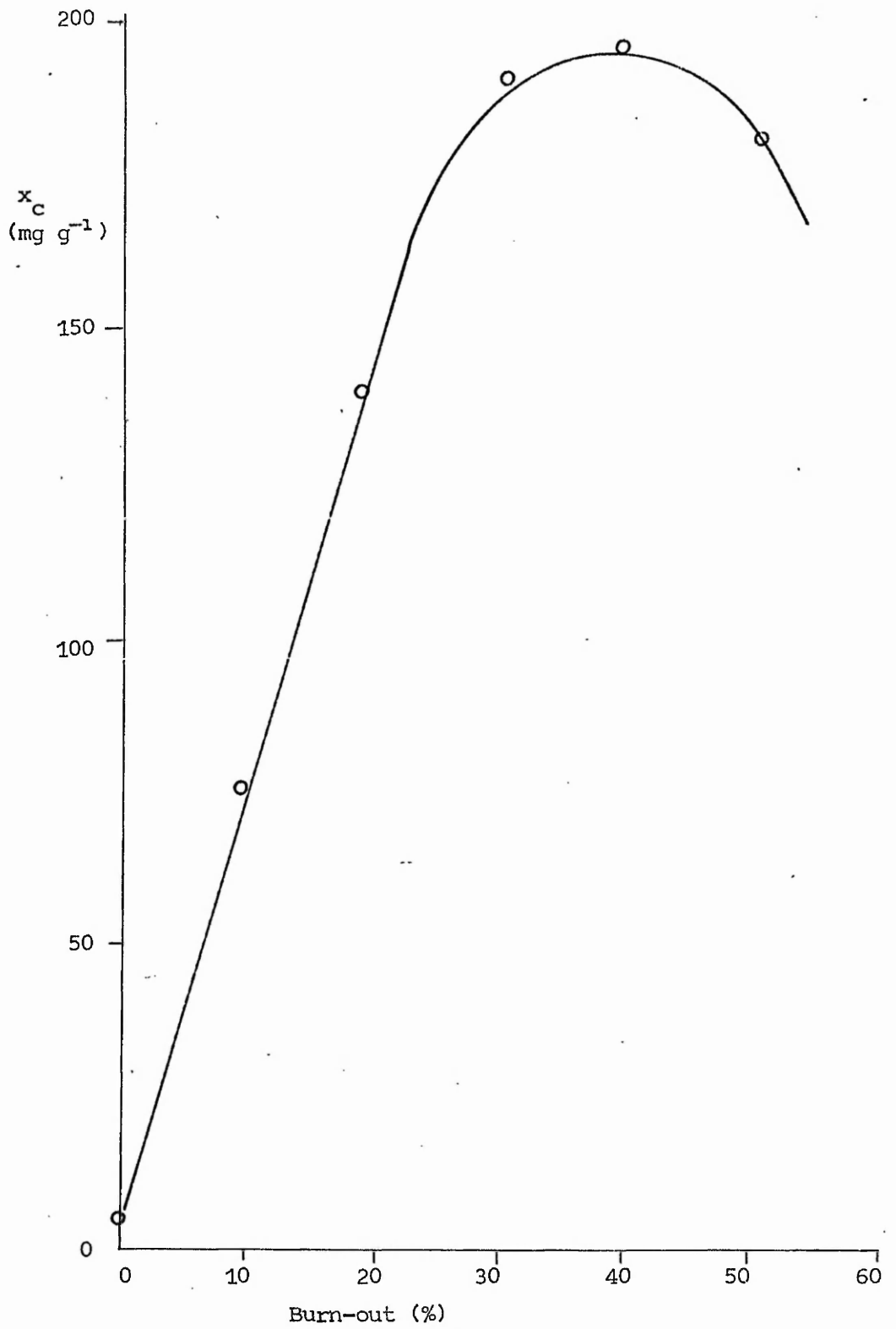


Figure 11.3(8)
Variation of x_c (mg g^{-1}) with burn-out (%) for W60/C40 carbon.

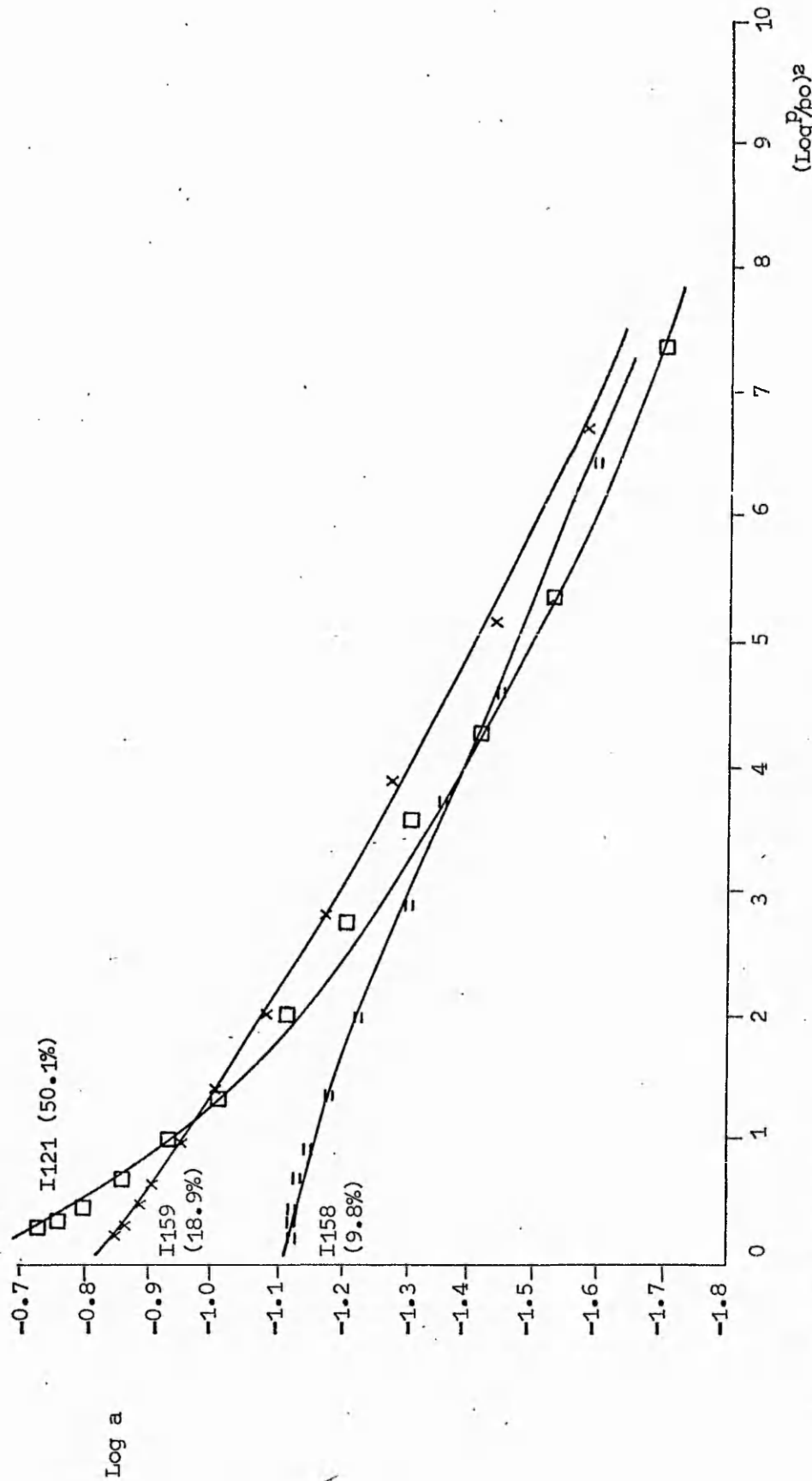


Figure 11.3(9)
Representative D-R type I plots for W60/C40 carbon

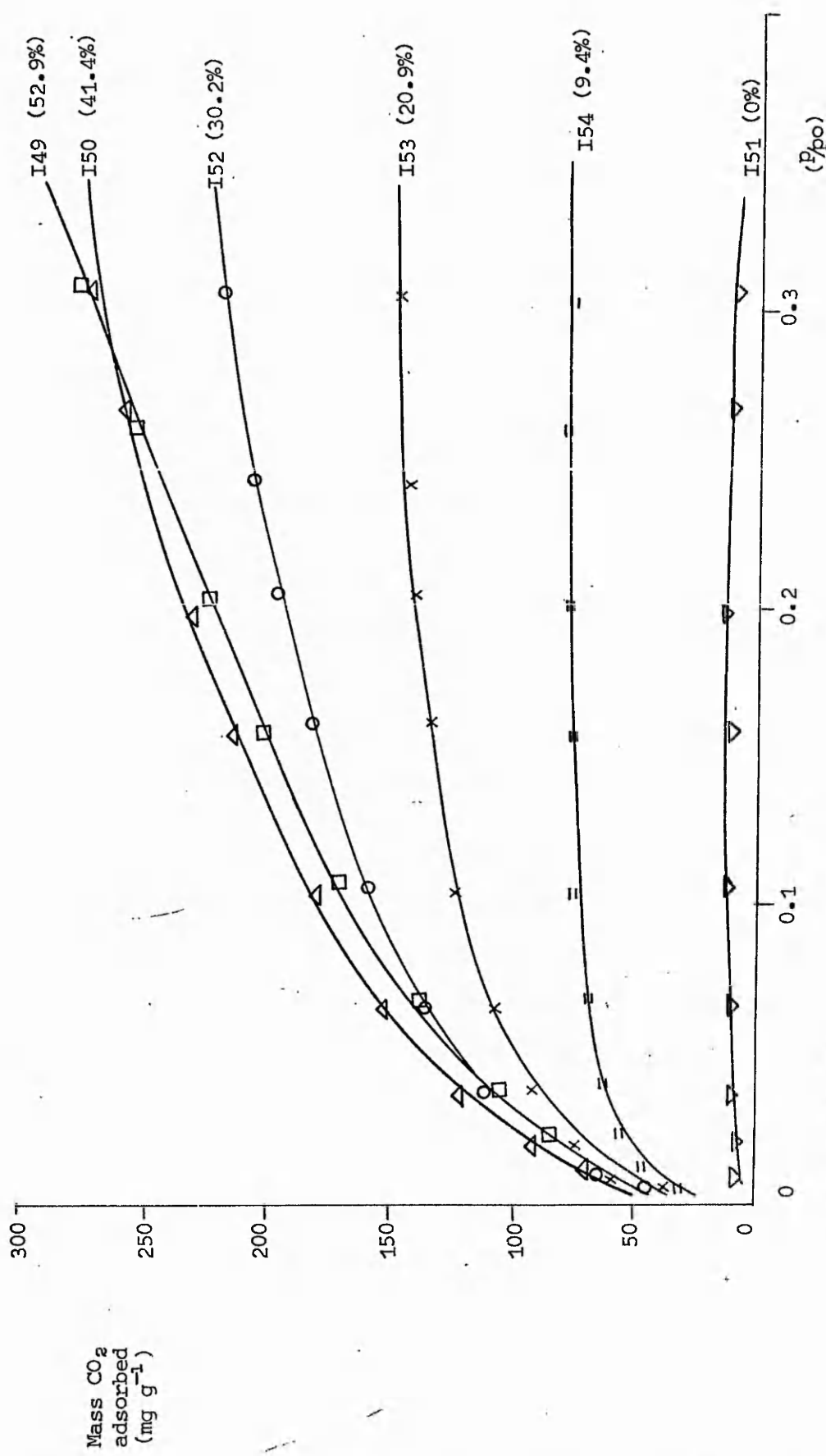


Figure 11.3(10)
 Adsorption of carbon dioxide at 195K on 1313K W50/C50 carbon activated by carbon dioxide at 1303K.

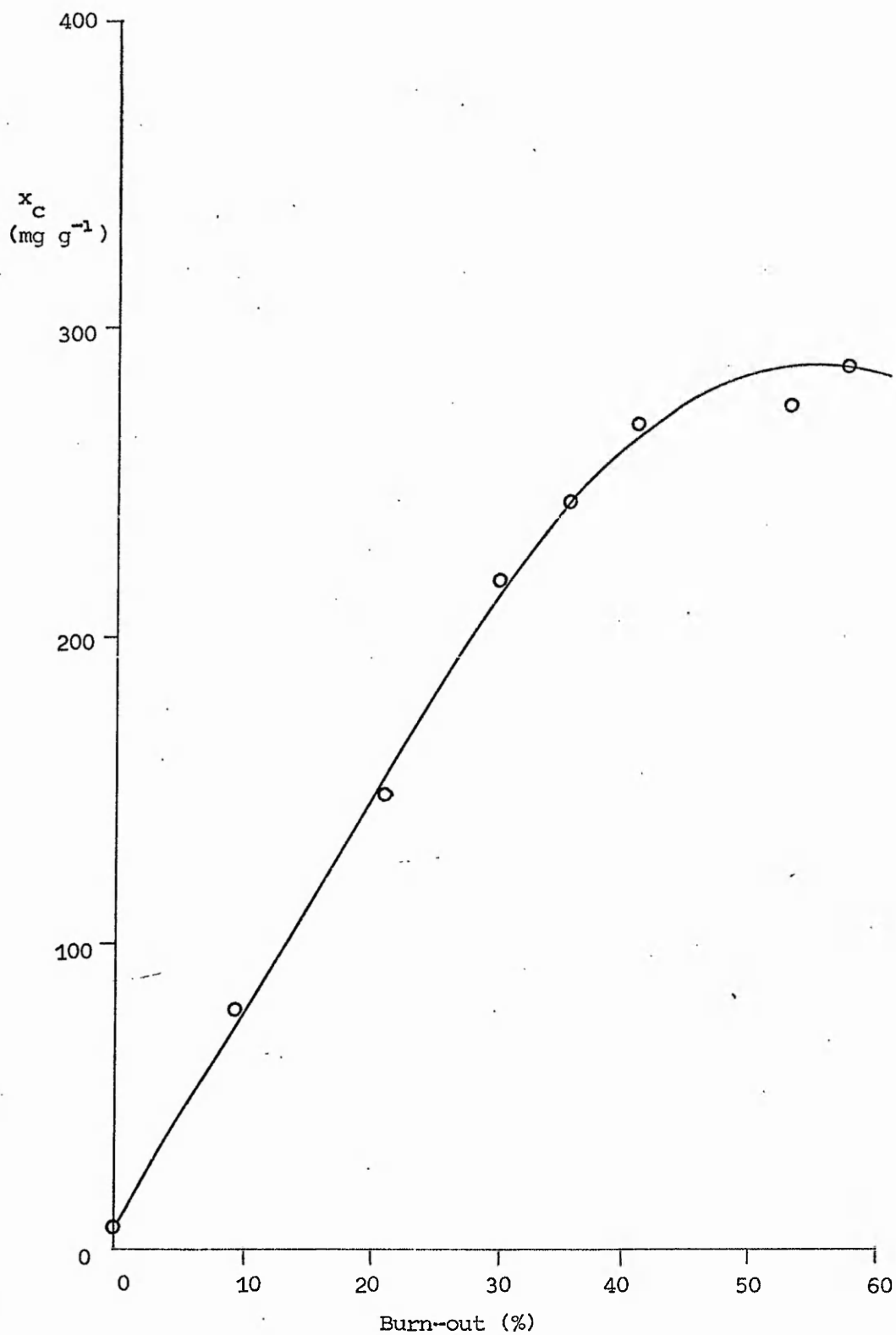


Figure 11.3(11)
Variation of x_C (mg g^{-1}) with burn-out (%) for W50/C50 carbon.

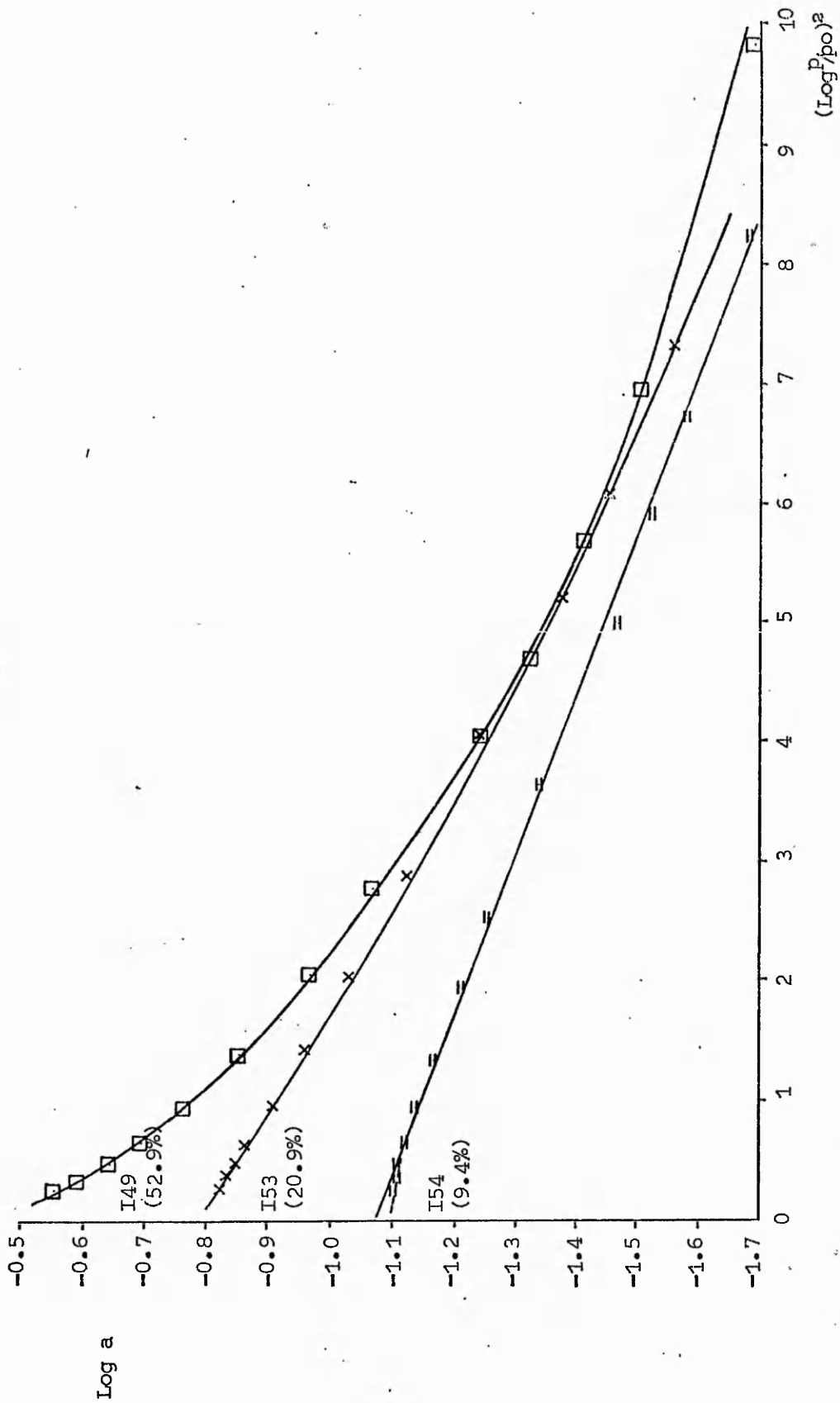


Figure 11.3(12)
Representative D-R type I plots for W50/C50 carbons.

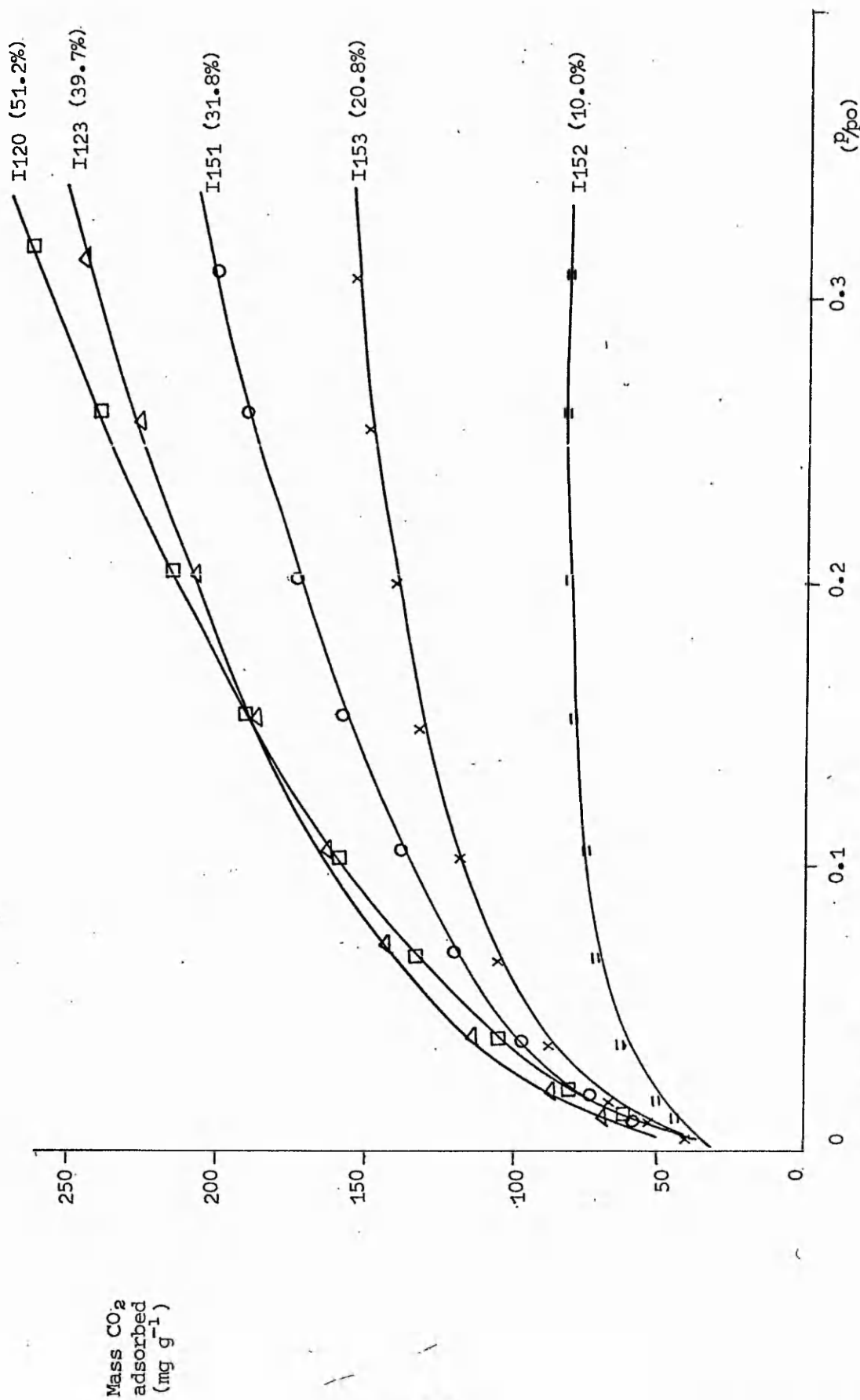


Figure 11.3(13)
Adsorption of carbon dioxide at 195K on 1313K W35/C65 carbon, activated by carbon dioxide at 1303K.

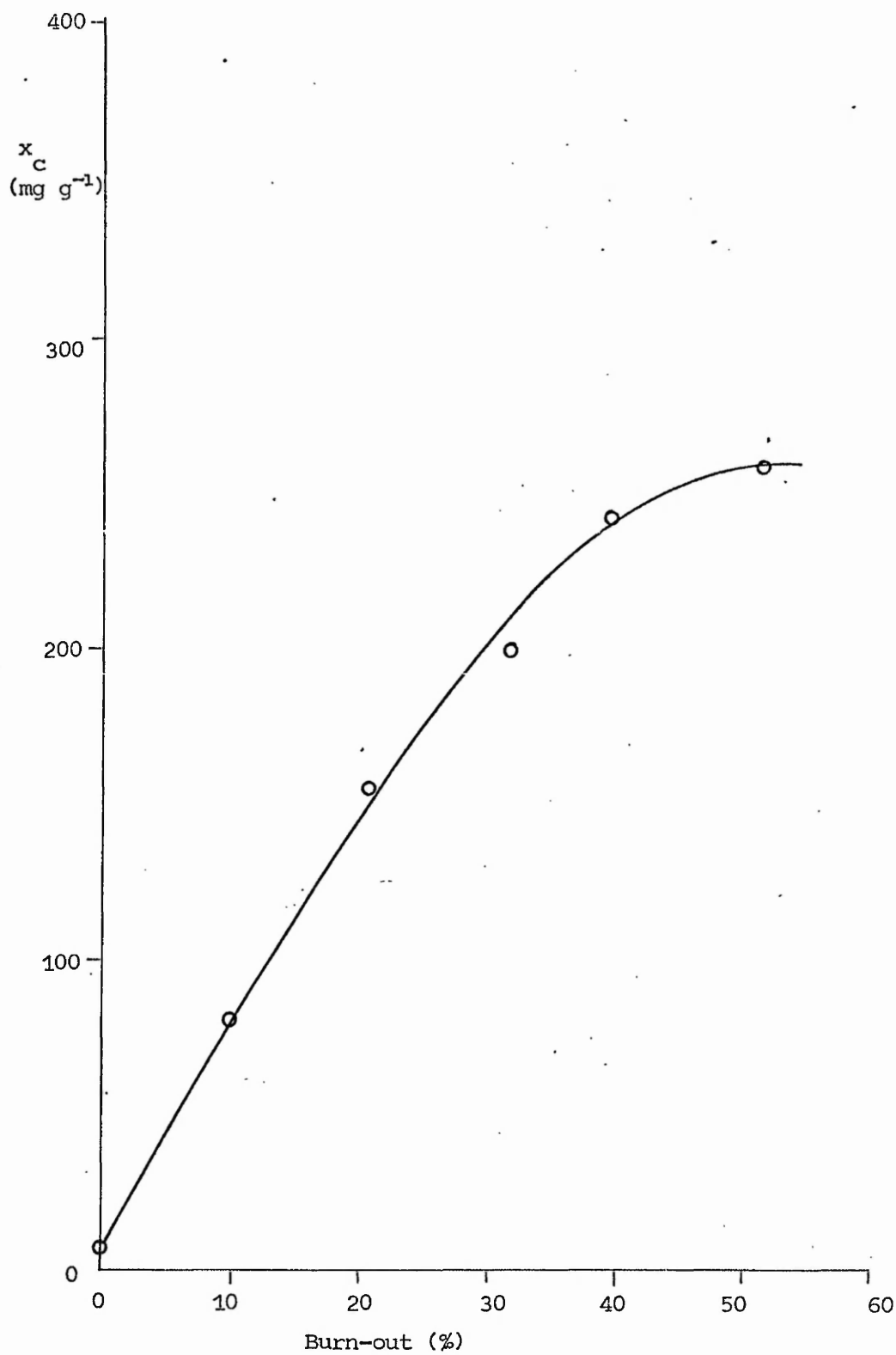


Figure 11.3(14)
Variation of x_c (mg g^{-1}) with burn-out (%) for W35/C65 carbon.

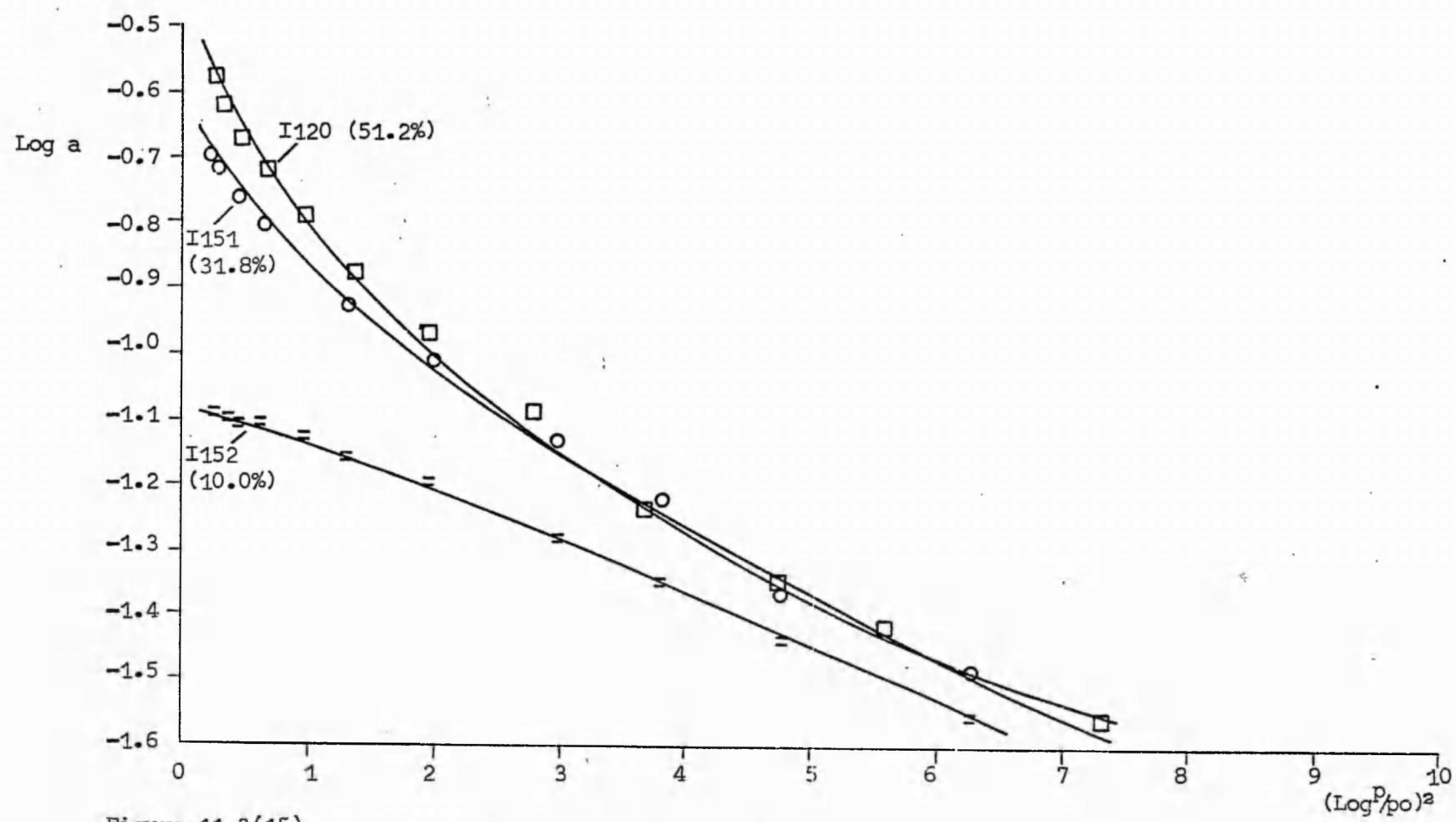


Figure 11.3(15)
Representative D-R type I plots for W35/C65 carbons

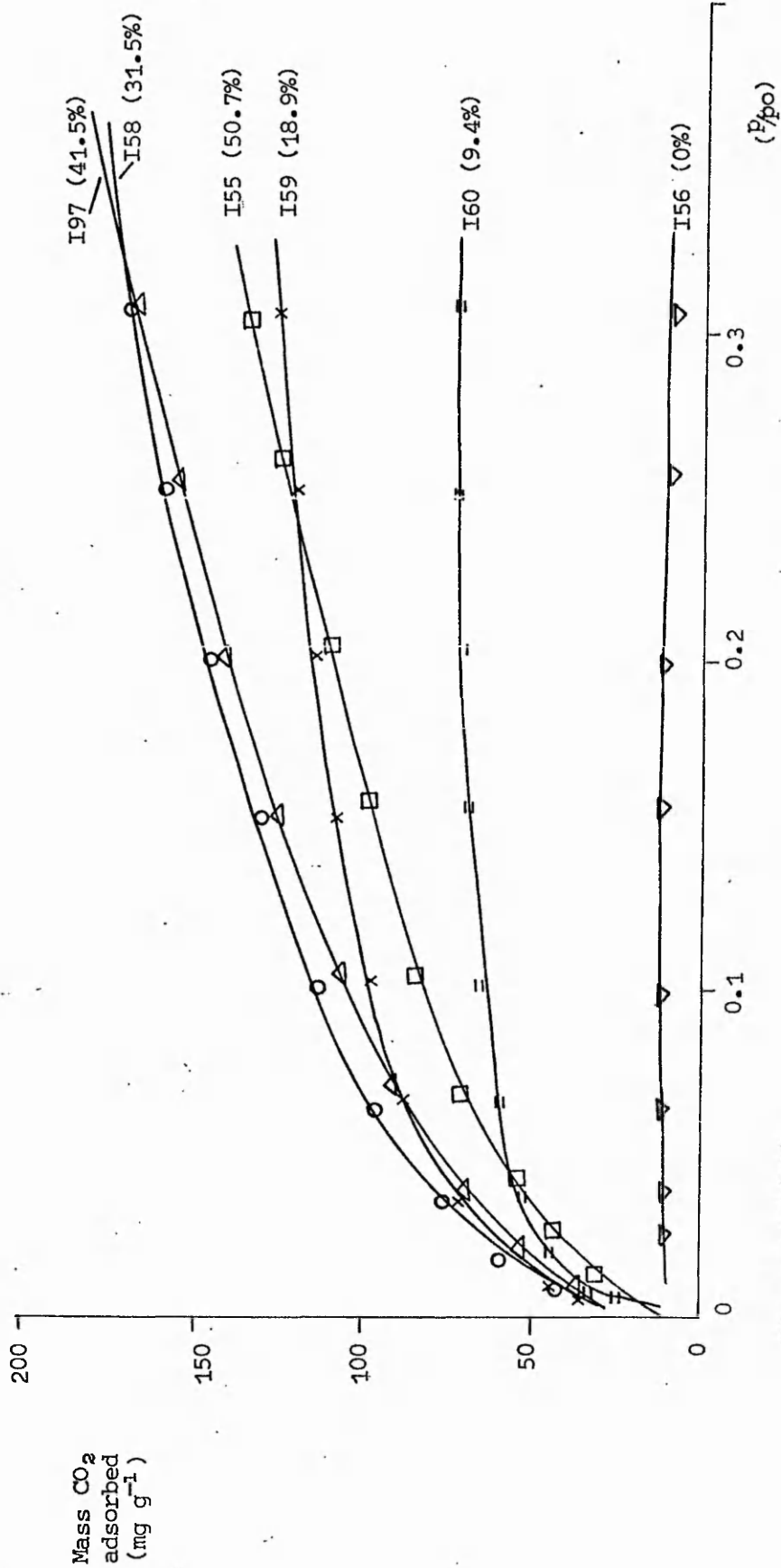


Figure 11.3(16)
 Adsorption of carbon dioxide at 195K on 1313K W75/C25 carbon activated by carbon dioxide at 1303K.

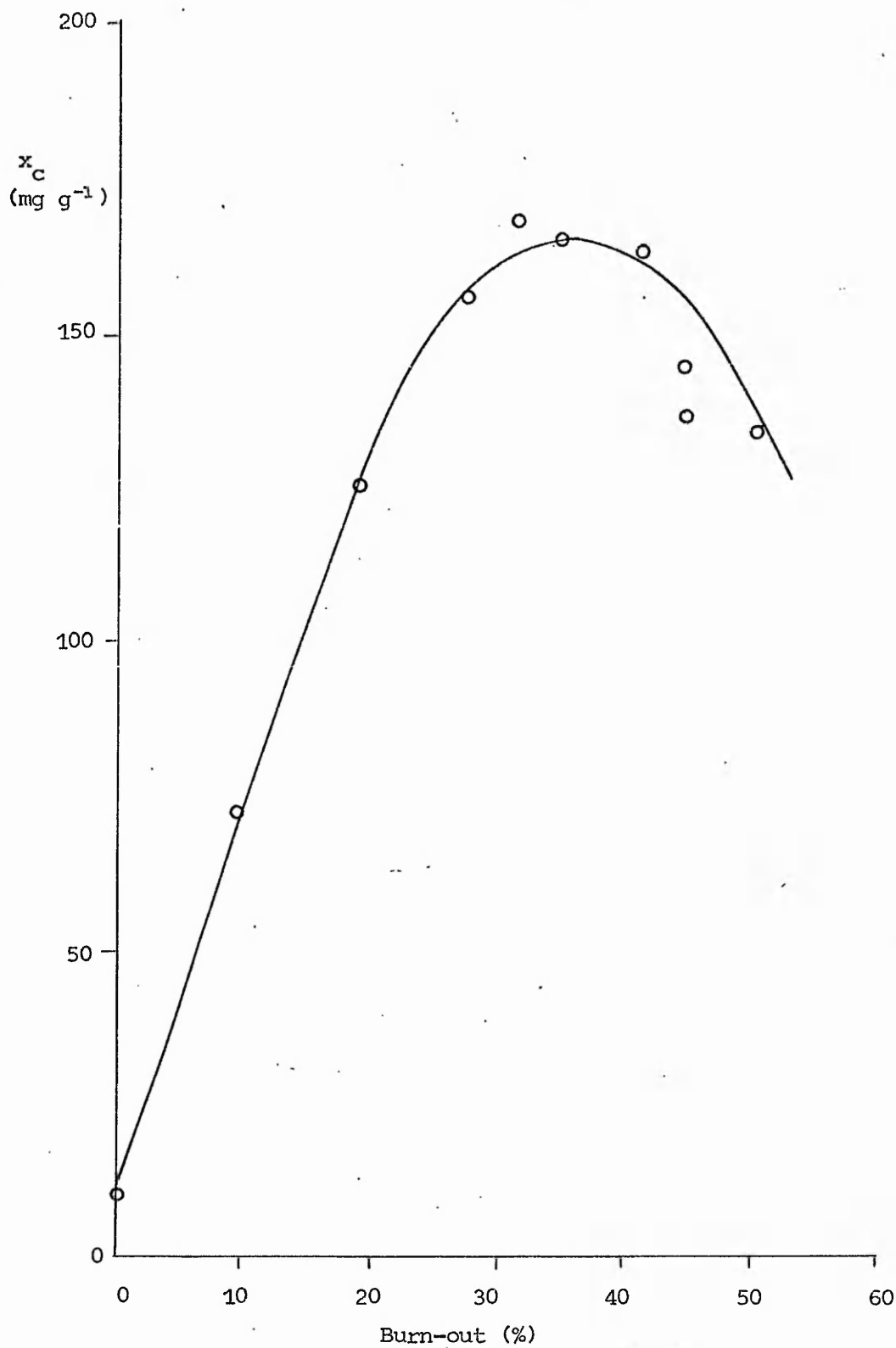


Figure 11.3(17)
 Variation of x_c (mg g^{-1}) with burn-out (%) for W25/C75 carbon.

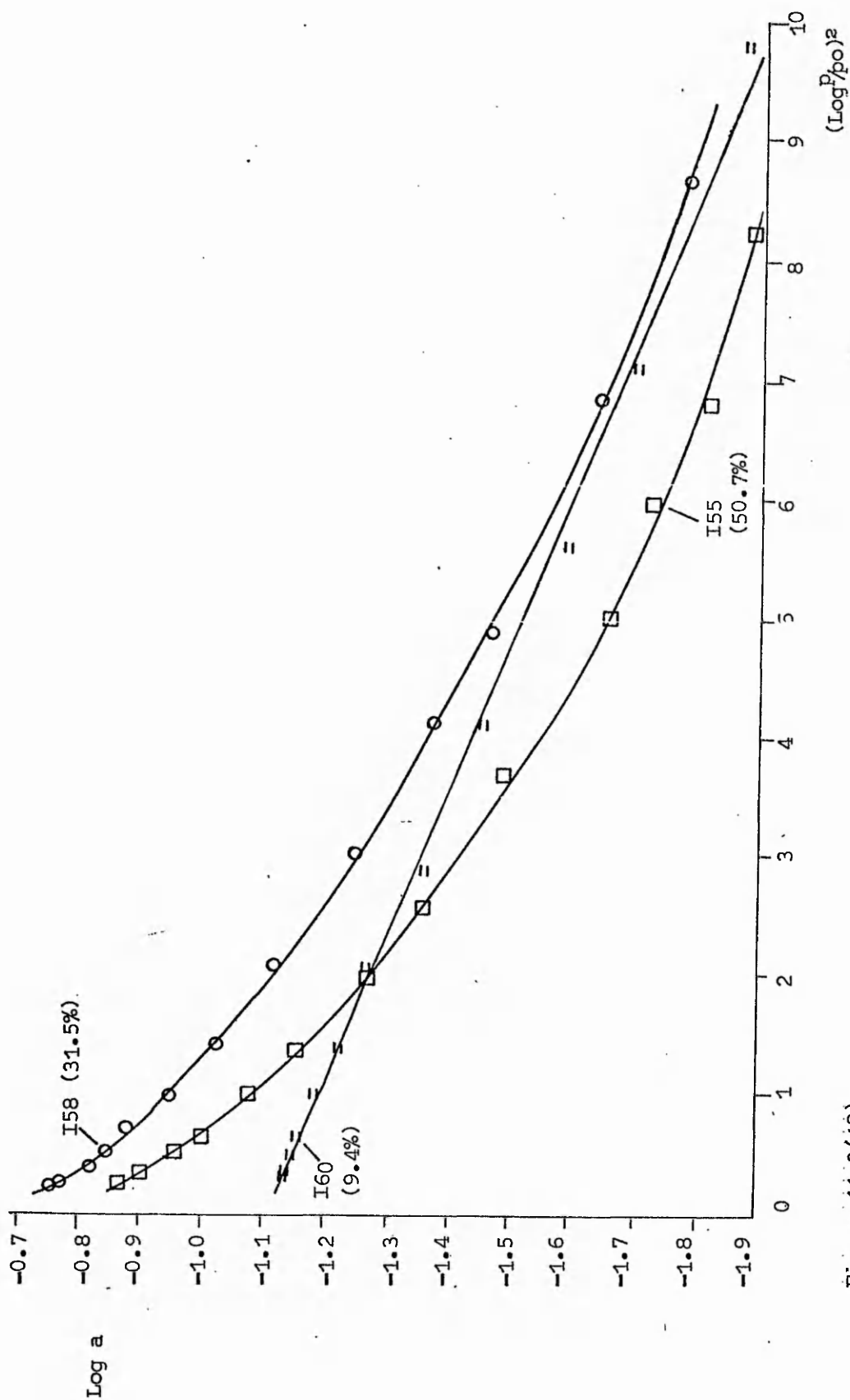


Figure 14.3(18)
Representative D-R type I plots for W25/C75 carbons.

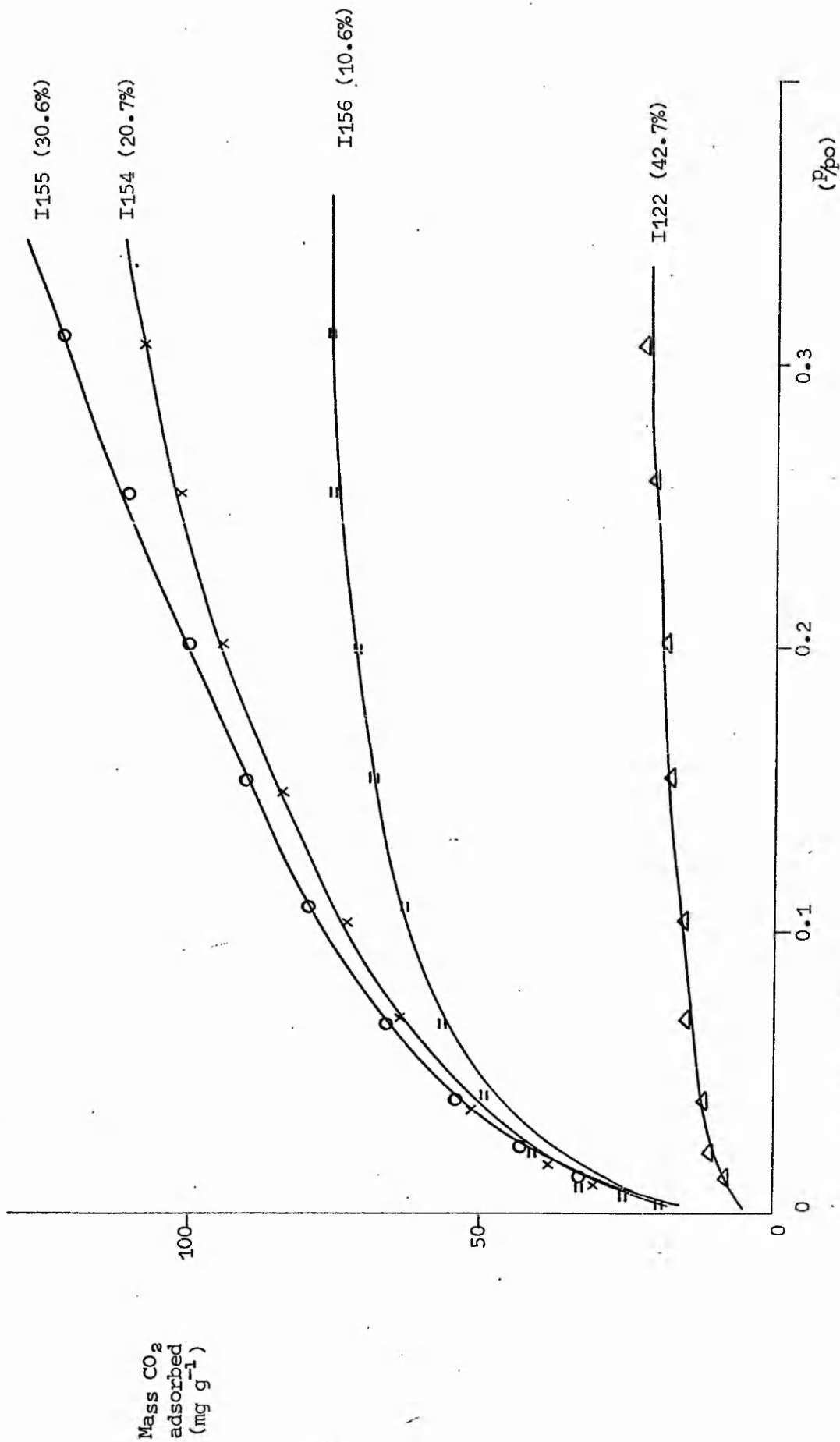


Figure 11.3(19)
Adsorption of carbon dioxide at 195K on 1313K W15/C85 carbon activated by carbon dioxide at 1303K.

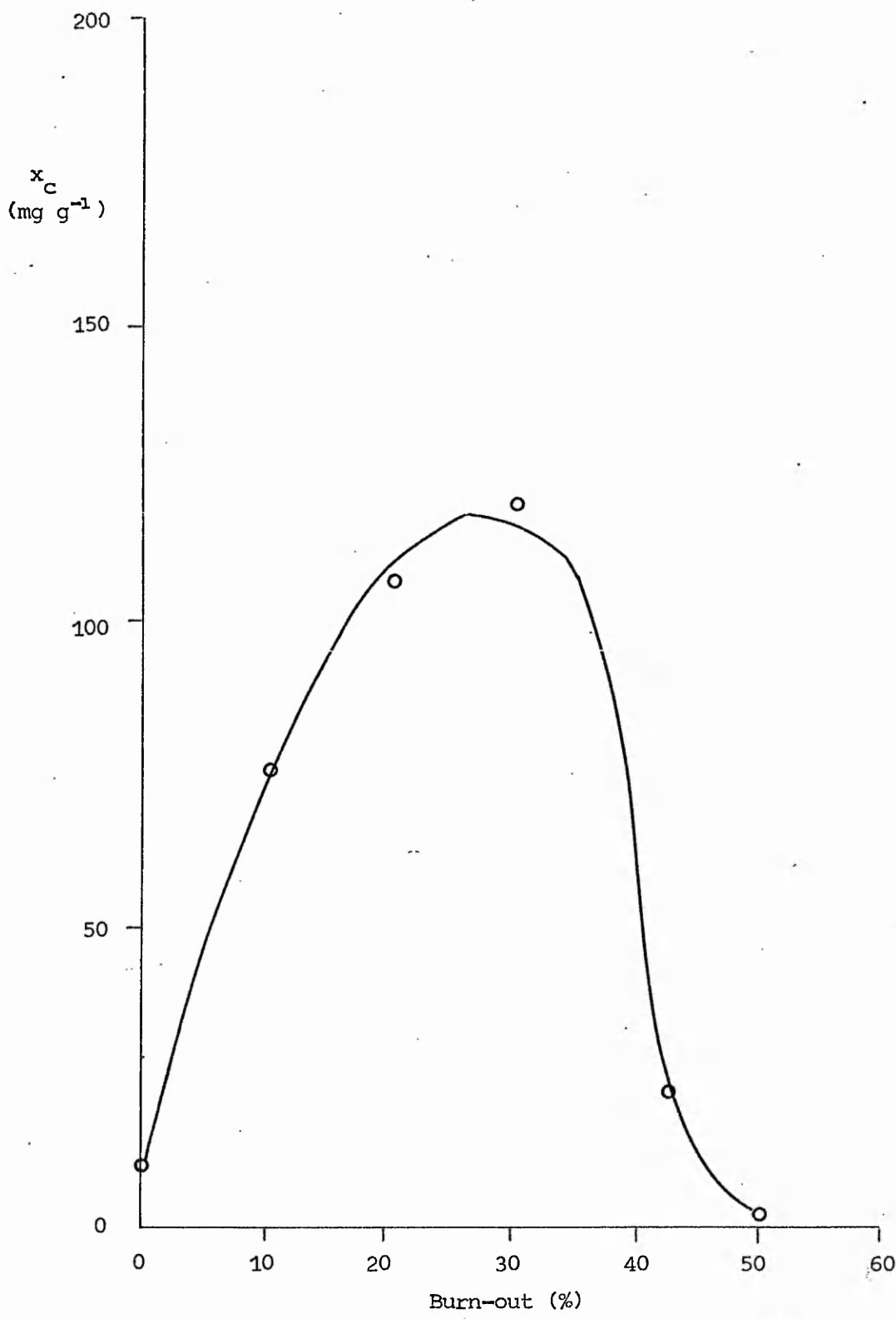


Figure 11.3(20)
Variation of x_c (mg g^{-1}) with burn-out (%) for W15/C85 carbon.

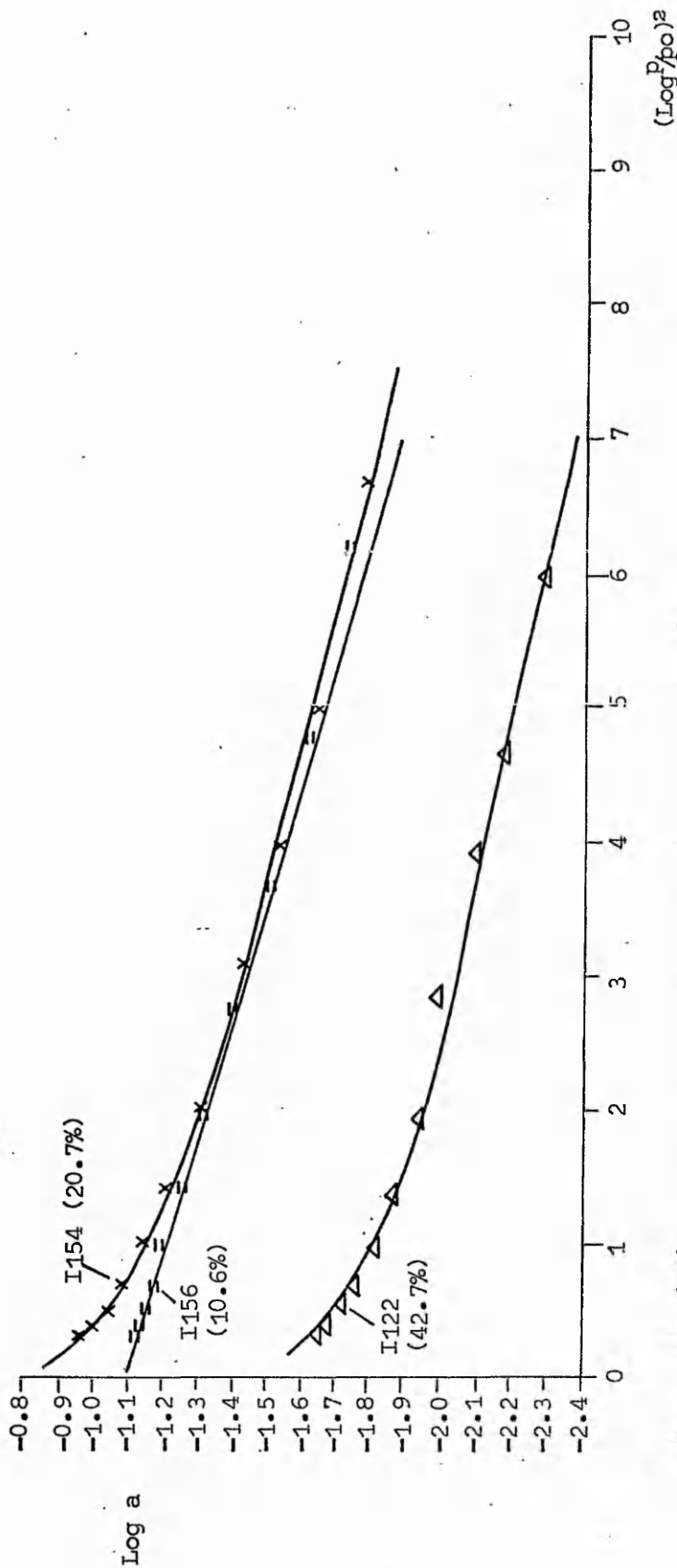


Figure 11.3(21)
Representative D-R type I plots for W15/C85 carbons.

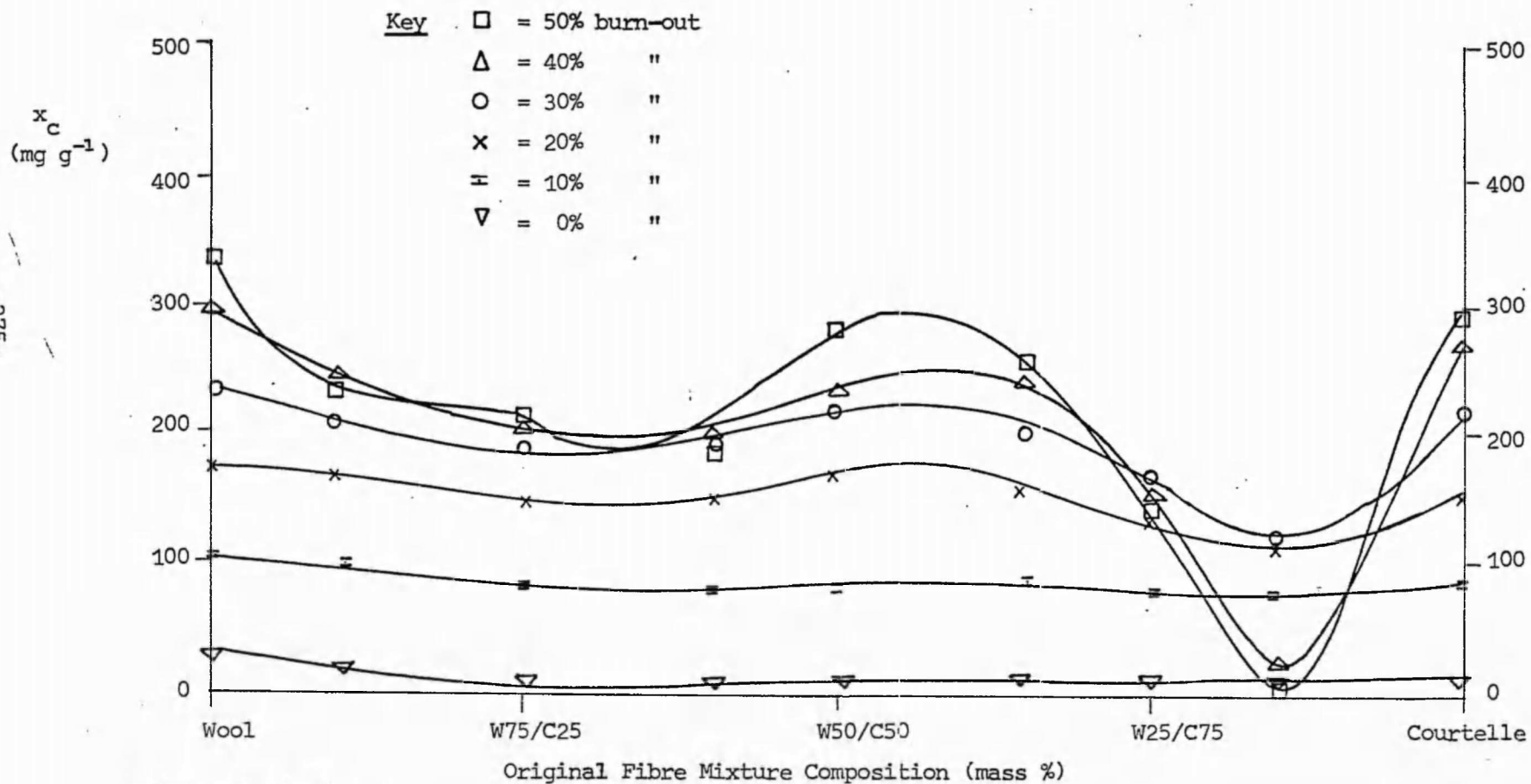


Figure 11.3(22)

Variation of x_c for burn-outs in the range 0-50% over the entire composition range for Wool/Courtelle carbons.

11.4 Terylene/Courtelle carbon

The textile polymer mixtures from which the Terylene/Courtelle carbons were prepared are listed in table 11.4(1). This table also provides a key to the location of all the adsorption data presented for this system of carbons.

The variation in \underline{x}_C with burn-out for each carbon of this system is summarised in table 11.4(2). The continuous increase in \underline{x}_C with burn-out observed for carbons prepared from Terylene was also observed for carbons prepared from fibre mixtures containing greater than or equal to 45% by mass of Terylene.

The maximum value of \underline{x}_C in the burn-out range 0-50% for these carbons was however observed to gradually decrease with decreasing Terylene content.

For carbons derived from fibre mixtures containing \leq 35% by mass of Terylene table 11.4(2) indicates a maximum in the variation of \underline{x}_C with increasing burn-out. Both the maximum value of \underline{x}_C and the burn-out at which it is observed decreased as the Terylene content decreased until the composition reached C90/T10 (mass %).

For the carbons C90/T10 and C85/T15 increasing burn-out had a relatively small effect on \underline{x}_C [figures 11.4(2) and 11.4(5)]. Indeed for both these carbons the value of \underline{x}_C at 40% and 50% burn-out was less than 10 mg g^{-1} .

Representative D-R type I plots are arranged as listed in table 11.4(1). The overall behaviour of the system in terms of the type of D-R type I plot observed is indicated in table 11.4(3). All the activated carbons prepared from Terylene exhibited type A deviation [figure 11.1(6)].

As the proportion of Terylene in the fibre mixture was reduced, a gradual decrease in the incidence of type A deviation was observed for the corresponding carbons and instead either linear plots or type B deviations were observed.

Type B deviation was observed at progressively lower burn-out with decreasing content of Terylene in the original fibre mixture.

As indicated in table 11.4(3) somewhat unusual behaviour was observed for carbons derived from fibre mixtures of high Courtelle content. Thus for both C90/T10 and C85/T15 carbons deviations with some type C character were observed at low burn-outs [figures 11.4(3) and 11.4(6)].

Table 11.4(1)

Location of (a) adsorption isotherms

(b) x_c /burn-out diagrams

(c) D-R type I plots

for the Terylene/Courtelle system.

Mixture (mass %)	(a) Adsorption Isotherms	(b) x_c /burn-out diagrams	(c) D-R type I plots
Courtelle (C)	figure 11.1(7)	figure 11.1(8)	figure 11.1(9)
C90/T10	" 11.4(1)	" 11.4(2)	" 11.4(3)
C85/T15	" 11.4(4)	" 11.4(5)	" 11.4(6)
C75/T25	" 11.4(7)	" 11.4(8)	" 11.4(9)
C65/T35	" 11.4(10)	" 11.4(11)	" 11.4(12)
C55/T45	" 11.4(13)	" 11.4(14)	" 11.4(15)
C50/T50	" 11.4(16)	" 11.4(17)	" 11.4(18)
C25/T75	" 11.4(19)	" 11.4(20)	" 11.4(21)
Terylene (T)	" 11.1(4)	" 11.1(5)	" 11.1(6)

Table 11.4(2)

Summary of the x_c /burn-out diagrams for the carbons of the Terylene/Courtelle system.

Mixture (mass %)	figure	behaviour observed	maximum x_c value observed in the burn-out range 0-50%
Courtelle (C)	11.1(8)	continuous increase in x_c value with burn-out	300 mg g ⁻¹ (at 50% burn-out)
C90/T10	11.4(2)	maximum x_c value occurs at 10-15% burn-out	45 mg g ⁻¹
C85/T15	11.4(5)	maximum x_c value occurs at 15-25% burn-out	55 "
C75/T25	11.4(8)	maximum x_c value occurs at 25-35% burn-out	145 "
C65/T35	11.4(11)	maximum x_c value occurs at 30-40% burn-out	160 "
C55/T45	11.4(14)	continuous increase in x_c value with burn-out	400 mg g ⁻¹ (at 50% burn-out)
C50/T50	11.4(17)	" "	450 " "
C25/T75	11.4(20)	" "	600 " "
Terylene (T)	11.1(5)	" "	650 " "

Table 11.4(3)

Applicability of the D-R type I equation to the Terylene/Courtelle carbon system. Deviations from linearity are classified according to the notation of Marsh and Rand.¹⁰²

Mixture (mass %)	Burn-out (%)					
	0	10	20	30	40	50
Courtelle (C)	X	A	L	B	B	B
C90/T10	X	(B/C)	(B/C)	(B/C)	X	X
C85/T15	X	C	B	B	X	X
C75/T25	X	B	B	B	B	B
C65/T35	X	L	B	B	B	B
C55/T45	(A)	L	L	B	B	B
C50/T50	X	A	L	L	B	B
C25/T75	C	A	A	A	L	B
Terylene (T)	A	A	A	A	A	A

Key

A = Type A deviation (according to Marsh and Rand)¹⁰²

B = " B " " " " " " "

C = " C " " " " " " "

L = Linear plot

X = Not plotted, negligible gas uptake.

Where A, B, C, L ringed indicates possible error range $\geq 25\%$ of corresponding x_c value.

The variation of mercury density with burn-out has been determined for C85/T15 carbon and the results are presented in chapter 12.

As discussed in the preceding section type C deviations were observed for carbons derived from fibre mixtures of high Courtelle content in the wool/Courtelle system.

The overall variation in \bar{x}_c with increasing degree of burn-out for all the carbons prepared from Terylene/Courtelle mixtures is illustrated in figure 11.4(22).

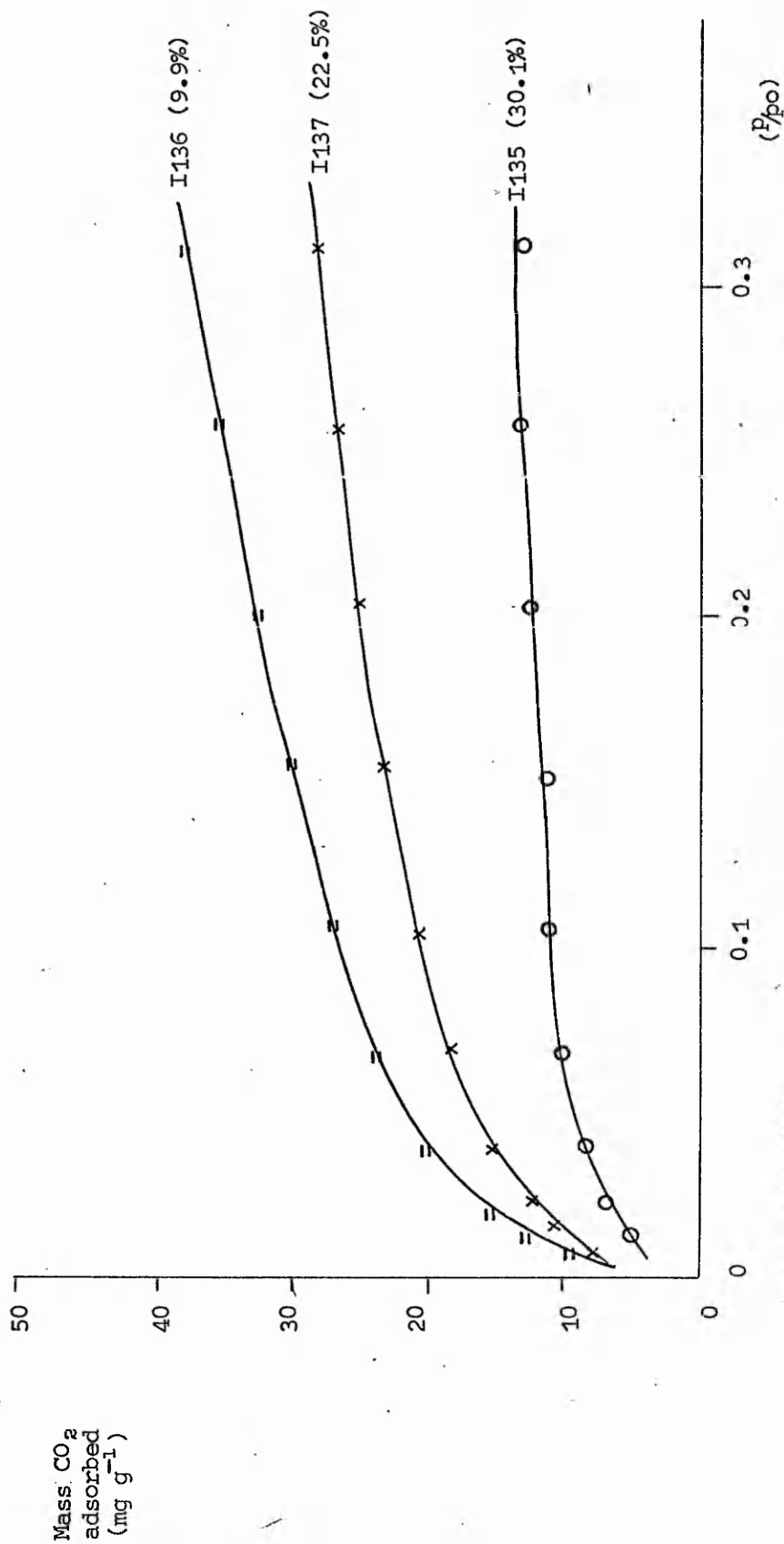


Figure 11.4(1)
Adsorption of carbon dioxide at 195K on 1313K C90/T10 carbon activated by carbon dioxide at 1303K.

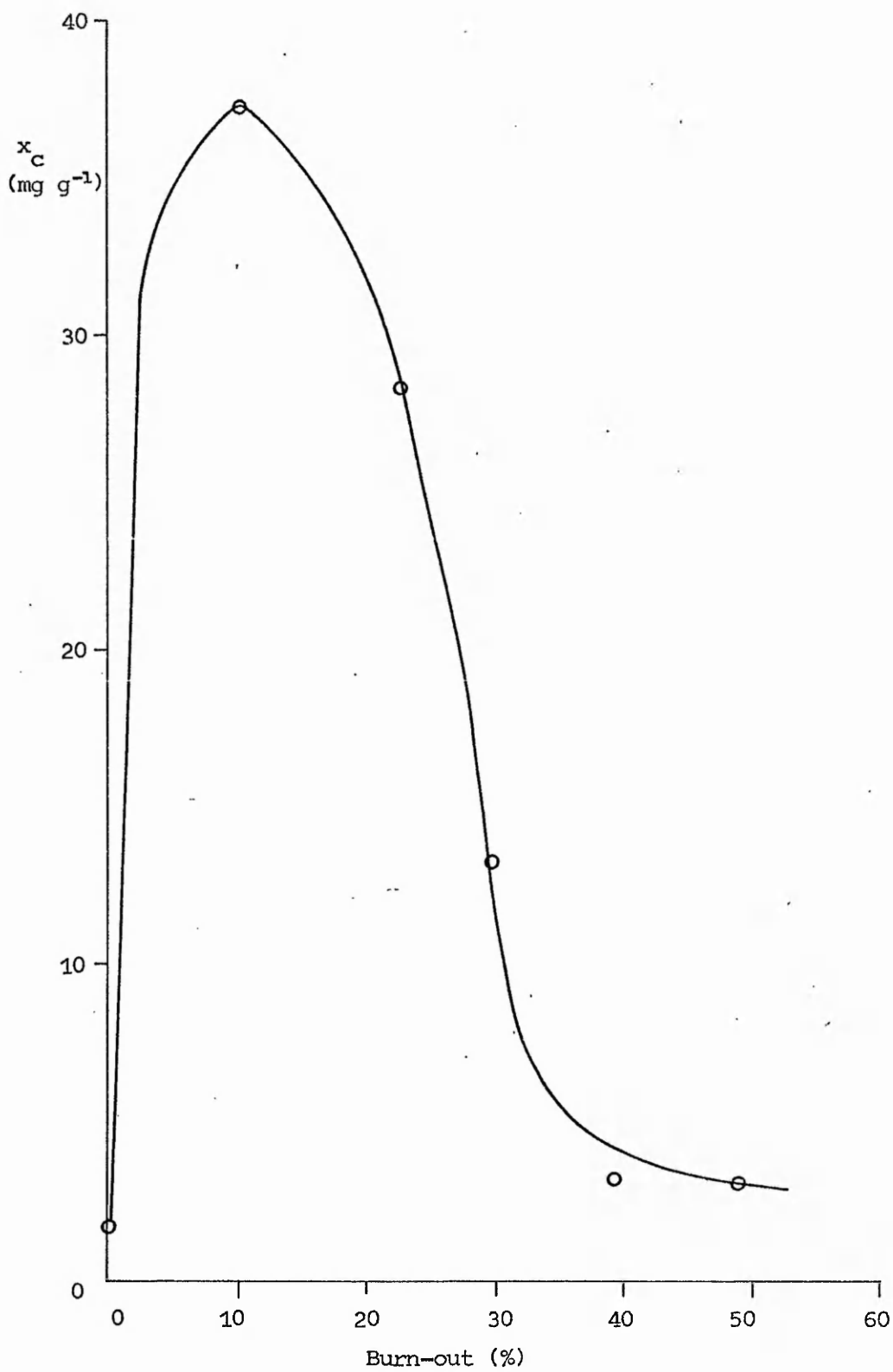


Figure 11.4(2)
Variation of x_C (mg g^{-1}) with burn-out (%) for C90/T10 carbon.

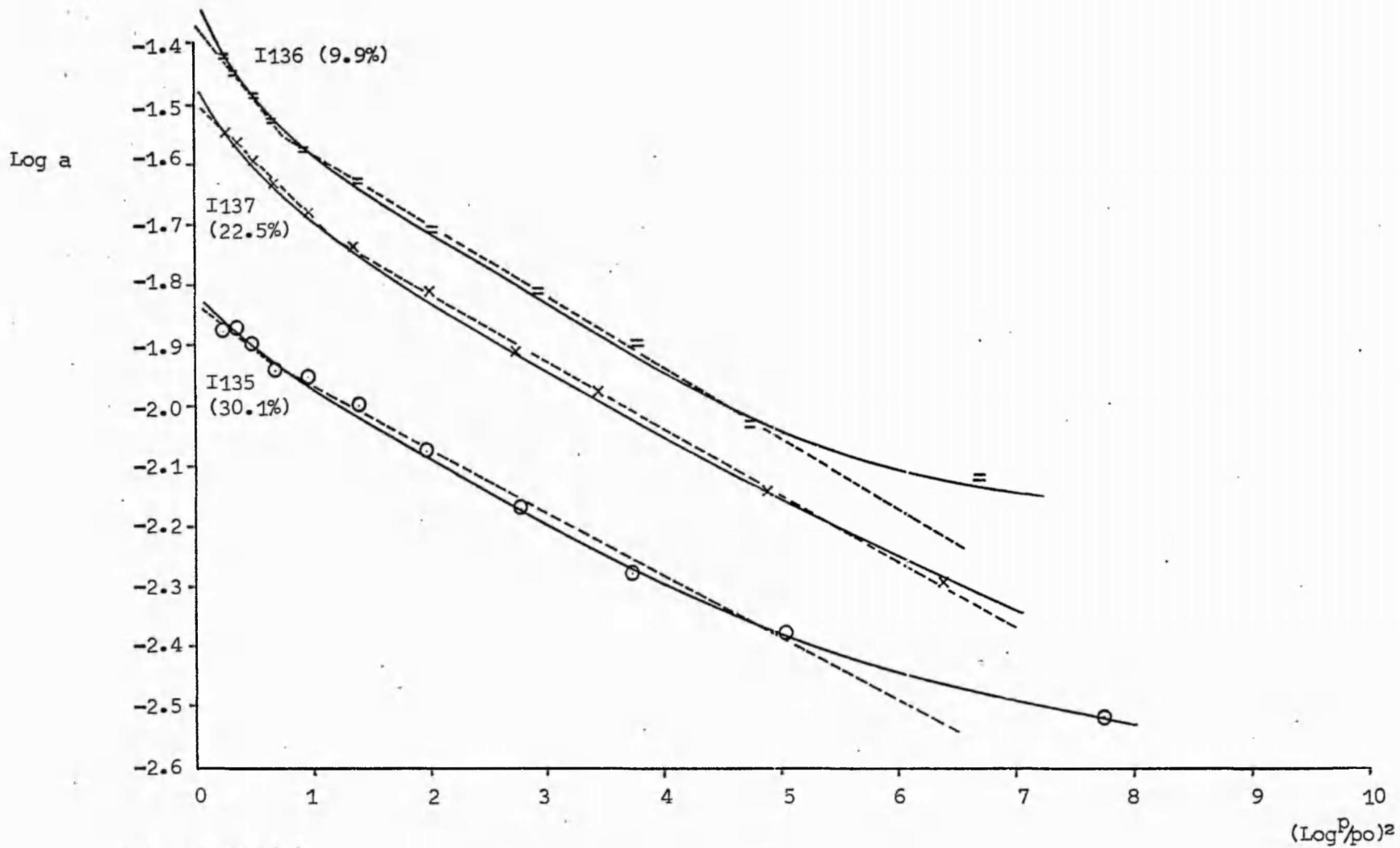


Figure 11.4(3)
Representative D-R type I plots for C90/T10 carbons.

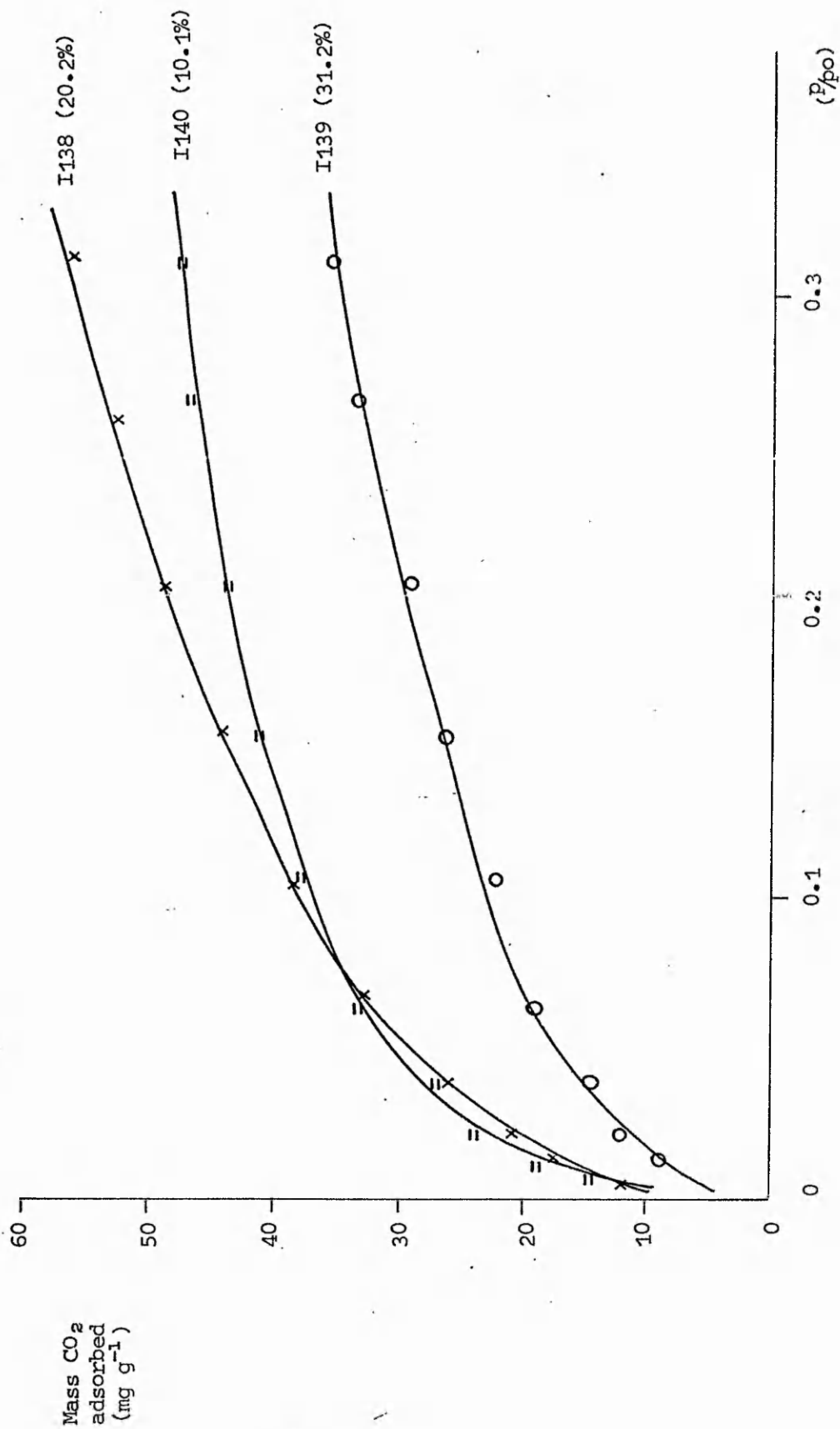


Figure 11.4(4)
adsorption of carbon dioxide at 195K on 1313K C85/T15 carbon activated by carbon dioxide at 1303K.

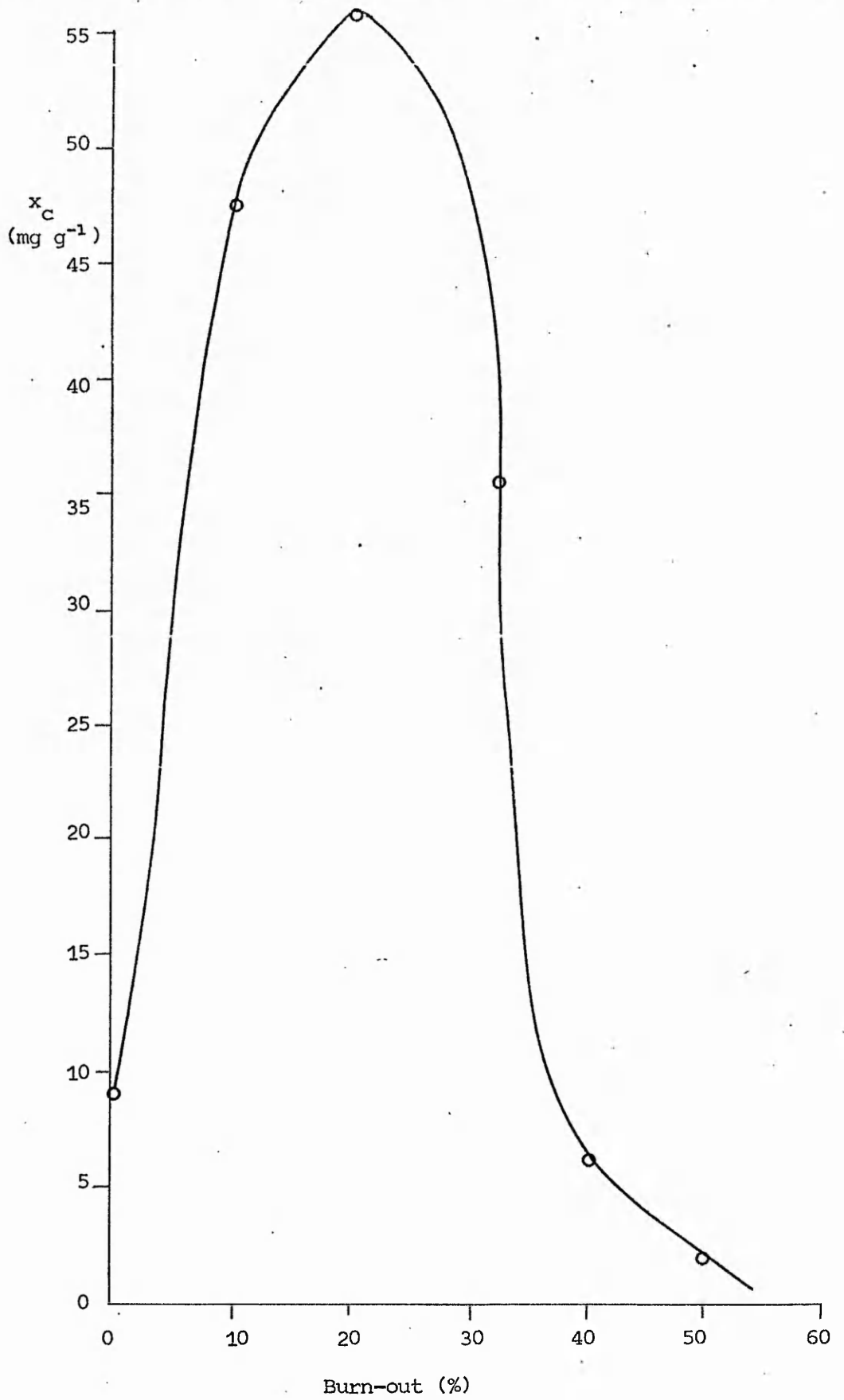


Figure 11.4(5)
Variation of x_C (mg g^{-1}) with burn-out (%) for C85/T15 carbon.

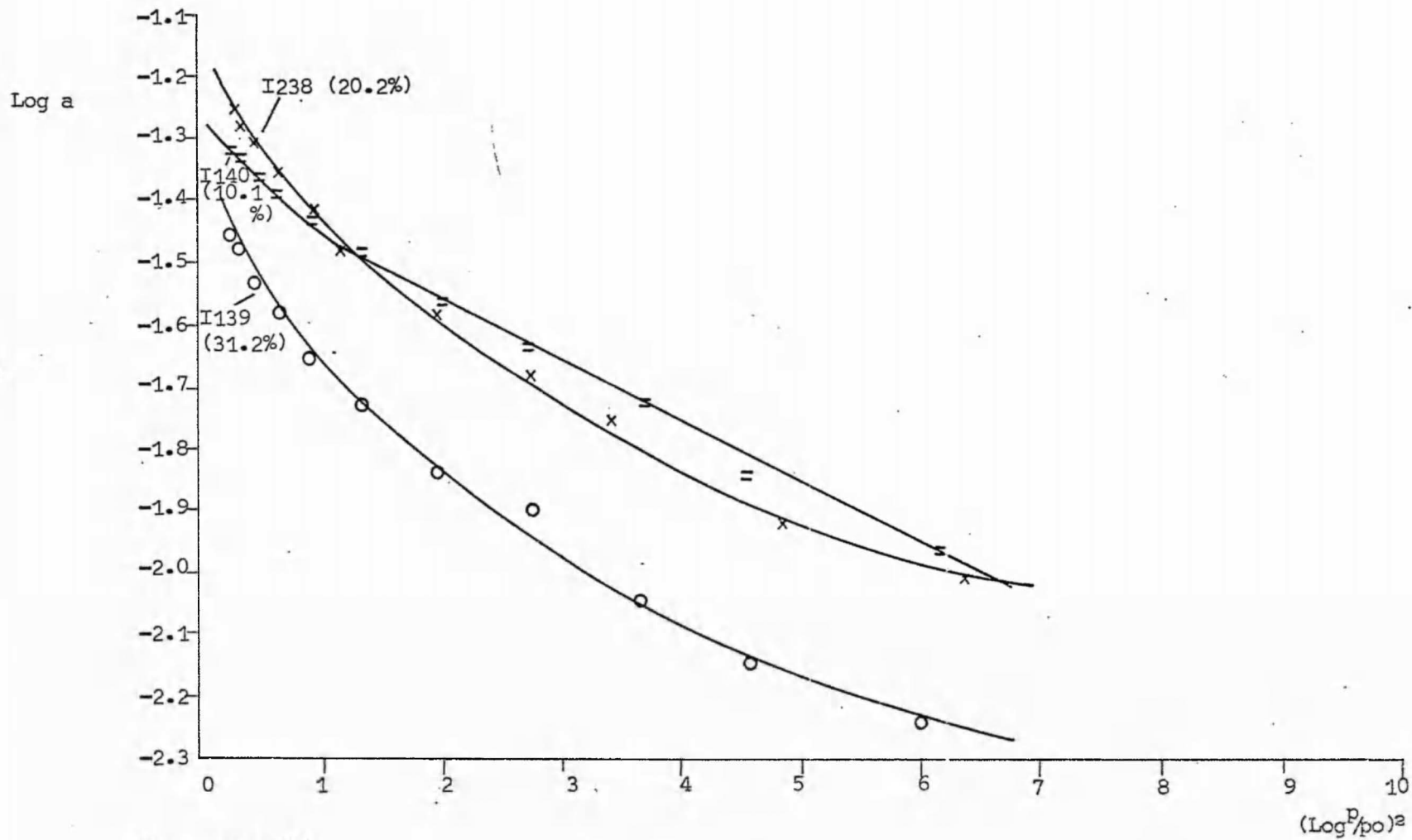


Figure 11.4(6)
Representative D-R type I plots for C85/T15 carbon.

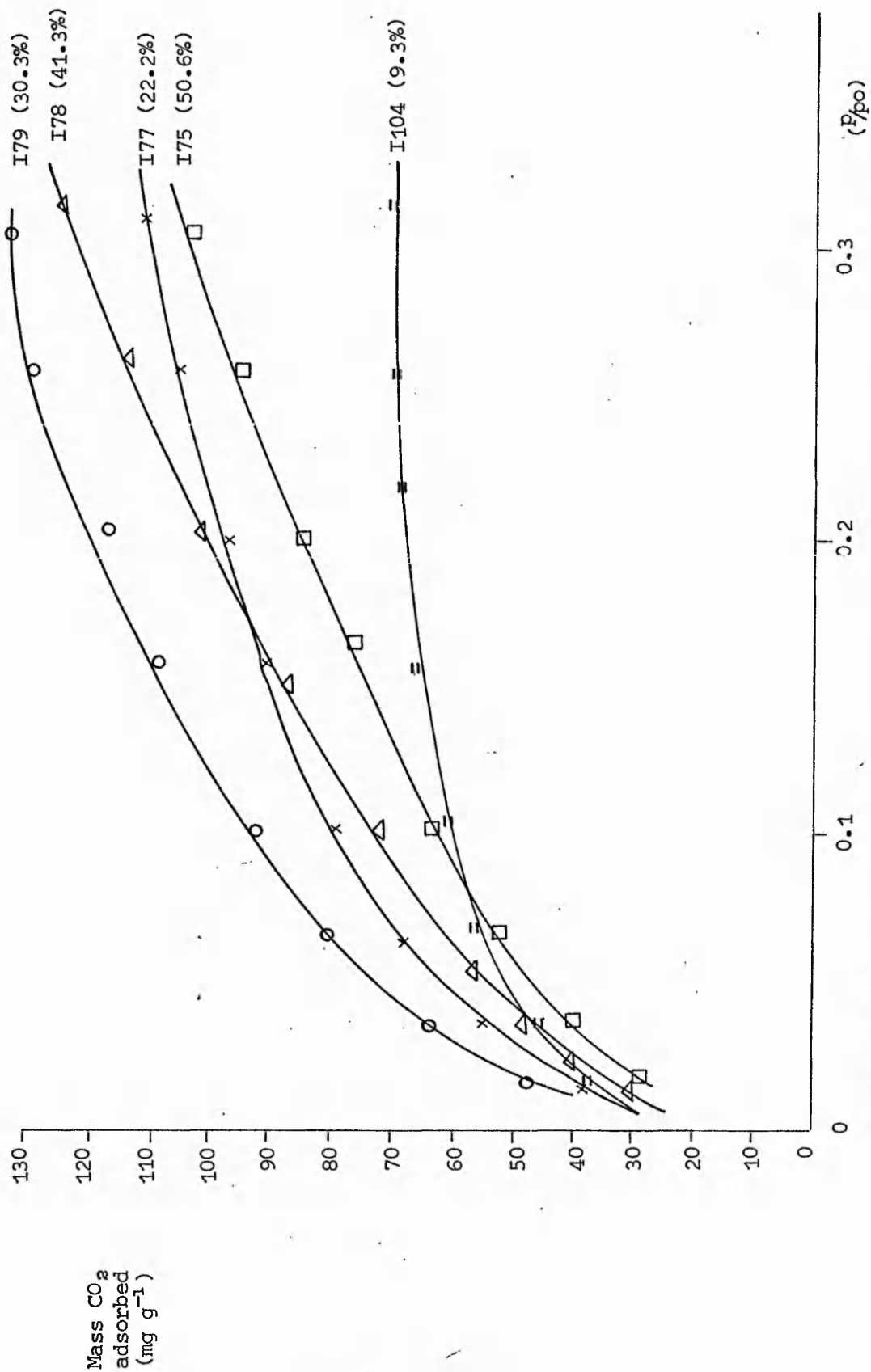


Figure 11.4(7)
Adsorption of carbon dioxide at 195K on 1313K C75/T25 carbon activated by carbon dioxide at 1303K.

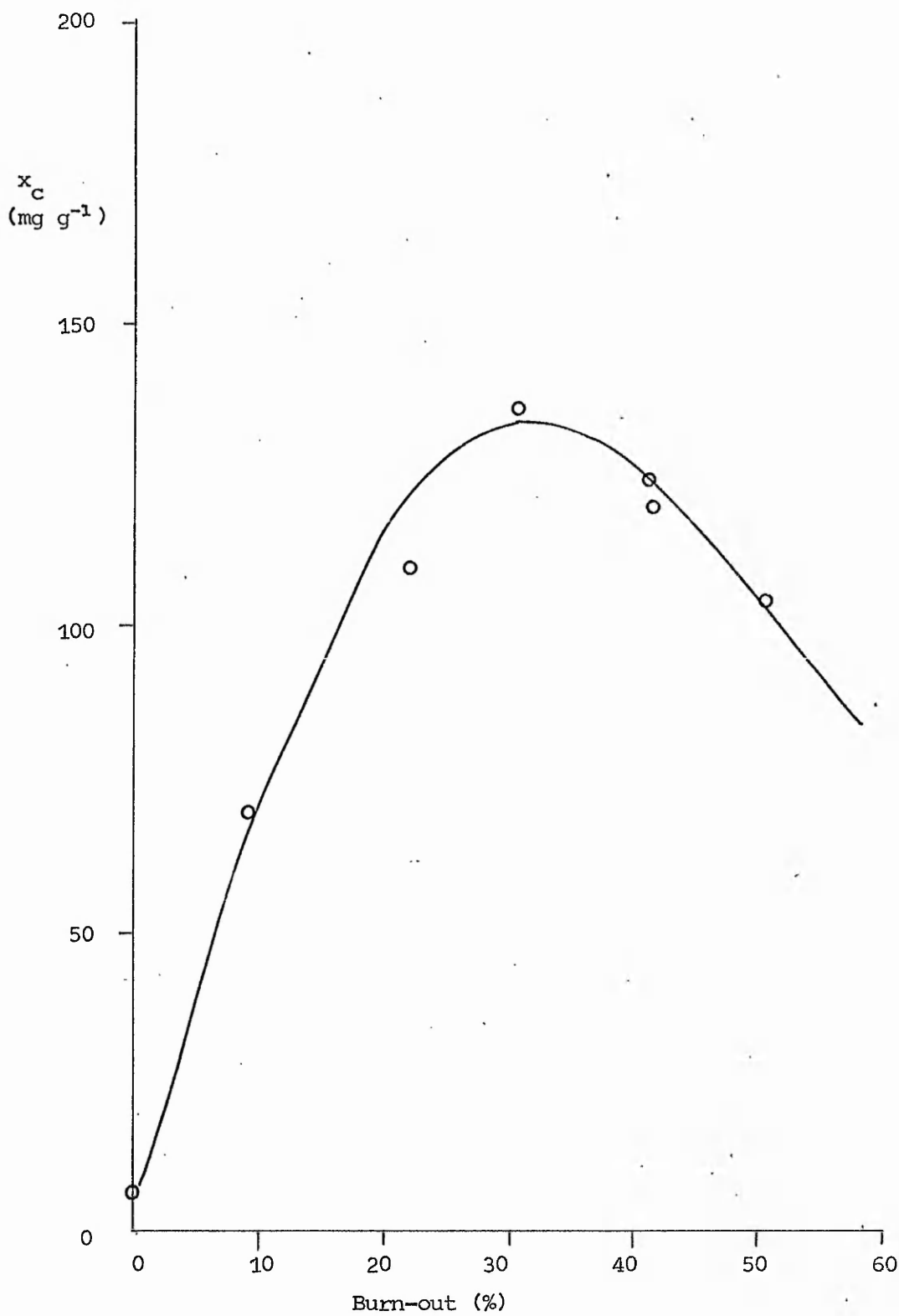


Figure 11.4(8)
Variation of x_c (mg g^{-1}) with burn-out (%) for C75/T25 carbon.

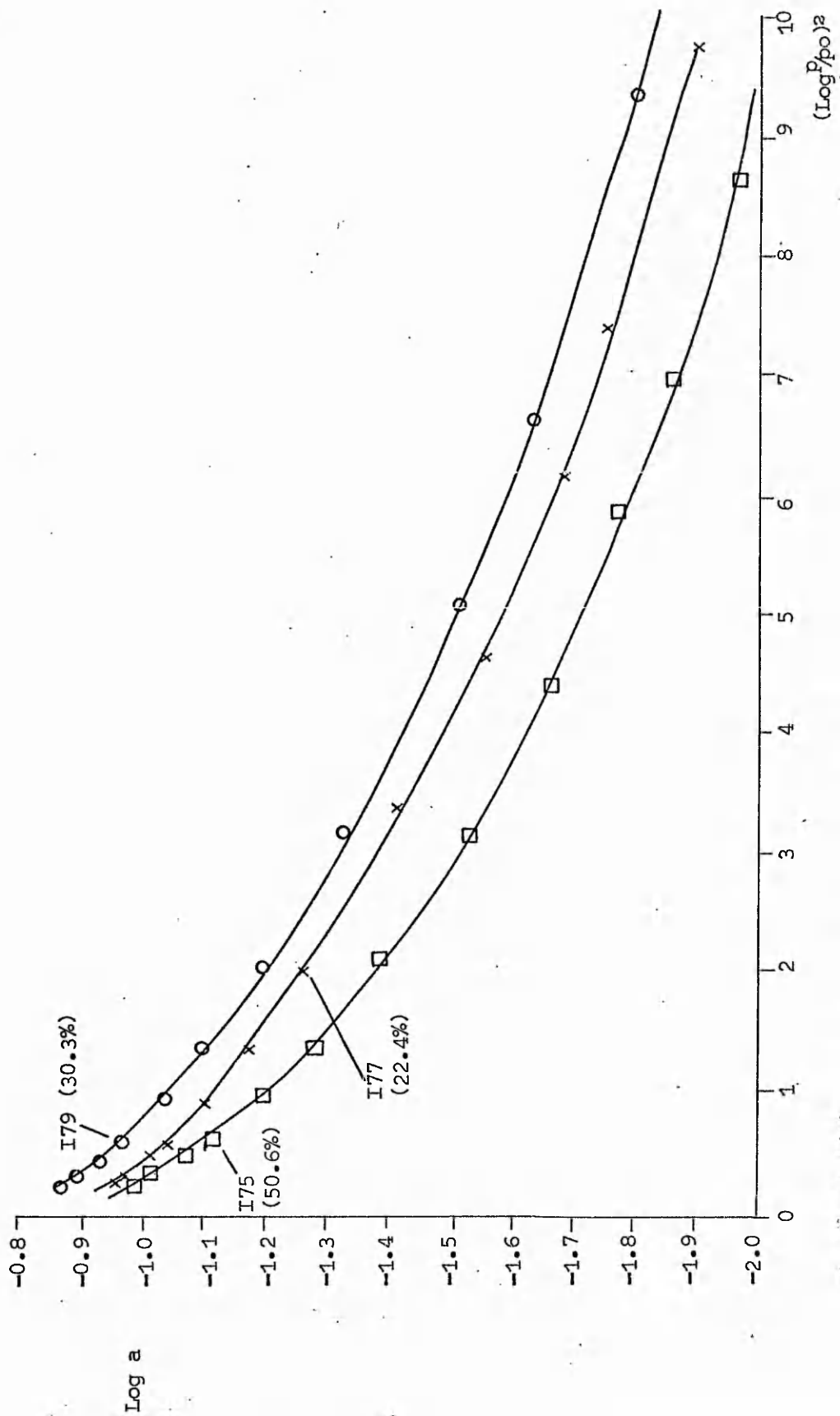


Figure 11.4(9)
Representative D-R type I plots for C75/T25 carbons.

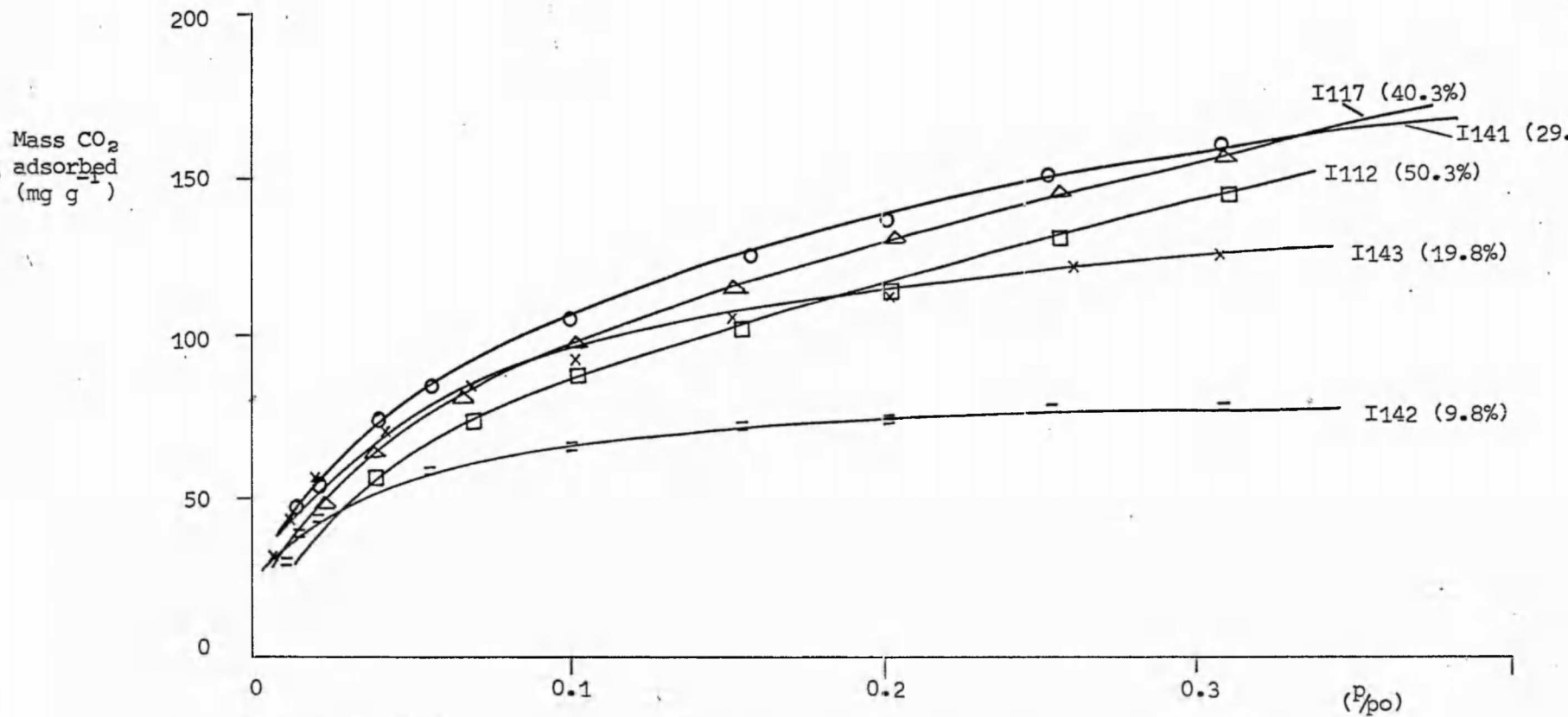


Figure 11.4(10)

Adsorption of carbon dioxide at 195K on 1313K C65/T35 carbon activated by carbon dioxide at 1303K.

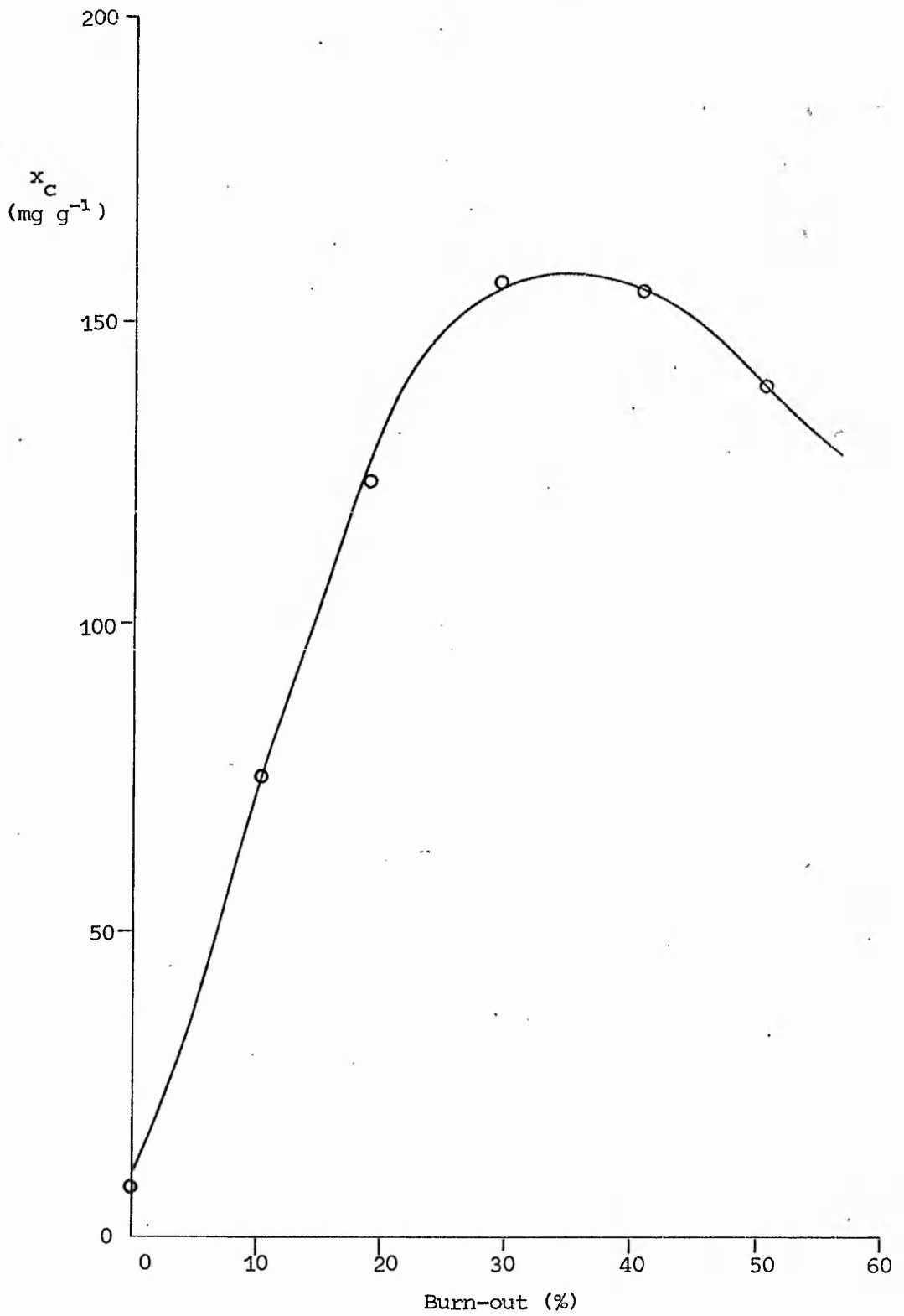


Figure 11.4(11)
Variation of x_c (mg g^{-1}) with burn-out (%) for C65/T35 carbon.

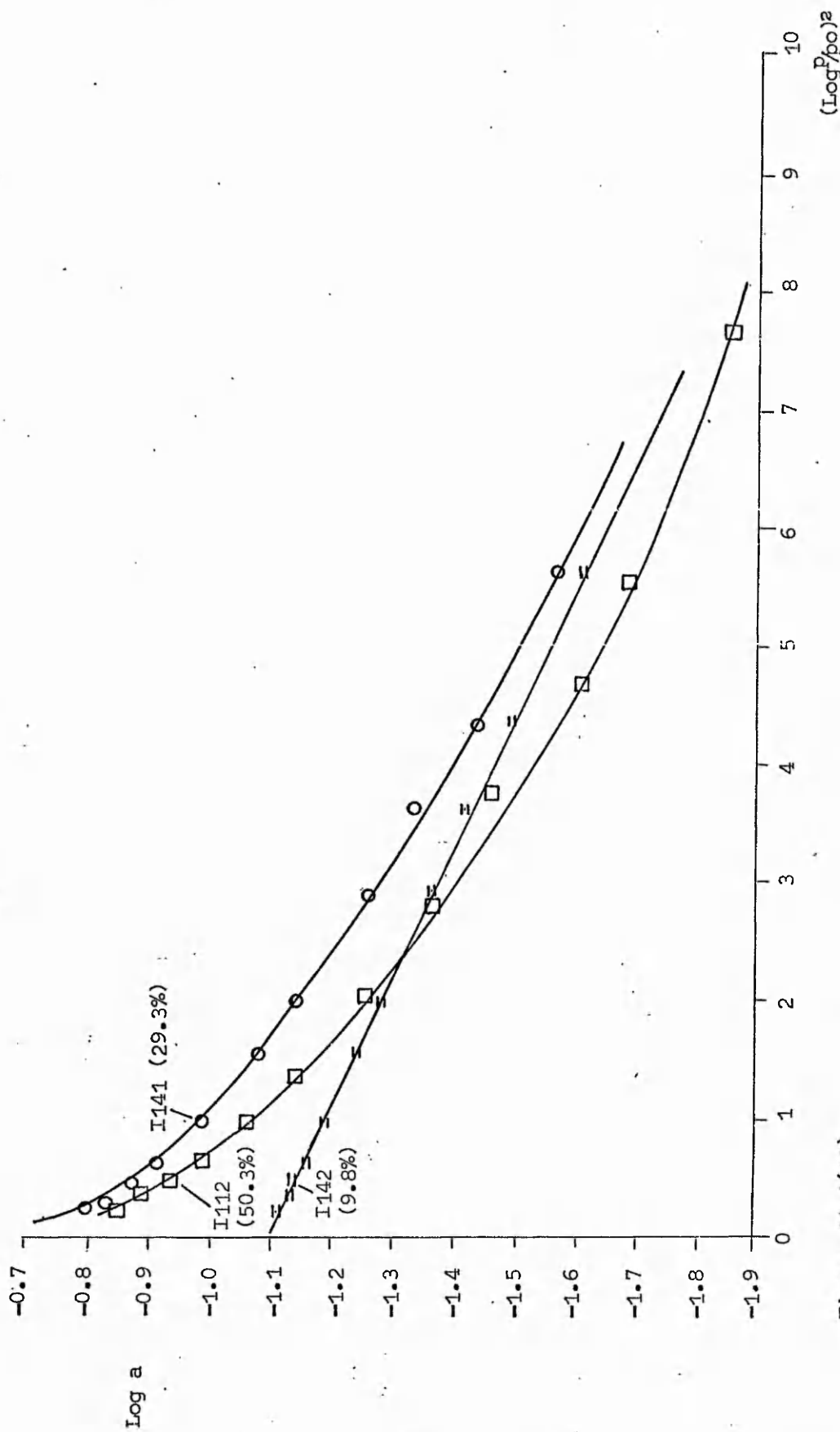


Figure 11.4(12)
Representative D-R type I plots for C65/T35 carbons.

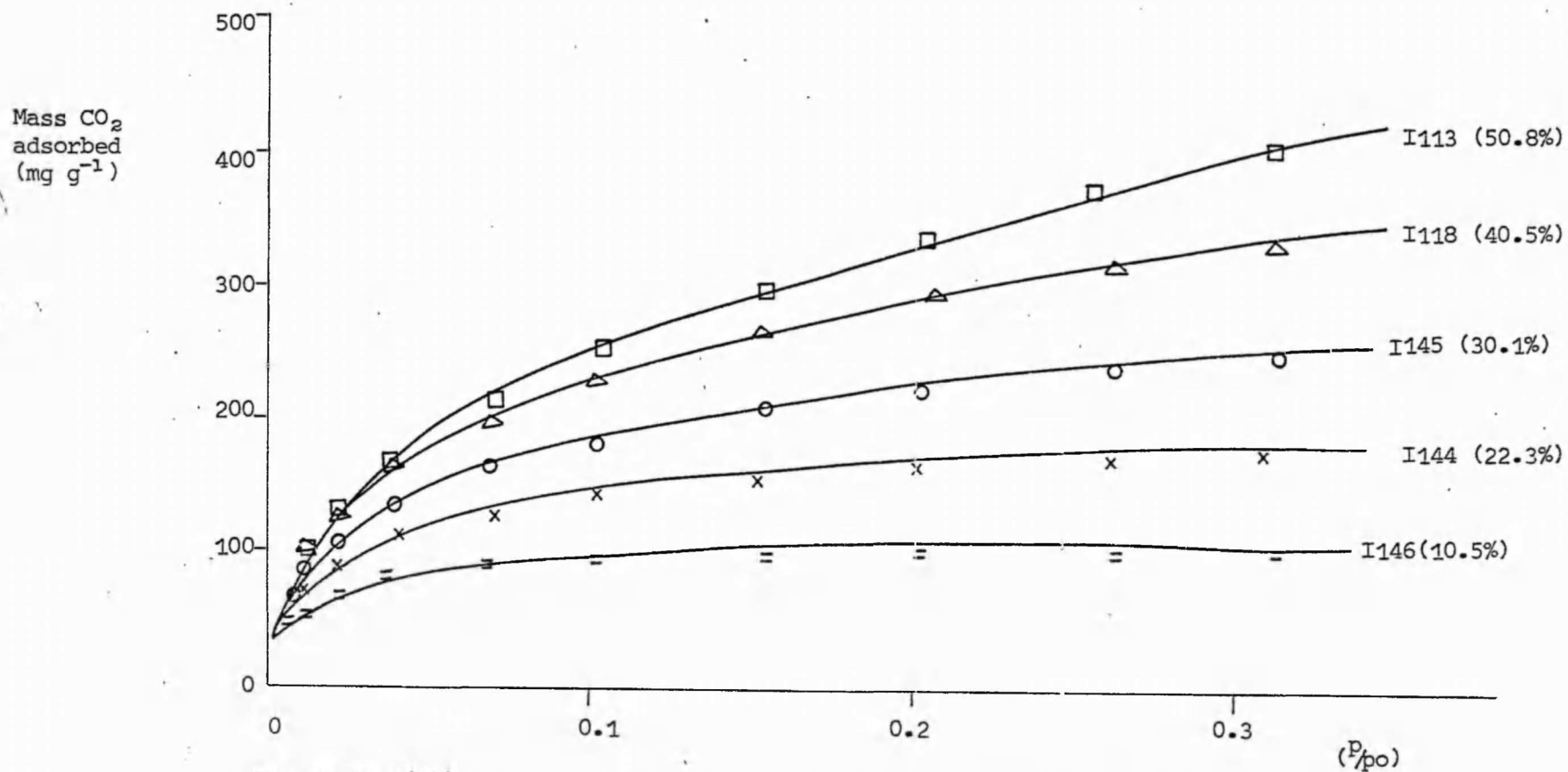


Figure 11.4(13)
Adsorption of carbon dioxide at 195K on 1313K C55/T45 carbon activated by carbon dioxide at 1303K.

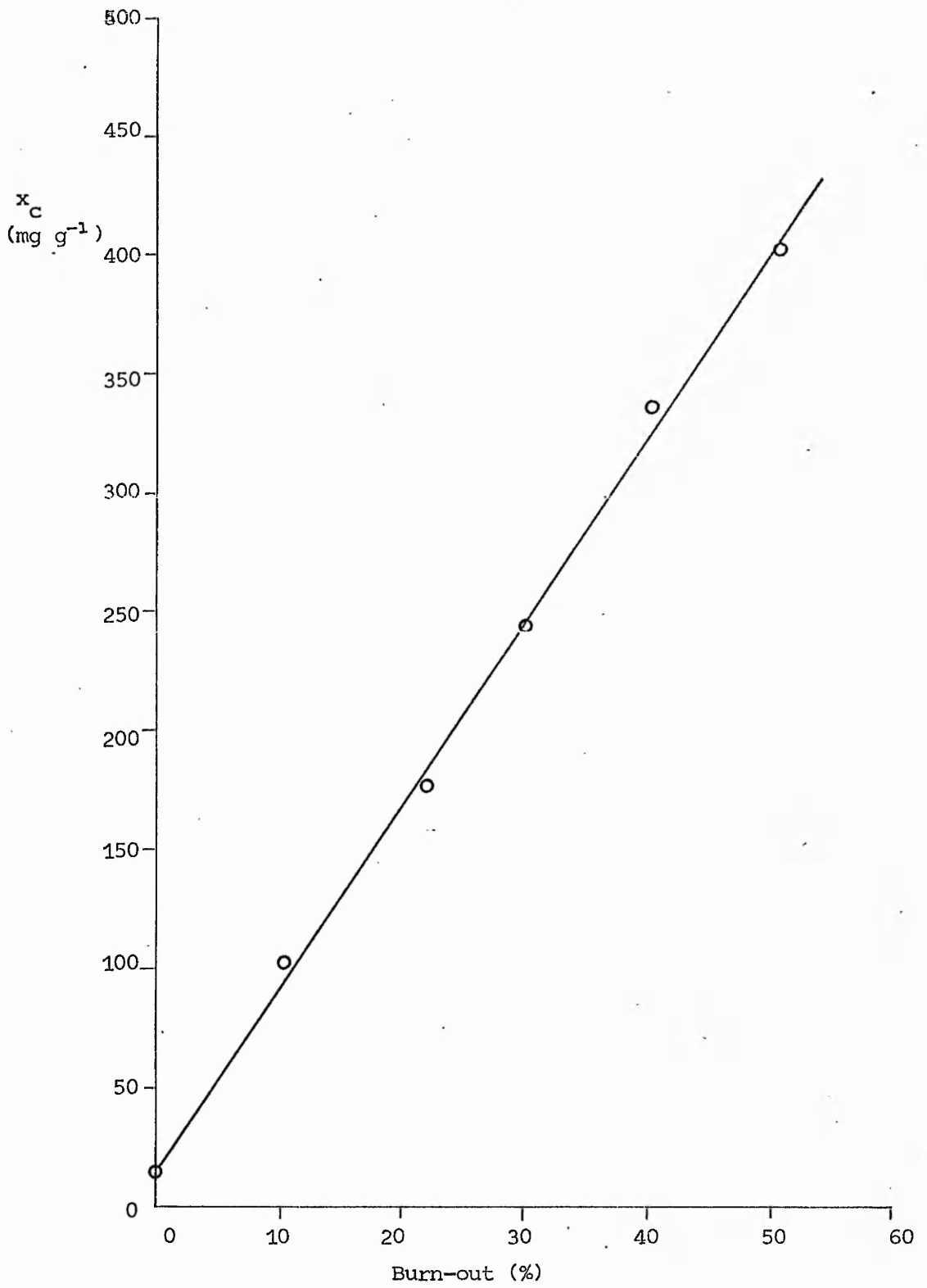


Figure 11.4(14)
Variation of x_c (mg g^{-1}) with burn-out (%) for C55/T45 carbon.

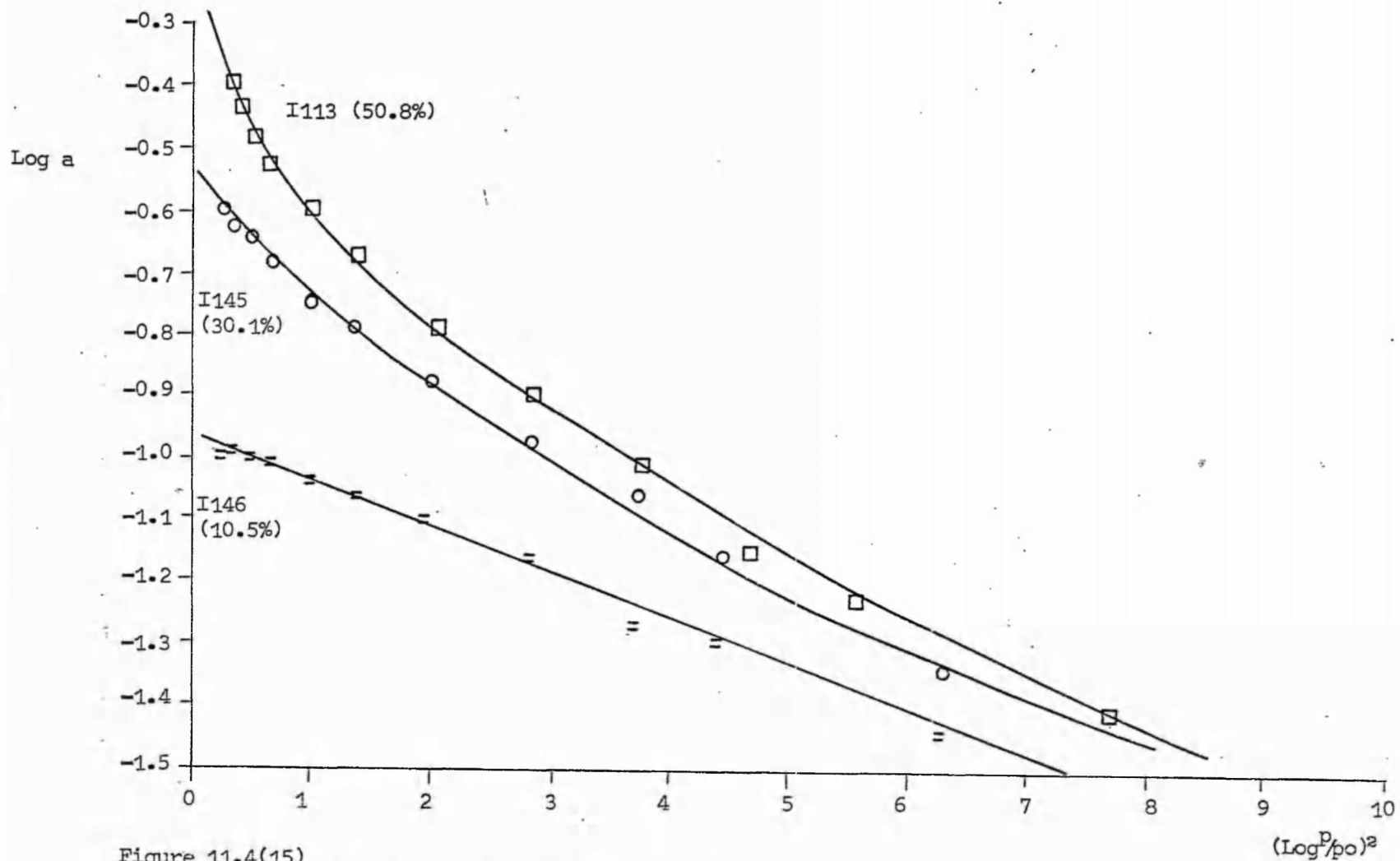


Figure 11.4(15)
 Representative D-R type I plots for C55/T45 carbons.

-IM Site

-295-

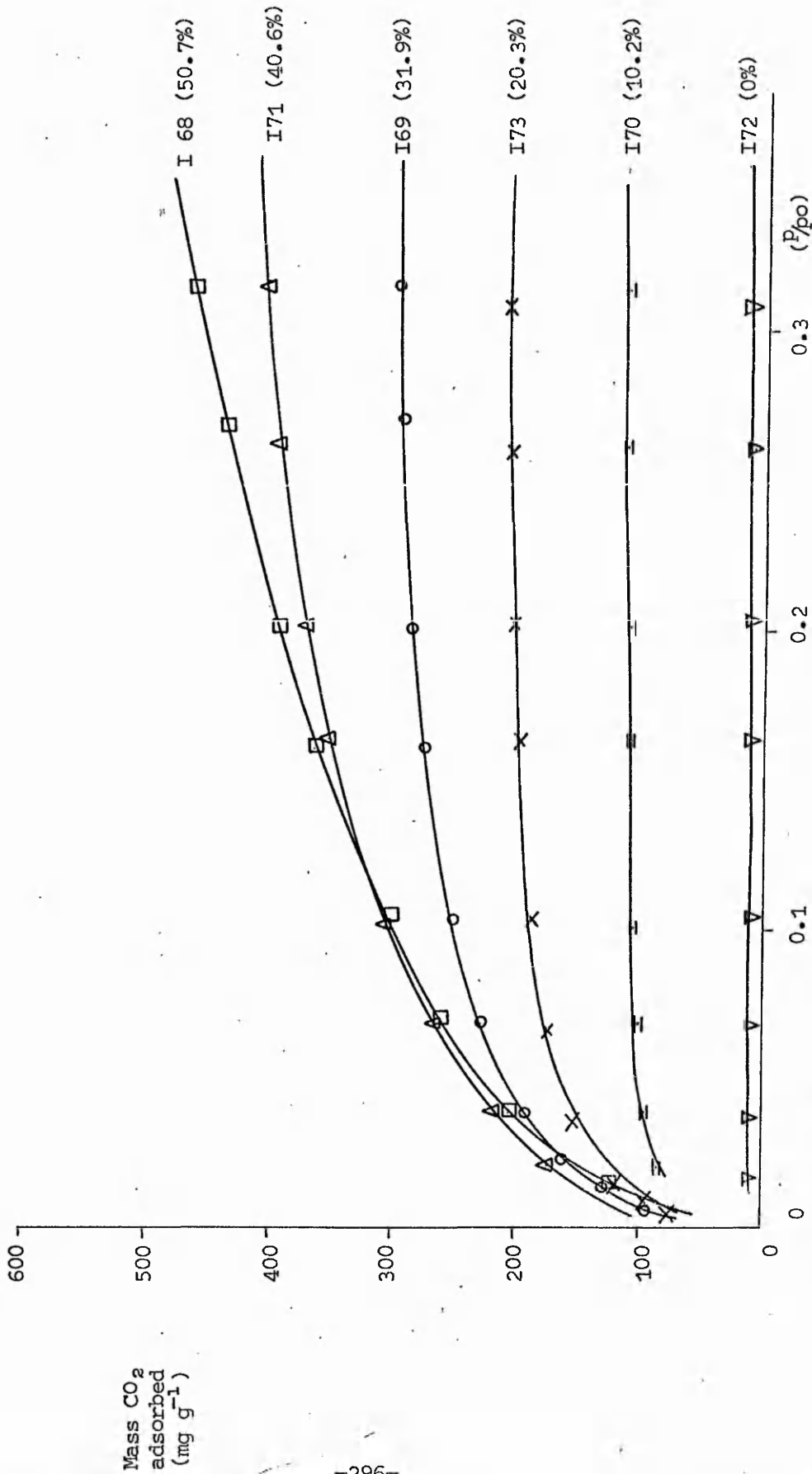


Figure 11.4(16)
Adsorption of carbon dioxide at 195K on 1313K C50/T50 carbon activated by carbon dioxide at 1303K.

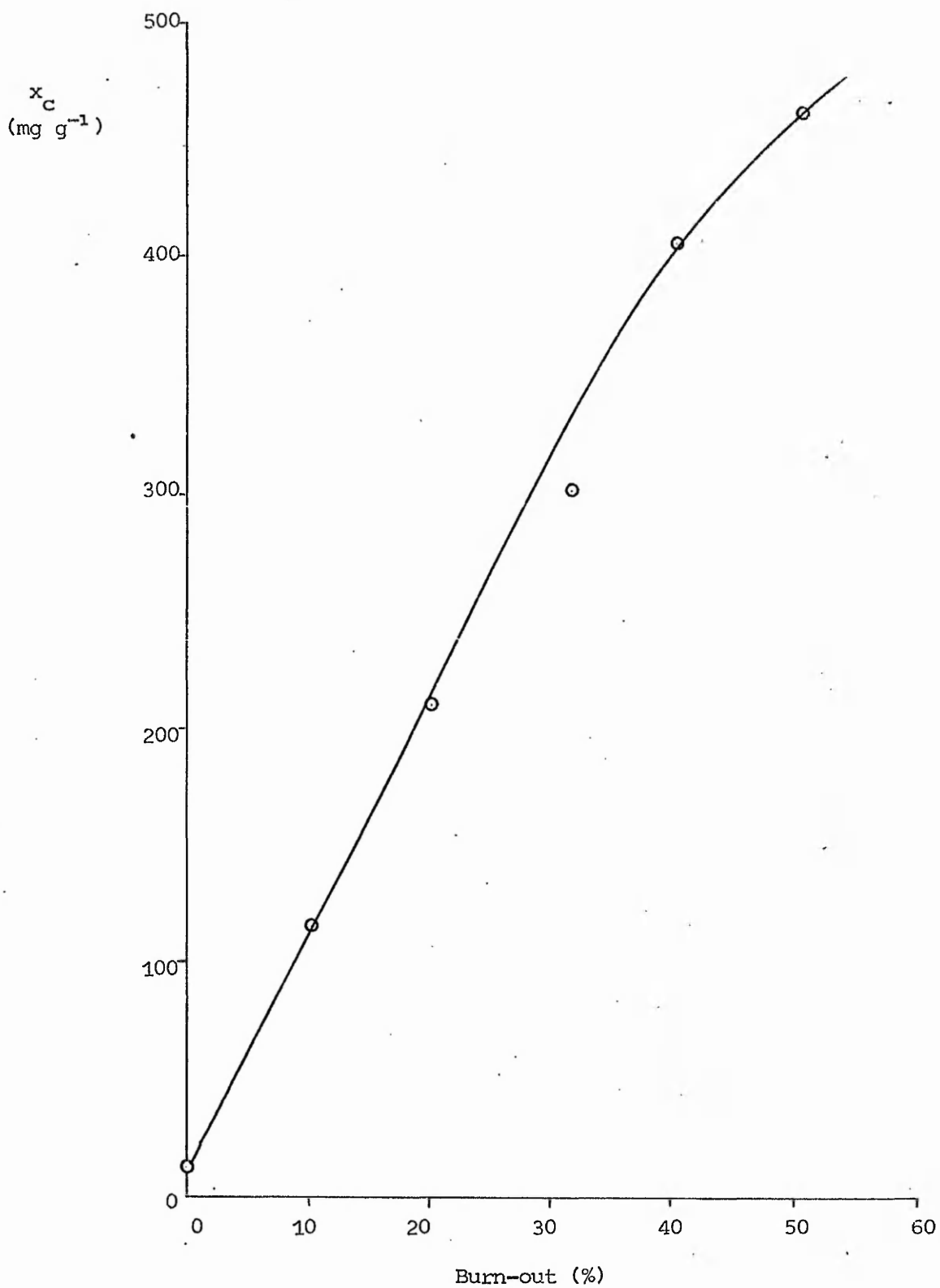


Figure 11.4(17)
Variation of x_c (mg g^{-1}) with burn-out (%) for C50/T50 carbon.

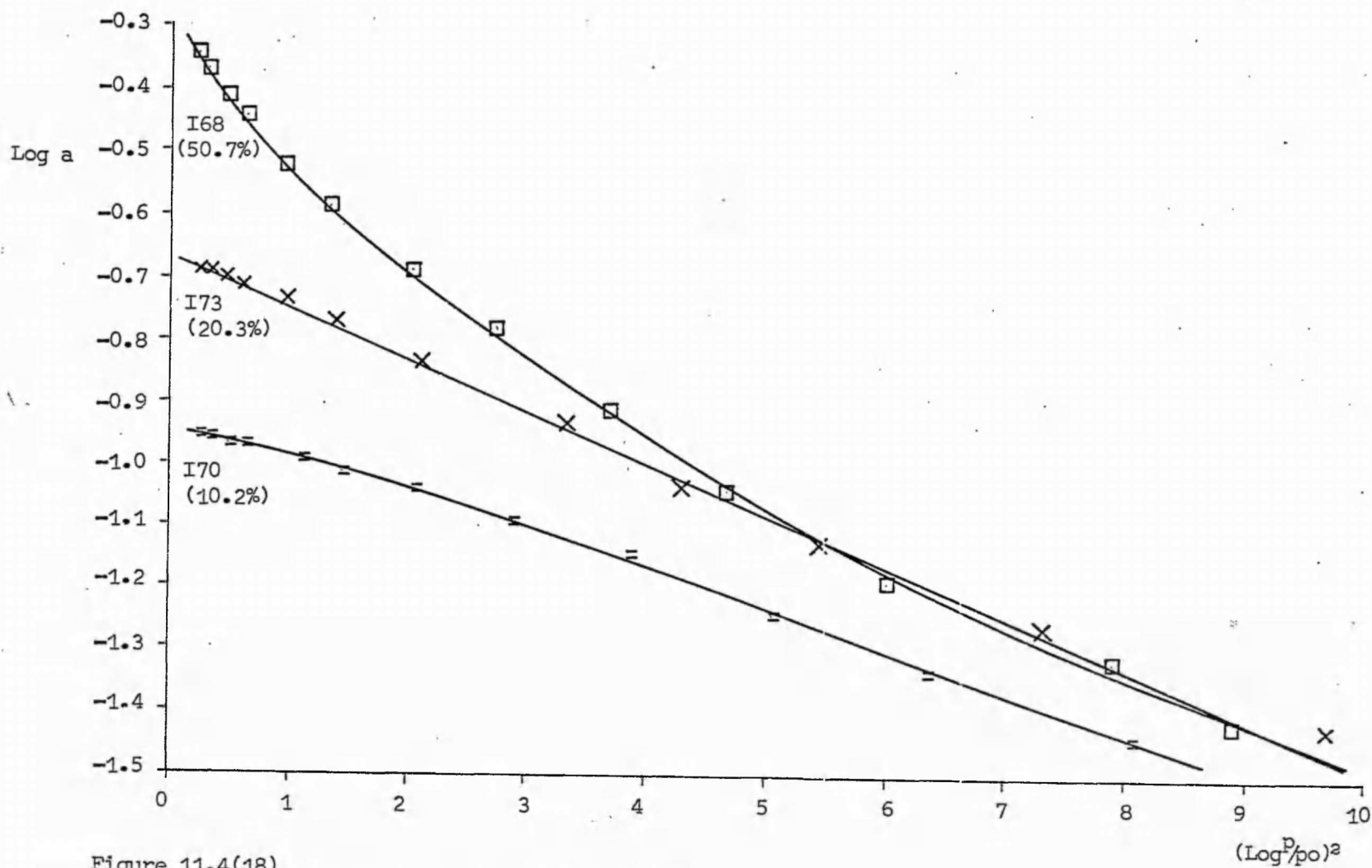


Figure 11.4(18)
Representative D-R type I plots for C50/T50 carbons.

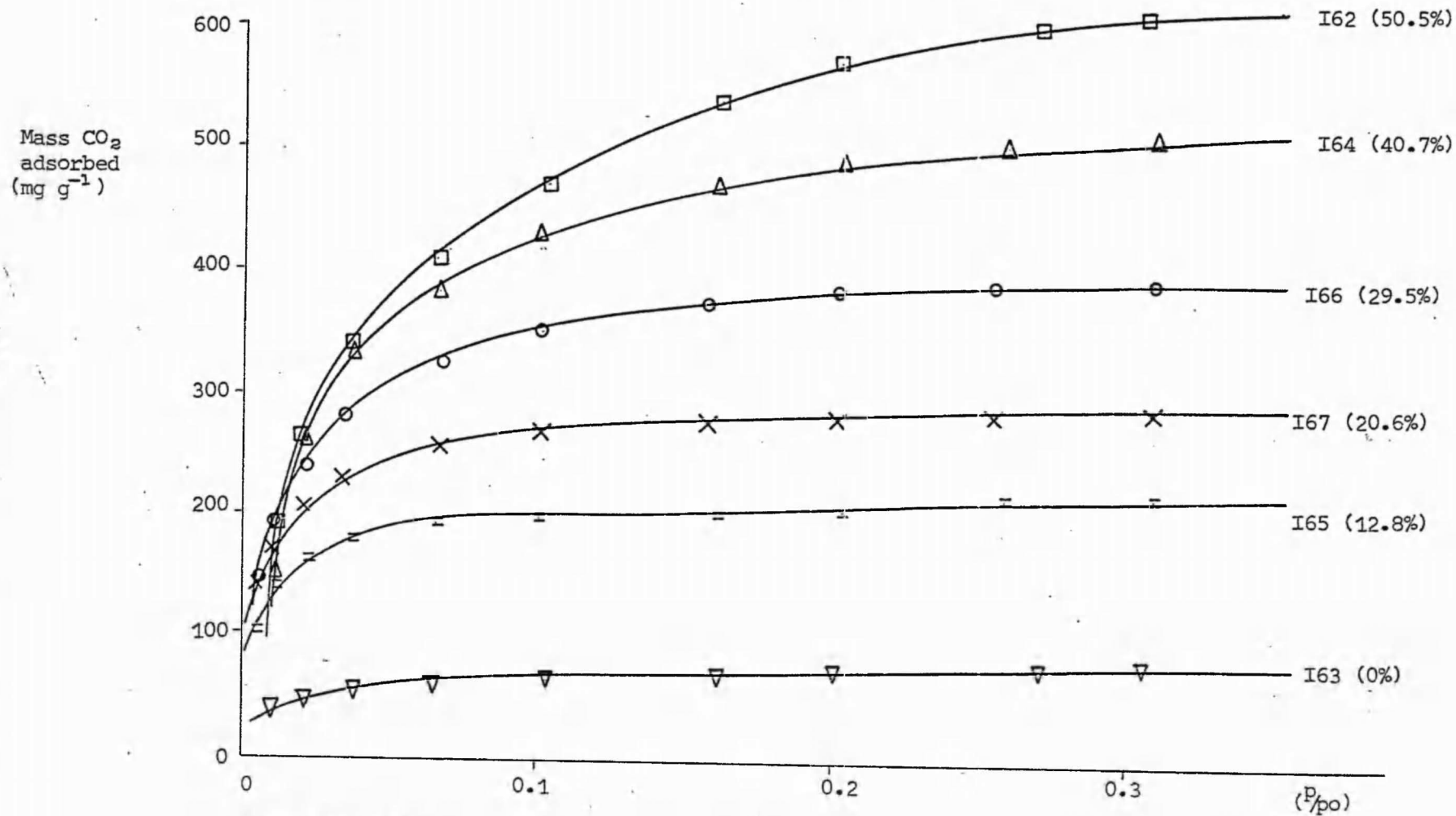


Figure 11.4(19)

Adsorption of carbon dioxide at 195K on 1313K C25/T75 carbon activated by carbon dioxide at 1303K.

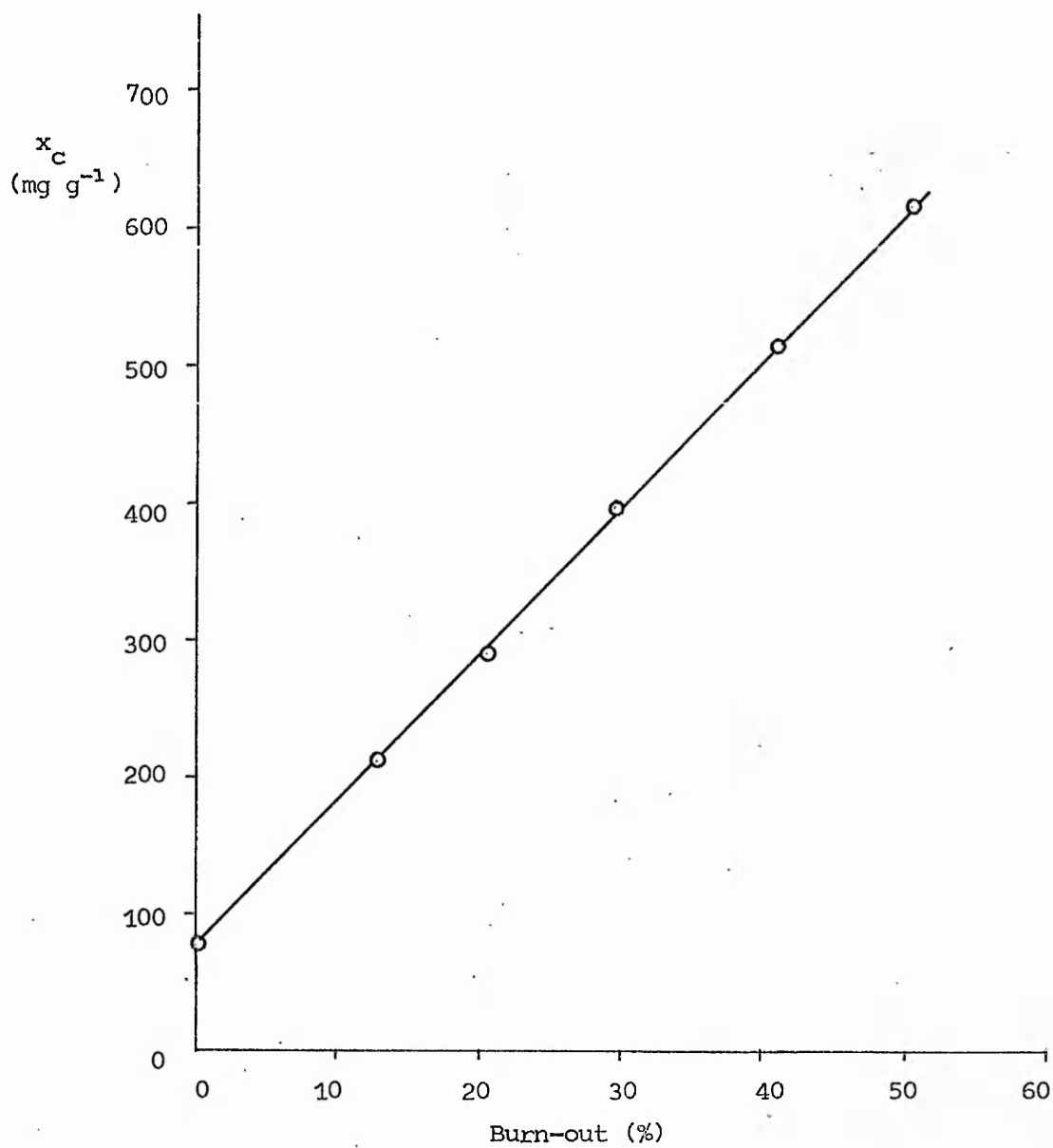


Figure 11.4(20)
Variation of x_c (mg g^{-1}) with burn-out (%) for C25/T75 carbon.

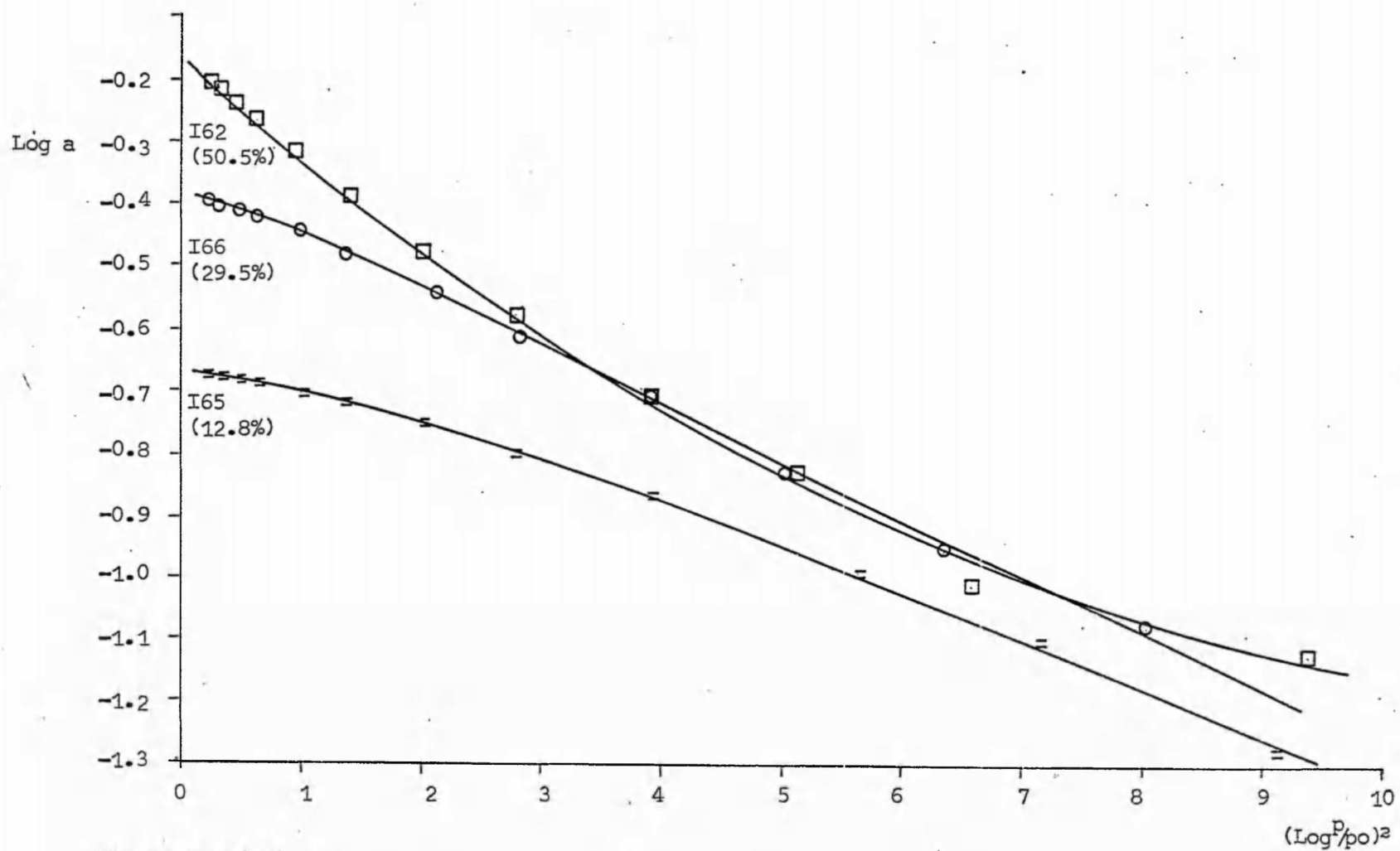


Figure 11.4(21)
Representative D-R type I plots for C25/T75 carbons.

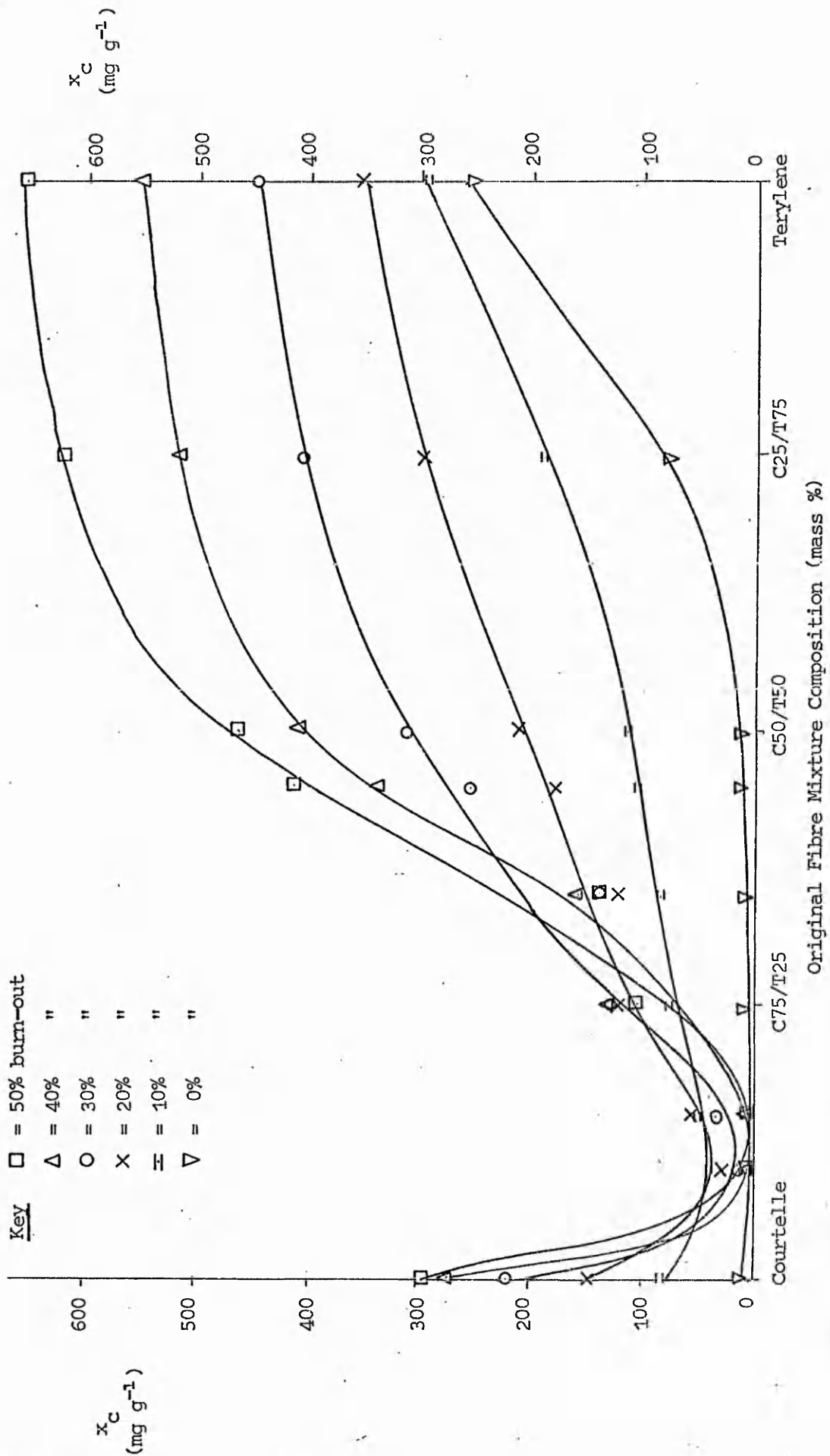


Figure 11.4(22) Variation of x_C for burn-outs in the range 0-50% over the entire composition range for Terylene/Courtelles carbons.

CHAPTER 12

Mercury Density Determination

12.1 Results and preliminary discussion

The variation of 'mercury density' with degree of activation for two carbon samples C85/T15 and C85/W15 is illustrated in figures 12.1(1) and 12.1(2) respectively.

It was decided to investigate the variation of 'mercury density' with degree of activation for these two carbons in view of the unusual behaviour observed in the x_c /burn-out diagrams and D-R type I plots for these particular samples [see figures 11.4(5), 11.4(6) and 11.3(20) and 11.3(21)].

As discussed in section 7.6 each point on the graphs illustrated in figures 12.1(1) and 12.1(2) is the arithmetic mean of two density determinations.

Once a 'mercury density' determination has been conducted on a particular sample of carbon it is contaminated with mercury. With the design of apparatus employed this contamination renders impractical any repetition of the density determination on that particular sample. Two separate 'mercury density' determinations could be performed with the quantity of carbon available, from a particular activation. The two limits included with each point in figures 12.1(1) and 12.1(2) indicate the two density values from which the mean was derived.

As described in section 7.6 the technique for the determination of carbon density by mercury displacement was developed using Sutcliffe Speakman Ltd carbon (type 203B). From four separate determinations the 'mercury density' of type 203B carbon was found to be $1.05 \pm 0.03 \text{ g cm}^{-3}$. Complete penetration by the mercury of all the accessible space in the density bottle was assumed to occur. Hence the experimental error arising from errors in weighing was estimated to be <1%. The range of 'mercury density' values observed for the type 203B carbon constituted approximately 6% of the mean density value and was therefore considered to reflect heterogeneity in the successive samples of type 203B carbon examined.

Whilst the 'mercury densities' recorded for carbon samples C85/T15 and C85/W15 are the arithmetic mean of only two separate determinations on different portions of the same sample, the observed differences in 'mercury densities' for these two determinations are

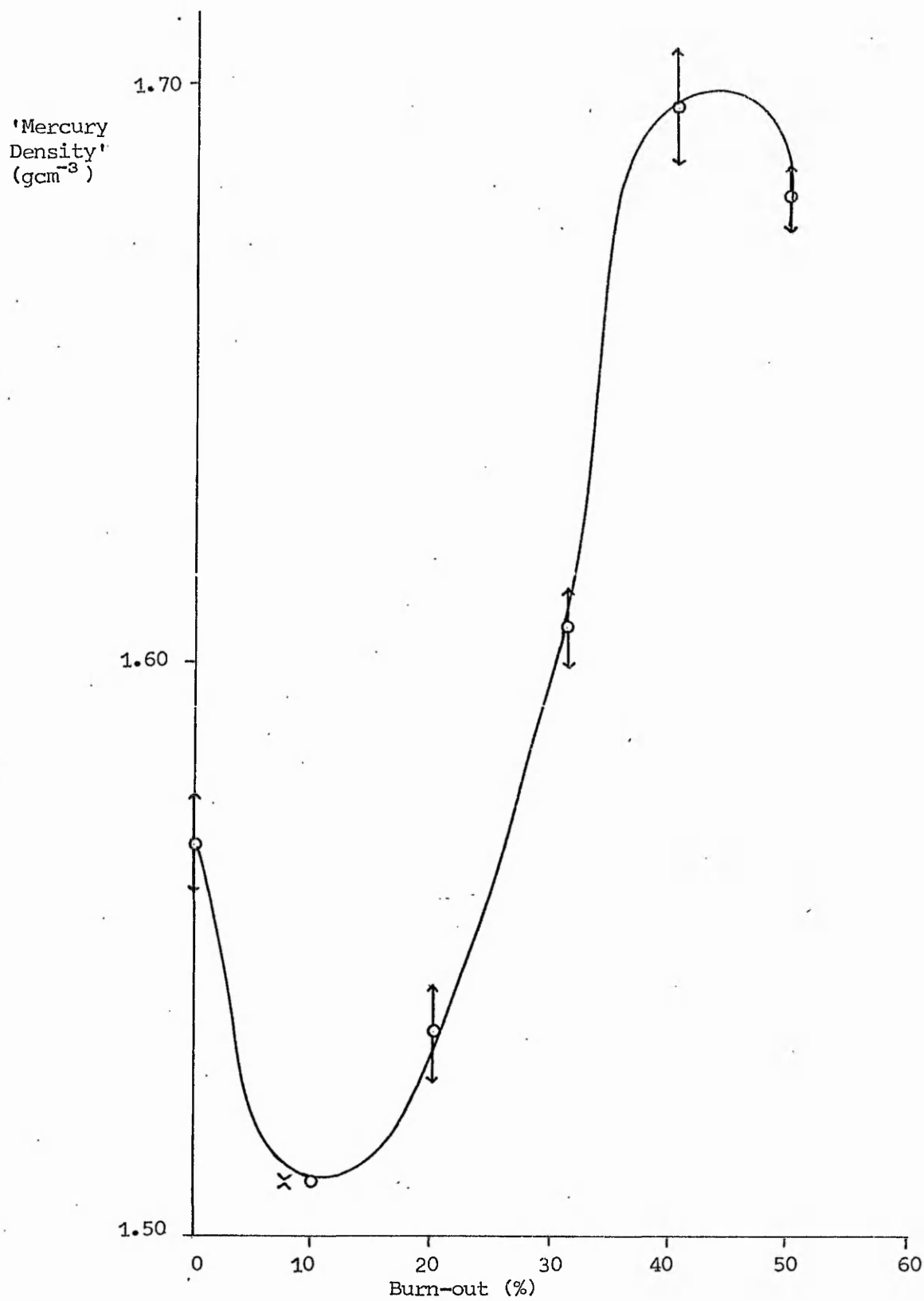


Figure 12.1(1)
Variation of 'Mercury density' (g cm⁻³) with burn-out (%) for C85/T15 carbon.

'Mercury
Density'
(g cm⁻³)

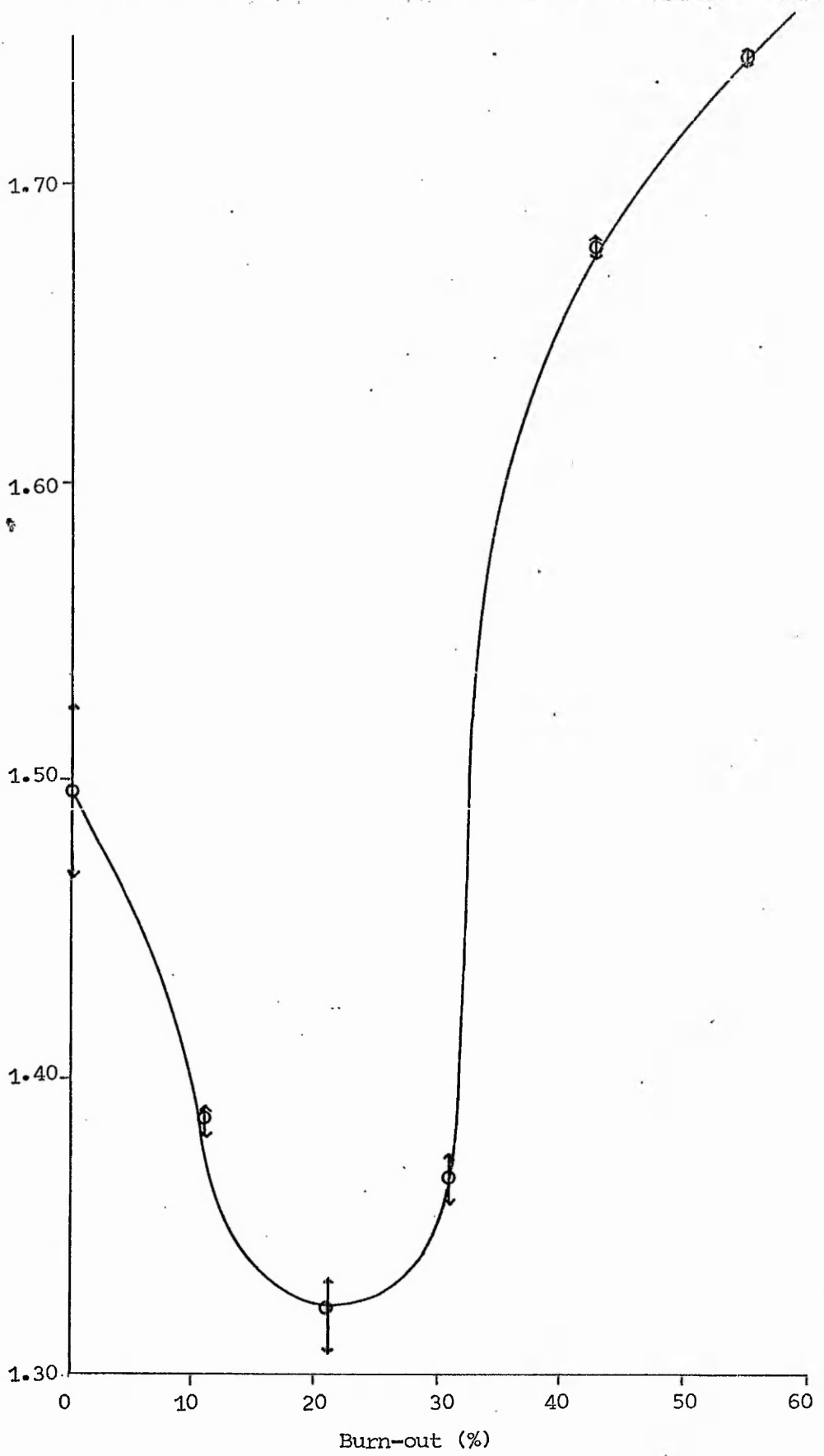


Figure 12.1(2)
Variation of 'Mercury density' (g cm⁻³) with burn-out (%) for C85/W15 carbon.

also believed to reflect sample heterogeneity rather than the effects of experimental errors associated with weighing.

A number of different factors affect the variation of mercury density with degree of activation, these factors will be discussed in the following paragraphs. Two features illustrated in figure 12.1(1) and 12.1(2) are of particular interest. First an initial decrease in 'mercury density' was observed followed by a significant increase with increasing degree of activation for carbons derived from both C85/T15 and C85/W15. Second for C85/T15 the mercury density of the unactivated carbon was significantly greater than either of the 'mercury densities' determined for the unactivated carbons derived from the single polymers Courtelle and Terylene [see table 12.1(1)]. With the design of the density apparatus employed it was not possible to determine a mercury density for the carbon derived from wool.

If impurities are assumed absent from the carbon then carbon loss during gasification from the particle exterior alone would result in a constant 'mercury density'. Carbon loss solely from the interior of the particles would however result in a decrease in the measured 'mercury density' assuming no collapse of the particle structure. The mode of the actual gasification reaction will thus affect the variation of 'mercury density' with degree of activation.

From the preceding argument it is clear that the initial decrease in 'mercury density' illustrated in figures 12.1(1) and 12.1(2) may be explained in terms of significant internal mass loss resulting from gasification. This conclusion is also valid in the case of an impure carbon as will be demonstrated in the following paragraphs.

It is now relevant to consider the possible effects of inorganic impurities present in the carbon samples C85/T15 and C85/W15 on the observed variation in 'mercury density' with degree of activation illustrated in figures 12.1(1) and 12.1(2).

The total inorganic impurity in each of the carbons derived from single polymers was estimated from measurements of ash content after gasification in an air atmosphere at 1206K. The ash contents of each carbon expressed as a percentage by mass of the 0% burn-out carbon are recorded in table 12.1(2).

Table 12.1(1)

'Mercury densities' of 0% burn-out carbons derived from Terylene and Courtelle.

Carbon	mercury density
Terylene	$1.40 \pm 0.01 \text{ gcm}^{-3}$
Courtelle	$1.47 \pm 0.05 \text{ gcm}^{-3}$

Table 12.1(2)

Ash content (mass %) of 0% burn-out single polymer carbons

Polymer carbon	wool	Terylene	Courtelle
Ash content (mass %)	3.2	5.1	2.7

It is assumed in the following argument that the 'mercury density' of the inorganic impurities is unaffected by gasification. Hence if inorganic impurities are present and their density as measured by mercury displacement differs from that of the carbon matrix then the 'mercury density' variation during gasification would be somewhat different from the cases considered so far where impurities are absent. The 'mercury density' of the inorganic impurity is likely to be greater than that of the carbon matrix and is therefore assumed so in the following example. In the case of carbon loss during gasification occurring solely from the particle exterior an increase in the 'mercury density' of this impure carbon would be expected through a decrease in the carbon/impurity mass ratio. Where impure carbon suffers carbon loss solely from the particle interior during gasification the situation is somewhat more complex. In general however a decrease in 'mercury density' will occur if it is assumed that there is no collapse of the particle structure.

The increase in 'mercury density' illustrated in figures 12.1(1) and 12.1(2) may therefore be explained through accumulation of impurity of higher 'mercury density' than the carbon matrix when gasification results in a high degree of external mass loss. It is also the case however that internal mass loss during gasification followed by collapse of the particle structure can also account for an increase in the 'mercury density' with increasing degree of activation.

As previously mentioned the 'mercury density' of the unactivated C85/T15 carbon is significantly greater than either of the 'mercury densities' determined for the unactivated carbons derived from the single polymers Courtelle and Terylene.

As reported in section 9.3 it was observed using Hot-Stage Microscopy that fused Terylene coated Courtelle fibres during the pyrolysis of Terylene/Courtelle mixtures. It was postulated that this coating retained Courtelle degradation products resulting in their incorporation in Courtelle pyrolysis residue. It thus follows that in C85/T15 carbon the carbon derived from Courtelle may possess an intrinsically higher 'mercury density' than that of the surrounding carbon derived from Terylene or carbon derived solely from Courtelle.

If increasing activation effects preferential removal of the coating carbon derived from Terylene (i.e. selective gasification takes place) then the 'mercury density' of the carbon derived from the polymer mixture C85/T15 might be expected to increase with increasing degree of activation, perhaps in the manner illustrated in figure 12.1(1).

The variation of 'mercury density' with increasing activation is thus a complex function of various factors. These factors include the impurity content, selective gasification where the carbon matrix contains regions of varying 'mercury density' and the mode of the actual gasification reaction i.e. extent of internal relative to external mass loss.

The complexity of the problem may be illustrated by the application to the data illustrated in figures 12.1(1) and 12.1(2) of Kipling's¹³⁷ method for calculating the mass of material lost from the exterior of carbon particles during gasification.

Using equation 12.1(1) Kipling¹³⁷ calculated the volume of carbon lost from the exterior of the particles during gasification to x% burn-out.

$$\frac{1}{\rho_{\text{Hg}}} - \frac{100 - x}{100(\rho_{\text{Hg}}^x)} = V \text{ ext.} \quad \text{Equation 12.1(1)}$$

where ρ_{Hg} = density of carbon prior to gasification as measured by mercury displacement (g cm^{-3})

x = degree of burn-out (mass %)

ρ_{Hg}^x = density of carbon after gasification to x% burn-out as measured by mercury displacement (g cm^{-3}).

The mass of carbon lost from the exterior of the particles was therefore $V \text{ ext.} \rho_{\text{Hg}}$ (g g^{-1} unactivated carbon). In this way Kipling¹³⁷ was able to determine the external mass loss during gasification and hence the ratio of internal to external mass loss.

Using this method Kipling¹³⁷ calculated that mass loss from phenol-formaldehyde carbon during gasification was almost totally from the particle exterior. Kipling¹³⁷ thus claimed that the absence of a substantial pore structure in unactivated phenol-formaldehyde carbon militated against the development of further pores and therefore

presumably interior mass loss during gasification. Kipling¹³⁷ considered that the work described above confirmed and extended the conclusions of Lamond and Marsh¹²⁸ that the extent of pore development during gasification depends on the basic structure of the original carbon. Kipling investigated the relationship between external mass loss (g g^{-1} unactivated carbon) and degree of gasification measured as percentage burn-out for a range of carbons. It was generally observed in the ranges of burn-out investigated that mass loss from the particle exterior was a linear function of percentage burn-out. However in the cases of carbon derived from coconut shell, cellulose and polyvinylidene chloride the observed ratios of internal to external attack during gasification did not correspond to the extent of pore structure present in the unactivated carbon as might have been expected from consideration of the work of Lamond and Marsh.¹²⁸

Using Kipling's approach,¹³⁷ embodying equation 12.1(1) plots of external mass loss (g g^{-1} unactivated carbon) against burn-out (mass %) are presented in figures 12.1(3) and 12.1(4) for carbon derived from fibre mixtures C85/T15 and C85/W15 respectively. In both these plots the broken line represents mass loss during gasification calculated as if it occurred solely from the particle exterior.

At burn-outs below 25% for C85/T15 [figure 12.1(3)] and 36% for C85/W15 [figure 12.1(4)] considerable mass loss was observed apparently from the particle exterior. However above these respective burn-outs in both cases the curves deviate above the line which represents mass loss from the exterior alone. This behaviour observed as a result of the application of equation 12.1(1) lacks reality purely from a physical stand point.

The apparent failure of Kipling's equation in these latter examples may arise from the assumptions implicit in its use. Thus one major assumption is the neglect of any effects arising from the presence of impurities in the carbon. It is further assumed that the carbon matrix is homogeneous (i.e. no 'mercury density' variations exist within the matrix) and hence selective gasification effects are absent.

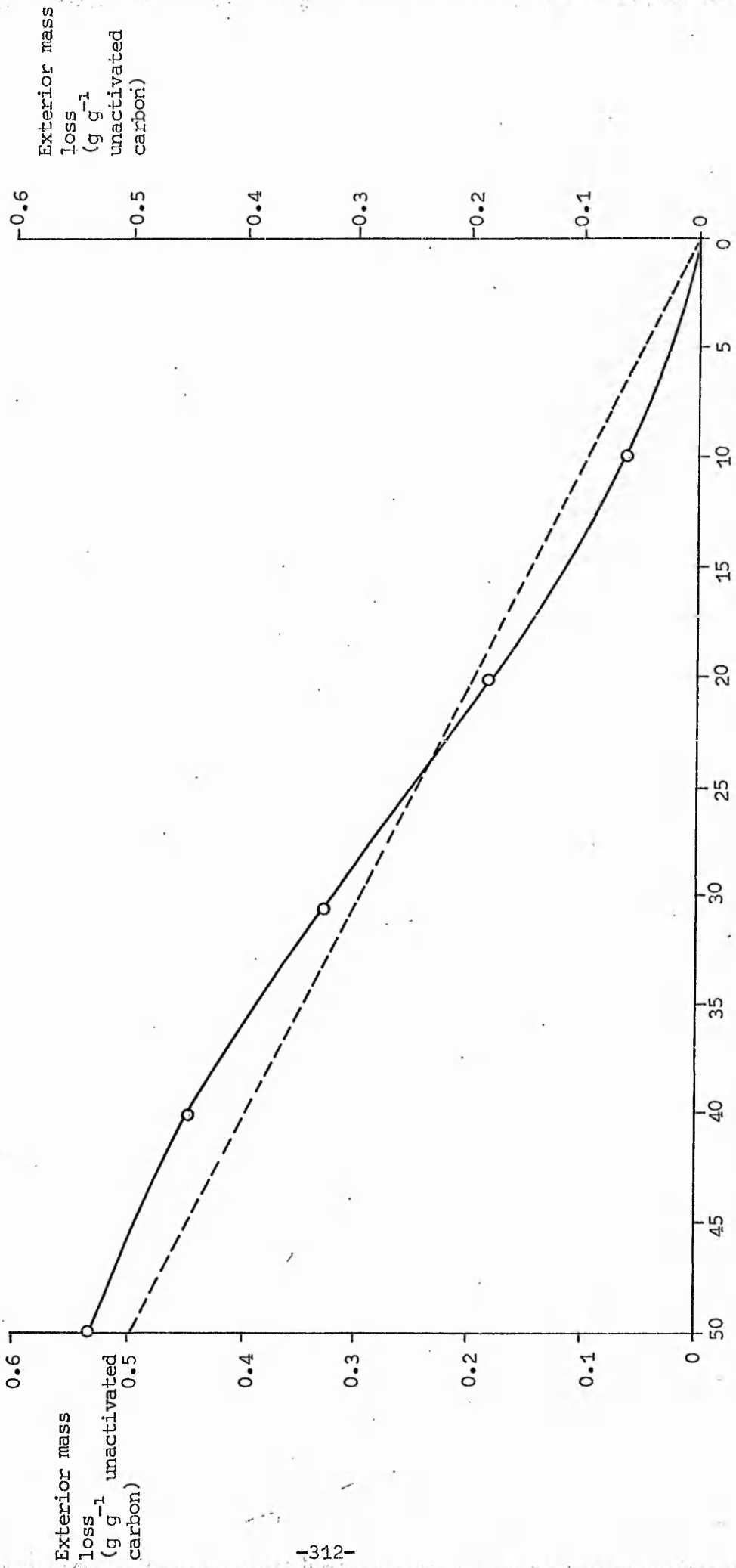


Figure 12.1(3)
Variation of exterior mass loss (g g⁻¹ unactivated carbon) with burn-out (%) for C85/T15 carbon.

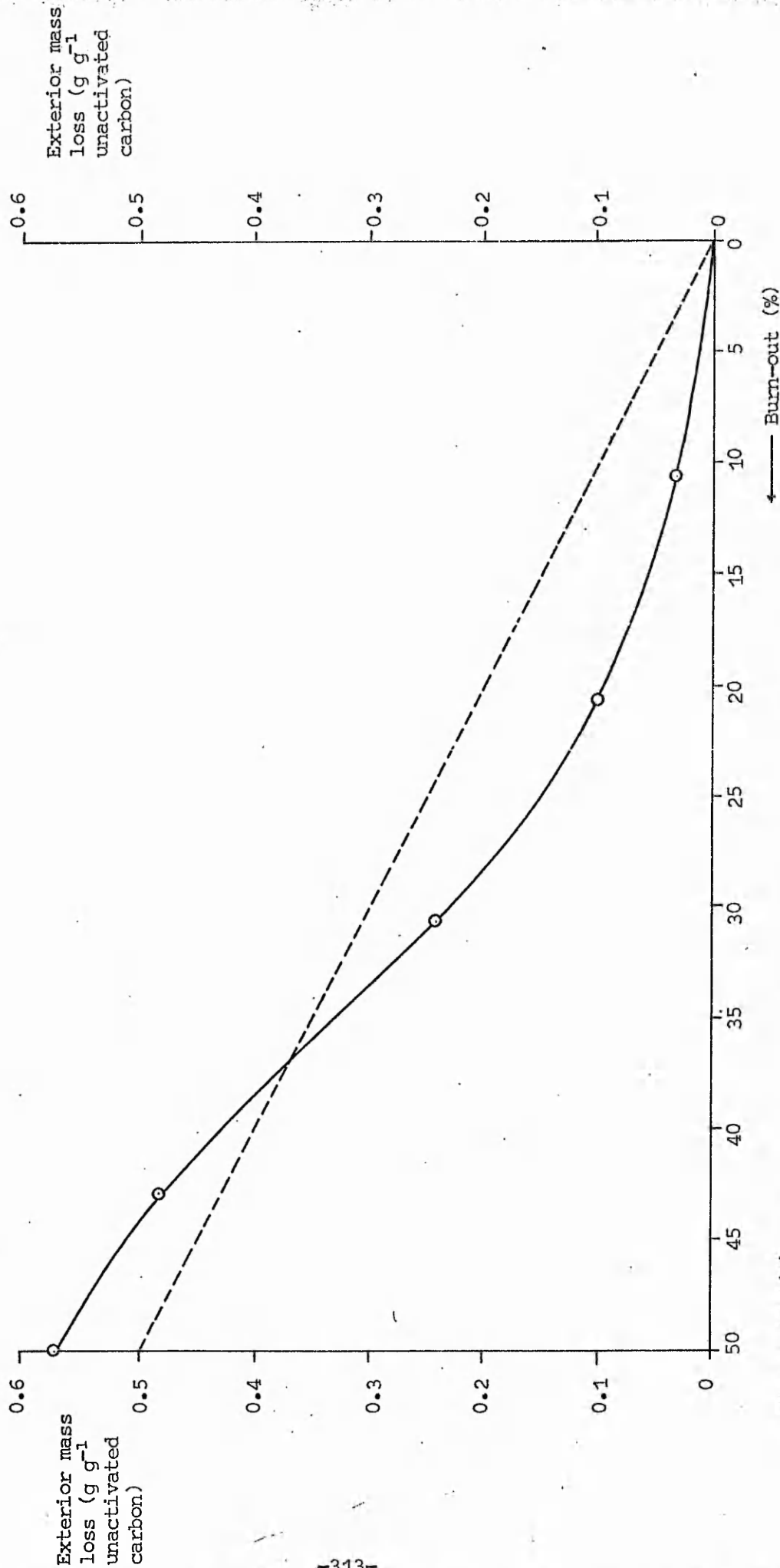


Figure 12.1(4)
 Variation of exterior mass loss (g g⁻¹ unactivated carbon) with burn-out (%) for C85/W15 carbon.

It would thus appear that Kipling's equation may be correctly applied to carbons prepared from single high purity organic compounds.

However the application of equation 12.1(1) to impure carbons or those prepared from binary mixtures of organic compounds appears basically unsound. Further any interpretations based on the magnitude of 'mercury densities' or their variation with gasification must include some consideration of impurity effects and effects associated with heterogeneity of the carbon matrix before any reliance can be placed on resulting conclusions.

Final Discussion of Results and Conclusions13.1 Pyrolysis Study

The most significant information arising from the pyrolysis study concerns the thermal stability of Terylene when it is pyrolysed in the presence of a second polymer.

In the D.T.A. curve of Terylene an endotherm was observed at 710K (702-712K). The T.G. data for Terylene indicated that significant mass loss was associated with this endotherm which has been attributed to the occurrence of main-chain breakdown^{51,52}.

The T.G. data for both wool/Terylene and Terylene/Courtelle systems indicated that significant mass losses, apparently associated with main-chain breakdown reactions in the Terylene component, occurred at temperatures lower than that observed for main-chain breakdown in the pyrolysis of Terylene alone.

Further the corresponding endotherm at 710K (702-712K) in the D.T.A. curve of Terylene was observed at lower temperatures in the D.T.A. curves obtained for both the wool/Terylene and Terylene/Courtelle systems [see figures 13.1(1), 13.1(2)]. From figure 13.1(1) it is clear that the peak displacement observed for the wool/Terylene system may be regarded as significant. However as explained in section 9.3 the peak displacement illustrated for the Terylene/Courtelle system in figure 13.1(2) cannot be regarded as significant.

As illustrated in figures 13.1(3) and 13.1(4) significant displacement to lower temperatures of the Terylene exotherm 745K (741-746K) was also observed in the D.T.A. data of both the wool/Terylene and Terylene/Courtelle systems. As discussed in section 8.3 this exotherm is believed to reflect the process leading to the formation of a highly cross-linked PET residue.

From a consideration of figures 13.1(1)-13.1(4) it is clear that where significant peak displacement is observed, the amount of displacement is a linear function of composition of the polymer mixture. Further the displacement observed for the Terylene exotherm [745K (741-746K)] at a given Terylene content of the original fibre mixture is different for the two systems wool/Terylene and Terylene/Courtelle.

It would thus appear that the processes of main-chain breakdown and cross-linking occurring during the pyrolysis of Terylene, took place at lower temperatures when pyrolysis was conducted in the presence of either wool or Courtelle.

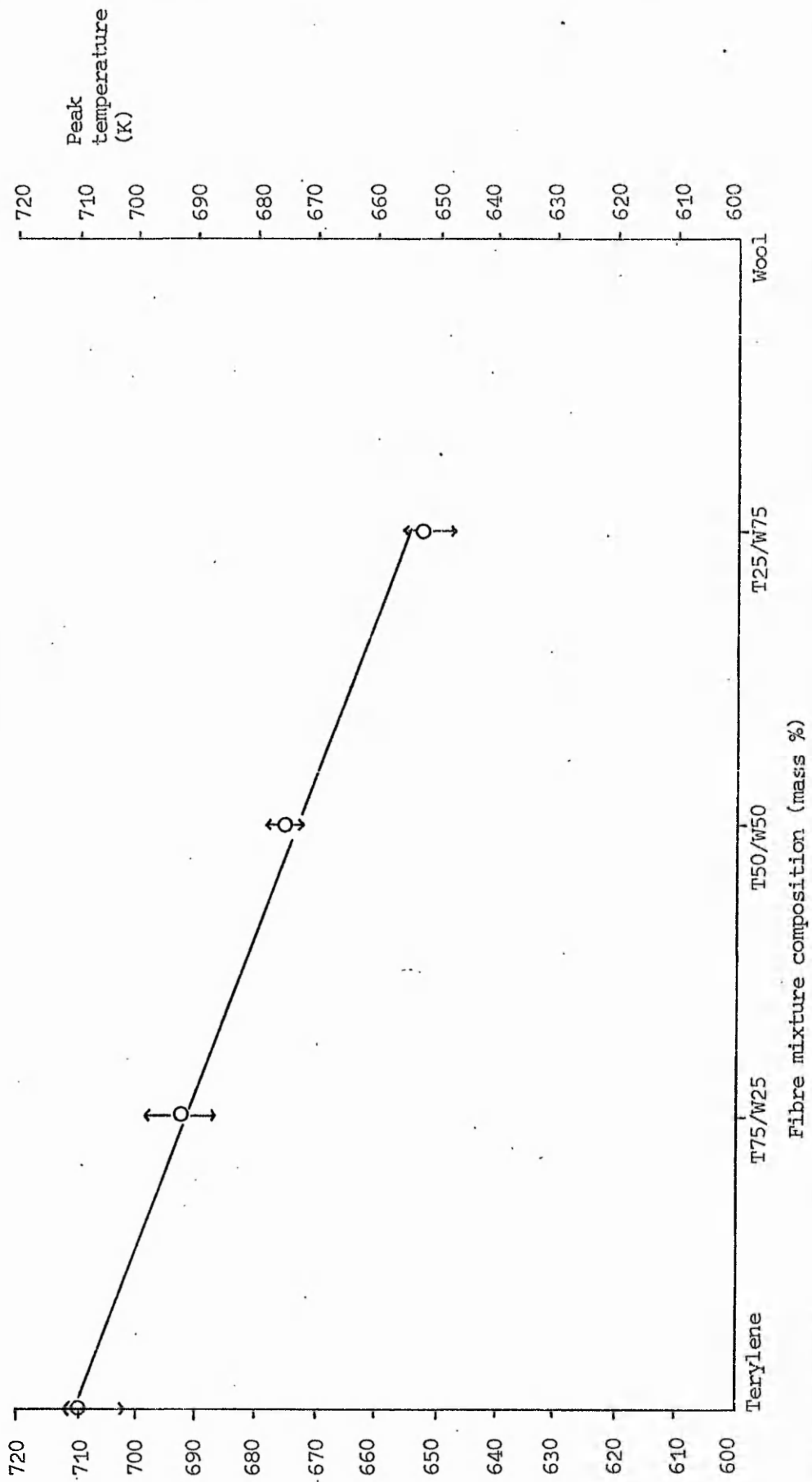


Figure 13.1(1)
 Position of the Terylene endotherm [710K (702-712K)] in the D.T.A. curves of wool/Terylene mixtures.

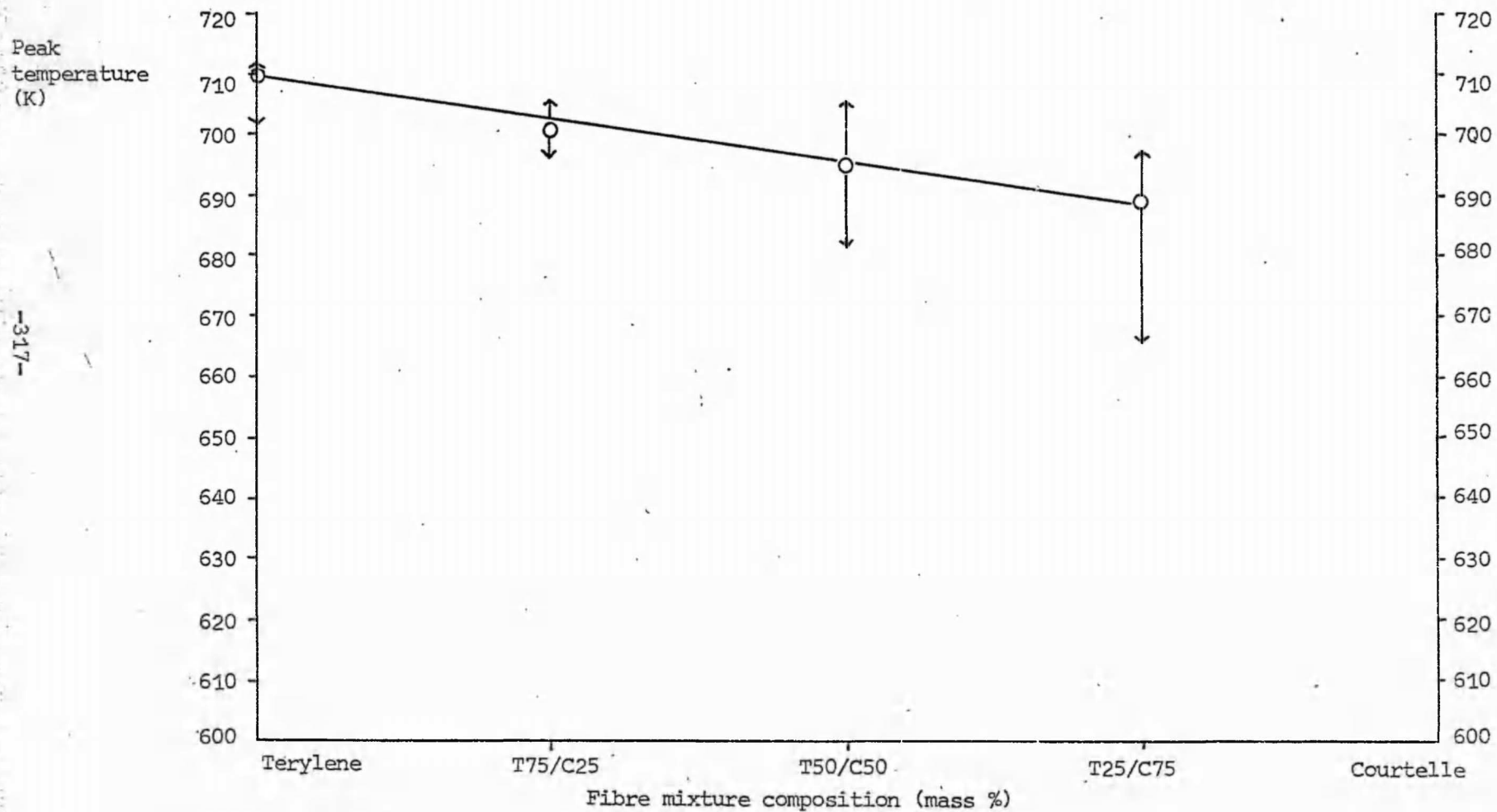


Figure 13.1(2)

Position of the Terylene endotherm [710K (702-712K)] in the D.T.A. curves of Terylene/Courtelle mixtures.

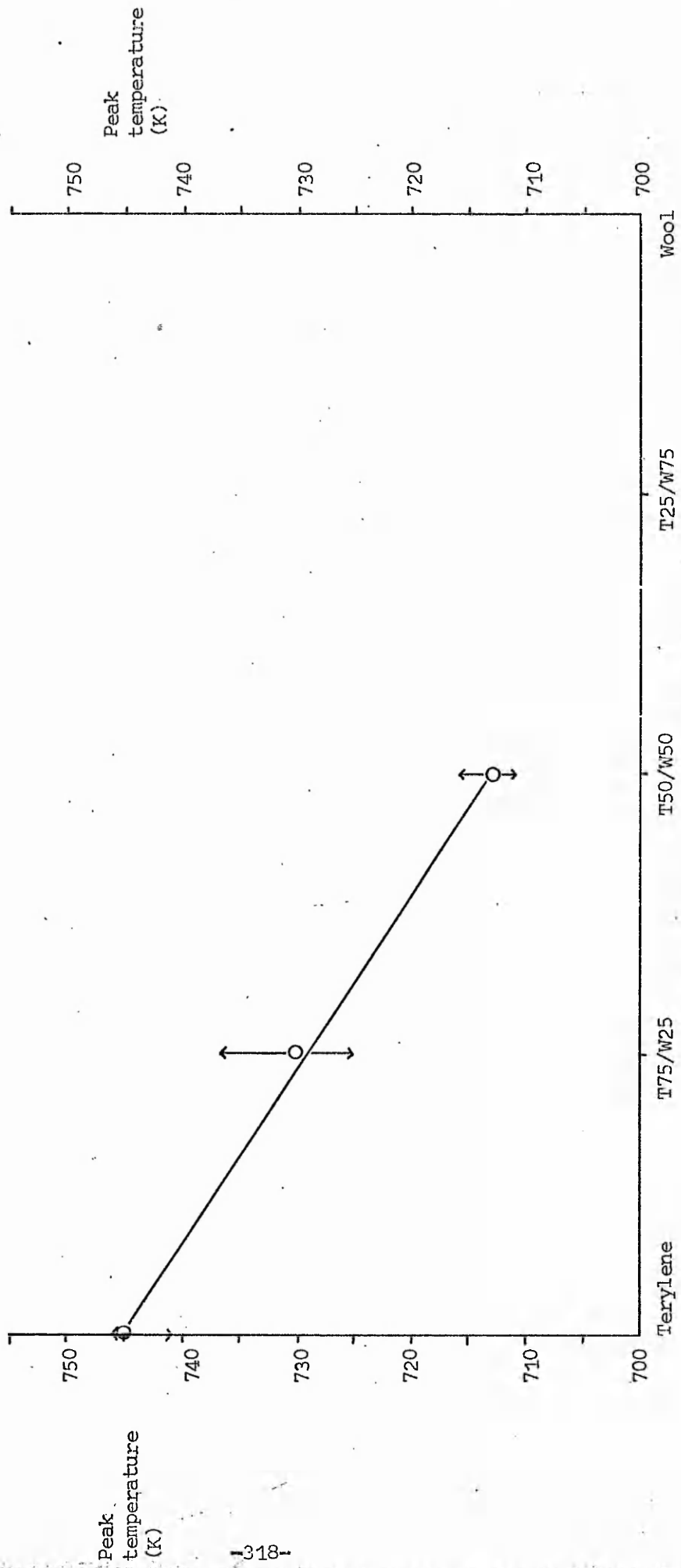


Figure 13.1(3)
 Position of the Terylene exotherm [745K (741-746K)] in the D.T.A. curves of wool/Terylene mixtures.

Peak
temperature
(K)

-319-

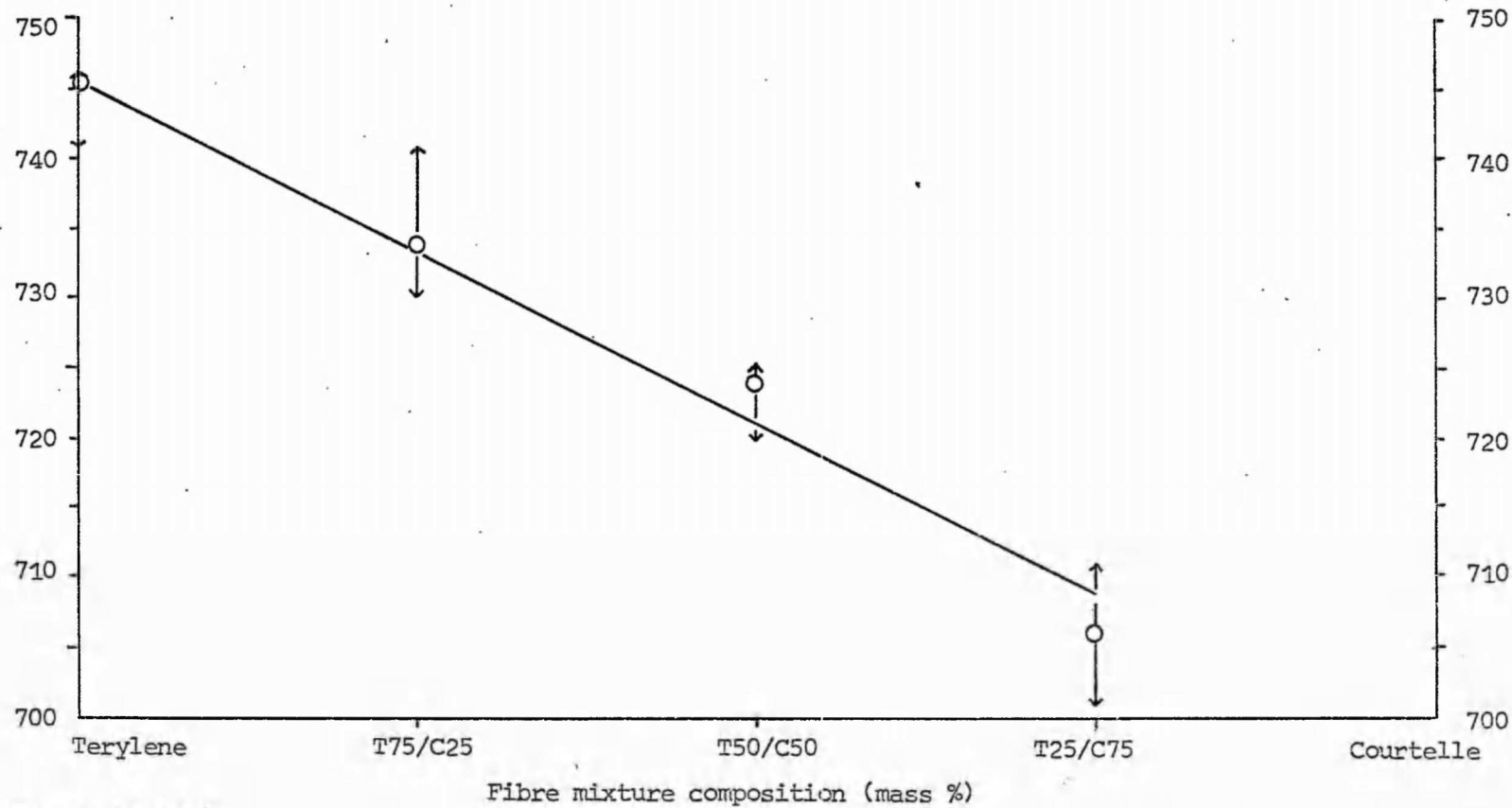


Figure 13.1(4)

Position of the Terylene exotherm [745K (741-746K)] in the D.T.A. curves of Terylene/Courtelle mixtures.

Physical interactions in the form of heat transfer effects cannot be invoked to explain the peak displacements illustrated in figures 13.1(1) - 13.1(4) since the maximum observed differential temperatures are an order of magnitude less than the peak displacements observed (see section 5.2).

The D.T.A. data for kieselguhr/Terylene mixtures is presented in table 9.1(4). In these mixtures kieselguhr is considered to act as a chemically and thermally inert support material. The only significant peak displacement was that observed for the Terylene exotherm [745K (741-746K)] between Terylene and the mixture K25/T75. Whilst the degree of this displacement is of the same order of magnitude as that observed between the corresponding members of the wool/Terylene and Terylene/Courtelle systems, there was no increase in the degree of displacement in the D.T.A. curves of mixtures of higher kieselguhr constant [c.f. figures 13.1(3) and 13.1(4)]. It is therefore considered that an inert support effect alone cannot account for the observed decrease in the temperature of the Terylene pyrolysis processes.

Therefore, whilst no direct evidence is available it would seem reasonable to argue that chemical interactions are responsible for this observed decrease in the thermal stability of Terylene.

The D.T.A. and T.G. data for both wool/Terylene and Terylene/Courtelle mixtures have indicated that significant degradation of the second polymer (e.g. wool and Courtelle respectively) occurred prior to the Terylene degradation reactions. It is therefore postulated that the thermal stability of Terylene is reduced through chemical interaction with the degradation products arising from the second polymer present.

The differences in the degree of peak displacements observed for the Terylene endotherm [710K (702-712K)] and exotherm [745K (741-746K)] in wool/Terylene and Terylene/Courtelle mixtures [see figures 13.1(1) - 13.1(4)] may reflect interactions with the different degradation products arising from the respective second polymers present in these two systems.

These observed peak displacements may however be due to chemical interaction with a degradation product common to both wool and Courtelle. Hence the differences in degree observed for these displacements may be ascribed to differences in the relative abundance

of this common product or differences in the temperature at which such a product was formed.

As discussed in sections 3.2 and 4.2 the degradation products arising from the pyrolyses (in inert atmospheres) of wool and Courtelle respectively have been determined by other workers^{131,57}. Degradation products common to both pyrolyses include ammonia, hydrogen cyanide and methane.

It has been previously reported that the thermal stability of PET was reduced in the presence of amines.¹⁴⁰ It may be possible that ammonia, a product common to both the pyrolysis of wool and Courtelle, can reduce the thermal stability of PET through a mechanism related to that of attack by amines.

Turner and Johnson⁵⁷ initially detected ammonia from the pyrolysis of Courtelle at 498K, the maximum rate of evolution being observed at 553K. Ammonia evolution during wool pyrolysis was detected initially at 473K by Goodall.¹³¹ The quantity of ammonia evolved increased to a maximum at a temperature of 873K. In both these studies ammonia was detected in relatively large quantities.

The results reported by these workers^{57, 131} suggest that in the current work ammonia evolution from the decomposition of wool in wool/Terylene mixtures and Courtelle in Terylene/Courtelle mixtures commenced prior to Terylene fusion (530K) and continued to temperatures above those at which the main Terylene degradation reactions occurred. Whilst no firm experimental evidence can be offered to support the postulate that ammonia reduced the thermal stability of Terylene, the characteristics of ammonia evolution from both wool and Courtelle are consistent with this postulate.

Two other significant peak displacements have been observed. These displacements involve the Courtelle exotherm 568K (568-570K) in wool/Courtelle mixtures and the wool endotherm 505K (505-507K) in wool/Terylene mixtures.

The Courtelle exotherm 568K (568-570K) followed the wool endotherm 505K (505-507K) in the D.T.A. curve of wool/Courtelle mixtures and was displaced to lower temperature [see table 9.2(1)] between Courtelle and the polymer mixture W25/C75. This displacement cannot be attributed to heat transfer and may have been due to the

initiation of the reaction leading to the formation of ladder polymer structure at somewhat lower temperatures by wool degradation products.

The displacement of the wool endotherm at 505K (505-507K) to higher temperatures between wool and W75/T25 in the wool/Terylene system may be related to the occurrence of the Terylene endotherm at 530K (529-531K). It is observed that this wool endotherm lies approximately within the temperature range of the Terylene endotherm at 530K (529-531K). Hence the fact that both polymers are absorbing heat may serve to delay the occurrence of the wool endotherm.

The second major observation from the pyrolysis study concerns the T.G. behaviour and large scale pyrolysis yields of the wool/Courtelle and Terylene/Courtelle systems. For the majority of wool/Courtelle mixtures and for all the Terylene/Courtelle mixtures significantly higher than predicted yields i.e. excessive yields were observed at 1213K from large scale pyrolysis, (see figures 9.2(5) and 9.3(5) respectively). Further the T.G. data for both systems suggested that initial mass loss from the Courtelle component was reduced [see figures 9.2(2), 9.2(3), 9.2(4) and 9.3(2), 9.3(3), 9.3(4)].

As previously discussed both the wool/Courtelle and Terylene/Courtelle systems are comprised of a fusing and a non-fusing polymer.

Hot-Stage Microscope photographs of Terylene/Courtelle mixtures indicate that following fusion at 530K the molten Terylene coats the Courtelle fibres [see plates 9.3(2), 9.3(3)].

Wool fusion was observed to occur at approximately 583K [see plates 8.2(3) and 8.2(4)]. In wool/Courtelle mixtures wool fusion was observed to occur although to a more limited extent [see plate 9.2(3)]. Once fused, the wool did not however appear to flow as extensively as fused Terylene.

It is considered that the excessive yields obtained from large scale pyrolyses and the apparent reduction in the loss of mass from Courtelle in wool/Courtelle and Terylene/Courtelle systems may be explained in terms of the coating of the non-fusing polymer by the fusing polymer during pyrolysis. It is postulated that this coating of fused polymer is effective in reducing mass loss from the non-fusing

polymer (Courtelle) by preventing the escape of volatile degradation products.

This postulate may be illustrated with reference to the Terylene/Courtelle system. Since Terylene fusion occurred at 530K it is reasonable to suppose that a coating of this fused Terylene had formed around the individual Courtelle fibres prior to the initiation of Courtelle mass loss at 543K. If this coating of fused Terylene was effective in trapping volatile Courtelle degradation products then the initial Courtelle mass loss would be reduced. Further the incorporation of these degradation products in the Courtelle pyrolysis residue might be expected to lead to an increase in the residual yield observed at 1213K from such a polymer mixture.

Whilst excessive residual yields from large scale pyrolyses and a reduction in the initial Courtelle mass loss were observed for both Terylene/Courtelle and wool/Courtelle systems the effects were less marked for the wool/Courtelle mixtures. This observation may be related to the fact that a Courtelle mass loss of approximately 12% has occurred prior to wool fusion at 583K. In addition a major wool degradative reaction occurs shortly after fusion at 583K, and is reflected by the endotherm in the D.T.A. curve of wool at 596K (582-616K). This degradation reaction may reduce the effectiveness of the fused wool coating in retaining volatile Courtelle degradation products. In contrast no degradation reactions were observed in the D.T.A. curve for Terylene following fusion at 530K until the exotherm with reported peak temperatures of 653K⁴⁹ and 662K.⁵¹

A final comment concerns the relationship between the observed reduction in the thermal stability of Terylene when pyrolysed in the presence of a second fibre and the excessive residual yields observed for the mixture Terylene/Courtelle. As previously discussed the decreased thermal stability of Terylene is attributed to chemical interactions and the excessive residual yields to product retention within a fused polymer coating.

However the effect of the decreased thermal stability of Terylene on the magnitude of the residual yield at 1213K cannot be accurately assessed. If the decomposition of Terylene at lower temperatures leads to a reduction in the amount of carbon derived from Terylene in

the residue at 1213K then the magnitude of yield increases observed at 1213K and attributed to product retention may be greater than those actually observed.

13.2 Adsorption study

(a) Single polymer carbons

It is relevant to consider first the pyrolysis behaviour of the three polymers employed in this study.

Previous workers^{10,11} have demonstrated that carbons prepared from Terylene and Courttelle to a final heat treatment temperature of 1213K were non-graphitising.

Franklin⁴ postulated that for crystallite growth and graphitisation to occur the system of cross-linking which unites the crystallites must not be too strong and that neighbouring crystallites should lie in near parallel orientation. In view of the accepted chemical and structural heterogeneity of wool it is considered that this latter condition is not fulfilled to any great extent in the carbon derived from wool. Wool carbon prepared at a final heat treatment temperature of 1213K is therefore also considered to be non-graphitising.

Franklin⁴ observed by X-ray diffraction techniques that non-graphitising carbons exhibited considerable fine structure porosity.

The adsorption data for the unactivated single polymer carbons [figures 11.1(1), 11.1(4), 11.1(7)] indicated that only in the case of Terylene carbon was there extensive porosity accessible to carbon dioxide at 195K.

A comparison of the 'mercury densities' recorded for Terylene and Courttelle carbon in table 12.1(1) (i.e. Terylene 'mercury density' $1.40 \pm 0.01 \text{ g cm}^{-3}$ Courttelle 'mercury density' $1.47 \pm 0.05 \text{ g cm}^{-3}$) with the 'true' density value of 2.10 g cm^{-3} adopted by Kipling¹⁸ for non-graphitising carbons, indicates the presence of extensive porosity in both carbons. In view of the relatively low adsorption of carbon dioxide at 195K by unactivated Courttelle carbon it is possible that this porosity is inaccessible to this adsorbate. Alternatively the porosity may consist only of a few relatively large pores (i.e. 'macropores') inaccessible to mercury at atmospheric pressure and contributing little to the adsorptive capacity of the carbon.

The mercury density of unactivated wool carbon has not been determined and therefore no similar estimate of pore volume is available. If the assumption is correct that carbon prepared from wool is non-graphitising then fairly extensive porosity might be expected to be

present. However from figure 11.1(1) it is clear that a low uptake of carbon dioxide at 195K was observed for unactivated wool carbon. Reasoning similar to that applied in the case of unactivated Courtelle carbon may explain the low adsorption of carbon dioxide at 195K by unactivated wool carbon.

From an examination of figures 11.1(2), 11.1(5) and 11.1(8) it is evident that any increment in degree of burn-out up to the limit of 50% for the three carbons derived from single polymers resulted in an increase in adsorption as measured by the corresponding x_c value. This is also true in respect of the majority of carbons prepared from binary polymer mixtures.

The conditions adopted for the activation of the carbons suggest that activation took place in zone 2 of the Hedden and Wicke classification.¹⁴¹ In this zone the rate of the gasification reaction is controlled jointly by the rate of the chemical reaction and by in pore diffusion. Zone 2 gasification is therefore considered to result in both internal and external attack by the oxidising gas.

As previously discussed, Franklin⁴ deduced from X-ray diffraction studies that generally non-graphitising carbons exhibit extensive fine structure porosity. Further this porosity once formed is preserved on further heating. Franklin⁴ estimated the dimensions of this porosity to be of the order of tens of Angstrom units. These findings suggest that in the non-graphitising carbons prepared from wool, Terylene and Courtelle a large proportion of the porosity is contained within pores of molecular dimensions. If this is indeed the case then the low adsorption of carbon dioxide at 195K observed for unactivated carbons derived from both wool and Courtelle may be attributed to the inaccessibility of porosity rather than the situation where the porosity is contained within a few relatively large pores (i.e. macropores).

It thus seems reasonable to suggest that the increases in x_c values observed with increasing degree of burn-out for the single polymer carbons prepared from wool and Courtelle resulted from increased accessibility of existing porosity together with some development of new porosity. Certainly if activation occurred under zone 2 conditions a degree of internal attack would be expected. It is however difficult to assess the exact character of this internal attack with the data available.

The character of the D-R type I plots observed for the carbons derived from single polymers are presented in table 13.2(1). Deviations from linearity are described according to the notation of Marsh and Rand.¹⁰²

For all three single polymer carbons at low degrees of activation (i.e. 0%, 10%) and where x_c values exceed 40 mg g⁻¹ type A deviation was observed. As previously discussed in section 6.4 type A deviations are generally observed at low degrees of activation.

At high degrees of activation (i.e. 30%, 40%, 50%) in carbons prepared from wool and Courtelle, type B deviation was observed. As previously discussed, type B deviation is generally observed for more highly activated carbons. The character of the D-R type I plots for carbons prepared from Terylene was however somewhat unusual. Thus for burn-outs in the range 0% - 50% type A deviation was observed.

Some changes were observed however in the D-R type I plots of carbons prepared from Terylene. With increasing degree of burn-out the slopes of both linear portions of each D-R type I plot increased and the point of intersection of these two linear portions moved to lower values of $(\log^D/p_0)^2$ [see figure 11.1(6)].

Chiche et al¹³⁸ considered that the two linear portions of the plot where type A deviation is observed represent parts of two distributions of partial molar free energy change on adsorption with adsorption volume. The point of intersection of these linear portions reflects a change in the mechanism of adsorption from one distribution to the other.

It is clear from the discussion contained in section 6.2 that the slope of the D-R type I plot controls both the mode and the spread of the distribution. This relationship is illustrated in figure 6.2(1)¹⁰³. Thus the observed increase in the slope of both linear portions of the D-R type I plot with increasing degree of activation may be interpreted in terms of a decrease in the spread and the $\Delta\bar{G}$ value at the mode for each of the two distributions present. Further the movement of the point of intersection of the two linear portions to lower values of $(\log^D/p_0)^2$ with increasing degree of activation reflects an increase in the relative pressure range over which one

Table 13.2(1)

polymer carbon	burn-out (mass %)					
	0	10	20	30	40	50
wool	Ⓐ	A	L	B	B	B
Courtelle	X	A	L	B	B	B
Terylene	A	A	A	A	A	A

Key

A = Type A deviation (according to Marsh and Rand¹⁰²)

B = " B " " " " "

C = " C " " " " "

L = Linear plot

X = Not plotted, negligible gas uptake.

Where A, B, C, L ringed, indicates possible error $\geq 25\%$ of corresponding x_c value.

distribution is effective in describing the adsorption process. As a result the relative pressure range over which the second distribution is effective in describing the adsorption process is correspondingly reduced.

Since no generally accepted relationship exists between the distribution of partial molar free energy change on adsorption with adsorption volume and the pore structure of an adsorbent no further comment is yet possible concerning the porosity present in carbon derived from Terylene. It would however appear that the mode of activation and hence possibly the porosity developed in Terylene carbon differs considerably from that for the carbons prepared from wool and Courtelle.

13.2 (b) Carbons prepared from binary polymer mixtures

The adsorption results for carbons prepared from the binary polymer mixtures wool/Courtelle and Terylene/Courtelle may be considered in terms of the coating model for pyrolysis behaviour proposed in section 13.1.

The adsorption results for the carbons prepared from wool/Terylene mixtures are discussed separately as these carbons arise from the pyrolysis of two fusing polymers.

Terylene fusion was observed to occur at 530K. From plate 9.1(3) taken during the pyrolysis of a wool/Terylene mixture it appears that the fused Terylene coated the wool fibres prior to wool fusion recorded at approximately 583K. If both polymers exist in a fused state even over a short temperature range it is possible that some kind of solution may be formed. If this is the case then the coating model will almost certainly be inadequate in terms of the interpretation of the adsorption data for the carbons prepared from wool/Terylene mixtures.

If however at the final heat treatment temperature of 1213K, Terylene carbon does in fact exist as a coating around the carbon derived from each wool fibre then the carbons prepared from wool/Terylene mixtures of high Terylene content might be expected to exhibit adsorption properties characteristic of carbon prepared from Terylene.

In fact a continuous increase in x_c values over the range of burn-out investigated was observed for carbons prepared from the mixture range Terylene - W90/T10. Further the maximum x_c value decreased regularly with decrease in the Terylene content of the original polymer mixture from Terylene to W50/T50. However type A deviations in the D-R type I plot at high degrees of activation (i.e. 30%, 40%, 50%) and characteristic of Terylene carbon were not observed for the carbon prepared from the polymer mixture W25/T75.

It would thus seem that whilst the adsorptive properties of carbons prepared from wool/Terylene polymer mixtures of high Terylene content reflect the presence of carbon derived from Terylene there is no evidence to suggest that this carbon exists as a coating around carbon derived from the wool component of the original fibre mixture. The adsorption data for carbons prepared from wool/Terylene polymer

mixtures do not therefore support the tentative conclusion from the pyrolysis study that the coating model is applicable in describing the pyrolysis behaviour of the wool/Terylene system.

It is however interesting to note that type C deviation of the D-R type I plot was observed for 0% burn-out carbon prepared from the polymer mixture W25/T75. Type C deviation was also observed for the corresponding carbon of the Terylene/Courtelle system (i.e. T75/C25), activated to 0% burn-out. The occurrence of type C deviation will be discussed later in this section.

As discussed in section 13.1 both the mixtures wool/Courtelle and Terylene/Courtelle are comprised of a fusing and a non-fusing polymer. If in fact the coating model for pyrolysis behaviour is applicable then the carbons prepared from these binary polymer mixtures would be expected to consist of areas of carbon from the non-fusing component surrounded by carbon derived from the fusing component.

As previously reported, activation is believed to take place under conditions corresponding to zone 2 of the Hedden and Wicke classification.¹⁴¹ In this case mass loss from both the interior and exterior of the carbon particles would be expected as a result of activation. Thus for carbons prepared from polymer mixtures of high fusing polymer content, the process of activation to low degrees of burn-out might be expected to result to a large extent in activation of the outer coating carbon derived from the fusing polymer. Thus the adsorptive properties of these carbons, both unactivated and activated to low degrees of burn-out would be expected to resemble the adsorptive properties of the carbon prepared from the fusing polymer alone.

This postulate is examined first with respect to the x_c /burn-out behaviour observed for the carbons prepared from wool/Courtelle and Terylene/Courtelle polymer mixtures [see tables 11.3(2) and 11.4(2)]. For the carbon prepared from wool a maximum value for x_c of 330 mg g⁻¹ was observed at 45-55% burn-out. As the proportion of wool in the original wool/Courtelle mixture is decreased to the composition W60/C40, a corresponding decrease was observed in both the maximum value of x_c and the burn-out at which this maximum was observed.

For the carbon prepared from Terylene a continuous increase in x_c with burn-out was observed over the entire range of burn-out

investigated. At 50% burn-out an x_c value of 650 mg g^{-1} was recorded. As the proportion of Terylene in the original polymer mixture decreased in the composition range Terylene - C55/T45, a corresponding decrease was observed in the value of x_c at 50% burn-out.

The relative success of the coating model in describing the pyrolysis behaviour of wool/Courtelle and Terylene/Courtelle polymer mixtures may be further assessed by a consideration of the character of D-R type I deviations observed for these carbons [see tables 11.3(3) and 11.4(3)].

No trends in behaviour are observed in table 11.3(3) since the carbons prepared from both wool and Courtelle exhibit similar D-R type I plot deviations in the range of burn-out investigated. However it is clear from table 11.4(3) that the adsorptive character of Terylene carbon (i.e. type A deviation) is also displayed by carbons prepared from polymer mixtures of high Terylene content. The occurrence of type A deviation decreasing only gradually with decreasing Terylene content of the original fibre mixture. The trends outlined above in the adsorption results for carbons prepared from wool/Courtelle and Terylene/Courtelle mixtures thus tend to support the coating model proposed to describe the pyrolysis behaviour of mixtures containing fusing and non-fusing polymers.

The significance of the type C deviations observed in some of the D-R type I plots reported in this study will now be considered.

Examples of type C deviation reported by other workers are listed in table 13.2(2). It is clear from these data that type C deviation has generally been observed for various carbonaceous adsorbents at high degrees of burn-out with a variety of adsorbates. The value of $(\log P/p_0)^2$ below which deviation from linearity was observed to occur is also seen to vary considerably.

As discussed in section 6.3 thermodynamic arguments limit the relative pressure range within which the basic assumptions of Dubinin's theory of volume filling are valid. Whilst the lower relative pressure limit for applicability of the D-R type I equation varies with the identity of the adsorbate/adsorbent system under consideration, it is possible that in some of the examples listed in table 13.2(2) the linear portion of the D-R type I plot occurs at

Table 13.2(2)

Adsorbate/adsorbent systems where type C deviation of the D-R type I plot has been observed. Also indicated is the value of $(\log P/p_0)^2$ below which the deviation from linearity is observed.

Reference	Adsorbate/ adsorption temperature	Adsorbent	Burn-out (%)	$(\log P/p_0)^2$ below which deviation observed
106	benzene/293K	activated sugar charcoal	57.9	<12
120	benzene/293K	activated coal	65	<15
120	benzene/293K	activated coal	70	<15
120	benzene/293K	activated coal	75	<13
118	carbon dioxide/ 195K	activated carbon (type 207C)	burn-out not quoted	<3
118	carbon dioxide/ 195K	activated carbon (type 112C)	burn-out not quoted	<3
102	nitrogen/77K	activated 850K polyfurfuryl alcohol carbon	71.5	<3

values of P/P_0 below the relative pressure limit for the system concerned. If this is the case then the plot must be regarded as a curve and therefore an example of type B deviation.

Since the necessary thermodynamic data to determine this lower relative pressure limit are not available for the current work it is not possible to advance this argument further. However in those examples where deviations from linearity are observed at $(\log P/P_0)^2$ values greater than 10 doubt may exist concerning the applicability of the D-R type I equation to the linear portion of the plot.

As discussed in section 6.4 where type C deviations have been reported various theories have been advanced to explain their occurrence. Whilst some success has been claimed through the application of equations containing two D-R type I terms^{105,120} or one D-R type I term and a D-R type II term,¹⁰⁶ these explanations may be considered simply as curve fitting exercises. Further, until independent evidence is available, explanations based on particular pore shapes¹⁰⁴ or pore filling processes¹¹⁸ must be regarded as conjectural.

The occurrence of type C deviation in this study for the carbons prepared from polymer mixtures W25/T75 and T75/C25 and activated to 0% burn-out is interesting. Some similarities exist in that both carbons were activated to 0% burn-out and were prepared from polymer mixtures comprising 75% by mass of Terylene. The second polymer of the mixture differed however in that one was a fusing type (wool) and the other non-fusing (Courtelle). From a consideration of table 13.2(2) it is clear that type C deviation is not generally observed at burn-outs as low as 0%.

Tables 11.3(3) and 11.4(3) indicate that type C deviations were also observed for carbons prepared from the polymer mixtures W15/C85 and T15/C85. In addition deviations of partial type C character were observed for carbons prepared from the polymer mixture T10/C90. These carbons were all prepared from mixtures of fusing and non-fusing polymers which had a high proportion of the non-fusing polymer (Courtelle). From an examination of the x_c /burn-out diagrams for these carbons [see figures 11.3(20), 11.4(5), 11.4(2)] it is clear that activation resulted initially in an increase in the value of x_c .

recorded for each carbon. However with further increase in the degree of activation the value of \bar{x}_c in all three cases showed a marked reduction. Thus the value of \bar{x}_c at burn-outs of 40% and 50% for all three carbons was less than 25 mg g^{-1} .

The 'mercury density' data for the carbons prepared from the polymer mixtures W15/C85 and T15/C85 [see figures 12.1(1) and 12.1(2)] indicated that as the value of \bar{x}_c for these carbons increases and then decreases with increasing degree of activation the 'mercury densities' show a corresponding decrease and increase in magnitude.

Utilising the coating model of pyrolysis behaviour the carbons prepared from polymer mixtures W15/C85 and T15/C85 would be expected to consist mainly of carbon derived from the non-fusing polymer (Courtelle) surrounded by a layer of carbon arising from the fusing polymer. Activation of these carbons under conditions corresponding to zone 2 of the Hedden and Wicke classification¹⁴¹ should as previously discussed result in some degree of internal mass loss. Internal porosity may therefore be developed by both increasing accessibility to existing porosity and by the creation of new porosity. Certainly at low degrees of burn-out increased values of \bar{x}_c together with decreased 'mercury densities' were recorded for these carbons. However in view of the observed decrease in the values of \bar{x}_c and corresponding increase in the 'mercury densities' with further increase in degree of activation it would seem that the porosity initially developed was then gradually destroyed leaving a core of carbon of relatively high 'mercury density' and porosity inaccessible to carbon dioxide at 195K. As discussed in chapter 12 for carbons prepared from wool 15/Courtelle 85 and Terylene 15/Courtelle 85 the observed increases in 'mercury density' with increasing degree of activation may be explained in terms of accumulation of relatively dense impurity or selective gasification of a carbon matrix composed of regions of carbon varying in 'mercury density'.

In these cases it is proposed that the core carbon, remaining after activation to 40% and 50% burn-out, is essentially carbon derived from Courtelle. Further the lack of accessible porosity observed after burn-out to 40% and 50% arises as a result of the

coating of fused polymer formed during pyrolysis around the non-fusing polymer. Hence in these cases the normal internal porosity developed in Courtelle carbon during pyrolysis is modified by the presence of the fused polymer coating. This modification may take place in two ways. First volatile Courtelle degradation products trapped within the fused polymer coating may be incorporated into the structure of the Courtelle carbon thus filling internal porosity. Secondly the fused polymer coating may actually enter the internal porosity of the Courtelle carbon as it develops thus filling or at least sealing off this porosity from the particle exterior.

The production of a graphite of low gas permeability and therefore presumably low porosity has been reported elsewhere.¹³⁹ The graphite in the form of a tube designed to hold nuclear fuel was impregnated with furfuryl alcohol plus a polymerisation catalyst. The resin formed was cured in situ and the tube then pyrolysed to 1273K. A measure of the reduction in gas permeability achieved is recorded in table 13.2(3) for a typical graphite tube.

Furfuryl alcohol polymerised into a solid resin, gave a carbon yield of 50% by mass on pyrolysis to 1273K. During pyrolysis the resin shrank uniformly without going through a liquid phase giving rise to a carbon of reported density 1.3 g cm^{-3} . The carbon prepared from polyfuryl alcohol was non-graphitising.

Whilst the details of this process differ from that employed in producing the W15/C85 and T15/C85 carbons it is possible that the pore blocking postulated to account for the observed reduction in gas permeability in the impregnated graphite also occurred in the carbons W15/C85 and T15/C85 if by a somewhat different mechanism.

It is clear from examination of table 13.2(2) that the type C deviations for carbons prepared from the polymer mixtures W15/C85, T15/C85 and T10/C90 were observed at lower burn-outs than the type C deviations reported by other workers.

The coating model for pyrolysis behaviour would suggest that these samples consist mainly of carbon derived from individual Courtelle fibres surrounded by carbon arising from the fusing polymer present in the original polymer mixture (e.g. wool or Terylene).

Table 13.2(3)

Size of tube	initial permeability to nitrogen at room temperature $\text{cm}^2 \text{s}^{-1}$	treatment	permeability to nitrogen at room temperature after treatment $\text{cm}^2 \text{s}^{-1}$
1" outside diameter 1/2" internal diameter 3" long	2.7×10^{-8}	two impregnations with pyrolysis to 1273K	1×10^{-7}

If, as is apparent, activation of these particular carbon samples develops porosity predominantly in the external layer of carbon and does not penetrate the seemingly impermeable core carbon then the rate of gasification for the external carbon layer might be expected to be considerably greater than that for the core carbon. In that event the external layer of carbon is effectively subjected to a greater degree of burn-out than that indicated by the overall burn-out. Further if this external layer of carbon then dominates the observed adsorption behaviour by virtue of its more extensively developed porosity then the occurrence of type C deviation in the D-R type I plot can readily be attributed to the adsorption behaviour of a more highly activated carbon.

13.3 Final conclusions

The pyrolysis behaviour of the single polymers wool, Terylene and Courtelle and the binary polymer mixtures wool/Terylene, wool/Courtelle and Terylene/Courtelle have been investigated. Both wool and Terylene were observed to fuse during pyrolysis separately giving rise to soft non-graphitising carbons at the final heat treatment temperature. Fusion was not however observed during the pyrolysis of Courtelle, the final product being a physically hard non-graphitising carbon.

The D.T.A. and T.G. data indicated that the thermal stability of Terylene was reduced when pyrolysis took place in the presence of either wool or Courtelle. It is considered that this decreased thermal stability was due to chemical interaction of the Terylene with degradation products formed during the pyrolytic breakdown of the second polymer. It was further observed that the thermogravimetric behaviour of Courtelle was modified when pyrolysed in the presence of either wool or Terylene. Residual yields from the pyrolysis of wool/Courtelle and Terylene/Courtelle mixtures at 1213K were observed to be excessive i.e. higher than would be predicted if the pyrolysis of a polymer in a mixture was unaffected by the presence of a second polymer. It is considered that both the modified Courtelle thermogravimetric behaviour and the excessive residual yields may be explained in terms of the coating model of pyrolysis behaviour as discussed in detail in section 13.1.

The surface properties of activated carbons prepared from both the single polymers and the binary polymer mixtures were also investigated. It is considered that the surface properties of carbons prepared from Terylene/Courtelle polymer mixtures are consistent with those suggested by the coating model. Whilst the surface properties of carbons prepared from wool/Courtelle polymer mixtures are not inconsistent with those suggested by the coating model, the similarity in the D-R type I deviations observed for the carbons prepared from both wool and Courtelle [see table 13.2(1)] does not allow such a definitive conclusion.

However it is considered that the coating model may be applied to explain the pyrolysis behaviour of binary polymer mixtures consisting of fusing and non-fusing components. The occurrence of excessive residual yields may thus be predicted for such a system.

Variations in x_c values both with burn-out and composition of the original polymer mixture, are in general difficult to predict but observed variations have been explained in terms of the coating model for Terylene/Courtelle and wool/Courtelle carbons.

As discussed in section 1.2 the aim of this project was to investigate the conversion of binary mixtures of textile fibres, containing wool as one fibre into active carbons. It is clear that the majority of carbons prepared from wool/Courtelle mixtures and all those from wool/Terylene mixtures when activated to burn-outs between 30% and 50% exhibited extensive porosity as measured by their respective x_c values. Depending upon the required properties (i.e. pore size, particle strength etc) activated carbons prepared from the binary polymer mixtures wool/Terylene and wool/Courtelle may constitute commercially useful active carbons.

This conclusion also applies to the active carbons prepared from Terylene/Courtelle mixtures in the composition range Terylene - T50/C50.

It must be added that the excessive residual yields observed from the pyrolysis of mixtures of fusing and non-fusing polymers provide an obvious advantage for the production of active carbon on a commercial basis.

REFERENCES

1. Gee N.C., 'Shoddy and Mungo Manufacture' Emmott Co. Ltd., King Street, Manchester, 1950.
2. Rainnie G.F. (editor), 'The Woollen and Worsted Industry - an Economic Analysis' Clarendon Press, Oxford, 1965, 17.
3. Central Statistical Office, Annual Abstract of Statistics HMSO, 1970, No. 109.
4. Franklin R.E., Proc. Roy. Soc., 1951, A209, 196.
5. Milner G., Spivey E., Cobb J.W., J. Chem. Soc., 1943, 578.
6. The British Wool Manual, published in association with the Textile Recorder. Harlequin Press, 1952, p. 87.
7. Fitzer E., Mueller K., Shaeffer, W., 'Chemistry and Physics of Carbon' Editor Walker P.L., 1971, 7, 237, E Arnold.
8. Turner W.N., Johnson F.C., Private communication.
9. Cotton F.A., Wilkinson G., 'Advanced Inorganic Chemistry' Second Edition 1966, p. 295, Interscience.
10. Kipling J.J., Sherwood J.N., Shooter P.V., Thompson N.R., Carbon 1964, 1, 315.
11. Kipling J.J., Shooter P.V., Proceedings of the Second Conference on Industrial Carbon and Graphite 1965, p. 15, Society of Chemical Industry (London).
12. Kipling J.J., Shooter P.V., Carbon 1966, 4, 1.
13. Ramdohr P., Arch. Eisenhüttenw., 1928, 1, 669.
14. Blayden H.E., Westcott D.T., Proceedings of the Fifth Carbon Conference 1963, 2, 97. Pergamon Press, London.
15. Brooks J.D., Taylor G.H., Carbon 1965, 3, 185.
16. Ihnatowitz M., Chiche P., Dedit J., Pregermain S., Tourant R., Carbon 1966, 4, 41.
17. Loch L.D., Austin A.E., Proceedings of the First and Second Conferences on Carbon. University of Buffalo, New York, 1953/1955.
18. Kipling J.J., Sherwood J.N., Shooter P.V., Thompson N.R., Carbon 1964, 1, 321.
19. Rossman R.P., Smith W.R., Ind. Eng. Chem., 1943, 35, 972.
20. Kipling J.J., Sherwood J.N., Shooter P.V., Thompson N.R., Young R.N., Carbon 1966, 4, 5.
21. Maggs F.A.P., Schwabe P.H., Williams J.H., Nature (London) 1960, 186, 956.

22. Mackenzie R.C., 'Differential Thermal Analysis' Volume I (1970) Volume 2 (1972), Mackenzie R.C. (editor) Academic Press, London.
23. Textile Institute of Great Britain. 'Identification of Textile Materials' 5th edition, 1965.
24. American Association of Textile Chemists and Colorists, 'Analytical Methods for a Textile Laboratory' 2nd edition 1968.
25. Alexander P., Hudson R.F., Wool, Its Chemistry and Physics, 2nd edition Revised Earland C., Chapman Hall, London, 1963.
26. Woods H.J., Proc. Roy. Soc., 1938, 166, 76-79.
27. Bradbury J.H., 'Advances in Protein Chemistry' editor Anfinsen C.B. et al, 1973, 27 130.
28. Horio M., Kondo T., Text. Res. J., 1953, 23, 373.
29. Peters D.E., Bradbury J.H., Aust. J. Biol. Sci, 1972, 25, 1255.
30. Crewther W.G., Harrap B.S., Nature (London) 1965, 207, 295.
31. Leach S.J., Rogers G.E., Filshie B.K., Arch. Biochem. Biophys., 1964, 105, 270.
32. Pauling L., Corey R.B., Branson H.R., Proc. Amer. Acad. Sci., 1951, 37, 205.
33. Hildebrand D., Textilindustrie, 1969, 71(4), 274-280.
34. Skerchly A., Woods H.J., International Wool Textile Research Conference, Harrogate, Yorkshire 1960, 1, T517.
35. Crighton J.S., Happey F., Symposium on Fibrous Proteins, Academy of Sciences, Canberra, Australia, 1967, editor Crewther W.G., published 1968, 409-420, Butterworths, Australia.
36. Felix W.D., McDowall M.A., Eyring H., Text Res. J., 1963, 33, 465.
37. Watt I.C., Kennett R.H., James J.F.P., Text. Res. J., 1959, 29, 975.
38. Horio M., Kondo T., Sekimoto K., Funatsu M., 111^e Congres International de la Recherche Textil Lainiere, Paris 1965, section 2, p. 189.
39. Schwenker R.F., Dusenbury J.H., Text. Res. J., 1960, 30(10), 800.
40. Crighton J.S., Findon W.M., Thermal Analysis, 1971, 3, 431.
41. Haly A.R., Snaith J.W., Text. Res. J., 1967, 37(10), 898.
42. Carroll-Porczyński C.Z., Thermal Analysis, 1971, 3, 273.
43. Bendit E.G., Text. Res. J., 1966, 36, 580.

44. Menefee E., Yee G., Text. Res. J., 1965, 35, 801.
45. Mecham D.K., Olcott H.S., Ind. Eng. Chem., 1947, 39, 1023.
46. Tarim S.T., Cates D.M., Applied Polymer Symposia, 1966, 2, 1-13.
47. Schwenker R.F., Beck L.R., Zuccarello R.K., American Dyestuff Reporter 1964, 53(19), 30-40.
48. Shenai V.A., Silk and Rayon Industries of India, 1965, 6(1), 85-9.
49. Gillham J.K., Schwenker R.F., Applied Polymer Symposia, 1966, No. 2, 59-75.
50. Petukhov B.V., The Technology of Polyester Fibres, 1963, Macmillan, New York.
51. Schwenker R.F., Beck L.R., Text. Res. J., 1960, 30(8), 624-626.
52. Pande A., Lab. Pract., 1965, 1048.
53. Buxbaum L.H., Angewelt Chemie International Edition, 1968, 7(3), 182-190.
54. De Puy C.H., Kong R.W., Chem. Reviews 1960, 60, 431.
55. Pohl H.A., J. Amer. Chem. Soc., 1951, 73, 5660.
56. Standage A.E. Prescott R., British Patent Number 1,128,043, April 1965.
57. Turner W.N., Johnson F.C., J. Appl. Polym. Sci., 1969, 13, 2073-2084.
58. Grassie N., McGuchan R., Europ. Polym. J., 1970, 6, 1277-1291.
59. idem, ibid, 1971, 7, 1091-1104.
60. idem, ibid, 1971, 7, 1357-1371.
61. idem, ibid, 1971, 7, 1503-1514.
62. idem, ibid, 1972, 8, 243-255.
63. idem, ibid, 1972, 8, 257-269.
64. idem, ibid, 1972, 8, 865-878.
65. idem, ibid, 1973, 9, 113-124.
66. idem, ibid, 1973, 9, 507-517.
67. Houtz R.C., Text. Res. J., 1950, 20, 786.
68. Grassie N., Hay J.N., J. Polym. Sci., 1962, 56, 189-202.

69. Takata T., Hiroi I., J. Polym. Sci., 1964, 2, 1567-1585.
70. Thompson E.V., Polymer Letters, 1966, 4, 361-366.
71. Hay J.N., J. Polym. Sci., 1968, A1, 6, 2127-2135.
72. Grassie N., McNeill I.C., J. Chem. Soc., 1956, 3929.
73. Burlant W., Parsons J., J. Polym. Sci., 1956, 22, 249.
74. Shindo A., Industrial Research Institute, Osaka, Report 317, 1961 (Studies on graphite fibre).
75. Miyamichi K., Okamoto M., Ishizuka O., Katayama M., J. Soc. Fibre Sci. and Tech. (Japan), 1966, 22, 538.
76. Strauss S., Madorsky S.L., J. Res. Nat. Bur. Standards, 1958, 61, 77.
77. Monahan A., J. Polym. Sci. 1966, A1, 4, 2391.
78. Watt W., Green J., Proceedings of the Conference on Carbon Fibres, The Plastics Institute 1971, paper 4, p. 23.
79. De Winter W., Macromol. Chem. Rev., 1966, 1(2), 336.
80. Noh I., Yu H., Polymer Letters, 1966, 4, 721.
81. Kasatochkin V.I., Kargin V.A., Dokl. Acad. Nauk, SSSR, 1970, 191(5), 1084-1087.
82. Kasatochkin V.I., Smutkina Z.S., Kasakov M.A., Churbrova M.A., Radinov N.P., Khimicheskie Volokna 1972, No. 4, 10-12.
83. Schurz J., J. Polym. Sci., 1958, 28, 438.
84. Dunn P., Ennis B.C., J. Appl. Polym. Sci., 1970, 14, 1795.
85. Peebles L.H., Brandrup J., Friedlander H.N., Kirby J.R., Macromolecules, 1968, 1, 53.
86. Saunders R.E., Chem. Proc. Eng., 1968, 49, 100.
87. Gokcen U., Cates D.M., Applied Polymer Symposia, 1966, No. 2, 15-24.
88. Crighton J.S., Holmes D.A., Thermal Analysis, 1971, 3, 411.
89. Perkins D.L., Drake G.L., Reeves W., J. Appl. Polymer Sci., 1966, 10, 1041.
90. Schwenker R.F., Zuccarello R.K., Beck L.R., Final Report, U.S. Navy Contract Number N140 (133) 67979B. (Text. Res. Instit. 1963 (March 29th)).
91. Ubaidullaev B.Kh., Geller A., Geller B.E., Vysokomol Soedin Ser. B., 1972, 14(5), 382-383.

92. Langmuir I., J. Amer. Chem. Soc., 1916, 38, 2221.
93. Brunauer S., Emmett P.H., Teller E., J. Amer. Chem. Soc., 1938, 60, 309.
94. Polanyi M., Verh., dtsh. physik Ges., 1914, 16, 1012.
95. Polanyi M., Trans. Farad. Soc., 1932, 28, 316.
96. Polanyi M., Verh. dtsh. phys. Ges., 1916, 18, 55.
97. Titoff A., Z. Phys. Chem., 1910, 74, 641.
98. Berenyi L., Z. Phys. Chem., 1920, 94, 628.
99. Dubinin M.M., Chemistry and Physics of Carbon Volume II (Editor P.L. Walter) Arnold, London, 1966, p. 51.
100. Bering B.P. Dubinin M.M., Serpinsky V.V., J. Colloid Interface Sci., 1966, 21, 378-393.
101. Young D.M., Crowell A.D., Physical Adsorption of Gases, Butterworths, London, 1962.
102. Marsh H., Rand B., Third Conference on Industrial Carbon and Graphite, Society of Chemical Industry, London, 1970, p. 172.
103. Marsh H., Rand B., J. Colloid Interface Sci., 1970, 33, 101.
104. Freeman E.M., Siemieniewska T., Marsh H., Rand B., Carbon, 1970, 8, 7.
105. Dubinin M.M., Polystyanov E.F., Izv., Akad, Nauk., SSSR Ser. Khim, 1966, 793.
106. Dubinin M.M., Zaverina E.D., Zh. Fiz. Khim., 1949, 23, 1129.
107. Radushkevich L.V., Zh. Fiz. Khim., 1949, 23, 1410.
108. Dubinin M.M., First Conference on Industrial Carbon and Graphite, Society of Chemical Industry, London, 1958, p. 219.
109. Sutherland J.W., Porous Carbon Solids, Editor Bond R.L., Academic Press, New York, 1967, p.1.
110. Marsh H., O'Hair T.E., Fuel 1966, 45, 301.
111. Brunauer S., Pure Appl. Chem., 1966, 10, 293.
112. Flood E.A., The Solid-Gas Interface Volume I, Arnold, London, 1967, p. 73.
113. Rand B., Ph.D. Thesis University of Newcastle upon Tyne 1968.

114. Culver R.V., Watts H., Rev. Pure Applied Chem., 1960, 10, 95.
115. Dacey J.R., The Solid-Gas Interface Volume II, Editor, Flood E.A., Arnold, London 1967, Chapter 34.
116. Dovaston N.G., McEnaney B., Weedon C.J., Carbon, 1972, 10, 277.
117. Bering B.P., Serpinsky V.V., Dokl. Akad. Nauk, SSSR, 1963, 148, 1381.
118. Marsh H., Siemieniowska T., Fuel 1967, 46, 441.
119. Marsh H., Rand B., Carbon, 1971, 9, 63.
120. Izotova T.I., Dubinin M.M., Zh. Fiz. Khim., 1965, 39, 2796.
121. McEnaney B., Rowan S.M., Chem. Ind., 1965, 2032.
122. Dollimore D., Elliott G.E.P., Hutton T.R., Stock R., J. Physics Section E. Scientific Instruments, 1970, 3, 465.
123. Yariv S., Birnie A.C., Farmer V.C., Mitchell B.D., Chem. & Ind., 1967, 1744-1745.
124. Manley T.R., Chem. & Ind., 1969, 421.
125. Coates A.W., Redfern J.P., Analyst, 1963, 88, 906.
126. Spencer W.B., Amberg C.H., Beebe R.A., J. Phys. Chem., 1958, 62, 719.
127. Dubinin M.M., Bering B.P., Serpinsky V.V., Vasilev B.N., 'Surface phenomena in Chemistry and Biology' 1958, Pergamon Press, London.
128. Lamond T.G., Marsh H., Carbon, 1964, 1, 293.
129. Bridgeman O.C., J. Amer. Chem. Soc., 1927, 49, 1174.
130. International Wool Textile Organisation, Bradford 'The determination of wool fibre thickness by the projection microscope'.
131. Goodall A.R., Private communication.
132. Scott N.D., Polymer, 1960, 1, 114-116.
133. Schwenker R.F., Proceedings of the Second Symposium on Thermal Analysis (editor McAdie M.G.) Toronto Section of Chemical Institute of Canada 1967.
134. Bromley J., Proceedings of the Conference on Carbon Fibres. The Plastics Institute, 1971, paper 1, p. 3.
135. Brunauer S., Emmett P.H., Teller E., J. Amer. Chem. Soc., 1938, 60, 309.

136. Handbook of Chemistry and Physics, The Chemical Rubber Co., 54th Edition 1973-1974.
137. Kipling J., McEnaney B., Proceedings of the Second Conference on Industrial Carbon and Graphite 1965, p. 380, Society of Chemical Industry, London.
138. Chiche P., Marsh H., Pregermain S., Fuel, 1967, 46(4-5), 341.
139. Watt W., Bickerdike R.L., Brown A.R.G., Johnson W., Hughes G., Nuclear Power 1959, 4, 86.
140. Zahn H., Pfeifer H., Polymer (London), 1963, 4, 429.
141. Hedden K., Wicke E., Proceedings of the Third Carbon Conference 1959, Pergamon Press, New York, p. 249.